Bulletin 36
Part 7
(of 7 Parts)

THE SHOCK AND VIBRATION BULLETIN

FEBRUARY 1967

A Publication of
THE SHOCK AND VIBRATION
INFORMATION CENTER
Naval Research Laboratory, Washington, D.C.

Office of
The Director of Defense
Research and Engineering

DISCLAIMER NOTICE

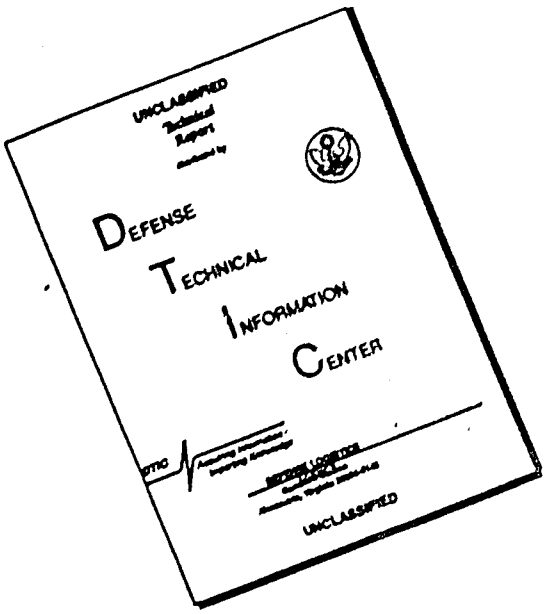

THIS DOCUMENT IS BEST QUALITY AVAILABLE. THE COPY FURNISHED TO DTIC CONTAINED A SIGNIFICANT NUMBER OF PAGES WHICH DO NOT REPRODUCE LEGIBLY.

Bulletin 36
Part 7
(of 7 Parts)

THE SHOCK AND VIBRATION BULLETIN

FEBRUARY 1967

A Publication of
THE SHOCK AND VIBRATION
INFORMATION CENTER
Naval Research Laboratory, Washington, D.C.

The 36th Symposium on Shock and Vibration was held in Los Angeles, California, on 18-20 October 1966. The U.S. Air Force was host.

Office of
The Director of Defense
Research and Engineering

SYMPOSIUM MANAGEMENT

The Shock and Vibration Information Center

William W. Mutch, Director

Henry C. Pusey, Coordinator

Rudolph H. Volin, Coordinator

Jean B. Goldbecker, Editor

Katherine G. Jahnel, Administrative Secretary

36th Program Committee

William R. Forlifer, NASA Goddard Space Flight Center

Edward H. Schell, Air Force Flight Dynamics Laboratory

George Stathopoulos, Naval Ordnance Laboratory

James M. Taylor, U.S. Army Missile Command

Air Force Liaison

Los Angeles Scientific and Technical Liaison Office, Research and Technology Division, Air Force Systems Command

Lt. Col. Kenneth W. Cook

Arthur E. Kimberly

Bulletin Production

Graphic Arts Branch, Technical Information Division, Naval Research Laboratory

CONTENTS

PART 7

Structural Reliability

Design Data and Methods

PAPERS APPEARING IN PART 1
Part 1 - Confidential
(Titles Unclassified)

PAPERS APPEARING IN PART 4

Damping

STRUCTURAL RELIABILITY

ESTIMATE OF EFFECT OF SPACECRAFT VIBRATION QUALIFICATION TESTING ON RELIABILITY

Clyde V. Stahle, Jr.
The Martin Company
Baltimore, Maryland

The purpose of this paper is to provide an estimate of the effect of a spacecraft vibration qualification test (SVQT) on the vibration reliability of a spacecraft system, i.e., the probability that the spacecraft will perform satisfactorily while and after the spacecraft is subjected to the vibration of the launch phase of flight. The increase in the vibration reliability of the spacecraft provided by the SVQT is quantitatively evaluated by a stress-strength reliability analysis which treats the vibration-induced spacecraft failures as resulting from log normal distributed equipment vibration stress and strength. If the SVQT is required, the spacecraft equipments are considered to be randomly selected from an equipment population having a strength distribution truncated at the equipment vibration qualification test level. If the SVQT is not required, the equipments are considered to be selected from two populations: one having the strength distribution of the unqualified equipments and the other having a strength distribution truncated at the equipment qualification test level. The vibration stress distribution, estimated from statistically analyzed vibration measurements and specification requirements, is formulated in terms of the equipment qualification test level and combined with the equipment strength distribution, obtained using the variance estimated from the analysis of extended level tests of launch vehicle equipment and a median strength estimated from the results of spacecraft equipment qualification programs so that it is a function of the equipment vibration qualification test level. An independent serial systems model is used to relate the vibration reliability of the equipment to that of the spacecraft.

Using the estimated statistical distributions for equipment stress and strength, the vibration reliability of the spacecraft is formulated in terms of the equipment qualification test level and the number of equipments to be qualified. The estimated reliability is given for the range of vibration levels for which data were obtained.

C. V. Stahle, Jr.

INTRODUCTION

The purpose of this paper is to estimate the reliability of a general spacecraft model with and without a spacecraft vibration qualification test (SVQT). Environmental qualification tests may be applied to parts, equipments, subsystems, or systems to verify the capability of the design to perform satisfactorily in the anticipated service environments. The tests are concerned with the reliability of the design, i.e., the probability of a device performing its purpose adequately for the period of time intended

under the operating conditions encountered. Because of the small sample size and relatively short test time, the data do not provide a statistical measurement of reliability. In spite of this, on successfully passing these tests, the unit is considered to be qualified for the service environment which it will encounter.

It has become common practice that environmental qualification tests be performed at the equipment level. The various equipments are then integrated into a spacecraft system by the system contractor. There are technical reasons for performing additional vibration qualification tests on the system level as well as on the equipment level. Some of the reasons cited are:

1. Removal of artificial restraints of test fixtures imposed during equipment testing;

2. Evaluation of subsystem interactions;

3. Evaluation of connectors, wiring and many small components not adequately evaluated during equipment qualification testing; and

4. Evaluation of changes in electrical parameters resulting from the environment.

In view of these considerations and the costs involved, it is important that the decision to perform SVQT be made on a rational basis. This rational basis will be probabilistic rather than deterministic, since the major effect of the test is to improve the reliability of the spacecraft, i.e., the probability that the spacecraft will perform satisfactorily. Although the effects of the environment on reliability are vague, there is a definite need to place decisions of this type on a quantitative rather than an intuitive basis. Golovin defends the "managerial insistence that all design criteria, design decisions and approved specifications likely to affect the probability of a system meeting its overall performance are explicitly defined and defended in quantitative terms" [1].

In this paper, the stress-strength concept is used to estimate the vibration reliability of equipment and to formulate the vibration reliability of a spacecraft system in terms of system parameters using the equipment reliability. The stress-strength concept is briefly reviewed, and the important factors of the equipment vibration stress and strength are discussed. A model which relates equipment reliability to system reliability is established, and through the evaluation of the equipment vibration reliability, the system vibration reliability is estimated with and without the SVQT.

STRESS-STRENGTH CONCEPT

The statistical concept of a stress vs strength analysis appears to be well suited to the consideration of the effect of the vibration environment on spacecraft equipments [2,3]. This concept, which has been applied to the Titan II structure [4], evaluates the reliability of any item by considering that the stress and strength have statistical distributions (Fig. 1) rather than by considering failures in the time domain. The probability of failure is determined by the probability that the stress exceeds the strength. Although this concept of describing the reliability of an item appears to fit the vibration stress effect of interest, this idealized model must be investigated further to determine its applicability to the present problem.

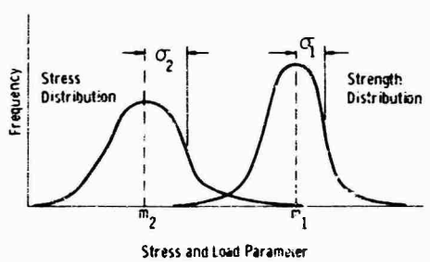

Fig. 1 - Stress-strength concept

EQUIPMENT VIBRATION STRENGTH

The vibration strength of equipment, i.e., the capability of the equipment to function while subjected to vibration, is difficult to determine. The strength will vary considerably from equipment to equipment. A motor-driven switch may have an extremely high vibration strength as compared to a relay. The variation in the vibration strength of equipments of a particular design can also vary from unit to unit as evidenced by the emergence of "Production Monitoring" vibration test programs of flight equipments after the equipment design has been qualified. It appears reasonable to consider that the variation in the vibration strength of equipments results primarily from design differences, although differences between units of a particular design will also occur.

The vibration strength of equipment is generally not determined analytically. As a result, the vibration strength is based on engineering judgment and past experience which may be translated into basic design practices.

The strength is frequently provided by testing the equipment to the qualification requirements and making those modifications which are necessary to pass the test. Consequently, a wide variation in the vibration strength of equipment designs will be present; however, the equipment designs will provide a minimum strength dictated by test requirements as design changes are made during qualification.

The statistical distribution of equipment strength as a function of vibration level after qualification testing will be a relatively broad distribution appearing to be truncated at the qualification test level. Although development testing will generally eliminate a number of equipment failures prior to qualification testing, qualification test data indicate that the mean strength of all the untested equipments may not be much higher than that required for qualification. Typical failure data from equipment qualification programs indicate that the percentage of failures range from approximately 10 percent to as high as 40 percent of the equipments tested. The strength distribution of qualification tested equipments is not truly truncated at the qualification level because the equipment designs that fail are modified and placed back in the equipment population, and because the variance from unit to unit of a particular design still exists; however, equipment strength should not fall significantly below the level used for qualification testing unless quality control procedures permit defective units to be flown. A truncated distribution should provide a good approximation of the strength distribution of the equipment used in the flight vehicles.

The vibration strength distribution of untested equipment can be approximated from available data, although the type of data required for the accurate determination of the statistical distribution of equipment vibration strength is generally not obtained; i.e., equipments either pass or fail the qualification tests but are not tested at varying levels to failure. The strength distribution of the untested equipment is broad in comparison with the vibration level as discussed previously. A normal distribution would not be applicable because this would permit negative strengths. In view of the broad distribution, it is reasonable to consider that the vibration strength of the equipments has a log normal distribution prior to qualification testing. Assuming that the vibration strength has a log normal distribution makes it possible to estimate the strength distribution from failure data obtained from tests at two vibration levels; i.e., the mean and variance can be estimated. Limited data on equipments tested at the qualification level and at 1.5 times the qualification level are available. The distribution after qualification testing can then be approximated if the equipment strength distribution is considered to be truncated at the qualification test level as a result of equipment design changes incorporated during the test program.

The vibration strength of equipment is, in fact, a two-dimensional statistical distribution. It is a function of vibration level and of time. However, the exposure time of the equipment to high vibration will not vary significantly for a particular spacecraft configuration and can be accurately predicted from trajectory calculations. On the other hand, experimental data show that the fatigue life is much more dependent on the stress level than on the exposure time [5]. Considering the relatively small variation in exposure time and the greater dependence of equipment failure on vibration level, a one-dimensional statistical distribution is warranted.

EQUIPMENT VIBRATION STRESS

To apply the stress-strength concept to the estimation of the equipment vibration reliability, a variable representing the vibration stress must be determined. From the previous discussion of the vibration environment and equipment strength, the effect of exposure time can be considered insignificant in comparison with the intensity of the vibration. Therefore, the vibration stress can be adequately represented by a variable which reflects the damaging effect of the vibration intensity on equipments.

Several mathematical models have been studied to relate the vibration damage of equipment to the vibration environment [6]. Based on these studies, the vibration stress variable to be used with the stress-strength concept will be related to the square root of the power spectral density (PSD) for random vibration and to the amplitude of the acceleration for sinusoidal or transient acceleration.

EFFECT OF SPACECRAFT VIBRATION QUALIFICATION TESTING

During the SVQT, vibration is introduced into the spacecraft. The response of the spacecraft tends to be relatively uniform at the equipment locations. On the other hand, statistical analyses of flight data combine the response, by frequency band, in all axes. Since the resonances of the spacecraft do not

generally occur at the same frequency in each axis, the statistically analyzed vibration data provide a broader distribution than would be obtained if the data were analyzed by direction. Since the high equipment vibration levels will occur at spacecraft resonances during the SVQT and since the levels will have a much narrower distribution than obtained by statistically analyzing flight data, it is reasonable to consider the vibration level of equipment during the SVQT as single valued; i.e., the variation in the equipment vibration levels during the SVQT will be neglected. Considering current test methods, the equipment vibration probability level will be the same as that used for individual equipment qualification tests.

Although equipments of a particular spacecraft may have been vibration qualification tested, subsequent system level tests of the spacecraft often reveal equipment deficiencies at the same probability level as the vibration input. These failures result from a variety of causes. The equipment or component (e.g., connectors, wire bundles, small components) may not have been tested during the equipment test program, or interactions between either equipments or the equipment and the spacecraft structure, which were not possible in the equipment test, may occur during the system level test. Interactions and interface problems are a major contributor to observed failures during spacecraft tests [7]. Because these equipments exhibit strength characteristics different from those evaluated during equipment tests or because these equipments were not tested as equipments, the strength distribution can be approximated by that of the original untested equipments, i.e., the strength distribution prior to equipment qualification testing. If the SVQT is performed, equipments having design deficiencies relative to the qualification test level will be uncovered, and design changes can be made to improve their vibration strength. On the other hand, if the SVQT is not performed, these weak equipment designs will be retained in the spacecraft system.

The change in the equipment vibration strength distribution as described above is shown conceptually in Fig. 2. Figure 2a shows the strength distribution of the untested equipment, i.e., the strength of the various relay, switch, transmitter, antenna, etc., designs before the design changes are incorporated so that they will pass the equipment qualification test. Figure 2b shows the truncated strength distribution of the equipment designs after the improvements required by the equipment qualification tests are included. For those equipments having interactions or not having been adequately evaluated in the equipment qualification tests, the original strength distribution, before truncation, will apply. If the SVQT is performed, all equipments will have the truncated distribution since the deficient designs will be corrected. If the SVQT is not performed, the system reliability will be associated with that of an expected number of equipments with the original distribution, as well as with a majority of equipments having the truncated distribution.

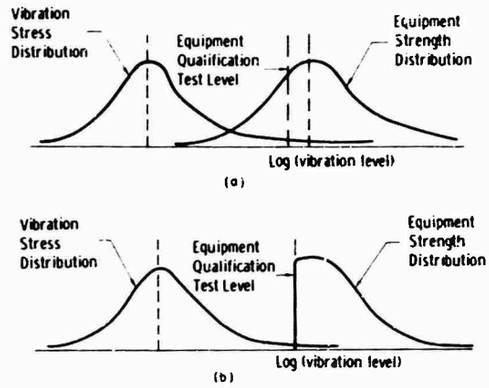

Fig. 2 - Effect of vibration qualification testing on equipment vibration strength and stress distributions: (a) before equipment qualification testing, and (b) after equipment qualification testing except for equipments having interactions

SPACECRAFT RELIABILITY MODEL

The basic steps in establishing a reliability model are to develop block diagrams for various system functional levels and subsequently to derive mathematical models for these block diagrams. Although block diagrams which accurately represent all spacecraft systems and subsystems cannot be developed, close approximations can be formulated. Usually, the requirements of minimum weight and volume of the spacecraft impose stringent requirements on the spacecraft design. As a result, unless reliability analyses indicate redundancy requirements, all subsystems and equipments are necessary to the successful operation of the system. On this premise, typical reliability block diagrams of the system and subsystem levels will be as shown in Fig. 3. The reliability diagram uses only a single line to show that the successful operation of the system or subsystem requires that all blocks perform without

failure. In some spacecraft an entire subsystem may be contained in a single package or reliability may be improved by providing redundant components of the same design combined in a single equipment package. For these systems, the block diagram of Fig. 3 is still applicable. In view of the overall design considerations of spacecraft, reliability block diagrams representing the spacecraft system and subsystems as composed of a number of blocks in series appears to provide an adequate representation. The reliability block diagram of Fig. 3 describes the system as a serial system; it operates successfully if, and only if, all the equipments perform successfully [8].

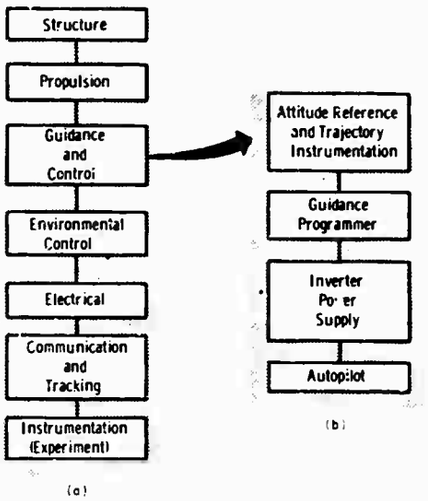

Fig. 3 - Typical reliability block diagram of spacecraft at (a) system and (b) subsystem (guidance and control) functional levels

The functional reliability model of the spacecraft system is the basis for the reliability model of the system under vibration stress. Three types of models for determining the vibration reliability of the serial system are the weakest link, the chain, and the independent serial system [9].

Weakest Link Model

As indicated by the name, the reliability of the system is determined by considering only the reliability of the most unreliable element. This model provides a high estimate of the system reliability and can approximate the system reliability if a single equipment reliability is much lower than that of the other equipments. Because of the numerous failure modes that exist under vibration, this model only provides a rough approximation, and a more accurate model is required.

Chain Model

The chain model of a serial system considers that all the equipment links have the same statistical strength distribution and are subjected to identical stress. However, the vibration load applied to all the equipments is not the same. The vibration stress is a function of equipment location and direction, although it is also related to a variation between flights. If a smooth flight to rough flight variation is the predominant factor affecting the vibration stress, this chain load concept would be applicable.

Independent Serial System Model

This model considers that the reliability of all the elements are mutually independent, i.e., that the reliability of the individual equipment elements is the same irrespective of the successful performance or failure of the other equipment elements. The difficulty with this model is that it does not consider interactions between components. The interactions can be accounted for by using two strength distributions for the equipments, as described previously. Another source of statistical dependence is the vibration environment as discussed for the chain model. Because the spacecraft design generally does not consider the vibration environment in selecting equipment locations, and because a large variation in the vibration stress has been shown to result from location and direction within the spacecraft, a model considering the equipments to be mutually independent elements can be applied. This independent serial system model shall be used to estimate the reliability of the spacecraft system under vibration stress using the original untested equipment strength distribution for equipments having interactions or inadequate equipment tests.

The vibration reliability of the spacecraft system can be determined with the product rule for the independent serial system model. The product rule states that the reliability of the system is equal to the product of the reliabilities of the elements of the system. This can be expressed as:

$$R^v = \prod_{j=1}^{n} R_j^v . \qquad (1)$$

where

R^v = system reliability for vibration environment,

R_j^v = vibration reliability of jth equipment,

n = total number of equipments, and

π = product of the function for all equipments.

The system vibration reliability can also be estimated by applying the product rule to the two types of equipments separately:

$$\left(R^v = \prod_{j=1}^{n-m} R_j^v\right)\left(\prod_{i=1}^{m} R_i^{v\,1}\right). \qquad (2)$$

where

R_j^v = vibration reliability of equipment not having interactions, and

$R_i^{v\,1}$ = vibration reliability of equipment having interactions.

This formulation is based on the model in which the equipments are considered to be randomly selected from two different equipment populations. The n equipments are drawn from the population of equipment designs which have passed equipment qualification tests and do not exhibit system interactions so that the vibration strength distribution of the designs has a truncated log normal distribution. Since the system interactions and system conditions cause them to behave in a different manner than under equipment test conditions, the remaining m equipments are considered to be randomly selected from an equipment population which has the log normal vibration strength distribution of the untested equipments. The values of R_j^v, $R_i^{v\,1}$, n, and m can be estimated from available failure data. This will be discussed in detail in the subsequent sections.

The system reliability under vibration stress can be estimated with and without the SVQT from Eq. (1) and (2). If an SVQT is performed, interactions causing equipment failures at the test level will be exposed and corrected; the system reliability can then be estimated from Eq. (1). If the SVQT is not performed, the system reliability can be estimated from Eq. (2) using available data to estimate n, m, $R_i^{v\,1}$ and R_j^v. The vibration reliability of the system can be estimated if an SVQT is not performed. (To evaluate the overall spacecraft system reliability, the system reliability for the vibration environment, R^v, must be combined with the estimated operating reliability of the system, assuming that the system has survived the vibration stresses of launch. This is beyond the scope of this paper.)

VIBRATION STRESS DISTRIBUTION

The statistical representation of the vibration environment as a log normal distributed random variable has been used by numerous investigators [8,10,11]. The equipment vibration stress was found to be best described by the square root of the acceleration PSD for random vibration, or the amplitude of the acceleration for periodic or quasi-periodic vibration. The root-mean-square (rms) acceleration can be used to describe the vibration stress for random vibration as well as for periodic types of vibration. Available data from actual measurements of the vibration environment and from test specifications are used here to evaluate the vibration stress distribution for equipments. The vibration stress is then formulated in terms of the equipment qualification test level using the log normal distribution. Before this is discussed, however, the characteristics of a log normal distributed variable are briefly reviewed.

If a variable has a log normal distribution, the logarithm of the variable is normally distributed. The mean and variance of the variable g_s are defined as

$$M(\log g_s) = \log \tilde{g}_s \qquad (3)$$

and

$$V(\log g_s) = M[(\log g_s - \log \tilde{g}_s)^2] = \sigma_s^2 . \qquad (4)$$

where the median of the distribution is $\tilde{g}_s$, the 50th percentile value, and the variance is defined as σ_s^2 [12]. By using the relation that the difference between the logarithms of two quantities is equal to the logarithm of the quotient of the quantities, the variance can be written as:

$$V(\log g_s) = M\left\{\left(\log \frac{g_s}{\tilde{g}_s}\right)^2\right\}. \qquad (5)$$

which indicates that the variance is a function of the ratio of the variable to the median value.

The cumulative distribution function and the probability density function, respectively, are

$$G(g_s) = \Phi(u) \tag{6}$$

and

$$g(g_s) = \frac{M}{\sigma_s g_s}\,\phi(u), \tag{7}$$

where

$\Phi(u)$ = standardized cumulative normal distribution function,

$\phi(u)$ = standardized normal distribution function,

$$u = \frac{\log g_s - \log \bar{g}_s}{\sigma_s} = \frac{1}{\sigma_s}\log\left(\frac{g_s}{\bar{g}_s}\right), \tag{8}$$

$M = \log e = 0.4343$,

and

$0 < g_s < \infty$.

Because the vibration stress of the equipment under random vibration is best described by the square root of the acceleration PSD and the vibration test requirements for equipments are based on a statistical analysis of the PSD, the test requirements can be used to estimate the statistical distribution of the vibration stress. The vibration tests for qualification are based on the 99th percentile levels of the PSD, and the vibration tests for acceptance are based on the 95th percentile levels [13,14]. Since the PSD is a log normal distributed variable, the values of the PSD(W) at two probability levels, defined by standardized variables u_{1s} and u_{2s}, can be written, from Eq. (8), as

$$u_{1s} = \frac{1}{\sigma_W}\log\left(\frac{W_1}{\bar{W}}\right) \tag{9}$$

and

$$u_{2s} = \frac{1}{\sigma_W}\log\left(\frac{W_2}{\bar{W}}\right), \tag{10}$$

where σ_W is the standard deviation and $\bar{W}$ is the median of the PSD log normal distribution as defined in Eqs. (3) and (4). Subtracting Eq. (9) from Eq. (10) yields

$$u_{2s} - u_{1s} = \frac{1}{\sigma_W}\left(\log\frac{W_2}{\bar{W}} - \log\frac{W_1}{\bar{W}}\right) = \frac{1}{\sigma_W}\log\left(\frac{W_2}{W_1}\right). \tag{11}$$

which shows that the ratio of the PSD values for the two percentiles indicates the variance in the PSD distribution. A typical statistically analyzed PSD is shown in Fig. 4 which presents the PSD values in 50-cps frequency bands from 50 to 2000 cps for the 95th and 99th percentiles [15]. The ratio of the PSD values at the two percentiles as a function of frequency is seen to be relatively constant; therefore, the variance of the PSD values (W) in all of the frequency bands can be approximated by a constant value as indicated by Eq. (11).

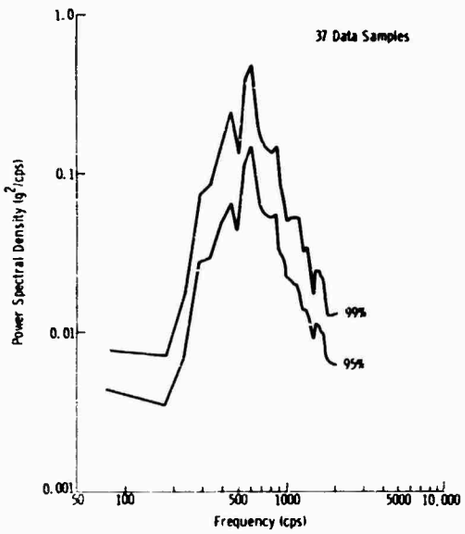

Fig. 4 - Acceleration power spectral density statistical distribution by frequency band, Titan guidance truss, Stage II firing

To evaluate the vibration stress, the square root of the PSD or, alternately, the square root of the mean square acceleration, g^2, can be evaluated since the vibration stress is dependent on the square root of the PSD. It is convenient to use the mean square acceleration since this is readily available from test specifications. Using the basic properties of logarithms, the variable can be written as

$$\log (g^2)^{1/2} = \frac{1}{2}\log (g^2), \tag{12}$$

which will be normally distributed since log W is normally distributed; however,

$$V\left\{\frac{1}{2}\log (g^2)\right\} = \frac{1}{4}V\left\{\log (g^2)\right\}. \tag{13}$$

since the variance of a constant times a normally distributed random variable ($\log g^2$) is equal to the square of the constant times the variance of the variable. Either the square root of the mean square acceleration (rms) can be used to evaluate the vibration stress or the square root of the PSD can be used since the variance of the PSD in all frequency bands is approximately equal. Using the equations derived above, the variance of the vibration stress can be estimated for random vibration.

For periodic types of vibration, i.e., periodic or quasi-periodic, either the peak or rms value of the equivalent sinusoidal test acceleration can be used to estimate the vibration stress since the vibration stress of a given equipment is a linear function of the amplitude of the acceleration.

To determine the mean and variance of the vibration stress, it is convenient to relate these parameters to the 95 and 99 percent vibration levels, g_A and g_Q, respectively, which are used to specify vibration test requirements. In terms of the log transformation of the vibration level used for acceptance and qualification testing, the mean and variance can be determined as:

$$\sigma_s = 1.45 \log \left(\frac{g_Q}{g_A}\right) \tag{14}$$

and

$$\log \bar{g}_s = \log g_Q - 3.38 \log \left(\frac{g_Q}{g_A}\right). \tag{15}$$

Equations (14) and (15) can be used to evaluate the median and variance of the vibration stress distribution from the vibration qualification g_Q and acceptance g_A test levels.

Because the basic phenomena causing the vibration environment are similar for all spacecraft, it is not surprising that the variance of the vibration stress is approximately the same. Available information obtained from specifications and actual data are shown in Table 1 for four different launch vehicles [13,15,16,17]. Although there is a considerable variation in levels for the various boosters, it can be seen that the ratio of the rms acceleration at the 99th percentile to that at the 95th percentile is approximately 1.5 for all the launch vehicles. It will be noted that the statistically analyzed data from the Titan is slightly higher than those values obtained from the various specifications. The ratios from the Titan data determined the variance of the PSD in those frequency bands having the highest value, e.g., the 575-cps center frequency band of Fig. 4, which is slightly greater than the variance in the other frequency bands. In view of the fact that the test levels reflect the variance in all frequency bands, the ratio of the test levels is slightly less than the ratio determined from the PSD. Using the ratio of 1.5 from Table 1 in Eqs. (14) and (15), the vibration stress is defined as a log normal distributed random variable, where

$$\sigma_s = 1.45 \log (1.5) = 0.255 \tag{16}$$

and

$$\bar{g}_s = 0.254\, g_Q. \tag{17}$$

Using the basic expressions for the log normal distribution with the values of the median and

TABLE 1
Comparison of Equipment Vibration Levels for Various Launch Vehicles

Launch Vehicle	Type of Vibration	Acceptance	Qualification	Ratio
Scout	Random	7.7	11.5	1.5
	Sine	14.0	21.0	1.5
Delta	Random	7.7	11.8	1.53
	Sine	Not required	21.0	–
Atlas/Agena	Random	9.0	16.4	1.82
	Sine/random[a]	6.7	10.3	1.54
Titan - guidance truss	Stage II firing	0.15[b]	0.5[c]	1.82[d]
	Transonic flight	0.22[b]	0.6[c]	1.65[d]

[a]Sinusoidal acceleration superimposed on random acceleration.
[b]95th percentile of measured acceleration PSD levels in highest frequency band.
[c]99th percentile of measured acceleration PSD levels in highest frequency band.
[d]Determined from the square root of the acceleration PSD.

variance determined above, the vibration stress probability density distribution can be written in terms of the qualification test level from Eq. (7) as

$$g_s(g) = \frac{M}{\sigma_s x}\,\phi(u_s) = \frac{1.705}{g}\,\phi(u_s)\,. \qquad (16)$$

where $\phi(u_s)$ is the normal distribution function, and

$$u_s = \frac{1}{\sigma_s}\log\left(\frac{g}{\bar{g}_s}\right) = 3.94\log\left(\frac{g}{g_Q}\right) + 2.33\,. \qquad (19)$$

The vibration stress distribution is shown in Fig. 5.

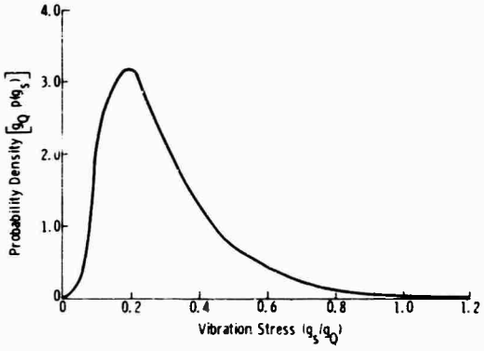

Fig. 5 - Probability density distribution of vibration stress

EQUIPMENT STRENGTH DISTRIBUTION

Since equipment failure data at two test levels is the only type of data available, these can be used to estimate the equipment strength distribution. If the strength distribution is log normal, the percentage of equipments failing at each test level can be used to estimate the mean and variance of the distribution. If the lower test level is taken as the equipment qualification test level (g_Q) and the higher test level is taken as some multiple (axg_Q), the percentage of equipments falling at each level can be used to estimate the strength distribution. If a random sample of size n is taken from an infinite population, some of which have a given attribute, an unbiased estimate of the proportion of the population having the attribute will be

$$P = E\left\{\frac{m}{n}\right\}, \qquad (20)$$

where P is the proportion of population having the attribute, m is the number of items in the sample having the attribute, n is the random sample size, $E\{\ \}$ is the expected value, and an unbiased estimate of the variance of this estimate, $\hat{P}$, will be

$$v(\hat{P}) = \frac{P(1-P)}{n-1}\,.$$

If the vibration strength of the equipment is a log normal distributed random variable as a function of vibration level, the relations for the log normal distribution given in Eqs. (6) and (7) correspond to the probabilities P_1 and P_2; $\bar{g}_f$ and σ_f, the median and standard deviation, respectively, of the equipment strength distribution can be shown to be

$$\bar{g}_f = \frac{g_Q}{10^{\sigma_f u_{1f}}}\,, \qquad (21)$$

$$\sigma_f = \frac{\log a}{u_{2f} - u_{1f}}\,, \qquad (22)$$

where

$P_1 = \Phi(u_{1f})$ = proportion of equipment failing at the qualification test level,

$P_2 = \Phi(u_{2f})$ = proportion of equipment failing at or below a times the qualification test level,

$$u_{1f} = \frac{1}{\sigma_f}(\log g_Q - \log \bar{g}_f)\,, \qquad (23)$$

and

$$u_{2f} = \frac{1}{\sigma_f}\log(axg_Q) - \log \bar{g}_f\,. \qquad (24)$$

These relations were used to estimate the variance of the strength distribution of untested equipment using results obtained from launch vehicle equipment tests. The data indicate that 19.5 percent of the equipments fail at the qualification level and 49.3 percent fail at 1.5 times the qualification test level. Since these data provide the only available means of estimating the vibration strength distribution of equipments, the variance, determined from the data by Eq. (22), is felt to be the best available estimate of the variation in the design strength. The variance of the log normal distribution represents the power to which the ratio of the vibration level to the median vibration level is raised, as indicated in Eq. (8). It is shown in

TABLE 2
Summary of Spacecraft Results

Question	Program[a]												
	1	2	3	4	5	6	7	8	9	10	11	12	13
Vibration requirements:													
Equipment vibration requirement	16.4	2.83	8.48	9.50	14.85	14.85	14.1	14.85	10.61	NA	14.85	16.1	14.85
Equipment qualification performed	Yes	Yes	Yes	Yes	Yes	Yes	Yes	Yes	Yes	Yes	Yes	Yes	NA
Equipment test:													
Equipment tested	NA	20	20	50	28	19	97	46	20	366	NA	NA	NA
Equipment failures	30	2	1	2	22	2	29	10	1	51	NA	NA	NA
Equipment types tested	56	20	10	10	28	16	97	46	20	28	NA	NA	NA
Different types failed	14	2	1	2	11	2	29	10	2	15	NA	NA	NA
Retest failures	NA	0	0	0	10	0	NA	0	0	4	NA	NA	NA
S/C tests:													
No. S/C tested	1	1	7	8	1	1	1	1	1	NA	1	5	2
No. failures	3	0	1	1	4	17	1	4	3	NA	7	1	11
No. different equipment failures	3	0	1	1	3	8	1	3	3	NA	7	1	9
Causes:													
Interactions	-	0	0	1	3	8	1	4	0	NA	-	NA	5
Unqualified	1	0	1	-	-	-	-	-	-	NA	-	NA	NA
Untested	1	0	0	0	-	-	-	-	3	NA	7	NA	NA
Other	1	0	0	0	-	-	-	-	-	NA	-	NA	NA

TABLE 2 (Continued)
Summary of Spacecraft Results

Question	Program[a]												
	14	15	16	17	18	19	20	21	22	23	24	25	26[b]
Vibration requirements:													
Equipment vibration requirement	14.85	14.85	9.2	-	14.8	14.85	14.85	14.85	14.85	14.85	14.85	NA	NA
Equipment qualification performed	Some	NA	NA	-	NA	Yes	Yes	Yes	Yes	No	No	Yes	Yes
Equipment test:													
Equipment tested	NA	NA	NA	NA	NA	NA	NA	NA	NA	ND	ND	150	410
Equipment failures	NA	NA	NA	NA	NA	NA	NA	NA	NA	ND	ND	5%	NA
Equipment types tested	NA	NA	40	NA	NA	70	28	42	32[c]	ND	ND	30-50	82
Different types failed	NA	NA	NA	NA	NA	NA	NA	NA	NA	ND	ND	3-5	56
Retest failures	NA	NA	NA	NA	NA	NA	NA	NA	NA	ND	ND	NA	NA
S/C tests:													
No. S/C tested	2	1	1	1	1	2	1	1	1	1	1	1	ND
No. failures	6	7	5	1	2	16	11	2	4	0	6	4	ND
No. different equipment failures	6	7	5	1	2	10	9	2	3	0	5	4	ND
Causes:													
Interactions	2	3	3	1	1	10	9	2	3	-	-	1	ND
Unqualified	NA	NA	-	-	NA	-	-	-	-	-	-	-	ND
Untested	NA	NA	-	-	NA	-	-	-	1	-	4	-	ND
Other	NA	NA	2	-	NA	-	-	-	-	-	2	-	ND

[a]NA = not available.
[b]ND = not done.
[c]These data for launch vehicle. Two equipments tested at 1.5 times qualification level without failure.

the previous section that the variance of the vibration stress does not vary significantly for the various launch vehicles and Fig. 6 indicates that, with the exception of the propulsion system, the various subsystem equipments have nearly the same variance. Therefore, the use of launch vehicle data to estimate the variance of the spacecraft equipment vibration strength distribution appears to be a reasonable approximation. The standard deviation of the log normal vibration strength was estimated to be 0.209. However, the ratio of the median vibration strength to the qualification test level can be expected to vary with the vibration severity.

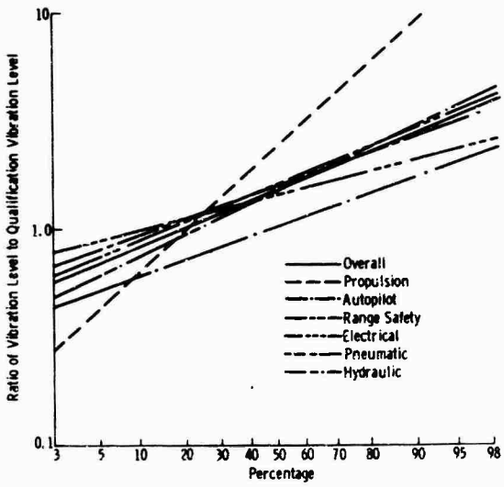

Fig. 6 - Comparison of estimated failure distribution of total system and subsystems

To estimate the relation between the median vibration strength of spacecraft equipment and the vibration level, spacecraft equipment qualification test data from nine spacecraft programs were analyzed (Table 2). The logarithm of the proportion of equipments which were qualification tested and did not fail are plotted as a function of the vibration qualification test level in Fig. 7. Since no equipment vibration failures will occur when the vibration qualification test level is zero and since all the equipments will tend to fail when the vibration qualification test level is infinite, the curve on this semilog graph should be a straight line passing through unity at a vibration level of zero. Using the method of least squares with the number of equipments tested as a weighting factor, a straight line was fitted to the data, as shown in Fig. 7 As can be seen in the figure, the data appear to fit the selected straight line transformation. Using the curve of Fig. 7 to estimate the probability of spacecraft equipment failures at the vibration qualification test level and the variance of the equipment vibration strength determined from the launch vehicle data, the equipment vibration strength distribution was obtained. The strength distribution of the untested spacecraft equipments is compared in Figs. 8 and 9 with the stress distribution for a vibration qualification test level of 5 and 15 g.

After qualification testing has been completed and modifications have been made to the equipments to provide vibration strength in excess of the qualification vibration value, the strength distribution of the equipment will be considered to be truncated at the qualification test level, as discussed previously. The strength distribution can now be described by a

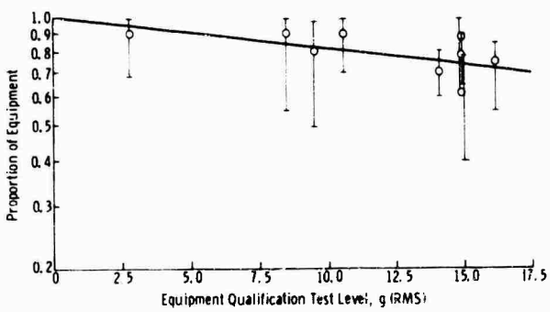

Fig. 7 - Variation of proportion of spacecraft equipments which did not fail during qualification tests with qualification test level, including 95 percent confidence limits for individual spacecraft samples

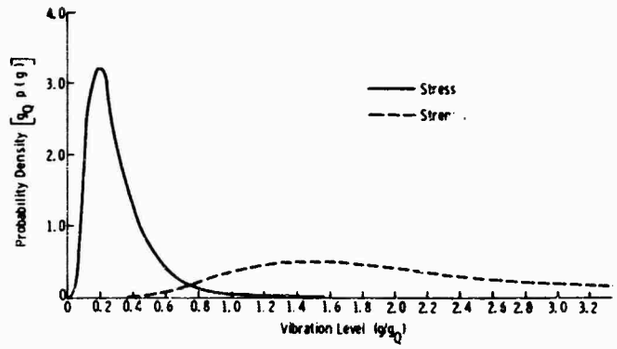

Fig. 8 - Comparison of estimated probability density distributions of vibration stress and equipment strength for qualification test requirement of 5 g rms

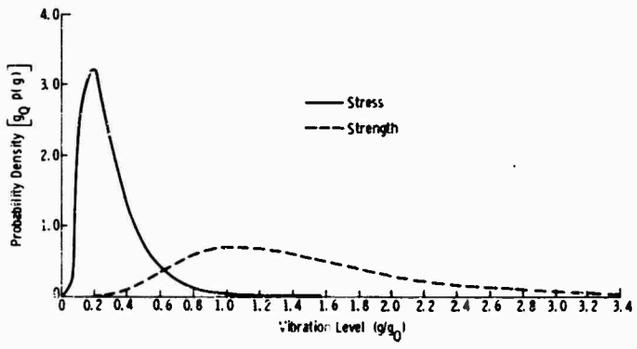

Fig. 9 - Comparison of estimated probability density distributions of vibration stress and equipment strength for qualification test requirement of 15 g rms

truncated distribution where the truncation point is a function of the vibration level, as shown in Fig. 7.

SPACECRAFT RELIABILITY UNDER VIBRATION STRESS WITH SVQT

After the vibration stress and strength distributions are estimated for the equipment, the reliability of the total spacecraft system under vibration stress can be determined if all equipments are assumed to have the truncated log normal strength distribution formulated in the previous section. The stress-strength concept can be used to determine the reliability of each equipment, and the total system reliability under vibration stress can then be determined from the reliability model.

The reliability of an equipment under a statistically varying stress is the probability that the strength of the equipment exceeds the stress. The reliability can be expressed in terms of the stress and strength distributions by letting $g_s(g)$ be the probability density distribution of the vibration stress and $g_f(g^*)$ be the probability density distribution of the vibration strength. Using the general expression for the reliability of an item having a statistically varying strength and subjected to a statistically varying stress, the reliability of the jth equipment under the vibration stress can be written as:

$$R_j^v = P\{\text{strength} > \text{stress}\}$$

$$= \int_0^\infty \int_s^\infty g_f(g^*)\, g_s(g)\, dg^* dg$$

$$= \int_0^\infty g_s(g)\,[1 - G_f(g)]\, dg\,. \qquad (25)$$

where $G_f(g)$ is the cumulative distribution of the equipment strength. R_j^v obtained with this equation is shown in Fig. 10 as a function of the qualification test level. The system reliability under vibration stress can be determined from Eq. (1) as

$$R^v = \left[R_j^v\right]^n \qquad (26)$$

when the SVQT is performed on the spacecraft, i.e., when all the equipments have the truncated log normal statistical strength distribution as a result of the SVQT. Consequently, the spacecraft vibration reliability R^v can be determined from the equipment vibration reliability given in Fig. 10, combined with Eq. (26) for the number of equipments, n, contained in the spacecraft system.

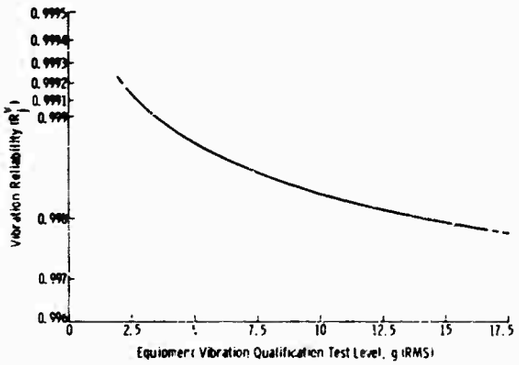

Fig. 10 - Variation in vibration reliability of qualification tested equipment with qualification test level

SPACECRAFT RELIABILITY UNDER VIBRATION STRESS WITHOUT SVQT

The spacecraft reliability under vibration stress without the SVQT requirement can be determined in the same manner as in the previous section, except that there will now be m equipments which do not have a truncated strength distribution. For the m equipments which have a log normal strength distribution, the reliability can be obtained as in the previous section. The reliability under vibration stress for these equipments is shown in Fig. 11, as a function of the equipment qualification test level. The system reliability can then be determined from Eq. (2) as

$$R^v = \left(\prod_{j=1}^{n-m} R_j^v\right)\left(\prod_{i=1}^{m} R_i^v\right). \qquad (27)$$

where R_j^v and R_i^v are obtained from Figs. 10 and 11, respectively, for the estimated qualification test level of the equipment.

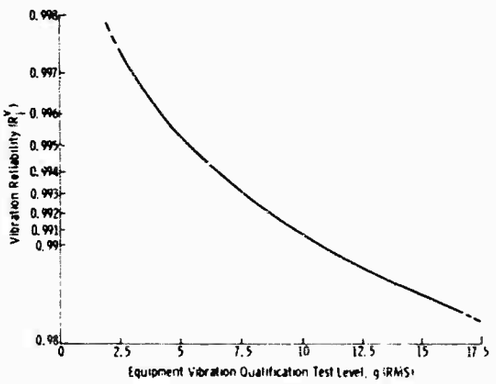

Fig. 11 - Variation in vibration reliability of unqualified equipments with equipment qualification test level

The number of equipments having the original vibration strength distribution of the unqualified equipment can be estimated from the number of failures which occur during the SVQT. If SVQT vibration failure data are obtained for various spacecraft for which the number of qualified equipments are known, the number of equipments having the original untruncated strength distribution can be estimated. Let t be the number of equipment failures observed during the SVQT, m be the number of equipments having the unqualified vibration strength distribution, n_Q be the number of equipments qualification tested, and P_f be the proportion of the unqualified equipments having a vibration strength less than the qualification test level. Then for those m equipments having the unqualified equipment vibration strength distribution, Eq. (20) gives

$$P_f = E\left\{\frac{t}{m}\right\}. \tag{28}$$

Because the SVQT is performed at the equipment qualification test level and the vibration strength distribution of the equipment has been estimated, P_f can be written as

$$P_f = \Phi(u_{1f}). \tag{29}$$

where

$$u_{1f} = \frac{1}{\zeta_f} \log\left(\frac{\xi_Q}{\bar{\xi}_f}\right). \tag{30}$$

Therefore, m can be estimated as

$$\hat{m} = \frac{1}{P_f}\, t. \tag{31}$$

where t is the observed number of failures during the SVQT and P_f is estimated from vibration failure data obtained during equipment qualification tests. The number of distinguishable equipments that are qualification tested, n_Q, can be used as a measure of the total number of equipments in the system since more complex space systems will result in a larger number of equipments to be qualified. Equation (31) can be written as:

$$\frac{\hat{m}}{n_Q} = \frac{1}{P_f}\left(\frac{t}{n_Q}\right). \tag{32}$$

so that the number of equipments having the original strength distribution can be estimated from the ratio of the number of equipment failures to the number of equipments qualification tested. It is reasonable to expect the number of equipment failures to be proportional to the number of equipments qualification tested in that any untested equipments are generally those which form an interface with and join together the individual equipments. Although the equipment failures which occur during the SVQT can be either qualified or unqualified equipments, analysis of failure data indicates that the failures occur primarily in the unqualified equipments (Table 2). The number of equipments having the qualified equipment strength distribution can be approximated as being equal to the number of equipments qualified. This leads to a slightly pessimistic estimate of the system vibration reliability, since the total number of equipments having the truncated strength distribution is increased. However, because the truncated strength distribution provides a higher vibration reliability than does the untruncated strength distribution, the added "fictitious" equipments in this category will have little effect on the estimated vibration reliability of the system.

Data obtained from SVQT tests of spacecraft were used to estimate the number of equipments having the original vibration strength distribution of the untested equipments. The results (Fig. 12) indicate that the number of equipments in this population is 0.39 times the number of equipments qualification tested. Using this result, Eq. (2) can be written as

$$R^v = \left(\prod_{j=1}^{n_Q} R_j^v\right)\left(\prod_{i=1}^{0.39 n_Q} R_i^v\right)$$

$$= \left[R_j^v\right]^{n_Q}\left[R_i^v\right]^{0.39 n_Q}. \tag{33}$$

where R_j^v, the vibration reliability of the unqualified equipment, is given in Fig. 10 and R_i^v, the vibration reliability of those equipments having the vibration strength distribution of the unqualified equipments, is given in Fig. 11.

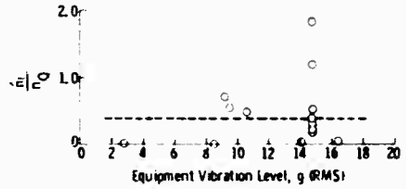

Fig. 12 - Comparison of overall estimated number of unqualified equipments to individual estimates

SUMMARY AND CONCLUSIONS

In this paper, the vibration reliability of the spacecraft system has been formulated using available data to estimate the parameters of the statistical distributions which determine the reliability. The vibration stress was considered to be a log normal distributed random variable. The variance of the vibration stress was estimated from specifications and measured data with the resulting distribution formulated in terms of the qualification test level. The vibration strength of spacecraft equipments was also treated as a log normal distributed random variable. The variance was estimated from available data at two vibration test levels. The median of the vibration strength was

estimated from spacecraft data as a function of the qualification test level. Finally, the estimated stress and strength distributions were combined to provide an estimate of the vibration reliability of the spacecraft system. If the spacecraft is required to pass an SVQT, the vibration reliability is determined by considering all equipments to have a truncated log normal strength distribution. If the SVQT is not performed, the equipments are considered to be randomly selected from two equipment populations, one having the truncated log normal strength distribution and the other having the log normal strength distribution of the untested equipments. In either formulation, the number of spacecraft equipments is estimated to be 1.39 times the number of equipments qualification tested. The results of this paper provide a means of estimating the vibration reliability of the spacecraft system with and without the SVQT requirement, using the number of equipments to be qualification tested and the equipment vibration qualification test level as spacecraft parameters. The estimated system vibration reliability is shown in Fig. 13 for various values of n_Q and g_Q with and without the SVQT.

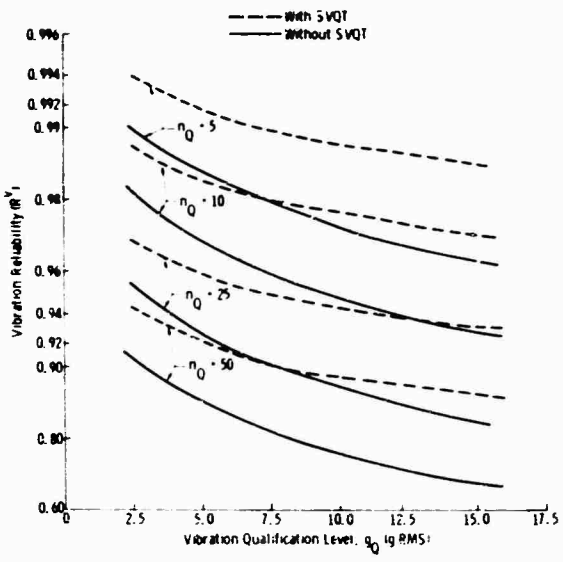

Fig. 13 - Estimated spacecraft vibration reliability

Based on the results presented in this paper, the following conclusions can be drawn:

1. Although numerous approximations and assumptions were required to arrive at the estimated spacecraft vibration reliability, the estimate uses the available data in a model which accounts for the major factors involved.

2. Data should be obtained to improve this estimate and substantiate the distributions of the environment and, particularly, the equipment vibration strength.

3. Until better data become available, the estimate contained in this paper should be used to evaluate the applicability of the SVQT requirement.

4. Substantial improvements in the vibration reliability of spacecraft can be obtained with the SVQT. The largest improvement will be provided for complex spacecraft and for spacecraft subjected to a more severe vibration environment.

REFERENCES

1. Nicholas E. Golovin, "Reliability Planning for Space Systems," IRE Trans. on Reliability and Quality Control, Vol. RQC-11, p. 21, Aug. 1961

2. Igor Bazovsky, Reliability Theory and Practice, p. 146. Prentice-Hall, Englewood Cliffs, N. J., 1961

3. Robert Lusser, "Reliability Through Safety Margins," p. 12, Army Rocket and Guided Missile Agency, Redstone Arsenal, Oct. 1958

4. Emory T. Haire, "Structure Reliability Analysis, Titan II," Martin Co. Rept. ER 11862, July 1961

5. Maurice Gertel, "Specification of Laboratory Tests," Shock and Vibration Handbook, Vol. 2, Chap. 24, p. 24-24. McGraw-Hill, New York, 1961

6. K. Eldred, W. Roberts, and R. White, "Structural Vibrations in Space Vehicles," WADD TR61-62, p. 411, Mar. 1961

7. John C. New, "Achieving Satellite Reliability Through Environmental Tests," NASA TND-1853, p. 16, July 1963

8. H. N. McGregor et al., "Acoustic Problems Associated with Underground Launching of a Large Missile," Shock and Vibration Bull. No. 29, Part 4, pp. 317-335, June 1961

9. David K. Lloyd and Myron Lipow, Reliability: Management, Methods and Mathematics, p. 221. Prentice-Hall, Englewood Cliffs, N. J., 1962

10. F. Condos and W. Butler, "Prediction of Vibration Levels for Space Launch Vehicles," Proc. IES. 1963

11. G. H. Klein and A. G. Piersol, "The Development of Vibration Test Specifications for Spacecraft Applications," NASA CR-234, May 1965

12. A. Hald, Statistical Theory with Engineering Applications. John Wiley and Sons, New York, 1952

13. William S. Shipley and James E. Maclay, "Mariner 4 Environmental Testing," Aeronautics and Astronautics, Aug. 1965

14. John H. Boeckel, "The Purposes of Environmental Testing for Scientific Satellites," NASA TND-1900, July 1963

15. C. J. Moening, "Comparative Discussion of Titan Missile Vibration and Temperature Environments with Test Levels Specified," Informal Martin Report, Nov. 16, 1960

16. "Environmental Test Specification and General Test Procedure for Design Qualification and Flight Acceptance Testing of Scout Launched Satellites," NASA Goddard Space Flight Center, Test and Evaluation Div., Aug. 11, 1961

17. "General Environmental Test Specification for Spacecraft and Components," Launch Environments Dictated by Delta Launch Vehicle, NASA Goddard Space Flight Center Spec. No. G-2-000, Sept. 10, 1963

DISCUSSION

Mr. Krause (Jennings Radio Mfg. Co.): Are you using a random vibration technique with fixed frequency limitations?

Mr. Stahle: The data were primarily from sinusoidal tests, although some random test results are also included.

Mr. Krause: Then this is fixed sinusoidal frequency as well?

Mr. Stahle: This would be a swept frequency. If the level varied, I selected the highest value.

Mr. Krause: How do you determine whether a qualification test is passed or failed? My experience in qualification testing is that one failure means failure of the test, but with the distribution you have shown, you can have failures but they can be predicted on a reliability basis.

Mr. Stahle: Two conditions can occur. In the first, you can decide to perform a qualification test on a complete spacecraft system in addition to equipment qualification testing; the entire spacecraft, with all the equipments included, can be vibrated, essentially subjecting the equipments to the qualification test level. In the second, you can decide to qualify the equipments but not to perform a test on the complete spacecraft system. In both cases it is assumed that any failures that occur will be corrected. The difference in the reliability with and without this test requirement reflects the ability to locate and repair design deficiencies within the total equipment population.

Mr. Krause: What is the difference between the 5 g and 15 g tests. Was the requirement for 5 or for 15 g?

Mr. Stahle: In Fig. 13, the vibration reliability with or without the test requirement was given as a function of the vibration qualification test requirement of equipment. The plot was from about 2-1/2 g to about 17-1/2 g, which sets the vibration qualification test requirement for equipment in the spacecraft tested. If the vibration requirement is higher, the median strength of the various equipment designs is not much greater; it is much closer to the equipment qualification test level. As a result, many more failures occur during the equipment qualification test program, and the distribution becomes very close to the qualification level which was fixed at some multiple of the vibration stress. As expected, more failures occur in the system with a more severe environment. If there were a failure using the independent serial systems model, which relates equipment reliability to system reliability, any equipment failure would constitute a system failure. From that standpoint it could be a pessimistic estimate of the system reliability.

Mr. Scott (Sandia Corp.): Was the qualification time fairly short, or was fatigue involved? If you increased the time, would you expect the same relationship? Also, what was the time of testing and was the testing done in all axes or just one?

Mr. Stahle: The data used here were obtained from a number of spacecraft programs, so I presume the durations of the qualification requirements varied. The data represent a cross section of spacecraft designs to reflect the current practices of qualification testing. Incidentally, the basic data were obtained through a questionnaire survey. The data are given in the paper and may be analyzed differently if anyone chooses to do so.

Mr. Roberts (Martin Co.): Is there anything significant that we have learned about the failure modes of these 300 different equipments?

Mr. Stahle: The intent of this paper was to estimate the vibration reliability with and without performing this test. The various failure modes, I believe, were in two general categories: one called interactions, and another classified as untested components. I think that in the untested component area, there would be many connectors and things of this sort. The objective of the paper was not really to try to uncover failure modes. I think it is evident that much failure data should be obtained and disseminated within the industry.

Mr. Jackman (General Dynamics/Pomona): How applicable is this to the NASA Saturn V program? Is the SVQT program being used as such, or is there a modification of it being considered?

Mr. Stahle: This program was for spacecraft rather than launch vehicles. I assume that because of the basic differences between spacecraft and launch vehicle design, there would be a question whether or not it would be applicable. I do not know whether or not this type of test is performed on a complete launch vehicle. Maybe somebody on the Saturn program could comment on that.

Mr. Roberts (Boeing Co.): The following paper (S-IC Reliability Program from Structural Life Viewpoint," Roy L. Rich and James A. Roberts, Shock and Vibration Bull. No. 36, Part 7) discusses the method used by the Boeing Co., New Orleans, to prove reliability of their hardware.

* * *

S-IC RELIABILITY PROGRAM FROM STRUCTURAL LIFE VIEWPOINT

Roy L. Rich and James A. Roberts
The Boeing Company
New Orleans, Louisiana

This paper defines critical hardware on the S-IC, the first stage of the Saturn V vehicle, and discusses the methods used to show reliability of this critical hardware, emphasizing the structural aspects of the program. Mechanical hardware, in which failures are chiefly attributable to fatigue, are proven reliable by a "safe-life" technique. This technique is developed using historical fatigue data established on airplanes. Components are proven capable of withstanding repeated life cycles of vehicle service environments by analysis and test. The vibration environments, hardware limitations, factors affecting the required life cycles, and test conditions are developed or defined. Reliability of electrical hardware is shown by comparing failure histories with maximum expected environments. Failures are caused by increasing, one at a time, the independent environments to which a component might be susceptible. Vibration environments, chief cause of S-IC problems, test conditions, and methods of establishing the reliability number are discussed.

J. A. Roberts

INTRODUCTION

The S-IC stage reliability test program is intended to provide assurance that the system reliability goal of 95 percent is met to the extent consistent with the program schedule, cost and state of the art. This program objective is accomplished by testing all critical hardware by the reliability program described in this paper. Reliability critical hardware is any vehicle hardware which causes the loss of stage or vehicle when a single failure occurs under vehicle life service environments. These environments produce structural loads on critical hardware causing metal fatigue, electrical discontinuities and relay and electrical contact chatter. The reliability critical hardware has been divided into the following two groups primarily because of physical and functional differences:

1. Propulsion/mechanical group which consists of gimballed ducting, pressure sensors, fluid level sensors and valves; and

2. Electrical/electronic group which consists of batteries and electrical power distributors containing timer cards, switches, relays, electrical contacts and/or associated electrical components.

The service environments are defined, with emphasis on the vibration environment and the test philosophy used for each group and the reasoning behind each test philosophy are discussed with emphasis on the structural aspect of the reliability program.

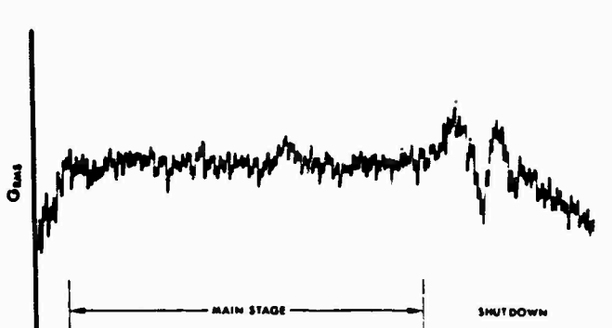

Fig. 1 - Time history

SERVICE ENVIRONMENTS

The first thing to be considered when developing a reliability program is the environment that the vehicle components must survive during their service life. On the S-IC, the environments producing structural stresses generally consist of vibration, fluid flow, pressure, and temperature. Vibration produces most of the structural loads causing metal fatigue, electrical discontinuities and relay and contact chatter. Although the test philosophies differ for each group of hardware, the derivation of environments are the same.

Flow rates, pressures, and temperature are generally steady state or slowly varying quantities and demonstrate little variance. They are generally known quantities, fairly easy to duplicate during test. The vibration environments are random in nature and are not well defined. A program was undertaken to define the vibration levels required.

VIBRATION ENVIRONMENT DEVELOPMENT

The vibration data are taken during captive firings of the S-IC stage and are modified as required to account for environments expected during flight. Accelerometers are installed on S-IC stage main structure at or near the attachment point of subsystems to be reliability tested. Figure 1 shows a typical plot of overall rms acceleration vs time. During the main stage, the g rms level remains approximately constant. However, a transient condition occurs when the engines are shut down. This sinusoidal transient is caused by an explosion of fuel and oxidizer which accumulates after engines are shut down.

The random vibration environment is developed to produce loads on reliability hardware which account for loads imposed on hardware during vehicle main stage vibration. Figure 2 shows typical measured data,

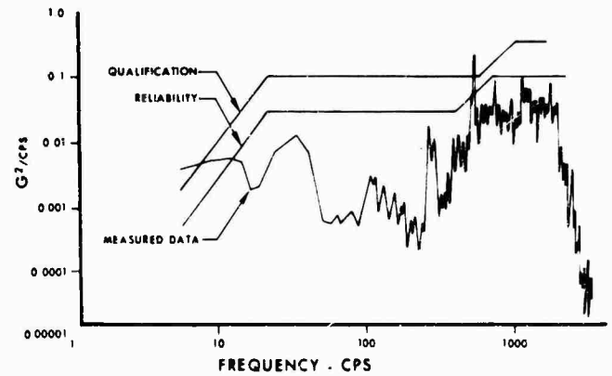

Fig. 2 - Main stage

established reliability environment and component qualification environment. The reliability test environment is derived by enveloping all applicable measured power spectrum data peaks. A superimposed sinusoidal dwell is used to envelope high sharp peaks which exceed by a large margin the other peaks in a general frequency range. The qualification test environment was established from scaled-up S-IC stage vibration data taken during captive firings and flight. In general, these predicted component qualification environments exceed the reliability test environment.

A sinusoidal sweep vibration test at 10 octaves/min from 5 to 2000 cps is performed to simulate shutdown transient loads on the reliability hardware. Figure 3 shows a typical sinusoidal sweep environment. The reliability environment is derived by enveloping all applicable measured peak data. The sinusoidal sweep test is only performed when shutdown transient levels exceed main stage levels.

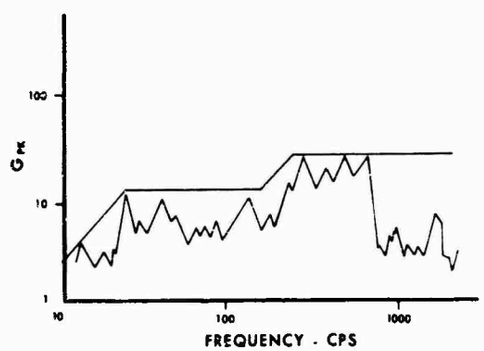

Fig. 3 - Shutdown transient

Once the environments are established, the methods of testing the hardware can be determined.

PROPULSION/MECHANICAL GROUP

The first group of critical hardware to be covered is the propulsion/mechanical hardware. There are eight critical propulsion/mechanical systems on the S-IC stage containing 85 critical components. Each component must be proven reliable by reliability testing or existing tests at a subsystem level or by similarity to a component which is reliability tested. Twelve components are proven reliable by similarity. A typical critical system (Fig. 4) is the fuel pressurization system. This system supplies and regulates helium gas flow, pressure and temperature as required to pressurize the fuel tank. A typical subsystem is the controller assembly (Fig. 5) which regulates the helium pressure and flow rate by opening orificed valves in a programmed sequence.

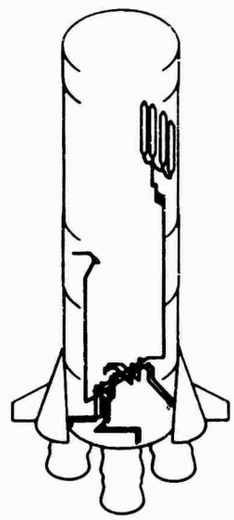

Fig. 4 - Typical propulsion/ mechanical hardware

The propulsion/mechanical subsystem test philosophy is to test three identical randomly selected production specimens for an extended number of life cycles at actual service life environments applied in sequence of occurrence during vehicle life. The extended number of life cycles is based on historical fatigue failure history.

The propulsion/mechanical hardware limitation of three specimens is due to high hardware and testing cost and the extended time required to set up and perform tests. All test environments are applied in sequence of occurrence and at levels expected during service life on the vehicle. All vibration, pressure, flow and temperatures are varied throughout the life cycle to be compatible with expected captive firing and flight profiles. Realistic stress distribution is obtained by applying proper service environments in the sequence of occurrence.

Vibration input is applied in only one axis at each input point which gives maximum stresses on hardware. This axis of vibration input is established from a mathematical model study.

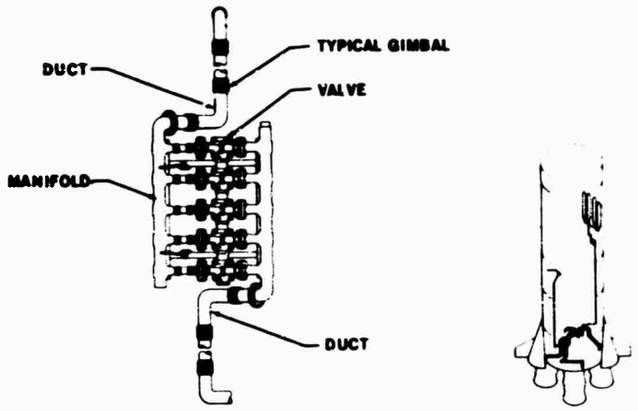

Fig. 5 - Typical propulsion/mechanical subsystem

The expected vehicle life is one life cycle and consists of one captive firing and one flight. This life cycle is repeated a number of times, depending on total variability and failure propagation factors. The number of times the life cycle is repeated is the product of the total variability factor, critical element factor, stress computation factor and the test severity factor.

The total variability factor (Fig. 6) is based on Ref. 1. The curve is established by testing a large number of test specimens to failure. The total variability factor is a ratio of test mean life to minimum life at first crack. The number of times a life cycle has to be repeated can be easily established once the number of test specimens is selected.

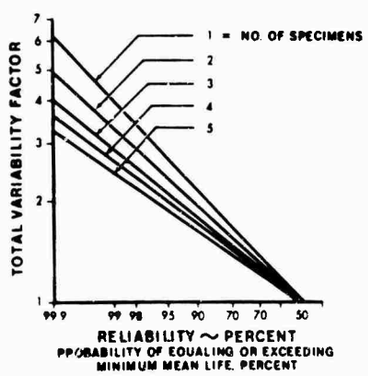

Fig. 6 - Total variability factor

The failure propagation factors also must be applied since vibration input is applied in one direction only at each input point. These factors are critical element factor, stress computation factor and test severity factor.

The critical element factor accounts for the possibility that some point on the structure may be more highly stressed than the critical point selected from mathematical model analysis. This factor varies between 1.0 and 2.0, depending on the complexity of the subsystem.

The stress computation factor accounts for the fact that only one axis of vibration input is applied to the specimen. Some fatigue loading on the critical element would be produced by inputs in the other two mutually perpendicular axes. This factor varies between 1.0 and 1.5, depending on the complexity of the subsystem.

The test severity factor is assumed to be 1.0 since conservative vehicle service environments are used as inputs and component installation and end conditions are duplicated closely.

A typical exercise performed on each subsystem to establish the reliability test is as follows:

1. The number of times the life cycle must be repeated is established from the total variability and failure propagation factors.

2. The existing test history from the component qualification test, captive firings of S-IC-T and single engine test firings is obtained. Only the total variability factor is used for this condition since all inputs are applied properly and the critical point is stressed properly. If properly tested (all environments imposed in proper sequence) and the test time

equals or exceeds reliability test requirements for the available number of specimens, the subsystem is considered reliable and no reliability testing is required.

3. All vibration, flow, temperature and pressure environments are established for the life cycle.

4. A mathematical model analysis of the critical subsystem, whether proven reliable or not by existing tests, is performed to establish loads. If stresses obtained from loads, increased by a stress-strain curve variation factor, are sufficiently low compared to the material endurance limit, the reliability test is not required. In general, the loads are high enough to require reliability testing. Also, the critical element and point of maximum stress are established along with the directions of vibration inputs at each input point which produces highest stresses on the critical element.

A reliability test must be run on all critical subsystems not proven reliable by other means. All tests are performed at subsystem level with all service environments imposed in sequence of occurrence. If a structural failure occurs, a failure analysis is performed followed by testing of additional specimens and/or redesign of the subsystem or component.

ELECTRICAL/ELECTRONIC GROUP

The second group of critical hardware to be covered is the electrical/electronic hardware. There are 32 critical electrical/electronic subsystems on the S-IC stage. Each subsystem must be proven reliable by reliability testing or existing tests at the subsystem level or by similarity to a subsystem which is reliability tested. Six subsystems are proven reliable by similarity. All critical electrical/electronic hardware is located on shock-mounted panels installed in the forward skirt and thrust structure regions of the S-IC stage (Fig. 7). The shock-mounted panels are designed to attenuate the high-frequency vibration environment which is damaging to vibration sensitive critical hardware. The critical electrical/electronic hardware consists of batteries and electrical power distributors which contain timer cards, switches, relays, electrical contacts and/or associated electrical components. The vibration environment causes relay chatter and electrical discontinuities which, when of sufficient duration, will cause loss of stage or vehicle.

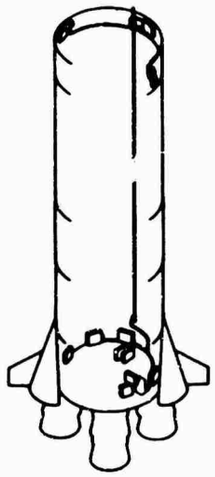

Fig. 7 - Typical electrical/electronic hardware

A typical electrical/electronic subsystem is a distributor (Fig. 8). All distributors are shock mounted to the shock-mounted panels to reduce further the high-frequency vibration. The function of these distributors is to sequence and time different vehicle operations, verify proper vehicle performance and shut down malfunctioning systems. The electrical/electronic reliability test philosophy is to increase service environments until a critical failure occurs and, based on this limited failure history, to perform a statistical reliability analysis.

The independent service environments which cause electrical characteristic failures are vibration, temperature and altitude. Any of these three service environments can be varied without affecting the other two environments. The electrical characteristics are always

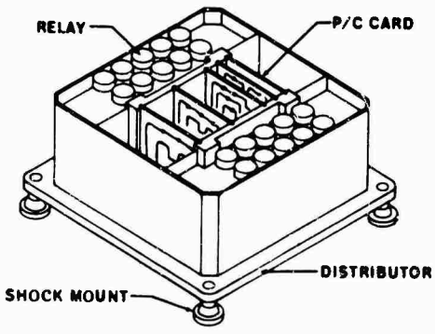

Fig. 8 - Typical electrical/electronic subsystem

monitored when hardware is subjected to any of the other service environments to determine when relay chatter or electrical discontinuity occurs.

During reliability testing, only environments which can cause critical failure of test hardware are imposed. In general, vibration loading is the major contributor to hardware critical failures. The vibration environment is applied for 5 min in the three mutually perpendicular axes on all tests since the maximum loading on each component within the critical subsystem cannot be obtained by vibrating in a single axis. Cross-axis loading is expected to be negligible during vibration. The vibration environment is increased in steps until hardware failure occurs or four times the overall rms acceleration is obtained.

A statistical approach is used to determine the subsystem reliability. A normal distribution is assumed about a mean stress produced by service environments (Fig. 9).

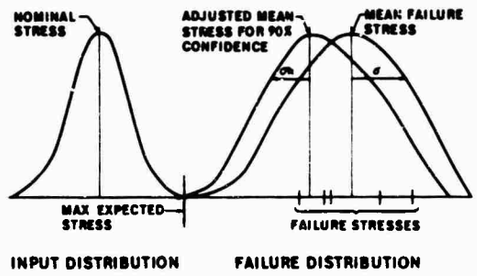

Fig. 9 - Reliability determination

A failure history is established as hardware fails when subjected to stepwise increases of the vibration input. The mean failure stress $\bar{X}$ is then established by the equation

$$\bar{X} = \frac{\sum_{n=1}^{N} X_n}{N} ,$$

where

X_n = stress at which nth specimen failed,

n = specimen number, and

N = total number of specimens tested.

The sigma value S is obtained using the equation

$$S = \sqrt{\frac{1}{N-1} \sum_{n=1}^{N} (\bar{X} - X_n)^2} .$$

By using this value of S, a normal distribution is then assumed about the mean failure stress. The failure history curve is adjusted as required to account for selected confidence level:

$$\bar{X}_R = \bar{X} - \frac{ts}{\sqrt{N}} .$$

where $\bar{X}_R$ is the adjusted mean failure stress, and t is the student distribution factor which is the probability of a mean failure stress falling outside of selected boundaries.

The adjusted sigma value (σ_R) is then calculated using the equation

$$\sigma_R = \frac{S\sqrt{N}}{\chi} ,$$

where χ is the chi factor which is based on a chi-squared distribution and is the probability of the sigma value falling outside of selected boundaries.

A safety margin K_S in standard deviations is now calculated using the equation

$$K_S = \frac{\bar{X}_R - M}{\sigma_R} ,$$

where M is the maximum stress expected during service life. This margin of safety can then be converted to a reliability value.

Any hardware which survives four times the overall rms acceleration has a reliability equal to or greater than the minimum required on S-IC subsystems.

SUMMARY

Three specimens of propulsion/mechanical hardware must survive a predetermined number of life cycles based on historical fatigue failures without failure. The service environments are identical for each life cycle.

The electrical/electronic hardware is tested using increasing environment levels until failure occurs. Based on this failure history, the reliability value at a predetermined confidence level is calculated.

REFERENCE

1. J. P. Butler, "Fatigue Scatter and a Statistical Approach to Fatigue Life Prediction," pp. 227-272, WADC TR 59-507, Aug. 1959

DISCUSSION

Mr. Jackman (General Dynamics/Pomona): What are you going to do about reliability between this stage of component testing and the time of takeoff with respect to vibration of the overall stacks which are 364 ft high and weigh 6.1 million pounds? I have heard that lateral but not longitudinal vibration testing is planned for the five major components. Therefore, the pogo effect and some of the other effects may not be checked out in the full-scale vehicle prior to flight.

Mr. Roberts: I cannot answer your question because we in New Orleans are basically associated with the S-IC. Our group in Huntsville is the Saturn V group.

Mr. Smith (Brown Engineering Co.): I work on the Saturn V at Huntsville. We do not plan right now to make a qualification test on the stacked vehicle. The vehicle testing will be basically a ground vibration test. There will be some evaluation of the pogo effect and of components, but it will not be a reliability or system reliability test.

Mr. Forkois (Naval Research Lab.): Was there actually a flow during the component vibration test, or was this done dry without the component function?

Mr. Roberts: On the subsystem shown there were five valves, the manifold and two ducts. There was flow through this unit while we imposed the expected vibration environment. Since it is located just aft of the LOX tank, a cryogenic condition was also imposed on the system. The valves had to operate in a programmed sequence to establish as realistic a condition as possible.

Mr. Roberts (Martin Co.): The use of only three specimens would ordinarily have been a deficiency in the paper. But then you correlated previous data to arrive at a total variability factor used to extend the number of cycles for testing. This is a very ingenious solution to the problem of trying to get a qualification and a stated level of reliability. If this would work for other systems, it would be a significant advance.

* * *

STRUCTURAL RELIABILITY

Panel Session

Moderator: William H. Roberts, The Martin Co., Orlando, Fla.

Panelists: Ralph E. Blake, Lockheed Aircraft Corp., Sunnyvale, Calif.
C. V. Stahle, Jr., The Martin Co., Baltimore, Md.
Innes Bouton, North American Aviation, Downey, Calif.
James A. Roberts, The Boeing Co., New Orleans, La.

The material on the following pages was presented during the panel session on structural reliability. All remarks have been edited for clarity, and some have been omitted, usually because they repeated points brought out earlier in the discussion. A summary statement prepared by the panel moderator follows the general discussion.

OPENING STATEMENTS

Mr. W. Roberts: One of the failings of the human experiment is to give ourselves more credit than we deserve. While there are obvious technical successes and a great deal of growth and development, the cost of our technical failures is greater than at any time in our history, many billions of dollars in a decade's time. These failures are related to just a few identifiable causes, all of which are more familiar to you and me than to anyone else. The annual maintenance cost very often exceeds the initial cost of the equipment. The equipment is often unavailable.

I would like to present a very definite challenge to the panel. The end product of all of our arbitrary processes is an attempt to build reliability by test. This will not work. When reliability requirements reach the very high levels they have, it is unreasonable to continue with this approach. Whether the systems used must have long or short lives, the number of costly specimens needed is too great. If you will accept my thesis that the present state of the art is intolerable, we can cast about for the reasons, which are not hard to find. First, we cannot design reliability into the system in advance and, second, we cannot design around fatigue. For many years there have been two types of discussions that have never supplied answers; one is about structural reliability and the other about fatigue. Fatigue is the most damaging failure mode in our technical history. It has been a first priority problem for more than twenty years. Through steady progress in electrical and electronic arts, most failures are now mechanical. With computerized circuit design, shortly 90 percent of the failures of electrical gear will be mechanical failures. So we must go back to fundamentals to develop an analytical capability in balance with our test capability. The proper tie between equipment reliability and structural reliability is that equipments are small structures. Equipments are an order of magnitude more failure prone than structures.

Mr. Bouton: My position on the question of structural reliability can be stated very quickly. I do not believe that the structural reliability of an aerospace vehicle can be calculated or otherwise determined accurately enough to serve as the basis for acceptance or rejection of a design of an individual structure. Therefore, a purely statistical structural reliability system is not a practical, workable, or administrable procedure for the design of structural systems. Neither is the present factor-of-safety structural design system completely satisfactory, although it has been very successful in the past. This success is based on a number of assumptions implicit in the procedures we use. Many of our structural systems are being designed for situations where the implicit assumptions of this present design system are no longer valid. The situation can be expected to get worse rather than better. I do believe that a modified version of the present system can be developed that will overcome the problems of the present system without introducing the

impracticalities of the purely statistical structural reliability system.

Let us examine what we want our structural design system to do. Professor Charles Stark Draper of MIT, in last year's 29th Wright Brothers Lecture, titled "The Role of Informetics in Modern Flight Systems" (AIAA Paper 66-131, 1966), noted that an operating system is an arrangement for the purposeful accomplishment of some desired result. Our structural design procedures are operating systems in themselves. While Draper was considering guidance and control system concepts that are probably well known to those in his field, I am not sure people concerned with structural reliability are familiar with what Draper said. I would suggest that any of you interested in the subject study his paper. Draper points out that the Wright brothers were successful because they performed all the necessary functions, even though many of these were done in their heads without an awareness of what they were actually doing. I believe that most structures people are doing the same thing. They are performing the functions which Draper has indicated are necessary because to do so is logical; they are not formalizing what they are doing.

Draper states that any function of an operating system falls into one of three categories. The first he calls informetics, information acquisition to generate instructions for realizing the desired results. In the structural design system these instructions are customer or contractor management decisions to do something. Draper's second category is called effectetics, the hardware and the software that constitute the operational system. The third category represents the control interface between the informetics and the effectetics. In the structural design system this is how management decisions are implemented by drawings, handbooks, verbal instructions, and so forth. Most of the areas of interest for our structural design and test problems fall in the informetics area. It has been an amazing revelation to examine our present and proposed procedures in this frame of reference. Informetics says very logically that decisions are made on the basis of our information about the "desired state" and the "actual state" of the structural system. In other words, decide what you want to do and how to measure whether or not you are really doing it. It is implied that the structural system state under consideration must be numerically definable.

How do the present system and a structural reliability system appear from the informetics point of view? First, consider the desired state system. In our present factor-of-safety structural design system there is a desire that the structure should have something that is vaguely characterized as structural integrity. Presumably this means zero or a very low failure rate, but the function is never quantified so there is no way to tell whether we have attained it or not. From this desire for structural integrity, we proceed to the structural design criteria and the shock and vibration design and test requirements. These are quantitative, and there are means for proving compliance. However, the requirements that represent the desired state do not have a direct link to our desire for a low failure rate. In fact, meeting the requirements does not guarantee that we will have a satisfactory structural system. Since requirements have evolved for the most part from experience, the new design will be satisfactory if it is comparable to previous designs. There is a slow evolution in the state of the art.

In the present system, a structure must show a positive margin of safety for ultimate loads, obtained by multiplying the loads at a designated limit condition by a factor of safety. For most shock and vibration situations, the desired state is simply survival at a designated test life. In the structural reliability design system, the problem definitely does not reside in the desired state. We simply say that we want a structural reliability corresponding to some number, such as 0.9999, and the job is done. Sometimes it is expanded slightly by assigning reliability requirements to the structural components. The procedure easily meets the requirements for a desired state information system.

Now let us examine the actual state information system to see what procedures are used. The factor-of-safety system is highly capable of measuring the actual state. The structural reliability system does not have the same capability. In the factor-of-safety system, a loads analysis and a strength analysis are performed. If the margin of safety is negative, the design is changed until the margin of safety has the desired positive value. In fatigue situations, the structural life is usually the parameter being compared. In the context of this discussion, the analysis is just as much a measure of the determination of the actual state as is a test. Unfortunately, experience has shown that the analytical determination is not consistently accurate enough to give a true measure. It can be considered only as an approximation. Jablecki, formerly head of the Static Test Laboratory at Wright Field, documented the fact that one out of every ten airplane wings failed at 2/3rd of its design value on the first

static test. One in 100 failed at 1/3rd of its design value. This must be considered a measure of the analytical inaccuracies in structural designs. Lest anyone say, "We don't make them kind of mistakes no more," I hasten to add that the record in recent years in high performance aircraft, space vehicles and launch vehicles is not much better. Thus, the analysis cannot serve as the final measure of the actual state. Instead, the structure is tested and qualified. One test proves almost nothing about structural reliability. Its basic function is to disclose errors in the analysis. Its ability to do so varies for different types of tests and structures, so the measure of the true state of the system is still somewhat in doubt after the test is completed. Further improvement is made by conducting operational tests to eliminate errors in the calculation of the loads and to define the actual environment better. All this is still done by the present factor-of-safety system. Finally, failures during actual operation disclose information on the actual state of the structure, that is, that the margin of safety was less than zero. When this information is fed back to management, a decision is made either to change the structure or the operation or to accept an occasional failure as being consistent with the vehicle mission.

In the structural reliability design system, this actual state information system bogs down. Structural reliability cannot be calculated accurately enough to serve as the sole measure of the actual state. All of the problems of making accurate analyses of the loads and strengths still exist, together with the added burden of determining the statistical functions. I suspect that the proponents of a purely statistical structural reliability design procedure are guilty of the mistake characterized by Catino at the last Reliability and Maintainability Conference, when he said, "In the eyes of the analyst, to predict means to determine." The test in this structural reliability system does not directly measure the actual state by determining the structural reliability function. As Gross said in the previous year's Reliability and Maintainability Conference, "Funding of test programs to prove reliability numbers like five nines would bankrupt the nation." It is more likely that excellent judgment, rather than unconcern, prevents such funding. Therefore, the analysis of structural reliability is not subject to the discipline of having to prove the accuracy of the prediction. If the actual state of structural reliability cannot be measured accurately, it is difficult to see how it can be expressed as a contract requirement.

I think that if we try to determine whether a proposed procedure can define the desired state of the structural system and then provide accurate information on the actual state, we will be less likely to advocate an impractical or useless structural design system.

Mr. Stahle: I would like to look at some of the basic characteristics of structural reliability analysis methods and try to apply these to equipment testing and reliability. In my paper I discussed the concept of a stress-strength reliability analysis. Some of the things evident in performing a stress-strength type of analysis are the following: the mean or expected load, the mean or expected strength, the variation in the load, and the variation in the strength.

Have these four facets of reliability analysis been considered in equipment design? With regard to load, some work has been done with vibration environments from a statistical standpoint, particularly with regard to captive firings and in-flight measurements of the vibration environment within launch vehicles. So we have a start toward defining both an expected or mean value of the vibration stress and a variation in this stress. On the other hand, the statistical distribution of equipment strength is an area that has only been explored to a very limited extent through fragility testing. The vibration level and duration of the exposure have been varied to determine margins for some launch vehicle programs. The method of qualification testing generally used requires that a design pass a set of test requirements. Generally, the qualification requirements do not give any data as to the failure distribution or how much margin there is, but only whether or not the equipment passes the test. This precludes the possibility of obtaining data describing the statistical distribution of equipment vibration strength. So in this area of vibration testing of equipment, much could be provided that is not available now to evaluate rellability. Testing to determine failure modes of equipments would provide the basis for more accurate, quantitative evaluation of the reliability of equipments in systems.

Another consideration evident from the review of structural reliability analysis is the ability to account for the variations in both the equipment strength and vibration stress in determining test requirements for equipments. The variation in the vibration strength of equipments does not seem to be considered. Reliability analysis requires that both the variation in the stress and the strength be considered,

but I do not believe that anybody has explored the variation in equipment strength to the extent necessary for generating a set of vibration test requirements. We have developed and are using a procedure which provides some degree of reliability. However, the question of whether or not this is the correct procedure remains unanswered.

In summary, there are two things that I think would be of utmost concern to those in the reliability area and which can place some of our qualification test programs and the determination of qualification test requirements on a more rational basis. First, in future programs, vibration tests of equipments to failure should be performed to explore the failure distribution, particularly in level but also in time. And second, this information on the variation and the distribution of the strength of the equipments should be used to arrive at a better definition of test requirements.

Mr. J. Roberts: On our Saturn program, a 95 percent stage reliability or system reliability could only be achieved on a strictly statistical basis if each critical component had a reliability of 0.999 999 5. It would take a million specimens with only one or two failures to establish this. When we selected three specimens, we were thinking about the state of the art and the cost of gaining any confidence, or an engineering judgment that this hardware would survive one life cycle. The cost of testing three specimens is of the order of three quarters of a million dollars which is enough to eliminate testing any more specimens. I would like to talk about the method described in our paper of establishing a reliability number using engineering judgment.

First, a more thorough comparative analysis of tests is needed. At Boeing New Orleans, computer programs are established, and we have found that for the particular systems analyzed we had good agreement between our analyses and the qualification tests. At the design stage on this hardware, however, this comparison cannot be made, so it is necessary to verify that the mathematical analysis models do agree well with test results. Furthermore, there is duplication in all the fields. If each company would avoid repeating what the other company is doing, money would be saved. In addition, better laboratory capability is needed. For example, on one of our system or subsystem tests seven shakers had to be used simultaneously, applying random excitation in an uncorrelated manner. This equipment is very expensive.

A better definition of the environments is needed. If there have been some captive firings, it is best to place accelerometers so that the actual environments are measured. However, this is not possible in the early stages of a program. We found that in nearly all cases, except for a few discrete frequencies, the environment established by the conservative method of enveloping all peaks was, in general, much lower than the qualification test levels. More data are needed to establish vibration levels more exactly.

To use our approach on the propulsion mechanical systems, a better knowledge of the material fatigue data is needed. This is found in the S-N curves, but we have found a tremendous scatter between two like specimens. This should be investigated more fully. We found that in measuring loads to the endurance limit of the material, we could not prove most of them reliable because of the large scatter in the material properties. We always had to assume that the load developed was a worse load, and was developed at some indeterminable number of cycles. Our problem with the random input was to establish how many effective cycles we had. This large spread kept us from eliminating a lot of the tests.

Finally, the number of conservatisms imposed on this hardware to prove it reliable should be reduced.

Mr. Blake: I think each of us on the panel has probably gotten interested in reliability from a different point of view or a different set of problems. The type of problem with which I might be faced is not concerned so much with what the contract says, what the requirements are, or how a management system is set up, but simply, given a particular design, what is the probability that that design will be successful in service? I think the essential element of this approach to reliability is basically that we are attempting to face the fact that environments and strengths are, in fact, statistical variables. Factors of safety in qualification test specifications also recognize this fact. These factors try to control reliability, but the control is subject to considerable error. It is easy to show that two designs may have the same margin of safety but considerably different reliabilities, and vice versa. So we are really talking about controlling a quality of the design, that is, reliability, which is of primary importance, and we are hoping to do it by more direct means than factors of safety and qualification tests. The changes which we hope to

bring about certainly will not, and should not come overnight. We should evolve gradually toward more rational and less arbitrary practices. This does not mean that we should turn our present system upside down and embark on something brand new and untried tomorrow. Conversely, the fact that we are not prepared to propose a complete change overnight does not mean that we should not make every effort to bring about these changes now. We should not sit on our hands and wait for all the obstacles to be removed. Much of the criticism which I have heard of the reliability approach involves such things as: you do not have enough data to make a reliability prediction; or, you do not know that the distribution is normal so how can you say what the reliability is? This is all true. But the person who is advocating some alternative approach also does not have these data. In the face of this ignorance, the problem is to determine which approach will give us a better chance at success. We should not judge a reliability approach or suggested method on the basis of what would be perfect. We have to judge it on the basis of whether or not it would be an improvement over what we are doing now.

Vibration testing is one area in which I have found a use for reliability prediction. That is, the system worked very nicely as long as no failures occurred, but as soon as a vibration test produces a failure, especially a failure which results in a lot of trouble to the project, there is liable to be a little meeting at which you are led to understand that they know that your test was overconservative and that was fine as long as you were not causing any trouble. But now let's look at the test realistically and decide whether or not we have to make a design change or whether this test failure is actually due to overconservatism in the margin of safety or in the test. When this happens, it is useful to reassess what is known about the design, its load and its strength to make a clear statement of the chance that this design will succeed in service.

An example is an assessment we made of the prospects of success of a large structure, a cylindrical structure in a space vehicle (Fig. 1). We had about 90 flight measurements, so we had a relatively accurate determination of the mean load and the variation of loads. The tolerances on those determinations are indicated by the black bars. As far as the strength is concerned, there had been one full-scale test of this structure to failure, and it was an expensive test. We had, therefore, one test result, one strength which we used as the mean strength. Now with one data point, a conventional statistician is rather helpless. We attempted to use a modern development of statistics called Bayesian statistics in which one blends together the direct data with information based on his past experience. In this case failure was due to buckling of a cylinder, and we had some information concerning the statistical variation of buckling strengths of cylinders. Therefore, we were able to put a tolerance on the mean strength and the standard deviation of the strength. This information obviously did not enable us to state a reliability number. We were able only to prepare a table, such as that on the upper right-hand side of Fig. 1, in which we stated a Bayesian confidence of 99 percent that the reliability exceeded 78 percent, ranging down to a 50 percent confidence that reliability exceeded 99.996 percent.

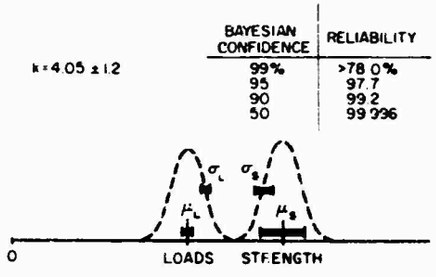

Fig. 1 - Probable errors in loads and strength of launch vehicle adapter

This is not intended to be a satisfactory answer to the question of what is this reliability; it is intended to be a summary of the state of our knowledge concerning the risk of failure. If our current knowledge is found to be unsatisfactory, it can be improved by further testing. In contemplating the different confidence levels, the question arises that these numbers are very interesting, but what do they mean? How do I decide whether these combinations are satisfactory? This is not a problem for vibration test engineers, but it certainly is a problem which we face in presenting these data. If the people to whom we present the data are unable to use them, the whole exercise is wasted.

Systems analysis provides a rational way of deciding for a given vehicle what the relative importance of weight, cost, reliability, and confidence may be. How much should we pay to increase confidence? The basic notion of tradeoff between reliability and weight is illustrated in Fig. 2, in which the possible effects are considered of increasing the size of a structure, which essentially means increasing the

weight. We should be able to use the proposed increase in structure weight to increase the reliability so that it approaches 1 asymptotically. However, the increase in weight means the payload must be decreased, thereby decreasing the effectiveness of the system. A rather plausible model for relating reliability and effectiveness is to assume that the effectiveness of the system is the product of the two dotted lines in Fig. 2, so the overall effectiveness of the system rises to a peak and drops off. Therefore, the ideal reliability for this structure is that corresponding to the size at the peak of effectiveness. This indicates that it is not necessarily a good policy to decide that all parts should have the same reliability goal. The optimum reliability for a structure depends on how fast the effectiveness decreases with weight. If the structure can have a considerable increase in strength for a very small increase in weight, the reliability goal can and should be higher than if the structure requires a large increase in weight for a small increase in reliability.

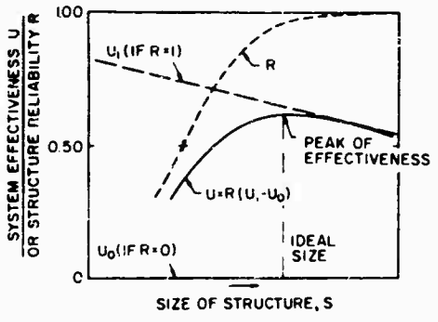

Fig. 2 - Criterion for ideal size of structure

GENERAL DISCUSSION

Mr. W. Roberts: I believe that Mr. Bouton is stating that it is a literal impossibility to develop this field of structural reliability. He has been the primary architect for many years working with probabilistic concepts. I think what we are searching for is a better system than the one we have, but that it need not be perfect. He expresses a fear, which is very common among the companies, that a reliability requirement will be forced on them. The questions here before the house are mainly ones of possibly directing our attention to the reliability of equipments, and particularly the mechanical failure modes of equipment. I wonder if Mr. Bouton sees any way in which this job may be accomplished, even if he sees no particular way in which he cares to recommend it for structural reliability at the present time.

Mr. Bouton: I think you overstated my case. There still is a future for structural reliability, but we must understand what we are dealing with. One of the points I tried to make was that since we do make errors in our calculations, our analytically determined structural reliability is questionable. We do not do enough testing, so we cannot determine structural reliability that way. However, one of the approaches that I am presently advocating and trying to develop is that we derive a statistically based deterministic system. In other words, we should establish deterministic conditions based on predicted statistics and then assign responsibility and develop procedures to see that these statistics come true. As an example, if someone had calculated the structural reliability of the DeHaviland Comet a few years ago, the day before it crashed, he would probably have calculated 0.999 999 reliability. The day after it crashed, he could have said it was just a random, one in a million, occurrence that wouldn't happen again. After the second one, it is difficult to accept this as a random failure. Now it becomes one in a trillion chance that these two occurrences are random, but the calculation hasn't changed a bit. So what did the calculation mean? The same thing could be applied to something like the Lockheed Electra. The day before and the day after a crash, things look very different in a structural reliability calculation.

A more pertinent example, I think, is a booster which has been in production. Each of the 150 built was proof tested before it left the factory. None had failed, and the shop was getting rather restive under this proof-test requirement. The engineering department was considering dropping the requirement for proof testing. With 20-20 hindsight, the engineering department now says that they would never have approved dropping the test, because before their decision was made, the 151st was tested, and it blew up. They considered that just a random occurrence and continued. The 152nd was tested and blew up, the 153rd also blew up, and by that time they thought they had a problem. It was found that somebody had changed a welding procedure in a way that shouldn't make any difference. It should have been just as good as the previous procedure, but it wasn't. What did the reliability calculation on that particular booster mean before and after this failure?

I think that almost all the failures we have, be they in gargantuan space launch vehicles,

Piper Cubs, or black boxes, are the result of errors of one kind or another. I think much of our attention should be directed toward finding methods to ferret out these errors. How do we discover the errors in a random world, in particular when one is apt to receive a strong structure for testing, and then pass a weak or a bad one. How do you handle this problem in a structural reliability world?

Mr. Blake: I think perhaps you are defining the structural reliability world as one which has no counterpart for the factor of ignorance which is talked about in connection with a factor of safety. Questions which one must ask oneself include: What is the probability that the analysis has omitted a critical factor? What is the chance that my qualification test has failed to include some important characteristic? What is the probability that the specimens I have tested happen to have been made very nicely, but the 50th or the 100th specimen might have a defect in manufacture which won't be caught by an inspector? I would like to imagine the reliability approach as including the question: what confidence do I have in my test, my calculations and my predictions?

Mr. Bouton: On this question of the factor of ignorance, a lot of people say that is the purpose of a factor of safety. I question that because when we disclose our ignorance by a test, we don't say the factor of safety covered that ignorance; we change the factor so that we get rid of our ignorance. Tests should be disclosing these errors. One has to establish an expected condition and develop steps which include statistical considerations that will, as far as possible, prevent failure at that condition. Next, one should establish who is responsible for failure if it should occur at that level, that is, establish the area of responsibility of the structural engineer and then establish an extreme environment, or ultimate condition in aircraft terminology. The vehicle should never be exposed to this extreme condition; if it is, the user is responsible and we should expect the structure to fail. These are two separate and distinct areas that we can predict by statistical methods, but we can only achieve reliability by making sure that the responsibility for preventing these occurrences is accepted by an individual or an organization.

Mr. Stahle: I agree with Mr. Blake on the need to quantify reliability. I have seen many cases where you are confronted with the basic question of changing specifications, thereby taking a calculated risk. If you cannot, or if you are not willing to quantify what this risk is, you are not performing your function to management so that they can elect to take or not to take the risk.

Mr. Fine (Litton Systems): I would like to disagree with Mr. Blake. The reliability prediction is just a statement of a number, of a condition; it is not a guarantee that the object will be built that way. Prediction is valid; it states merely that if you have a dispersion, a spread, or a variance, and you say that the load or the strength-to-load ratio is a certain value, then you assume and predict a certain number of sigmas. The carrying out of the prediction is left to someone else. So we are mixing two different things. If someone left a rivet out, is that the fault of the prediction?

Mr. Blake: Leaving the rivet out is probably an extreme example. One which is more within limits might be concerned with buckling strength of shells. These buckling strengths seem to be determined by the degree of waviness of the shell which in regular manufacturing practice cannot be eliminated. One cannot specify to an inspector how much is all right. The structural man must not take the position that he approved this on the condition that the waviness was not too bad and now he has been given a lot of hardware in which the waviness is too bad, so that is not his fault but someone else's. One can't pass the buck to somebody else if that somebody else is not in a position to inspect adequately.

Mr. Bouton: Does this mean that if you calculate 0.999 999 reliability and every one in service fails, this is 0.999 999 reliability because somebody else did it?

Mr. Fine: No, if the initial assumptions were correct, it should be achieved. You do not have to run a million tests to do this. In other words, if a wide enough spread is chosen between the medians and if a test is conducted which indicates that there is about a 2- or 3-σ deviation and a 10-σ deviation is used in the design, then, as far as you are concerned, the requirement is satisfied.

Mr. Bouton: What you are specifying, then, is a conditional reliability, rather than the true reliability of the structure. We should define each of these conditions. There is an Air Force requirement that inspection doors be designed so that any one rivet around the corners could be left out. Previously you could design it so that one was in. I think this is a very homely example of what the problem is. You could say we will make the structure good enough when the rivet is out. There are many reasons other than carelessness why these

fasteners keep coming loose, and it has to be tolerated. That is one requirement for the structure. On the other hand, you can say the structure does not have to tolerate this. We will make the line crew see that the rivets are properly put in, and we'll send somebody with an ultrasonic vibrator to make sure that they are tightly fastened. You can do either, but what does structural reliability mean in a situation like that; which one is right?

Mr. Fine: Since I took a rivet out, I would like to add something back. On the Lockheed X-17 program, there is a parachute which comes out of a door at the aft end of the craft. The technician was having trouble closing this door, so he added a piece of tape. Consequently, the parachute never came out, and the test failed.

Mr. Getline (General Dynamics/Convair): Aren't we confusing the ability to design a reliable structure with the ability to place a number on it? There are commercial aircraft that have been flying for 20 or 30 years, with 10's of thousands of hours on them, and people will still get in them. They are not afraid of the reliability of these aircraft. With regard to Mr. Bouton's remark about structures failing in static test at 2/3rd the design load, I might point out that it is the policy in some areas to design the structure to something less than the design load and stretch it, so the result is the most efficient structure possible with minimum weight.

Mr. Bouton: I am very much aware of the stretch testing philosophy. I haven't heard of anybody deliberately putting in a 2/3rd or a 1/3rd factor. However, I witnessed one case in which there was a decimal point error, and the structure failed at 10 percent. I think this is the purpose of testing, to disclose these errors and get rid of them. The result is increased reliability, though how much it increases is a moot question.

Mr. Getline: Eighty percent.

Mr. Bouton: I have also heard that one aerospace company following this policy thought that their designers were conservative so they went to 15 percent. They were very startled when they found that the structures were all failing at 15 percent under the point at which they were supposed to fail.

Mr. W. Roberts: Can the audience offer more information on the capability being developed in dynamic reliability of equipment? So far it is a stated position on the board that this is the problem.

Mr. Fine: There is a dearth of information, and I think this is one of the basic problems. Martin had to run their own tests on weldments because information on this distribution was not available in the literature. I don't know what has been done to accumulate these data, but I know each company had been accumulating data in-house. Gathering these data together somewhere and publicizing them would help to solve a lot of the problems we are facing.

Mr. Jackman (General Dynamics/Pomona): I would like to make a point about the practice of building factor on factor. I tried for a long time to get a tolerance matrix or funnel built into aircraft instruments, in the testing of aircraft instruments such as rate and body gyros and flight accelerometers, flight instruments of the inertial guidance type. It is amazing, when you go from designers to dynamicists and others, how you are building factor on factor. It is almost impossible to come down to a tolerance that the instrument manufacturer can live with and meet at low cost with sufficient production and on schedule. Do you think that there is anything that can be done to prevent us from building factor on factor in instrument metrology? The gyro manufacturers are the first people to say, "If we could only get a practical tolerance on this thing, regardless of what the environment might be." For example, during linear vibration of gyros, high cross-axis vibration is very critical. All sorts of values are found, and the dynamicist will certainly add 100 percent here and the structural man 100 percent there for certainty, and the poor old gyro just doesn't exist that will do that job.

Mr. W. Roberts: Gyros are one of the approximately 12 types of electrical equipments which fail at the rate of about 7 percent during their design life. The most unreliable piece of field equipment is a motor; this has a failure rate of about 20 percent.

Mr. Bouton: I think you would be quite surprised at what you could do with the informetics approach about the problem of building factor on factor. If you actually make a functional diagram of what you are trying to do with your factors and other things, you may find that a single factor will cover two or three different things. It will depend on how much margin you need for overloading and how much for under strength. Incidentally, we are beginning to report on the work we are doing on this for the Air Force. Nothing is published yet, but I could

arrange for distribution to a few individuals if you would contact me.

Mr. W. Roberts: Mr. Bouton, your presentation indicated that it would be possible to expand the existing system to do the job that we are hoping to do with the reliability approach. Would you define the improvements that you would make in the existing system?

Mr. Bouton: I have already described the development of a statistically based deterministic system and the assignment of responsibility to the control system people to see that we never exceed the ultimate condition. In other words, we would separate our environmental statistics from the strength statistics. I think the fallacy in some of the present structural reliability calculations is that no responsibility is assigned and, therefore, you cannot decide what to do to correct a failure when it does occur. I hope I make my point clear, that you can determine a limit condition of 0.99. One out of 100 structures would get to that environmental level, and then only one out of 10,000 would get to the extreme environment, so we set these up as separate from the strength. Now, we are approaching the fatigue problem by testing to the life cycle that is two or four times the nominal life. We don't know that this is achieving what we want. We should have more information on where the item will actually fail, that is, the nominal life. Testing to an extreme life may eliminate all of the ones that would be weaker than a certain value at the nominal life. We know next to nothing about how the strength of the system varies in a fatigue situation at the nominal life with respect to what it was at some extreme life.

Mr. W Roberts: In Harris' new book on structural fatigue, this arbitrary factor of 4 on life is being used as 10, 12 and 15 by the British to reach what they consider a safe position. This further illustrates the hidden factors in the fatigue problem for which satisfactory research has not provided us a suitable answer. The type of contract containing a clause with penalties for failure to meet the reliability goal seems to me to give a tremendous incentive to solve this problem. Often reliability goals are being defined which are more or less out of your control. The system simply requires it, and you do not have a capability at present to meet it or to satisfy your own desires to attain even the reliability that you need. Mr. Blake's comment seems to be that whether or not you are using your reliability techniques, you are making reliability estimates. Basically what you are doing by the factor-of-safety technique, or some personal modification of it, is making reliability estimates.

Mr. Forkois (Naval Research Laboratory): I think the problem here is that you cannot quantify the reliability number. For example, years ago a certain brand of coffee came in a tall can. By using differential calculus, minimizing the area involved to the volume, the producers came out with a smaller can that used less material. Now this is not facetious. This can is more economical and more reliable, especially if it were a pressure vessel, because the span is not as great and it would not blow up as easily. But how would you quantify the reliability? Another factor to consider is structural design vs weight. If the stress is high, as it is in a large structure, and the frequency of the structure is low, for example, 2 cps, you will have a lot of trouble with it. You will have more reliability in the small item, but I don't know how anyone can put it in numbers. I think we are up against something that is impossible to do.

Mr. Blake: I am not interested in quantifying reliability per se. I am interested in whether or not we are going to accept or change the design. If we simply admire the number, we haven't done anything to the coffee can or the vehicle. A reliability number is, in my mind, something to compare with the number associated with a different design to decide if a design change is an improvement worth the cost.

I agree fully with Aleck Fine when he advocates gathering data on the scatter of strength, and the statistical distribution of environments. By ignoring statistical distributions in the factors of safety, we have actually thrown away these data. I think it would be a positive improvement if we now actively gathered and assembled these data.

Mr. W. Roberts: I'm not sure Mr. Blake's first point was completely developed. I think he was pointing out that the reliability numbers could easily be looked at as relative numbers. We can do what we wish to the weak sisters of these numbers and whether a total system is absolutely correct or not, one thing has been accomplished — the design has been balanced. The reliability variations are not going to compare by 10 or 20 percent, but by factors of 3, 7, or 10, so what needs to be done to improve the system will be quite clear.

Mr. Stahle: I imagine Mr. Forkois is having considerable difficulty understanding the purpose of my paper, that is, to estimate the

effect on the vibration reliability while performing the spacecraft test. The obvious step after quantifying reliability with and without the additional test which burns up the spacecraft is to determine if it pays to conduct this test. This is one of the places where you are definitely in the corner. You may object to performing the test, but you are making a decision whether or not to make design improvements by doing so. Whether or not it is going to be worthwhile can be determined from the change in the reliability.

Mr. Forkois: The Navy has a vessel called the Enterprise; it is over 1100 feet long and weighs 70 or 80 thousand tons. We only make one of them.

Mr. W. Roberts: Is there an advantage in using reliability numbers derived from tests on present systems for later systems?

Mr. Getline: Mr. Bouton remarked earlier on the reliability of the Comet and the Electra before and after their respective accidents, saying that, assuming a number can be put on reliability, it can only be done on the basis of known loads. In those two instances, the loads were entirely unforeseen, so what price reliability?

Mr. Bouton: I would like to correct that. The Comet loads were, for all intents and purposes, exactly as predicted. It didn't fail when it was doing anything unusual. The strength was wrong.

Mr. Getline: The Comet underwent sonic fatigue failure primarily. It started around the windows, and these loads were never considered at all in the design. In fact, this was the first major incident of the type. On the Electra, the whirl mode was not even investigated until afterward.

Mr. Bouton: I'll modify my statement then. The aircraft failed in gusts which produced loads of about 1-1/2 or 2g. The sonic environment did not cause failure; it caused the deterioration in strength.

Mr. W. Roberts: Dr. Morrow, are you opposed to making reliability estimates on equipment?

Dr. Morrow (Aerospace Corp.): No. I worry a bit about this because from time to time I have observed a tendency to figure reliabilities from laboratory tests and to assume too glibly that this is field reliability. Laboratory conditions do not duplicate what happens in practice.

Mr. W. Roberts: Isn't this another example of using reliability numbers as relative numbers? Doesn't this avoid the error associated with using them as absolute numbers?

Dr. Morrow: I think it avoids most of the error, and this is a very good caution to keep in mind.

Mr. Bouton: Some studies we made show that . environment is chosen that gives the ultimat oad of one occurrence in 10,000 vehicles and if the mean strength of the structure is where it is supposed to be, the result would be greater than 0.9999 reliability. But if the incidence of failure as illustrated by the Jablecki data is added, reliability goes down to about 0.9. If the reliability is assumed to be ten times better than the whole industry produces, as exemplified by the Jablecki data, it is still only about 0.95. But if a single test is made of a structure whose coefficient of variation is 5 percent, then reliability increases to more than 0.9999 again. There may be a spread depending on the assumptions made and the accuracy from the start, but it is a minor difference, in the 5 to 10 percent range. If the same test is made with a structure whose scatter is 20 percent, as it is with high temperature and brittle materials, the power of disclosure decreases; the reliability increment is only between about 0.9 and 0.99 or 0.995. So apparently when you think you are doing the same thing, you are not. You are getting a different reliability by orders of magnitude.

Mr. W. Roberts: We have also found that reliability is associated with error somewhere in design, manufacturing, or process control. Possibly these are separate problems. There is a point at which they must meet, but we certainly do agree that there is a reliability problem associated with error as well as one associated with the design and manufacture.

Mr. Forkois: Can we get back to the Comet a minute? I think the Comet was a well designed plane, but there were two errors. The failure was the same as occurred in the Liberty ships during World War I. The reinforcement around the window was welded and a brittle material was used. There was crack propagation, a weak point, and the plane blew up. To prevent this the reinforcement should have been riveted as was finally done in the Liberty ships. The rivet acts as a crack arrester, preventing crack propagation. But these are factors which I can't quantify except to say that it is good design and the probability of a failure is remote.

Mr. Bouton: If the kind of a test had been made that in our greater knowledge we now

make of this type of aircraft, I think the crack would have been discovered and eliminated. As it was, the disclosure of the error was by the actual failure. I think what you are saying in a way is really just confirming what I am saying. Nobody miscalculated the environment. The cabin pressure, the ground-air-ground cycle, and so on, presumably were right. There was nothing unusual when the aircraft failed. The gust load encountered at the time of the failure was not unusual. As soon as the structure was replaced with one that could tolerate this environment, there was no further problem.

Mr. W. Roberts: It is a classical case of structural instability due to critical crack length. It also has another feature, that of stress concentration factor built on stress concentration factor around the window. But let's leave the Comet and go on to the dynamic reliabilities of equipment. What we are really discussing are the built-in errors in design or in other portions of the process of manufacturing and quality control. Perhaps we think these errors will be eliminated by the structural reliability approach. Of course, they won't. These are problems that have to be dealt with separately.

Mr. Jackman: I would like to return to my example of a gyro. You spoke about 7 percent rejections where the gyro actually fails to work. I'm talking about building in tolerances, which is a much broader thing. With a missile, the designers state that there must be a certain tolerance for a certain environment, so that that missile will hit its target. Later those tolerances probably could be loosened by 100 percent, and the missile would still hit the target. But we do not want to take chances. We want to keep the tight tolerances, and be safe. But how safe do we have to be? We may be 100 or 200 percent safe, the instrument manufacturers are finding it very hard to meet those tolerances. So don't just throw out the instrument because it doesn't work. Maybe you're trying to make it work under abnormal conditions.

Mr. Blake: It seems that you are objecting to the piling of conservatism on top of conservatism. Eliminating this may be one of the benefits of a statistical reliability attitude, though not necessarily in the situation you are talking about. I have in mind the common practice of multiplying factors of safety together. There is a factor of safety for one purpose and one for another. These are then multiplied together. This is not reasonable. If the reason for using the first factor is statistically independent from that for the second factor, you should take the difference between the factor and 1 and then take the square root of the sum of the squares of those quantities to get an appropriate factor for the combination of the two effects.

Mr. Bouton: Mr. Jackman's comment suggested something to me. In structural design criteria and specifications of various kinds, there is a tremendous built-in inertia. They are changed in reaction to something going wrong. Then maybe two or three years later, the requirement becomes obsolete. But to get something removed from the specification is nearly impossible. Nobody wants to be a hero, because it might happen that as soon as the specification is changed, there might be a failure, maybe even not as a result of the change. This problem might be overcome if we start developing a system that treats the desired state more rationally, that really approaches what we want to accomplish with our structural system.

Mr. Blake: A horrible example of this inertia is the prevalence of the 90, 95 or 99 percent confidence level. These confidence levels are used almost automatically in old statistics books. At the time these books were written, the confidence levels were applied to the testing of medical treatments and the improvement of the corn crop; these same numbers have been carried right up to missiles and spacecraft simply because they are traditional. There needs to be some thought as to what the number really should be. What is a rational number in view of the problem?

Mr. Bouton: This is again the problem that we don't always know what we want our systems to do. How do you decide whether you would rather ride in an airplane with a 99.996 percent structural reliability and a 50 percent confidence or one with a 78 percent structural reliability and a 99 percent confidence?

Mr. W. Roberts: I wish to take the other side for the moment and be critical of the approach under examination. I question, first, the normal distributions, second, the assumption that a structure fails because of an overlap in the extreme values of load and strength, and third, the idea that since fatigue is a principal failure mode and linear accumulative damage is a very poor description of what is going on in fatigue and since I need an estimate of the failure rate in the fatigue problem, I probably cannot make an estimate of reliabilities in equipments or structures until I have a significantly better understanding of the fatigue problem. I think answers to these questions should be found, although the questions will not really interfere with our progress in trying to make these estimates.

Mr. Blake: Would you take them one by one?

Mr. W. Roberts: Yes, how do we know that the details of the normal distribution are accurate? There is real reason to doubt that the 4- and 5-σ extremes exist

Mr. Blake: To answer that, I have to go back to my attitude that what I am attempting to do is to decide which of a population of designs I am going to strengthen and which I am going to leave alone. One wants to apply some consistent policy in separating these groups. If one assumes that all distributions are normal, he will arrive at a certain separation into good and bad designs. It would, of course, be great if we knew the exact statistical distributions. I think, however, that in assuming all distributions to be normal, we do a better job than if we use a factor of safety which implicitly is equivalent to assuming not only that all distributions are normal but also that all the strength distributions have the same variance. We are actually inspecting all the designs. We have some criterion by which we reject certain designs. Nobody should claim that all the designs we reject would in fact be rejected if we knew everything we would like to know. An inspector on the production line rejects parts which would probably function satisfactorily, but he cannot take a chance on them. So, we are willing to redesign 10 percent of our parts in the hope that we will pick up the 1 percent which really need redesigning. We can't be 100 percent efficient in our inspection, but we hope to be more efficient if we use one set of ideas than if we use another.

Mr. W. Roberts: I think at this point we would like to sum up.

Mr. Fine: I think the general discussion has revealed that a prediction should not be a number but rather something to indicate how good the design is or what might be expected of the product. Secondly, there is a necessity for data to enhance this estimate. Third, there are certain deficiencies in the actual building or construction of the hardware which may appear to negate the first assumption, but I claim this is not true. There have to be controls. Also, there should be some way to classify or to segregate the predictions. I believe this has been done by North American Aviation in their criticality numbers where they do not look at the number of nines.

Mr. Getline: I got this out of the discussion: Reliability numbers can be used to compare the design of item a to item b, but not to give an assurance of absolute reliability.

Mr. W. Roberts: Is the game worth the candle?

Mr. Getline: I don't know. I have my doubts.

Mr. McClymonds (Douglas Aircraft Co.): I think the game is worth the candle. All managers want good reliability. National Aeronautics and Space Administration, Washington, insists on good reliability and because to analyze it into a structure is difficult, the only thing that really is at our disposal is to run test programs. So we do what Jim Roberts has done. He manages to get the funding to test three more parts, and whether he is trying to get a reliability number of 0.999, I think, is beside the point. The managers will feel the money has been well spent; and Jim will have engineering confidence that his design is satisfactory. One of the significant things that he will learn is at what level failure occurs — do the three parts fail at the same level or does one fail at 50 percent, one at 100 percent, and one at 150 percent of the expected environment? With these three statistics he will know what to do with the design. He would not have those statistics if he did not have the reliability program.

A number of years ago at a sonic fatigue conference at Annandale, Minnesota, Dr. Freudenthal presented a paper showing that the linear damage rule was inadequate and that a group of polished beam specimens showed very wide scatter. The people in the aircraft business took exception to this. They had used a linear damage rule for years to design airplanes, and it seemed to work on built-up structures. Dr. Freudenthal said that he was, at that point, embarking on a program to check into built-up structures, and that it was entirely possible that the wide scatter would narrow down with an increase in inaccuracies in the design. Perhaps stress concentration factors would make the failure so definite that all parts would fail at about the same load. I have seen this happen during tests on built-up structures. The scatter is not anywhere near as great as predicted. I hope Jim Roberts can confirm this and say that there can almost be engineering confidence based on a margin-of-safety standpoint.

Mr. J. Roberts: We increase levels only when testing the electrical-electronic systems. In some cases we have found a weak item which did not get past the first level. This is a quality

control problem to be dealt with during production by applying vibration input, which is the main contributor to failures, isolating all the weak components, and replacing them. Through screening, we have found that most failures in the propulsion-mechanical systems occur at about 3 times the expected service environment. There is a small amount of scatter. In some propulsion-mechanical systems, when we test only three specimens at the same levels, we have had failures near the end of the required number of life cycles which were not critical. They were hairline cracks which did not allow critical amounts of pressurization gasses to leak out. To verify the stress-strain curve and the tolerances to be used, we did run the two specimens which has not failed up to a failure point of at least double the number of cycles required, from six to eleven life cycles. We found that when the specimen failed, it did so at the same spot. So far we have been able to calculate this critical point within reasonable accuracy. This extended test was done on a development basis to verify that this was a weak link. A metallurgical analysis proved that there was a material flaw that caused one specimen to be weak or that it was stretched beyond a critical point.

Mr. Bouton: To moderate some of the pessimism I have been radiating, I would point out that even if we only succeed in raising the reliability to 0.99 or 0.999 instead of the desired 0.9999, we must continue to test and eliminate as many weak spots as possible.

Mr. Stahle: This prediction is an estimate which is perhaps not as good as we would like, but it is something that has to be done in evaluating program decisions, the criteria we use, and how we spend our money. I think we need more data to reach better predictions.

Mr. J. Roberts: It is hard to establish a reliability number, but by testing we can help our engineering judgment that an item will survive at least one life cycle. This is important in manned flight.

Mr. Blake: The effort expended towards determining structural reliability is very small when compared to the research and study of the reliability of electronic systems. The work has been almost a hobby or a special interest of relatively few people. I hope that you will agree that the prospects of a payoff are sufficient to increase the horsepower we are applying to this field

SUMMARY

William H. Roberts

A new approach to structural safety permits one to deal with margins appropriate to the probabilities contained in load and strength. The difference between load and strength is used as well as the variance. The old approach to structural safety based on a fixed margin between load and strength was tantamount to assuming constant distributions and variances. Two designs may have the same margins but considerably different reliabilities. Our inspection for faulty design will be more efficient if we use this new set of ideas.

A stumbling block in this new concept is the position occupied by design error relative to the reliability statement. Mr. Bouton showed that if comparable statements are made, one including error and one without, error is shown to be the dominant quantity. If the reliability statement omits the loss in reliability due to error, is the statement valid? Our discussion was not definitive, but several good points were made. First, if we make a reliability statement ignoring error we need to add other information to include the effect of error if this is possible. Second, ignorance and error in engineering must not prevent our putting a number on reliability which assumes error-free design and manufacture. This conceptual improvement is an aid to design as well as to the safety analysis. On the other hand, failure is more often the result of error than the lack of reliability, and much of our attention must be directed towards discovering error.

As to the ability to handle reliability analytically and to quantify reliability, the ordering of this new portion of the science will be done because it is so much cheaper to solve the problem analytically than by testing. The improvements required to reach extreme reliability will be determined from the analysis of where lie the gains capable of giving the needed improvements. Designs may be optimized, new variables uncovered, and performance increased. There will be no lack of examples where the analysis will stand alone without experimental support when exigencies associated with certain projects require it. This statement in no way minimizes the testing.

In many contracts, clauses are being inserted which require radically improved structural safety. Incentive money is available if these improvements can be demonstrated, and profit is being subtracted when they cannot be shown. System reliability is more a function of equipment reliability where mechanical and electrical, as well as structural, aspects enter. In all areas, fatigue is a principal failure mode.

* * *

DESIGN DATA AND METHODS

DYNAMIC ANALYSIS OF ATS-B SPACECRAFT*

Saul M. Kaplan† and Victor Terkun
Hughes Aircraft Company
El Segundo, California

This paper briefly describes the analytical model and the digital computer techniques used in evaluating the dynamic characteristics and loads of the ATS-B Applications Technology Satellite. A vibration test was performed on a structural test model of the ATS-B spacecraft. Comparisons of the test data with analytically predicted accelerations at various locations on the spacecraft structure and components are presented and show excellent agreement.

S. M. Kaplan

INTRODUCTION

Dynamic effects play an important part in the design of spacecraft. Therefore, it is desirable to be able to predict with some degree of confidence spacecraft vibration characteristics as well as loads. In the past little was done on detailed vibration analyses of communication satellites. The approach usually taken was to perform an unsophisticated vibration analysis of the spacecraft and then to verify the design adequacy of the spacecraft by a vibration test. This design approach has been costly as well as unreliable. To rectify this condition an analytical method for accurately determining frequencies, mode shapes, and loads was developed at Hughes Aircraft Company, Space Systems Division, Dynamics Section.

The first spacecraft to be analyzed using this analytical method was the Applications Technology Satellite, "B" vehicle (ATS-B). This spacecraft (Fig. 1) is a 1550-lb scientific satellite that will serve as an orbital platform for a wide spectrum of communications, meteorological, environmental and other scientific experiments. The specific spacecraft configuration treated is a spin-stabilized vehicle that will perform its mission at synchronous altitude (22,300 mi).

The ATS-B spacecraft structure must possess the strength and rigidity to meet design requirements at a minimum expenditure of structural weight. The objective was achieved through the use of thin shell and plate construction. This construction yielded a ratio of structural weight to total weight of approximately 6 percent.

ATS-B SPACECRAFT DYNAMICS DESIGN CRITERIA

The ATS-B spacecraft is designed to withstand qualification level vibration testing with

*This work was performed under NASA/GSFC Contract NAS 5-3823.
†Now with General Electric Company, Missile and Space Division, Valley Forge, Pa.

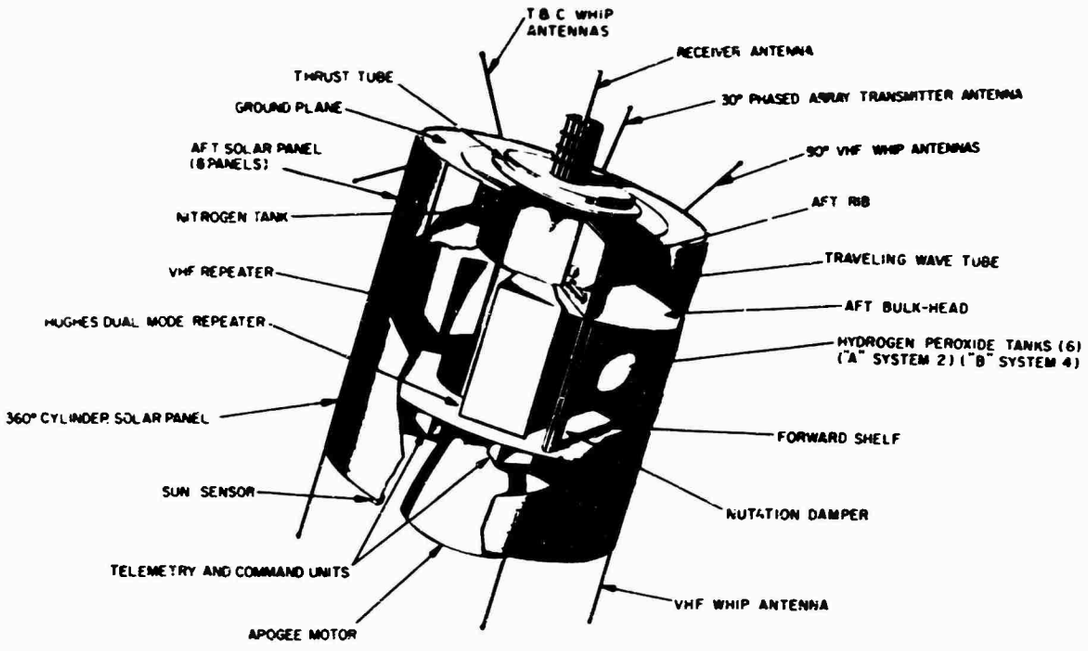

Fig. 1 - ATS-B synchronous altitude spin-stabilized vehicle

inputs applied at the base of the spacecraft adapter. These test levels (Appendix A), standard for all Atlas-Agena launched payloads, require that the vehicle be subjected to lateral, longitudinal and torsional sinusoidal vibration, lateral and longitudinal random vibration, modulated torsional pulses, and longitudinal shock pulses. In addition, to prevent booster coupling, a minimum allowable spacecraft-adapter frequency of 20 cps was required.

ANALYTICAL MODEL

Idealized Mass Stations

The ATS-B spacecraft was idealized by a 15-lumped-mass station physical model. These mass stations are defined in Fig. 2 and Table 1, together with their inertial and geometrical descriptions. Stations 3 through 8 and 15 represent primary structure, stations 1 and 2 describe the forward solar cylinder, stations 9 and 10 represent the apogee motor, and stations 11 through 14 portray major component mounting regions.

To facilitate analysis, components (experiments) were idealized as being constituents of or lumped into any one of four equivalent toroidal masses. This was accomplished by collating individual units in terms of their geographic

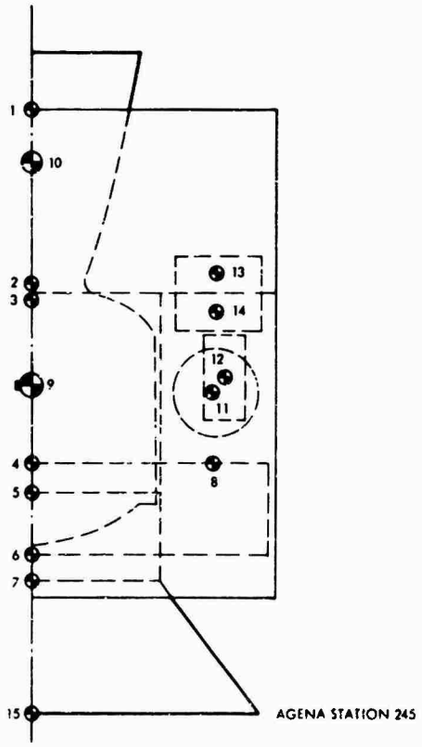

Fig. 2 - ATS-B spacecraft analytical model with mass stations

TABLE 1
Mass Station Description

Mass Station	Description	Weight (lb)	Location (Z)
1	Solar panel (cylinder)	13.4	53.3
2	Solar panel and shelf	46.15	32.3
3	Thrust tube and shelf	63.07	31.7
4	Thru . tube	16.35	13.1
5	Apogee motor attachment plane	14.35	10.3
6	Thrust tube	10.46	3.1
7	Separation plane	47.38	0.0
8	Forward rib flange	100.79	13.1
9	Apogee motor c.g.	792.00	22.3
10	Apogee motor nozzle c.g.	47.00	--
11	Rib-mounted components	212.86	22.3
12	Center thrust tube-mounted components	128.70	22.6
13	Shelf-mounted components – forward	55.23	34.0
14	Shelf-mounted components – aft	22.49	30.0
15	Agena station 245.0	45.00	--

attachment to the spacecraft proper; i.e., units were idealized as being either thrust tube-mounted components, rib-mounted units, components mounted to the forward shelf (bulkhead) aft of its plane, or components mounted to this shelf forward of its plane.

This analysis assumed that because of the symmetry of the ATS-B spacecraft there were no lateral-longitudinal-torsional vibrational couplings, i.e., that the axis of shear centers coincided precisely with the vehicular axis of symmetry throughout. Likewise, the mass of the vehicle at any spacecraft station had its center of gravity on this axis of symmetry. It was also assumed that the spacecraft lateral vibration characteristics were invariant from one lateral axis to another. Consequently, separate analytical models were established for lateral, longitudinal and torsional vibration. The discussion in this paper is concerned only with the lateral and the longitudinal cases.

Generalized Coordinates

Thirty-four lateral coordinates of motion (degrees of freedom) were selected. These include both translational and rotational motions, and incorporate the effects of rotational discontinuities across the structural joints. These are described in Table 2 and illustrated by Fig. 3.

Twenty longitudinal coordinates of translational motion were chosen. These also (Table 3 and Fig. 4) incorporate the effects of discontinuities across structural joints.

Structural Stiffness

The elasticity of the primary vehicular structure was taken into account in a gross sense. The structural idealization is illustrated schematically, together with appropriate coordinates of motion for the lateral (Fig. 3) and longitudinal (Fig. 4) cases.

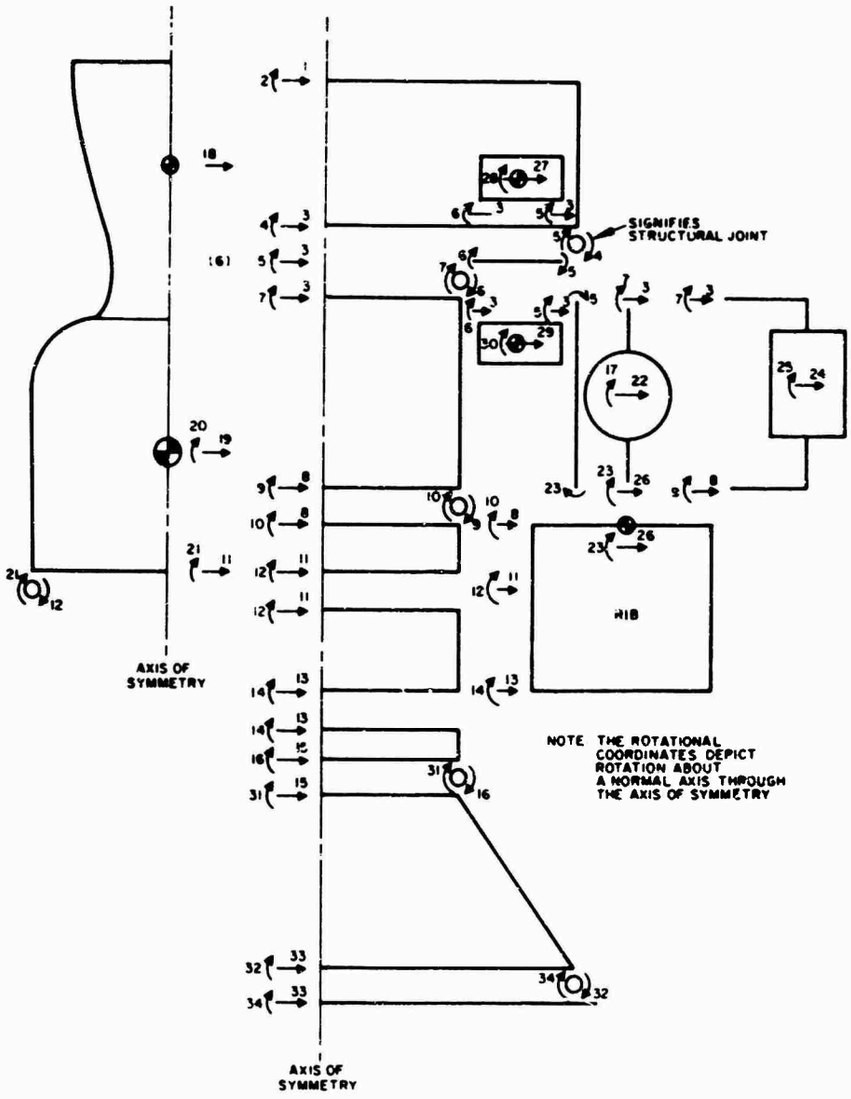

Fig. 3 - Schematic lateral coordinator fixed-free model

Essentially, the basic structure (thrust tube) has been treated as four cylindrical shells in series. Monocoque shell elements are employed aft of the forward rib flange, while the segment forward of this location is a semi-monocoque cylinder. The forward solar cylinder has also been idealized as a monocoque shell of honeycomb construction attached to the spacecraft at the outer periphery of the forward shelf (bulkhead). Stiffness distributions for the shelf, the eight-rib assembly cantilevered off the aft end of the thrust tube, and the eight posts between the forward shelf and the ribs were described implicitly. The Agena interstage structure (adapter) was idealized as a monocoque conical shell.

Stiffness coefficients derived for these thin shell elements were based on the assumption that a stress element within the surface of the shell was subjected only to membrane (normal) stresses and shear stresses.

The effects of the structural joints at appropriate mass stations have been taken into account using techniques described by Alley and Ledbetter [1].

TABLE 2
Coordinate Description of Lateral Analytical Model[a]

Mass Station	Coordinate (Degree-of-Freedom) Number			
	Lateral (X, Y) Translation	Pitching Rotation (θ)		
		At Mass Sta.	Fwd of Sta.	Aft of Sta.
1	1	2	-	-
2	3	-	4	5
3	3	-	6	7
4	8	-	9	10
5	11	12	21	-
6	13	14	-	-
7	15	-	16	31
8	26	23	-	-
9	19	20	-	-
10	18	-	-	-
11	22	17	-	-
12	24	25	-	-
13	27	28	-	-
14	29	30	-	-
15	33	-	32	34

[a]See Fig. 3.

Components were grouped into the four mounting regions (categories) described earlier. These components have been idealized as having supporting (secondary) structure with lateral frequencies of 60 cps and longitudinal frequencies of 80 cps.

The apogee motor has been idealized as a lateral 51-cps nozzle connected to a lateral 87-cps motor case, having a combined longitudinal frequency of 120 cps. These motor vibration characteristics were based on experimental data provided by the motor vendor.

The analytical model was used to establish spacecraft structural dynamic characteristics and design loadings with the aid of digital computer routines.

DIGITAL COMPUTER ROUTINES

The DYNAMO (Dynamic Analysis of Spacecraft) programs represent a series of five digital computer programs developed at the Hughes Company for structural dynamic and loads analysis of spacecraft. These five programs, their influences and their relative functions in the synthesis of structural design loads are illustrated through a flow diagram (Fig. 5). The digital computer routines are used in sequence to perform the following functions (details of which are presented in Appendix B).

1. MESS - lumps masses and inertias in accordance with the dynamic model;

2. SMOG - generates structural element stiffness matrices;

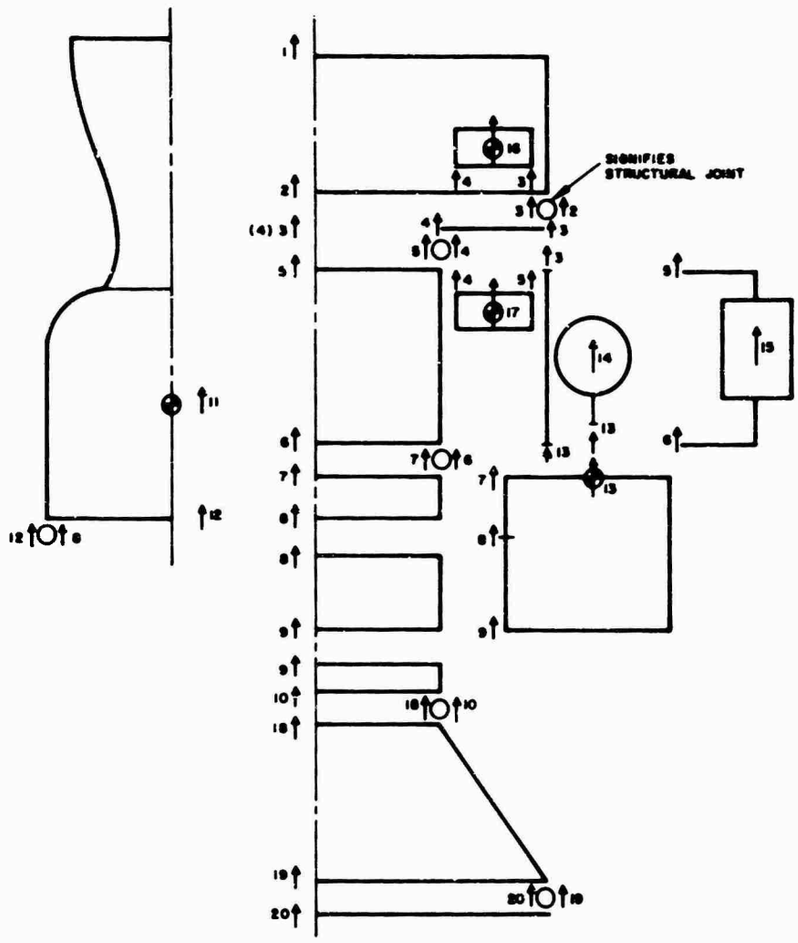

Fig. 4 - Schematic longitudinal coordinator fixed-free model

3. SMRR - reduces a system stiffness matrix by appropriate coordinate orthogonal transformation;

4. MOPUP, the heart of the program series - (a) formulates system stiffness and mass matrices, (b) computes mode shapes and frequencies through a Givvens diagonalization technique, (c) establishes acceleration response, structural deflections for sinusoidal vibration, and random vibration excitation by modal acceleration techniques, and (d) organizes mode shapes and frequency data into pages of dynamic analysis reports;

5. SLOP - organizes results into pages of formal loads reports.

These routines have been developed separately rather than in a combined package to provide better individual program flexibility and potential for their individual growth, and to enable their gradual development over a period of time during which they have been extensively used, even in embryonic form, to support Hughes Aircraft Company projects.

VEHICLE DYNAMIC ANALYSIS

Vibration characteristics and design loads for the ATS-B spacecraft were established through the use of the previously outlined computer routines.

A viscous modal damping coefficient of 5 percent of the critical value for all modes was used in the analysis of the ATS-B spacecraft. This damping function was based on previous test data obtained for the Advanced Syncom which is similar structurally and in weight to the ATS-B vehicle.

TABLE 3
Coordinate Description of Longitudinal Analytical Model[a]

Mass Station	Coordinate (Degree-of-Freedom) Number		
	Longitudinal (Z) Translation		
	At Mass Sta.	Fwd of Sta.	Aft of Sta.
1	1	-	-
2	-	2	3
3	-	4	5
4	-	6	7
5	8	12	-
6	9	-	-
7	-	10	18
8	13	-	-
9	11	-	-
10	11	-	-
11	14	-	-
12	15	-	-
13	16	-	-
14	17	-	-
15	-	19	20

[a]See Fig. 4.

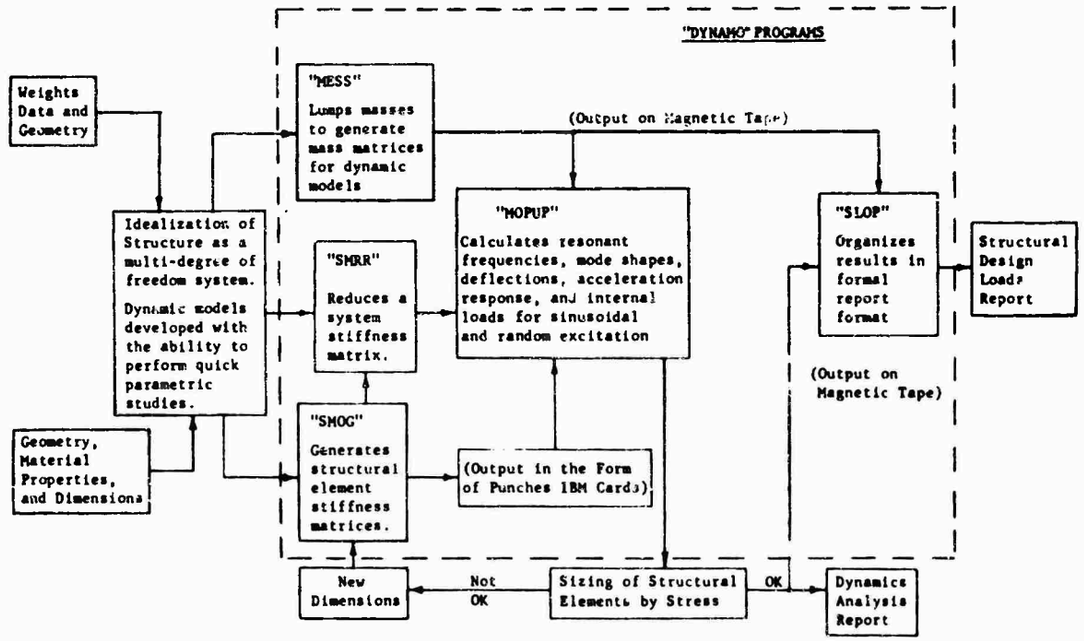

Fig. 5 - Flow diagram of DYNAMO programs

The spacecraft lateral and longitudinal analytical models, described earlier, were cantilevered at the base of the adapter for this investigation. These constraints were identical to those encountered during the spacecraft vibration test during which the vehicle, mounted on its Agena interstage structure (adapter), was cantilevered off the shaker.

The analytical models were subjected to base excitations (same as the test vehicle) specified by NASA/GSFC [2] and presented in Appendix A. The calculated response of the spacecraft to these vibration levels was determined using a modal acceleration method. The digital computer routine is presented in Appendix B. These computed loads were used in the design of the spacecraft structure.

Maximum predicted and measured response loads at the first three natural frequencies are presented in Tables 4 and 5 for the lateral and longitudinal cases, respectively.

TABLE 4
ATS-B Structural Design Load Factors Due to Lateral Response

Location	Load Factor (g)					
	First Mode		Second Mode		Third Mode	
	Measured	Predicted[a]	Measured	Predicted[a]	Measured	Predicted[a]
Forward solar cylinder, sta. 53.3	12.0	11.7	4.5	5.8	12.0	9.9
Forward solar cylinder, sta. 32.2	4.3	6.3	0.7	0.9	2.0	2.3
Spin-scan cloud camera, attachment	3.8	3.8	1.8	1.9	2.0	2.2
H_2O_2 tanks, forward attachment	4.0	3.8	1.7	1.9	1.7	2.2
H_2O_2 tanks, aft attachment	2.5	3.8	0.8	1.8	1.2	2.3
EME package, aft attachment	3.0	2.8	1.8	2.5	2.4	4.1
EME package, c.g.	5.0	6.9	1.1	2.7	2.7	4.8
Apogee motor case	5.2	5.2	0.7	0.8	3.1	3.5
Apogee motor mounts	2.1	2.6	1.5	2.4	2.7	4.1
Ion engine, attachments	4.4	6.2	1.4	2.7	1.8	2.0
Thrust tube, sta. 3.1	1.6	1.6	2.1	3.4	4.4	3.6
Thrust tube, sta. 10.3	2.7	3.0	1.6	2.3	1.8	2.8
Forward rib flange	2.9	3.8	0.9	1.9	1.7	2.3
Rib-mounted electronics, attachment	2.7	3.8	1.5	1.9	2.0	2.3
N_2 tank attachments	1.7	1.6	2.6	3.4	6.0	3.4
Thrust tube, sta. 32.2	4.5	6.3	0.9	1.0	2.5	2.3
Forward battery, attachment	4.6	6.3	0.6	1.0	0.6	2.3
Aft battery, attachment	3.0	3.0	2.2	2.3	2.6	2.8
EME package, forward attachment	3.7	6.3	0.6	1.0	1.8	2.3
Thrust tube, sta. 13.1	2.7	2.8	0.9	1.2	1.5	0.9

[a]See Ref. 3.

TABLE 5
ATS-B Structural Design Load Factors Due to Longitudinal Response

Location	Load Factor (g)							
	First Mode		Second Mode[a]			Third Mode[a]		
	Measured	Predicted[b]	Measured	Predicted[b]	Predicted[b] Plus Pitching Motion	Measured	Predicted[b]	Predicted[b] Plus Pitching Motion
Forward solar cylinder, sta. 53.3	22.0	21.8	12.0	3.4	9.0	8.8	3.0	7.1
Forward solar cylinder, sta. 32.2	21.0	21.5	9.0	3.3	9.3	7.0	2.9	5.5
Spin-scan cloud camera, attachment	19.0	19.0	3.5	3.4	9.4	6.0	4.4	5.0
EME package, aft attachment	9.6	12.1	6.1	2.4	4.8	6.6	6.7	7.7
EME package, forward attachment	10.5	13.6	7.0	2.5	5.5	7.0	6.3	7.7
Apogee motor case	11.0	13.6	7.6	3.9	6.3	8.0	12.5	12.8
H_2O_2 tanks, aft attachment	16.0	19.0	9.8	3.4	5.8	6.0	4.4	7.2
Ion engine, attachment	23.0	21.5	4.0	3.0	5.4	6.0	2.9	5.4
Thrust tube, sta. 32.2	9.6	13.6	6.6	2.5	5.5	5.2	6.3	7.9
Forward rib flange	11.0	19.0	6.5	3.4	5.8	4.0	4.4	7.6
Thrust tube, sta. 13.1	9.8	12.1	6.3	2.5	5.5	4.3	6.7	7.7
Thrust tube, sta. 3.1	9.0	10.5	5.8	2.2	4.6	2.8	6.6	7.1
Transponder, attachment	10.0	12.1	8.8	2.4	5.4	14.0	6.6	8.0
Apogee motor mounts	7.8	11.6	4.4	2.3	4.7	4.8	7.2	7.8
EME package, c.g.	22.0	24.8	11.0	11.2	14.2	18.0	21.4	22.8

[a]As discussed in paper, the shaker subjected the spacecraft to severe pitching motion as well as longitudinal excitation in the 60- to 85-cps frequency band (Fig. 10). This did not affect the first mode but severely affected data acquired experimentally for the second and third modes. The response of the spacecraft analytical model to this pitching motion has been established and appropriately superimposed onto data from Ref. 4.
[b]See Ref. 4.

Accelerations at different locations on the spacecraft structure are graphically illustrated in Figs. 6 through 14 for both the lateral and the longitudinal cases in the frequency range of 10 to 200 cps. It is evident from these figures and tabulated results that good correlation exists between analytical and measured acceleration responses. Further discussion of the comparison between analytical and test results are presented in the following paragraphs.

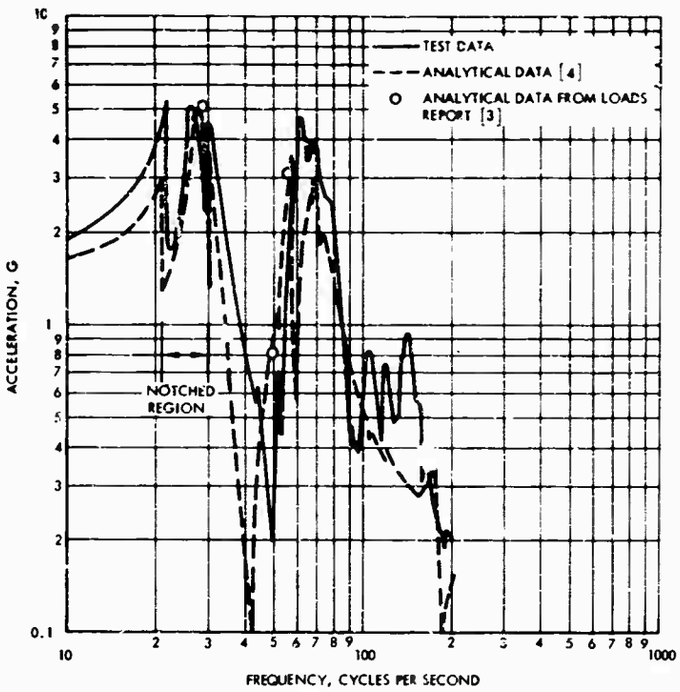

Fig. 6 - Apogee motor case lateral response spectra

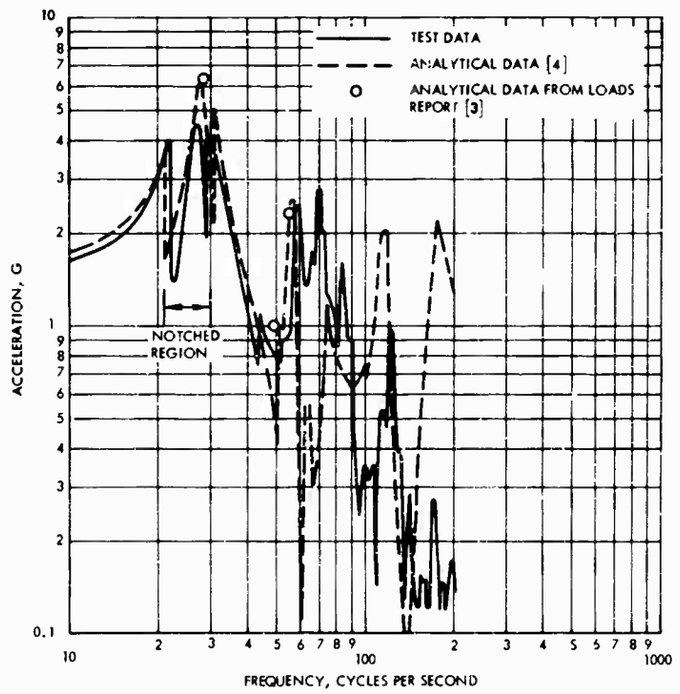

Fig. 7 - Lateral response spectra of thrust tube at sta. 32.2

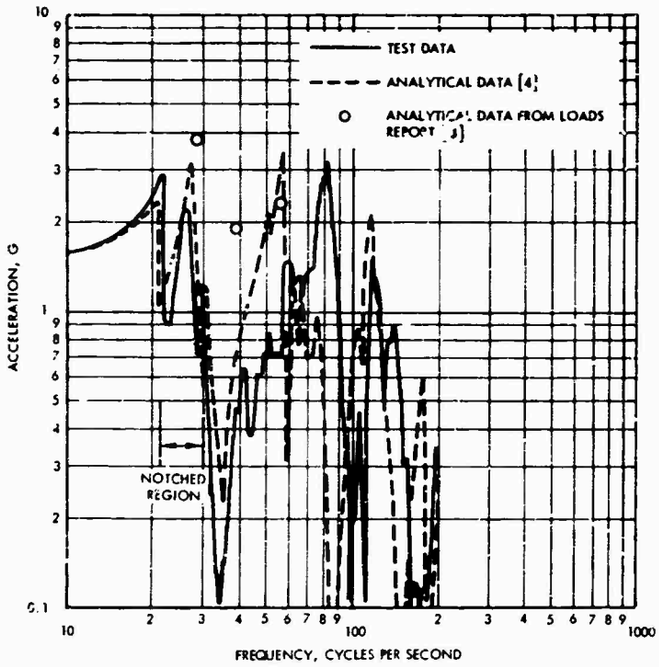

Fig. 8 - Forward rib flange lateral response spectra

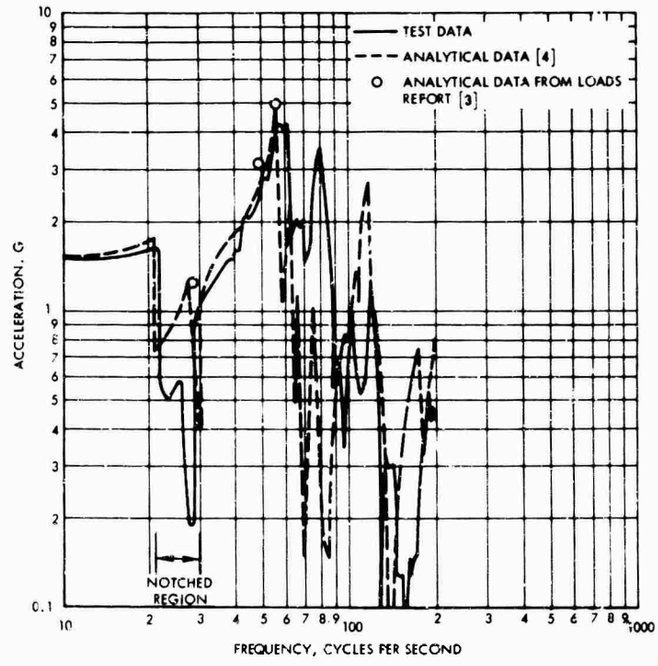

Fig. 9 - Lateral response spectra of thrust tube at sta. 3.1

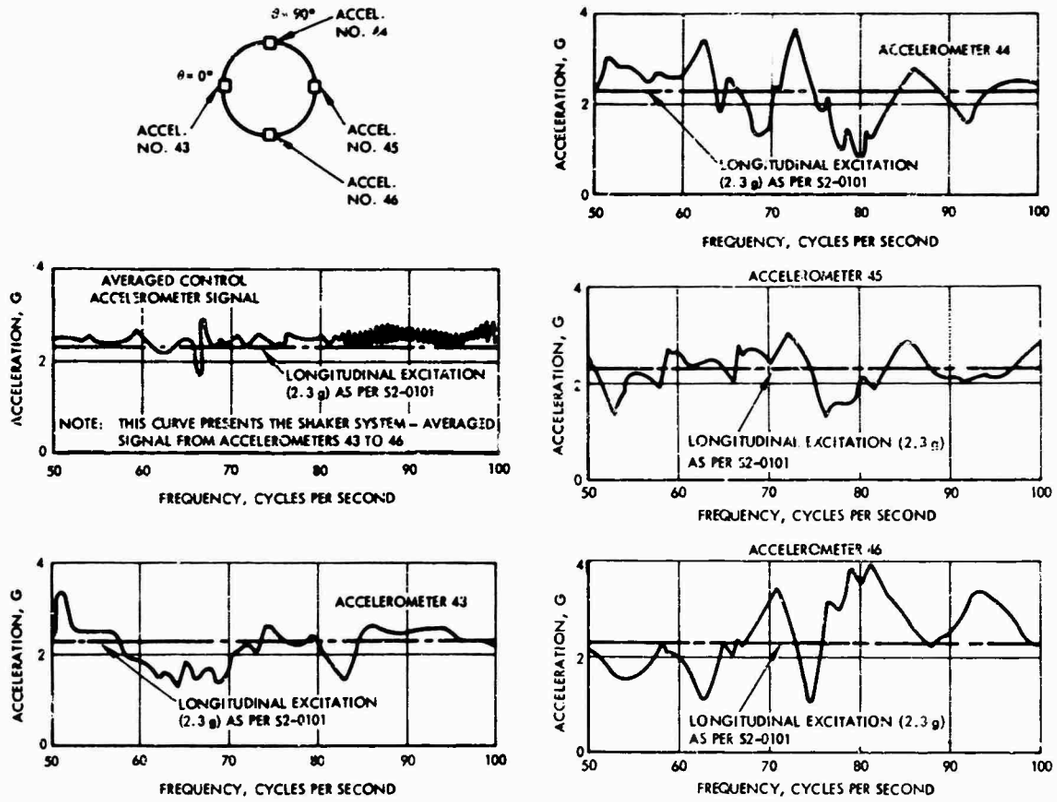

Fig. 10 - Shaker pitching motion during longitudinal test

SPACECRAFT VIBRATION TEST

Data acquired during the ATS-B vibration test provided the means for assessing analytical predictions. During this test the ATS-B structural model was subjected to the complete series of qualification test environments specified by NASA/GSFC (Appendix A). This test vehicle employed the actual spacecraft structural subsystem and brackets. Units, however, were simulated for the most part by dummy masses having inertial characteristics identical to the actual components. Fifty-one accelerometer channels were used to acquire the spacecraft vibration response data cited herein. Accelerometer blocks allocated to structural stations were positioned to facilitate loads comparison with the analytical models.

The vibration tests were conducted in the Hughes Aircraft Company's Space Simulation Laboratory (Fig. 15). A Ling 249 electromechanical shaker was used to provide the inputs to the spacecraft. The spacecraft is shown in Fig. 16 mounted to its adapter during lateral axis vibration testing.

ANALYTICAL PREDICTIONS COMPARED TO VEHICLE TEST RESULTS

Spacecraft Frequency Comparisons

Predicted spacecraft natural frequencies are compared with experimental results in Table 6. These experimental frequencies have been extracted from phase angle-frequency data plots and acceleration-frequency curves from the qualification-level sinusoidal vibration tests. The analytically predicted fundamental frequencies are within 6 percent of the measured frequencies. Other analytically derived resonant frequencies are shown to be in as good agreement with test data.

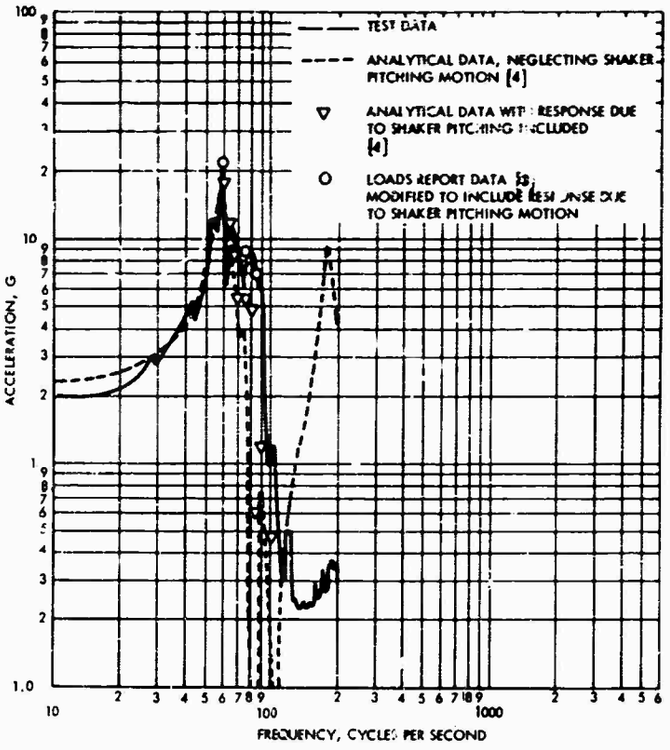

Fig. 11 - Longitudinal vibration spectra of forward solar cylinder, sta. 32.2

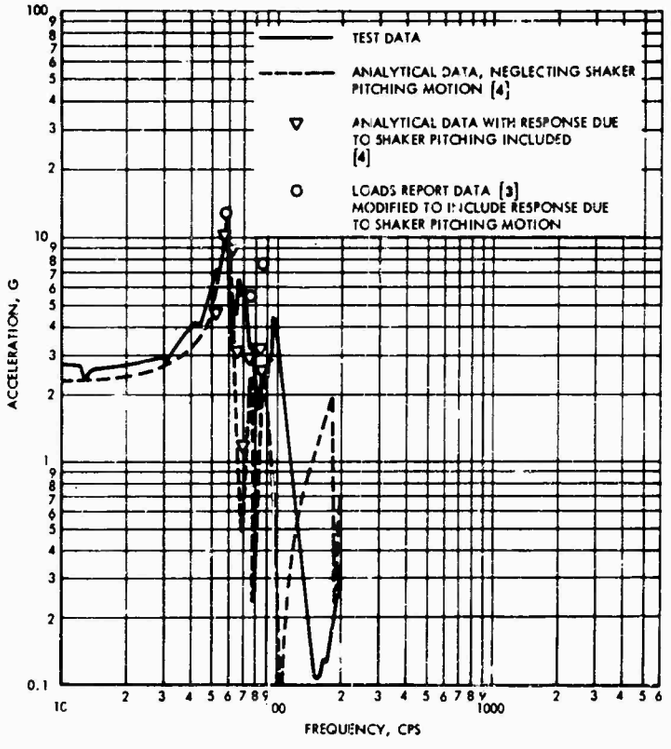

Fig. 12 - Longitudinal vibration spectra of thrust tube, sta. 13.1

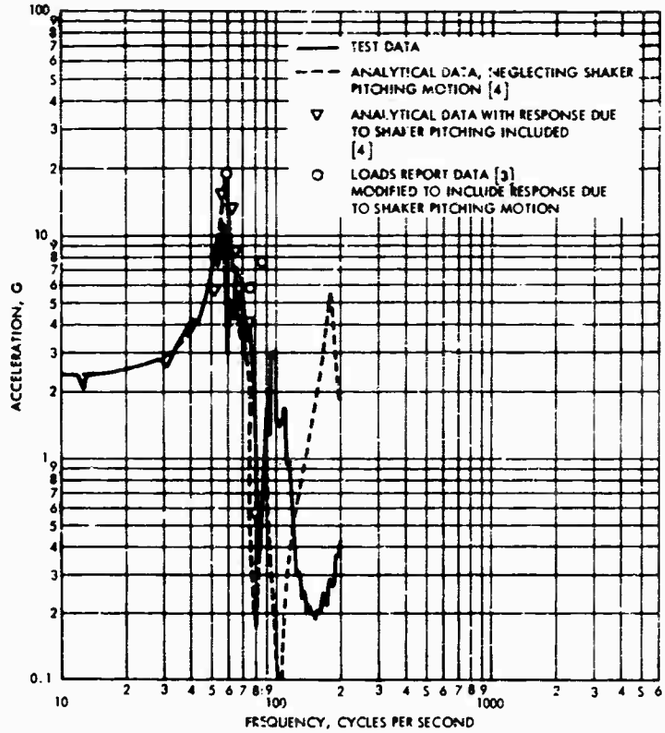

Fig. 13 - Forward rib flange longitudinal response spectra

Fig. 14 - Longitudinal vibration spectra of thrust tube, sta. 3.1

TABLE 6
ATS-B Spacecraft Natural Frequencies

Accelerometer Block	Natural Frequencies (cps)									
	f_1	f_2	f_3	f_4	f_5	f_6	f_7	f_8	f_9	f_{10}
(a) Lateral Sine Test, θ = 202.5° Axis										
1	27	44[a]	51	58	62	—	74	80 94	100 110	122
19	27	—	51	60	62	68	72	86	110	122
22	26	—	51	58	61	66	70	84	112	120
23	29	44[a]	51	58	60	66	69	80 90	109	120
60	26	—	53	59	60	65	72	86	115	120
Predicted[b]	27.6	—	51.6	57.6	59.9 60.2 62.2	66.7	72.8	98.3	106.6	117.1
(b) Lateral Sine Test, θ = 270° Axis										
8	29	48	58	62	69	78	87	109	117	—
18	27	48	54	60	66	70	88	98	118	—
19	26	48	54	59	68	78	88	100	115	—
22	27	48	54	60	69	.3 78	86	97	115	—
61	26	48	54	60	68	74	86	97	114	—
Predicted[b]	27.6	51.2	57.6	59.9 60.2 62.2	66.7	72.8	98.3	106.6	117.1	—
(c) Longitudinal Sine Test										
1	60[c]	70	78	94	100[d]	121	150	200	—	—
3	60[c]	70	79	93	102[d]	125	165	202	—	—
19	59[c]	69	77	92	—	120	—	190	—	—
22	59[c]	68	77	92	—	122	—	190	—	—
23	59[c]	68	79	92	100[d]	120	165	190	—	—
Predicted[b]	59.1	75.6	78.0 80.2	86.3	—	—	—	180.1	—	—

[a]This is attributed to localized resonance within magnetometer support bracket.
[b]See Ref. 4.
[c]Acceleration-frequency plots show spikes peaking at 53 and 59 cps while phase angle-frequency plots do not show any phase changes occurring until 59 cps. Consequently, 53-cps spike is felt to represent a "false mode."
[d]These are attributed to localized (secondary) resonances within magnetometer bracket and/or forward bulkhead.

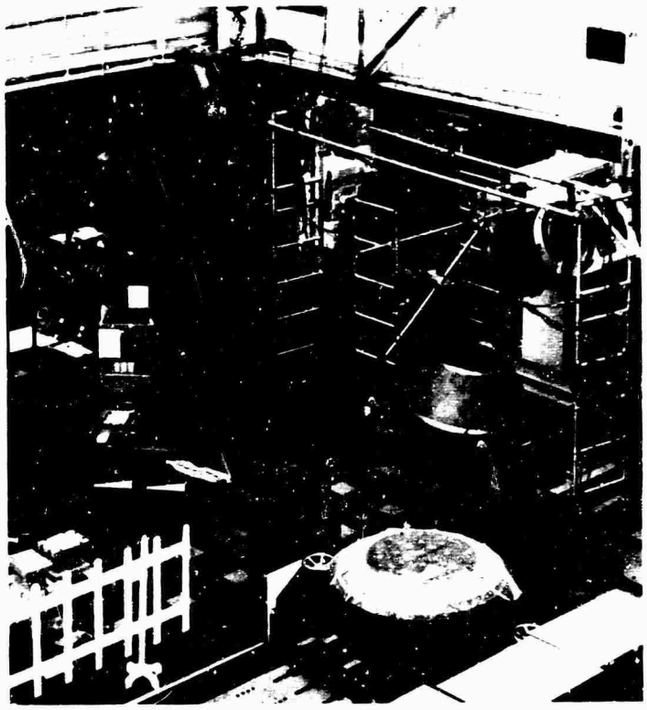

Fig. 15 - Testing arrangements for ATS-B vibration test

Structural Design
Loads Comparisons

In assessing validity of the analytically derived spacecraft mode shapes, comparisons of analytical and experimental structural design load factors (induced by sinusoidal vibration excitation) offers the most expedient and also the most severe test. The individual acceleration load factors due to sinusoidal vibration excitation are directly proportional to their corresponding modal displacements. Thus, the nature of agreement between predicted and measured acceleration responses throughout the spacecraft at a given resonant frequency is identical with agreement between corresponding analytical and experimental mode shapes at that resonance.

Lateral Load Factors — Experimental and analytical lateral acceleration load factors induced by qualification lateral sinusoidal vibration test levels are compared in Table 4. Analytical data used for this comparison were found in Ref. 3. The experimental load factors reflect data acquired by accelerometers oriented in the direction of shake for both lateral test axes. Illustrated comparisons of experimental and analytical acceleration-frequency curves are also presented in Figs. 6 through 9. Both analytical and experimental curves reflect a notched lateral input at the fundamental spacecraft resonance. The analytical curves are based on the mode shapes published in Ref. 4, i.e., the most recent spacecraft dynamic analysis data. Data from Ref. 3 are also presented to illustrate how slightly these loads changed over the 5-mo interval cited earlier. Both tabulated and illustrated data show very good correlation between analytical and experimental results.

Longitudinal Load Factors — In evaluating data from the ATS-B longitudinal sinusoidal qualification test, it was noted that the spacecraft was subjected to severe rocking (pitching) motions in the 62- to 85-cps frequency band. These combined longitudinal-pitching inputs to the spacecraft over this frequency band are illustrated in Fig. 10 for both the averaged input control accelerometer signal and the four individual control accelerometers.

To provide a rational and valid means of comparing analytical and experimental data, the

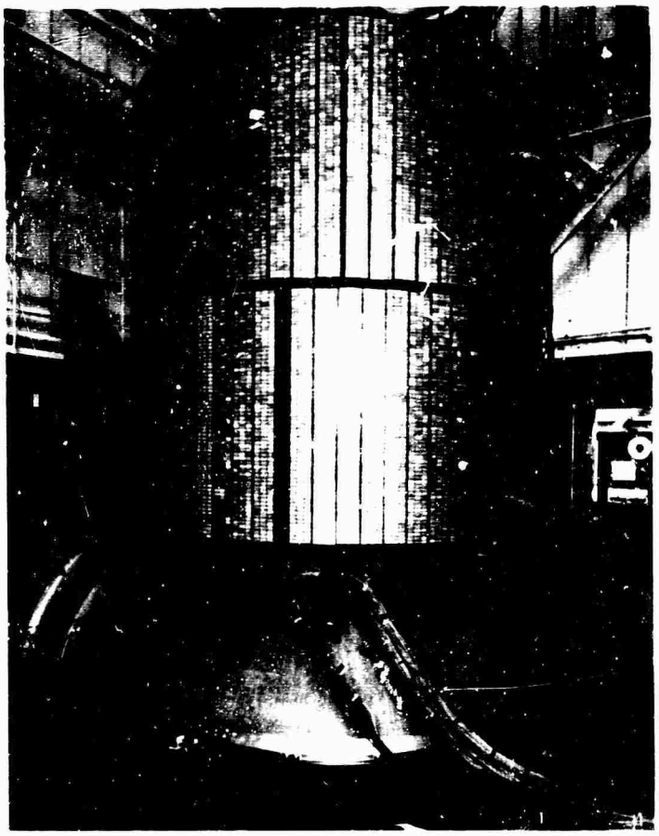

Fig. 16 - Spacecraft-adapter configuration during lateral qualification testing

response of the spacecraft to the combined pitching and longitudinal excitation experienced during the test has been determined analytically. To implement this, increments of longitudinal acceleration due to shaker pitching (from Fig. 10) were converted into a pitching acceleration vs frequency input spectra for the spacecraft. The spacecraft's response to this rocking excitation was established, using the lateral model of Fig. 2 for this investigation. Longitudinal load factors due to pitching motion were then superimposed onto their counterparts derived for purely longitudinal excitation [3,4]. This yielded combined longitudinal load factors reflecting the spacecraft's predicted response to the actual environments encountered during the test.

Experimental and analytical longitudinal acceleration load factors induced by the qualification longitudinal sinusoidal vibrational test levels are compared in Table 5. Analytical data presented therein consist of load factors reflecting both the accelerations predicted in Ref. 3 for a purely longitudinal excitation, and these same load factors onto which analytically derived loads due to the shaker pitching motion has been superimposed. The experimental loads presented therein reflect data acquired by accelerometers oriented in the direction of shake. The tabulated experimental data has been extrapolated from acceleration-frequency curves. Illustrated comparisons of experimental and analytical acceleration frequency curves are also presented in Figs. 11 through 14.

Both tabulated and illustrated data shown very good correlation between experimental data and those analytical results modified to reflect the combined longitudinal-pitching environment.

CONCLUSIONS

Based on the comparisons between analytically derived and experimentally measured data for the ATS-B spacecraft, it may be considered that:

1. Very good correlation was obtained between analytical predictions and experimental data;

2. Because of this, confidence may be placed in analytical data derived for this and other spacecraft;

3. The assumption of a modal damping rate of 5 percent of the critical value for all modes of this spacecraft yields good results; and

4. The assumption of structural symmetry i.e., no lateral-longitudinal vibrational couplings, is also valid.

REFERENCES

1. V. L. Alley, Jr., and S. A. Leadbetter, "Prediction and Measurement of Natural Vibrations of Multistage Launch Vehicles," AIAA J., Vol. 1, No. 2, pp. 374-379, Feb. 1963

2. "ATS Spacecraft Technical Requirements — Environmental Qualification and Acceptance Test Specification — Spacecraft Testing," NASA/GSFC Spec. S2-0101, Rev. B, July 20, 1965

3. S. M. Kaplan and V. Terkun, "Structural Design Loads for ATS Spacecraft, S/S Configuration," HAC IDC 2222.3/182, May 11, 1965

4. V. Terkun, "ATS Spacecraft, S/S Configuration Lateral and Longitudinal Modes," HAC IDC 2222.3/298, Oct. 3, 1965

Appendix A

ATS SPACECRAFT DESIGN QUALIFICATION VIBRATION AND SHOCK LEVELS

The ATS spacecraft design qualification vibration levels have been specified by NASA/GSFC [A-1]. Pertinent data from this source are described in Tables A-1 through A-4 and the following paragraphs.

TORSIONAL PULSE FOR SPACECRAFT DESIGN QUALIFICATION

This is interpreted as two separately applied torsional pulses with a finite (long) time

TABLE A-1
Sinusoidal Translational Vibration Schedule for Spacecraft Design Qualifications[a]

Frequency (cps)	Axis No.	Sweep Rate (octaves/min)	Level (0 - peak g)
10 - 250	3 (thrust)	2	±2.3
250 - 400			±3.7
400 - 2000			±7.5
5 - 10	2 and 4 (lateral)	2	—[b]
10 - 22			±1.5
22 - 29			±0.43
29 - 250			±1.5
250 - 400			±3.0
400 - 2000			±7.5

[a] To be applied at Agena interface structure (adapter) base, i.e., Agena sta. 245. Lateral test inputs at this location have been notched.
[b] 0.30 in. double amplitude.

TABLE A-2
Random Vibration Schedule for Spacecraft Design Qualification[a]

Frequency (cps)	Axis	Test Duration, each axis (min)	Acceleration (g rms)	PSD Level (g^2/cps)
20 - 150	3 (thrust)	4	9.2	0.0225
150 - 300				—[b]
300 - 2000				0.0450
20 - 51	2 and 4 (lateral)	4 per axis 2 and 4	9.2	—[c]
51 - 150				0.0225
150 - 300				—[b]
300 - 2000				0.0450

[a]To be applied at Agena interface structure (adapter) base, i.e., Agena sta. 245. Lateral test inputs at this location have been notched.
[b]Increasing from 150 cps at a constant rate of +3.0 db/octave.
[c]Decreasing beneath 51 cps at a constant rate of -9 db/octave.

TABLE A-3
Torsional Excitation Vibration Schedule for Spacecraft Design Qualification[a]

Frequency (cps)	Thrust Duration (thrust axis)	Level (rad/sec^2)
20 - 60	1 logarithmic sweep at 2 octaves/min	12.9
60 - 160		25.8

[a]To be applied at Agena interface structure (adapter) base, i.e., Agena sta. 245.

TABLE A-4
Shock Excitation Schedule for Spacecraft Design Qualification[a]

Axis	Pulses			
	Type	Level[b] (g)	Duration (msec)	No. of Pulses
3 (spin)	Terminal sawtooth	9	6 - 15	3

[a]To be applied at apogee motor mounts.
[b]This level has been reduced to 9 g from 30 g specified [A-1], with approval of NASA/GSFC.

separation between them. Each pulse shall have 0.2-sec duration and be applied at the Agena interface structure (adapter) base, i.e., Agena sta. 245.

Two torsional pulses shall be applied consisting of a high-frequency tone modulated by a 2.5-cps sine wave whose angular amplitude is 96.6 rad/sec^2 (vector value). The frequency of the high-frequency tone is determined as follows:

> If a major torsional resonance of the spacecraft is observed in the 60 to 75 cps band during the sinusoidal sweep, this resonance frequency is to be used as the high-frequency tone; if there is no resonance indicated in this band, 68 cps is to be used as the high-frequency tone.

A high frequency tone of 63 cps was employed for the T-4 test.

EXCEPTIONS

During vibration testing in the lateral axes, the vibration response of the spacecraft structure in its primary cantilever modes shall be limited so that the design ultimate strength of the structure is not exceeded. Design ultimate strength is defined (there) as: "the structural strength based on 1.5 times flight limit loads." The response shall be controlled and limited by the use of data from transducers (accelerometers, strain gages, load cells, etc.) installed on the spacecraft to monitor displacement, acceleration, bending moment, and/or axial load at critical points on the structure. The type and location of these monitoring transducers and the limiting values of the measured parameters shall be determined by extrapolation of the results of low-level sweeps.

REFERENCE

A-1. "ATS Structural Design Criteria Specification," NASA/GSFC Spec. S2-0111, Rev. A, June 21, 1965

Appendix B

DESCRIPTION OF DIGITAL COMPUTER ROUTINES

MESS (MASS ENUMERATION SORTING SYSTEM)

Function

MESS lumps the mass of the elements of a structural dynamic physical idealization to generalize mass stations as weights and mass inertias, to correspond to the related generalized coordinates.

Program Operations

1. Volume Sweep — The specification of a volume for a "generalized mass station" (g.m.s.) allows weights data generated by the Weights Section to be scanned and lumped at the g.m.s. Discrete masses are lumped within the prescribed volume to the associated g.m.s.

2. Proportion by length - Structural elements are proportioned by lengths specified for the model. This allows for lumping the mass of a structural element which has been idealized as a number of delta segments to the g.m.s. (This is done by association with the segments by a factor established by the ratio of the delta length to the total length.)

3. Percentage lump (for structural elements) — This lumps the mass of an element which is segmented by a fixed-percentage lumping factor input as a control.

4. Organization readout — Input data is organized without any calculation in same output format as items 1 to 3 for conformity.

Input Data

This comprises weights data and geometric coordinates, generalized mass stations, generalized coordinates, and geometric coordinates, limits of volume, dimensions, and percentage lumping factor.

Output

This consists of lumped weight, rotational and torsional weight inertias, generalized mass station number, description of g.m.s., generalized coordinates, and geometrical coordinates of g.m.s. These data are also stored on magnetic tape for input to MOPUP and SLOP.

SMOG (STIFFNESS MATRIX ORGANIZER AND GENERATOR

Function

The stiffness matrices for a large variety of basic structural elements are generated using analytical relationships presented in texts by Timoshenko, Flugge, Shanley, Wehle and Lansing, etc. These matrices describe the force-displacement relationship of the individual elements under longitudinal, transverse (coupled lateral-rotational) and torsional loading conditions.

Program Operations

Through the use of programmed force-displacement equations, elements of stiffness coefficient matrices are established. These equations presently are derived for the following structural shapes: monocoque, semimonocoque and sandwich cylindrical and conical shells; N-star conical space trusswork; quadrilateral shear panel; circular sandwich plate and circular plate (bulkhead) with circular hole in center (fixed-fixed or fixed-hinged boundary conditions); beam (linearly varying or constant EI) with varying boundary conditions at extremities; axial load (pin-ended) member (linearly varying or constant AE); capstrip or longeron (linearly varying or constant AE); and various component-support structures defined by frequency requirements, mass and inertial properties, and degree and number of restraints. This program is continuously being expanded as required.

Program Input

This comprises the code for the type of structural element, the mechanical properties of the material, and the elements geometry.

Program Output

1. Printout of input data and computer stiffness matrices.

2. Punched cards containing stiffness matrix inputs for MOPUP.

SMRR (STIFFNESS MATRIX REDUCTION ROUTINE)

Functions

1. Stiffness matrices for rib webs or plate structures of arbitrary shape are generated through the use of an equivalent beam gridwork (using theory developed in texts by Timoshenko and Flugge), for cases of both in-plant and transverse loadings.

2. An (N×N) stiffness matrix (generated for web or plate) is reduced to size (J×J).

3. An arbitrary (input) stiffness matrix of size (N×N) is reduced to order (J×J).

For a given structural element, a stiffness matrix of size (N×N) may be reduced to an equivalent reduced matrix of size (J×J) by applying zero forces at the undesired coordinate locations (designated herein by the subscript A, A = N - J. The partitioned force-displacement matrix equation,

$$\left\{\begin{matrix} F_J \\ F_A \end{matrix}\right\} = \left[\begin{matrix} K_{Jj} & K_{Ja} \\ K_{Aj} & K_{Aa} \end{matrix}\right] \left\{\begin{matrix} \delta_j \\ \delta_a \end{matrix}\right\} \qquad \left\{\begin{matrix} J = j \\ A = a \\ N = J + A \end{matrix}\right.$$

may be solved, with $\{F_A\} = 0$ and $[K_{Ja}] = [K_{Aj}]^T$, to yield

$$\{F_j\} = ([K_{Jj}] - [K_{Ja}][K_{Aa}]^{-1}[K_{Ja}]^T)\{\delta_j\}.$$

Program Operations

1. Establishment of stiffness matrices through the use of basic linear beam structure analysis program.

2. Partitioning of the matrices based on a pre-established loading pattern to reduce the order of the stiffness matrix. This is necessitated by "MOPUP" limitations on the maximum size of a single element stiffness matrix (12×12).

Program Input

This consists of the code identification for the type of structure, mechanical properties of the material, geometric dimensions, type of model (mass points, generalized coordinates, dimensions), and stiffness matrix (N×N).

Output

1. An (N×N) stiffness matrix; and

2. A reduced (J×J) stiffness matrix, where $N > J$ and $J \leq 12$.

MOPUP (METHOD OF PERMUTATING UNDULATING PROBLEMS

Functions

1. Combines individual elemental stiffness matrices to form a total system matrix.

2. Computes eigenvalues (frequency) and eigenvectors (mode shapes) by a Givven's diagonalization method.

3. Computes generalized masses and forces.

4. Determines structural responses to sinusoidal and random vibration.

5. Tabulates mode shapes into format suitable for the pages of dynamic analysis reports.

Program Operations

1. Establishment of system stiffness matrices.

2. Formulation of the dynamic matrix by orthogonal transformations involving the square root of the (symmetric) mass matrix.

3. Givven's diagonalization method is used to transform iteratively the symmetric dynamic matrix into a diagonal eigenvalue (frequency) array through a series of successive orthogonal transformations.

4. The response of the system is established through modal acceleration techniques.

5. Modal accelerations and displacements are transformed to yield acceleration load factors and structural deflections.

Program Input

This comprises stiffness matrices for individual structural elements (punched cards from SMOG), mass matrix (magnetic tape inputs from MESS), modal damping coefficients, boundary conditions, and descriptions and nature of excitation (shock, sinusoidal vibration or random vibration).

Output

1. Eigenvalues (resonant frequencies),

2. Corresponding mode shapes,

3. Structural displacements, and

4. Acceleration load factors.

SLOP (STRUCTURAL LOADS ORGANIZATION PROGRAM

Functions and Operations

1. To organize the weights and inertias in tabular form for both component and structural elements.

2. To compute and present in tabular form the load factors for component and structural elements. These are presented as loading conditions reflecting integrated structural response to sinusoidal, random, and shock excitation. This includes excitations applied along the lateral, longitudinal and torsional axes.

Program Input

1. Lumped weights and inertias, coordinates, etc., from MESS in the form of data stored on magnetic tape.

2. Acceleration response from MOPUP, in the form of data stored on magnetic tape.

Output

This is presented in tables in the format of those used in standard spacecraft structural design loads reports.

* * *

SPACECRAFT DESIGN FOR ATLAS TORSIONAL SHOCK TRANSIENT

Sol Davis
Fairchild Hiller
Republic Aviation Division
Farmingdale, Long Island, New York

The design and test criteria for the Advanced Orbiting Solar Observatory included a torsional vibration requirement and a severe torsional shock transient associated with a possible launch on the Atlas-Agena D. The effect of the torsional vibration and shock inputs applied to the base of the spacecraft were expressed in terms of response spectra for several values of damping. Since the shock input has several cycles at a discrete sinusoidal frequency, the analysis indicates that very high responses will occur in torsional modes whose natural frequencies lie between 60 and 75 cps. These shock responses can be much more severe than the response to the torsional steady-state vibration if torsional resonant frequencies lie between 50 and 80 cps.

An analysis of the AOSO configuration designed by all other significant design criteria except torsion shock indicated that the fundamental primary structure torsional frequency would fall within the worst part of the critical frequency band. Because it was feared that many experiments would not be able to survive this severe dynamic condition without major redesign, it was decided that the structural design should be modified to minimize the effects of the torsion shock transient on the experiments. After investigating and rejecting the possibility of designing the AOSO fundamental torsion frequency below 50 cps, the design criteria was established that the primary structure torsional natural frequency should be greater than 30 cps for all experiment array configurations.

S. Davis

INTRODUCTION

Design and test criteria for a spacecraft include many environmental conditions that may be encountered during its total mission life. Some of these critical environments occur during the short boost phase and are intimately related to the particular launch vehicle that is used. Familiar spacecraft dynamic criteria during the launch phase have included significant longitudinal and lateral shock and vibration requirements, acoustic noise environments, and minimum natural frequency requirements. The magnitudes of these requirements are heavily dependent on the particular launch vehicle used. A recent addition to these more familiar criteria is the requirement for torsional shock and vibration associated, for example, with a spacecraft launch on the Atlas-Agena D.

This paper will present some of the implications of these torsional requirements on the design of a particular spacecraft – the Advanced Orbiting Solar Observatory (AOSO). The spacecraft was initially designed for a TAT-Agena D launch, but was subsequently required to have the capability of a launch on the Atlas-Agena D. This new booster requirement introduced the

severe torsional shock transient which is the subject of this paper.

TORSION REQUIREMENTS

The torsion vibration and shock inputs to be applied at the base of the spacecraft adapter are presented in the Appendix. These requirements were specified for the AOSO by NASA [1].

The qualification level vibration is a sinusoidal sweep excitation about the spacecraft longitudinal axis at a sweep rate of 2 octaves/min from 20 to 250 cps. The input level of 12.9 rad/sec^2 jumps to 25.8 rad/sec^2 at 30 cps.

The qualification level shock consists of two separate applications of a transient pulse having several cycles at a discrete frequency. A pictorial representation of the torsional shock pulse is shown in Fig. 1. The maximum amplitude of the pulse is 96.6 rad/sec^2 and the sine wave frequency is specified as the resonant frequency of the spacecraft in the 60- to 75-cps band. Thus, if the torsional resonant frequency as determined by the vibration test is 64.9 cps, then this frequency must be used for the high-frequency tone of the torsion shock test.

CONCEPT OF RESPONSE SPECTRA

The response spectrum is defined as a plot of the maximum response experienced by a single-degree-of-freedom system, as a function of its own natural frequency, in response to an applied excitation. This definition is similar to that in the Shock and Vibration Handbook [2] except that "applied shock" has been replaced by "applied excitation." With the present definition, even the response to a steady-state vibration input may be expressed as a response spectrum. In general, the response spectrum is a function of the damping of the single-degree-of-freedom system.

The effect of the torsional excitations (both shock and vibration) will be expressed in terms of response spectra.

TORSION SHOCK RESPONSE SPECTRA

The shock response spectra (also called shock spectra or response spectra) for the torsional qualification shock test requirement of the Appendix were computed with the aid of an analog computer. The computer determined the time history of acceleration response of the mass to an acceleration input applied to the foundation of a single-degree-of-freedom system. The differential equation governing the response to the acceleration input is:

$$\ddot{q} + 2\zeta\omega_n\dot{q} + \omega_n^2 q = A(t) \qquad (1)$$

where

ω_n = undamped natural frequency of the single-degree-of-freedom system (rad/sec),

ζ = viscous damping factor (dimensionless),

$A(t)$ = acceleration input to the foundation (rad/sec^2),

$\ddot{q}$ = acceleration response of the mass with respect to the moving foundation (rad/sec^2), and

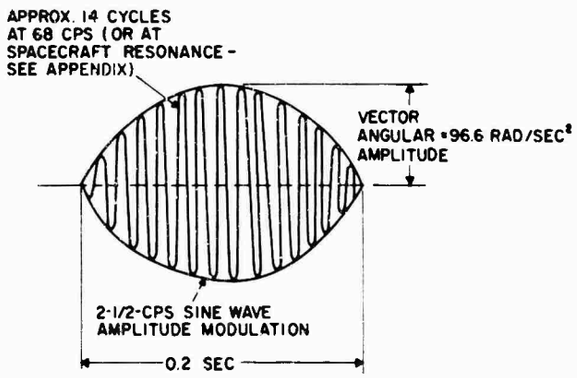

Fig. 1 - Torsional shock qualification test pulse

$\ddot{q} + A(t)$ = acceleration response of the mass in absolute coordinates relative to a fixed reference (rad/sec^2).

The shock spectra for $\ddot{q} + A(t)$ were obtained for the 68-cps high-frequency tone with a maximum input amplitude of 1.0 rad/sec^2 for two values of damping, $2\zeta = 0.02$ and $2\zeta = 0.20$. These values of damping were chosen as extreme upper and lower bounds for the damping associated with expected torsional modes of the AOSO. The shock spectrum value for $2\zeta = 0.07$ was also computed for a natural frequency of 68 cps so that interpolation in the high-response region of the shock spectra could be made for other damping values. Since the test requirement stipulates that a 60- through 75-cps pulse frequency must be used if a spacecraft natural frequency lies between these frequency limits, the response for f_n of 75 cps to a 75-cps pulse frequency was also computed for $2\zeta = 0.02$. The 75-cps pulse frequency was chosen because more cycles exist during the pulse duration of 0.02 sec, resulting in a slightly higher shock amplification.

The results of the analog computer study, scaled to a qualification input amplitude of 96.6 rad/sec^2, are presented in Fig. 2 for several values of damping. It is clear from the figure that the shock response spectra is very dependent on damping for natural frequencies in the 60- to 75-cps band. However, the shock response is almost independent of the damping value for natural frequencies outside the band of 50 to 80 cps.

TORSION VIBRATION RESPONSE SPECTRA

The vibration sweep rate of 2 octaves/min is slow enough to excite a single-degree-of-freedom system to almost its steady-state vibration response level when the sweep frequency passes the system natural frequency. Therefore, the vibration response spectra will be taken as that due to a steady-state torsional vibration at the natural frequency of the single-degree-of-freedom system. This approach is mildly conservative for the values of damping considered. The differential equation governing the response of a single-degree-of-freedom system to a steady-state sinusoidal acceleration input is the same as Eq. (1) with $A(t)$ having the special form $A_o \sin \omega_n t$

$$\ddot{q} + 2\zeta \omega_n \dot{q} + \omega_n^2 q = -A_o \sin \omega_n t . \qquad (2)$$

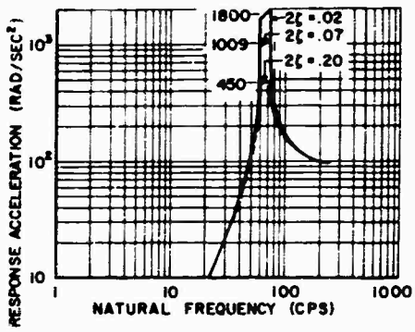

Fig. 2 - Torsional shock response spectra

A_o is the amplitude of the steady-state torsional vibration input and $\omega_n (= 2\pi f_n)$ is the undamped natural frequency of the system.

For the values of damping considered ($2\zeta < 0.2$), the use of the undamped natural frequency (ω_n) instead of the damped natural frequency

$$\left(\omega_d = \omega_n \sqrt{1 - \zeta^2}\right)$$

or the frequency of maximum response

$$\left(\omega_r = \omega_n \sqrt{1 - 2\zeta^2}\right)$$

is a reasonable simplification for the engineering accuracy required. It may also be assumed that the acceleration response of the mass with respect to the moving foundation ($\ddot{q}$) is equal to the acceleration response of the mass with respect to a fixed reference ($\ddot{q} + A_o \sin \omega_n t$). This assumption is appropriate for steady-state vibration at resonance because $\ddot{q}$ is much larger than A_o, and $\ddot{q}$ is almost 90° out of phase with $A_o \sin \omega_n t$. Reference 3 may be useful for a detailed review of the damped single-degree-of-freedom system under steady-state sinusoidal excitation.

The solution of Eq. (2) for $\ddot{q}$ yields $\ddot{q} = QA_o$, where Q is the steady-state amplification factor at resonance. Q is approximately given by $1/2\zeta$. The vibration response spectra for a single-degree-of-freedom system is merely a plot of $A_o 2\zeta$ at each natural frequency. Since $A_o = 12.3$ rad/sec^2 for natural frequencies between 20 and 60 cps, and $A_o = 25.8$ rad/sec^2 for natural frequencies between 60 and 250 cps, the torsional vibration response spectra for different values of damping are as shown in Fig. 3.

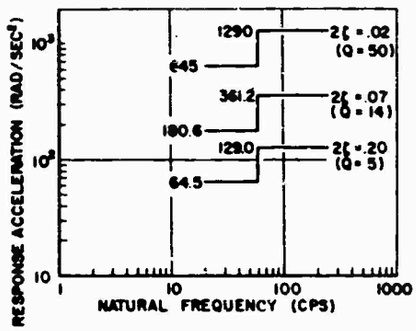

Fig. 3 - Torsional vibration response spectra

COMPARISON OF SHOCK RESPONSE WITH STEADY-STATE VIBRATION RESPONSE

The severity of the torsion shock transient in relation to the steady-state torsion vibration may be examined by comparing the response spectra for the two test conditions. This criterion, associated with maximum acceleration response, avoids cumbersome fatigue calculations which would consider number of cycles and acceleration response statistical distribution. The response spectra comparison method is considered a good engineering approach for a vehicle-launched spacecraft because of the small number of cycles of high-level vibration response at the structural natural frequencies.

Shock and vibration response spectra, obtained by interpolation of the spectra in Figs. 2 and 3, are shown in Fig. 4 for a damping value of $2\zeta = 0.10$. This value is an estimate of the damping in the primary structure fundamental torsion mode for the AOSO.

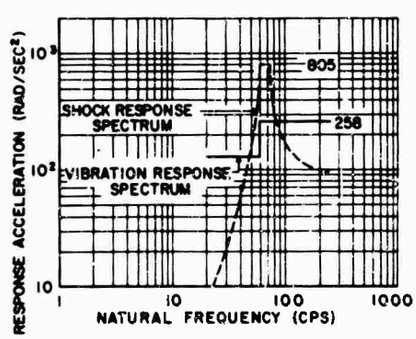

Fig. 4 - Torsional response spectra for $2\zeta = 0.10$

Figure 4 indicates that the shock response of a single-degree-of-freedom system (or a normal mode representing the primary structure in torsion) will be more severe than the steady-state vibration response if the system (or torsion mode) natural frequency lies between 50 and 80 cps.

AOSO DESIGN AND DYNAMIC CHARACTERISTICS

The AOSO launch configuration, attached to the forward end of the Agena D and enclosed within the aerodynamic shroud, is shown in Fig. 5. The highly delicate experiments that are the essence of the AOSO mission are attached to the external or internal faces of the experiment support tube. The tube is, in turn, attached to the three pylon supports, each of which transfers its loads to a local fitting at Sta. 68.5 of the thermal housing. These fittings, dictated by thermal distortion requirements in orbit, are designed to take tangential and axial loads but no radial loads. It is appropriate to mention here the significant design criteria other than torsion that established the configuration which was analyzed:

1. Support tube and pylons — spacecraft minimum lateral natural frequency requirement of 25 cps, and orbit thermal distortion requirements;

2. Thermal housing — spacecraft lateral natural frequency requirement of 25 cps;

3. Equipment bay skin — thermal heat sink requirements for electronic equipment;

4. Adapter — longitudinal vibration qualification test; and

5. Solar panels — lateral vibration qualification test and orbit natural frequency requirement.

For the purpose of analyzing the structure to the torsional inputs, the simplified 9-degree-of-freedom model of Fig. 6 was used where each circled coordinate represents a lumped roll inertia degree of freedom. The mass of the solar panels, which are fairly stiff in the tangential direction, was appropriately included in the roll inertia of the thermal housing. For the first flight experiment array which had all experiments attached to the outside of the support tube, the fundamental primary structure natural frequency of 64.9 cps was obtained. The mode shape normalized to the largest twist coordinate, the top of the support tube, is listed

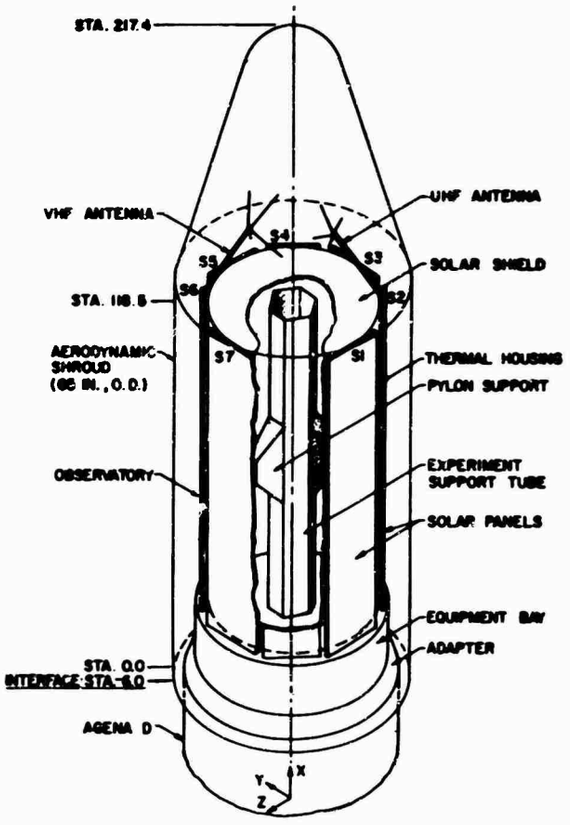

Fig. 5 - AOSO launch configuration with shroud

in Table 1. The worst possible shock condition has occurred; namely, the primary structure torsional natural frequency of the spacecraft is within the very critical frequency band of 60 to 75 cps. The logical question to be asked is, "Can the spacecraft, designed by all other design criteria, adequately survive the severe shock environment?"

PREDICTION OF TORSIONAL ACCELERATION RESPONSE AND STRUCTURAL LOADS

Using conventional normal mode theory, the actual peak torsion acceleration response distribution can be obtained from the shock response spectra. The peak torsional shock response distributions in any mode due to a foundation acceleration input is given in matrix notation as:

$$\{\ddot{\theta}_x\}_{shock} = R(f_n, 2\zeta)\, \frac{[V^T]\,[M]}{[V^T]\,[M]\,\{V\}}\, \{V\}\,, \qquad (3)$$

where

$\{\ddot{\theta}_x\}$ = torsional acceleration response distribution vector - $[N \times 1]$ (rad/sec^2);

$R(f_n, 2\zeta)$ = response spectrum acceleration at mode natural frequency, f_n, for modal damping value 2ζ - $[1 \times 1]$ (rad/sec^2);

$\{V\}$ = torsional mode shape vector - $[N \times 1]$ (dimensionless);

$[V^T]$ = transpose of mode shape vector - $[1 \times N]$ (dimensionless);

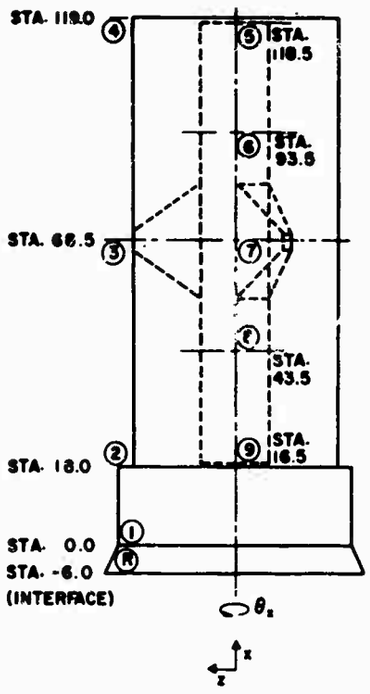

Fig. 6 - AOSO torsional dynamic model

TABLE 1
Primary Structure Fundamental Torsional Mode Shape[a]

Coordinate No.	Mode Shape Value {V}	Location
R	0.0	Adapter-Agena D interface
1	+0.055	Equipment bay-adapter interface
2	+0.121	Thermal housing - equipment bay interface
3	+0.482	Middle of thermal housing
4	+0.611	Top of thermal housing
5	+1.000	Top of support tube
6	+0.847	Upper quarter pt. of support tube
7	+0.580	Center of support tube
8	+0.747	Lower quarter pt. of support tube
9	+0.832	Bottom of support tube

[a]Generalized mass = 77.09×10^3 psi.
Natural frequency = 64.9 cps.

$[M]$ = diagonal matrix of weight or mass moments of inertia about the x-axis - $[N \times N]$ (psi or lb-in.-sec^2);

$\{M\}$ = column vector of the diagonal elements of $[M]$ - $[N \times 1]$ (psi or lb-in.-sec^2);

f_n = mode natural frequency (cps);

2ζ = two times the viscous damping factor for the mode (dimensionless); and

$[V^T][M]\{V\}$ = generalized mass in the mode (psi or lb-sec^2/in.).

As a special case, the response to steady-state torsional vibration at resonance requires the substitution of $\ddot{\theta}_o(f_n)\ 2\zeta$ for $R(f_n, 2\zeta)$ in Eq. (3). $\ddot{\theta}_o(f_n)$ is the magnitude of the torsional vibration acceleration input applied at the adapter base R at the natural frequency f_n of the normal mode.

With the data for the 64.9-cps mode and a value of R (f_n = 64.9 cps, 2ζ = 0.1) of 805 rad/sec^2 from Fig. 4, the maximum torsion shock acceleration response distribution is given by

$$\{\ddot{\theta}_x\}_{shock} = \frac{(805)(146.4 \times 10^3)}{77.09 \times 10^3}\{V\}$$

$$= 1529\ \{V\}\ \text{rad/sec}^2\,. \qquad (4)$$

where only the response in the fundamental mode is considered. The contributions of the second (f_n = 105 cps) and higher modes has been ignored because their modal response to the shock is comparatively small. The acceleration response distribution predicted for the AOSO is given in Table 2 together with the resulting dynamic inertia torque at each station obtained from the relationship:

$$T_x = \frac{I_x \ddot{\theta}_x}{386}\,. \qquad (5)$$

where

T_x = dynamic inertia torque (in.-lb),

I_x = moment of inertia about the x-axis (psi), and

$\ddot{\theta}_x$ = torsional acceleration response (rad/sec^2).

TABLE 2
AOSO Torsional Shock Acceleration Response and Inertia Torques

Coordinate No.	Acceleration Response, $\ddot{\theta}_x$ (rad/sec^2)	Moment of Inertia, I_x (psi, $\times 10^3$)	Inertia Torque T_x (in.-lb, $\times 10^3$)
R	0	21.4	0
1	84	151.0	32.9
2	185	182.1	87.3
3	737	92.8	177.2
4	934	50.9	123.2
5	1529	11.9	47.1
6	1295	10.4	34.9
7	887	11.2	25.7
8	1142	8.6	25.4
9	1272	7.9	26.0
Total	–	548.2	597.7

SPACECRAFT EVALUATION

It was found by subsequent stress analysis that the primary structure, dictated by other design criteria, was generally adequate to withstand the high torsional inertia loads shown in Table 2. However, a major concern was tne adequacy of the delicate experiments for which little fragility information was available.

Consider a typical experiment mounted near the top of the support tube, attached to the external surface by a set of nonredundant mounts. This nonredundant mounting requirement is necessary to minimize thermal distortions in orbit. A typical experiment may have radial dimensions as shown in Fig. 7. Its center of gravity is located 14.0 in. radially outward from the tube centerline. The linear tangential acceleration is related to the angular acceleration about the tube longitudinal axis by the simple equation:

$$\ddot{T} = \frac{r\ddot{\theta}_x}{386} , \qquad (6)$$

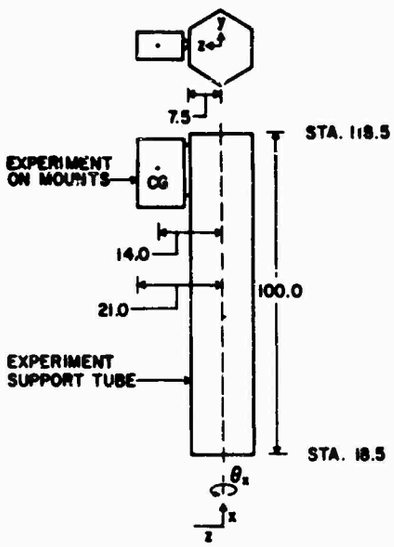

Fig. 7 - Typical experiment near top of support tube

where

$\ddot{T}$ = linear tangential acceleration at a distance r from the axis of rotation (g),

r = radius from the axis of rotation to the point of interest (in.), and

$\ddot{\theta}_x$ = torsional acceleration about the axis of rotation (rad/sec^2).

The predicted shock response angular acceleration of 1529 rad/sec^2 at the top of the tube converts to a linear tangential acceleration of 55.5 g at an experim ntal c.g. located at a

radius of 14 in. from the axis of rotation. The actual tangential acceleration varies through the experiment from 29.7 g at the mount interface with the support tube (radius of 7.5 in.) to 83.1 g at the extreme radial location (radius of 21.0 in.). If the experiment and mounts have their natural frequencies much higher than 65 cps, these accelerations could be treated as equivalent static load factors (with a limited number of completely reversed fatigue cycles) for evaluation of the experiments to survive the AOSO torsional shock condition. However, if the experiment on its mounts cannot be considered rigid in the tangential direction, then responses of experiment internal parts might well exceed the g levels computed above.

After considering the delicate nature of the experiments, it was feared that many experiments would not be able to survive this severe dynamic condition without major redesign or severe weight penalties. It was decided, therefore, that the structural design should be modified to minimize the effects of the torsional shock transient on the experiments.

ABOVE OR BELOW

It can be seen from Fig. 4 that the torsional shock transient can be eliminated as a significant design criteria if its effects are less severe than the torsional steady-state vibration requirement. This can be accomplished by designing torsional resonant frequencies (and, in particular, the primary structure fundamental torsional resonant frequency) outside the band of 50 to 80 cps. Is it better to design above 80 cps or below 50 cps?

In general, a weight penalty is associated with efforts to increase natural frequencies of a given geometric configuration. It was desirable, therefore, to investigate the possibility of designing the AOSO for a fundamental torsional frequency below 50 cps. The added advantage, observable from Fig. 4, is that the steady-state torsional vibration response load factors for a resonant frequency of 45 cps would be about half of the load factors associated with a torsional resonant frequency of 85 cps. This advantage is simply due to the lower torsional vibration input level below 60 cps.

Weakening the structure to get a torsional natural frequency below about 45 cps was found to be incompatible with the minimum lateral natural frequency requirement of 25 cps. If the AOSO were designed for 45 cps in torsion with a first flight array of experiments located on the outside of the support tube, it was found that the same structure with the second flight array would have a fundamental torsional frequency in the critical 60- to 75-cps band. This ironic situation occurs because the second flight array has a major experiment inside the support tube, resulting in a significant reduction in mass moment of inertia for coordinates 5 through 9 of Fig. 6. It was concluded, within the framework of other requirements, that the AOSO torsional frequency for all arrays could not be easily designed below 50 cps. The primary structure torsional natural frequency must, therefore, be greater than 80 cps with any proposed experiment array.

The first flight experiment array was expected to give the lowest torsional frequency because it had the largest moment of inertia about the roll axis. Succeeding flight configurations were expected to have their fundamental torsional frequency in the band of 80 to 110 cps.

SUMMARY AND CONCLUDING REMARKS

The severe torsional shock requirement for the Advanced Orbiting Solar Observatory associated with a possible launch on the Atlas-Agena D has been presented, analyzed, and compared with the torsional sweep vibration requirement in terms of response spectra. Significant AOSO structural design characteristics, dictated by other than torsional criteria, established the configuration whose torsional acceleration response and structural loading were computed at the torsional resonant frequency of 64.9 cps.

Spacecraft evaluation indicated that the primary structure was generally adequate to withstand the high torsional inertia loads; however, it was feared that many of the delicate experiments would not be able to survive this severe dynamic environment without major redesign or severe weight penalties. It was decided to eliminate the torsional shock transient as a significant design condition by designing major structural torsional frequencies outside the frequency band of 50 to 80 cps. Because of other design criteria, the AOSO torsional frequency for all experiment arrays could not be easily designed below 50 cps; therefore, the design criterion was established that the primary structure torsional natural frequency should be greater than 80 cps.

The importance of the torsional shock requirement on the AOSO design should be a caution to designers of other spacecraft to consider torsional problems very early in the design stage.

ACKNOWLEDGMENT

The support of J. Fussell of the Dynamics Subdivision in programming and running the analog computer to obtain the torsional shock response spectra is gratefully acknowledged.

REFERENCES

1. "Advanced Orbiting Solar Observatory Specification," NASA Goddard Space Flight Center, Rept. S-623-P-1, June 17, 1965
2. Cyril M. Harris and Charles E. Crede, Shock and Vibration Handbook, Vol. 1, p. 1-23. McGraw-Hill, New York, 1961
3. Robert H. Scanlon and Robert Rosenbaum, Introduction to the Study of Aircraft Vibration and Flutter, pp. 72-79. Macmillan Co., New York, 1962

Appendix

TORSION QUALIFICATION LEVEL TEST REQUIREMENTS

TORSION VIBRATION

Direction	Frequency (cps)	Level
About longitudinal axis	20-60	12.9 rad/sec^2 vector angular amplitude
	60-250	25.8 rad/sec^2 vector angular amplitude

Sweep rate: 2 octaves/min (log sweep)

TORSION SHOCK

Following the above sweep, two separate pulses shall be applied with a discrete time interval between them. Each pulse shall consist of a high frequency tone modulated by a 2.5-cps sine wave whose angular amplitude is 96.6 rad/sec^2 vector, and for a duration of one-half the period of the modulating sine wave. If a major torsional resonance of the observatory structure during the sweep test is indicated in the 60- to 75-cps band, this resonant frequency is to be used as the high-frequency tone. If no resonance is indicated in this band, 68 cps shall be used as the high-frequency tone (see Fig. 1 for a pictorial representation of this pulse).

DISCUSSION

Voice: Did you estimate the weight that would be required to raise the frequency? Would this be critical in the design of the vehicle?

Mr. Davis: Weight was critical on this vehicle; however, with the Atlas/Agena we had the possibility of an additional weight allowance. Unfortunately, the problem was solved the easy way – the program was cancelled.

* * *

COMPARISON OF PREDICTED AND MEASURED LAUNCH LOADS FOR SNAP 10A*

Everett A. Robb and A. P. Gelman
Atomics International
Canoga Park, California

The development of structural design criteria for SNAP 10A is discussed. The vibration-induced lateral bending moments critical for the SNAP 10A support structure are emphasized. The predicted loads used in design and testing of the satellite are compared with the actual loads encountered in flight.

F. A. Robb

INTRODUCTION

SNAP 10A was the first nuclear space power system launched into orbit. This system, part of the SNAPSHOT program, was developed by Atomics International (AI) for the AEC. In space, the reactor was remotely started by ground command, and the thermoelectric convertor delivered power to the satellite for 43 days. A spacecraft electrical system failure caused a premature shutdown of the reactor. A companion ground test unit successfully completed 10,000 hr of operation in March 1966 in a simulated space vacuum environment.

The SNAP 10A configuration (Fig. 1) was conical with the reactor and shield supported at the top of a semimonocoque titanium shell. The structure also supported the thermoelectric convertors and NaK piping system. An instrument compartment was attached at the lower end of the cone. The total weight of the flight unit was 960 lb, with the support structure comprising 85 lb of that total. The overall height was approximately 11 ft. The base diameter was 4-1/2 ft.

Flight test data of structural interest were acquired during the brief ascent phase of the SNAP 10A orbital test. Boosted by an Atlas/Agena launch vehicle, the SNAP 10A encountered the critical environments of acceleration, vibration, and noise that had determined most of its basic design criteria.

While the launch environment affected every component of the SNAP 10A system, it was the primary support structure that received the heaviest loading during ascent. The initial responses of the SNAP 10A to the transient events of launch were the principal source of these loads. The SNAPSHOT launch configuration had the following characteristics that distinguished it from other Atlas/Agena programs:

1. The Agena forward auxiliary racks and nose cone for SNAP 10A defined the longest Agena flight configuration to date.

2. The SNAP 10A reactor and shield subassemblies were mounted at the top of a corrugated titanium shell structure. Thus, the SNAP 10A heaviest components were cantilevered

*This work was supported by the United States Atomic Energy Commission under Contract AT(11-1)-GEN-8.

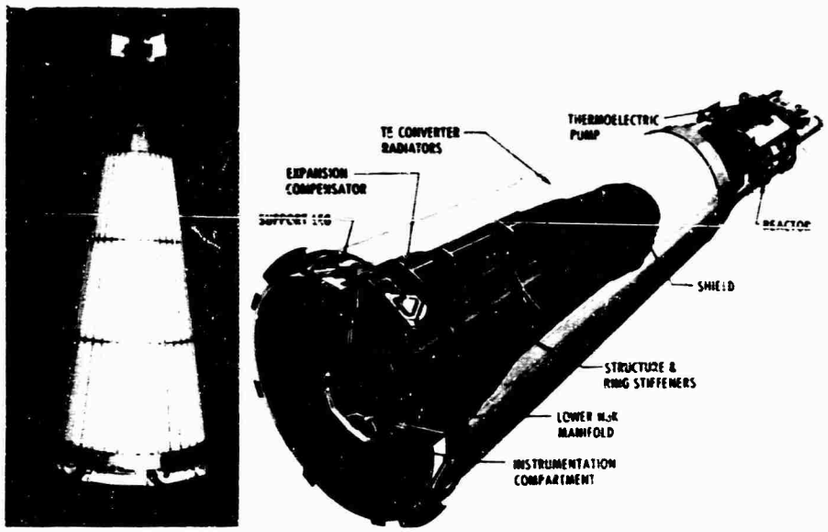

Fig. 1 - SNAP 10A system

several feet from the interface by a relatively flexible support.

The purpose of this paper is to discuss the development of the structural design criteria for SNAP 10A, and to compare measured flight test results with those criteria. The discussion is principally concerned with the vibrational aspects of the SNAP 10A loads environment.

DISCUSSION

In the early design stages of the SNAP 10A program, the structural design criteria were based on standard Agena environmental specifications. Also, at that time, AI vibration equipment was limited to sinusoidal sweep tests. Table 1 summarizes the qualification level sinusoidal vibration test specifications for the complete SNAP 10A. An important part of this specification was the response restrictions imposed, so that at the lowest frequencies the lateral response was to be limited to 2 g and the longitudinal response to 2.5 g as measured at the system center of gravity (c.g.). In other words, the specification allowed a reduction in input in the vicinity of critical resonant frequencies. Two main difficulties arose from this early specification. First, the SNAP 10A was a lumped system, with its c.g. located in space within the support shell. Thus, it was not

TABLE 1
Sinusoidal Vibration Test Inputs — Qualification Level

Test Axis	Magnitude (peak)	Frequency (cps)	Sweep Rate
Longitudinal (X-X)	[a]	5-9	Constant octave rate from 5 to 3000 cps in 25 min
	2.3 g	9-400	
	7.5 g	400-3000	
Lateral (Y-Y) and (Z-Z)	[a]	5-8	
	1.7 g	8-250	
	4.5 g	250-400	
	7.5 g	400-3000	

[a] 1/2 in. double amplitude.

possible to instrument the c.g. directly. Because of the complexity of the mode shapes, it was not possible to monitor system responses in terms of the c.g. Second, nearly every design review of the SNAP 10A, outside of those by structurally oriented groups, questioned the validity of the response restriction provisions in the vibration specifications. It soon became apparent that a specific load analysis for SNAP 10A was required, in terms of the complete launch system. By this time in the program, all of the structural parameters were known so that a good dynamic model of the SNAP 10A/Agena/Atlas launch configuration could be defined. The complete loads analysis was subsequently made to remove the arbitrariness and component level approach from vibration testing of SNAP 10A and to define realistic loads that could be simulated in the laboratory for final qualification of the structure.

ANALYSIS

A review of the overall loads situation for SNAP 10A, in terms of the program constraints that existed, indicated that a straightforward analytical approach was needed. A dynamic analysis, based on proven theoretical principles and including actual laboratory and flight test data, would be the approach most generally accepted by all concerned groups. Accordingly, in cooperation with Lockheed Missile and Space Company, the booster integration contractor, a dynamic model was established for the launch configuration. The lumped parameters that went into the model (mass, stiffness, and damping) were based on experimentally obtained values. Modal calculations were made by a modified Myklestad method. Figure 2 illustrates some of the elastic modes for the lift-off configuration. When these mode shapes were studied in terms of all flight conditions of lift-off, staging, and Agena firing, it became apparent that the low-frequency elastic responses of the system in the lateral direction would produce the critical conditions for the SNAP 10A support structure.

To predict the maximum lateral bending load for SNAP 10A, the calculated mode shapes for the system were normalized to a known acceleration level in the Agena. This level, referenced in the Agena c.g., was based on measured flight vibration data from 44 launches and was adjusted to 0.45 g. The probability of not exceeding this derived level in the low-frequency bandwidth was 99 percent. Figure 3 is an enlarged scale of the critical mode, normalized to 0.45 g at Agena station 255. It can be seen that the maximum response for SNAP

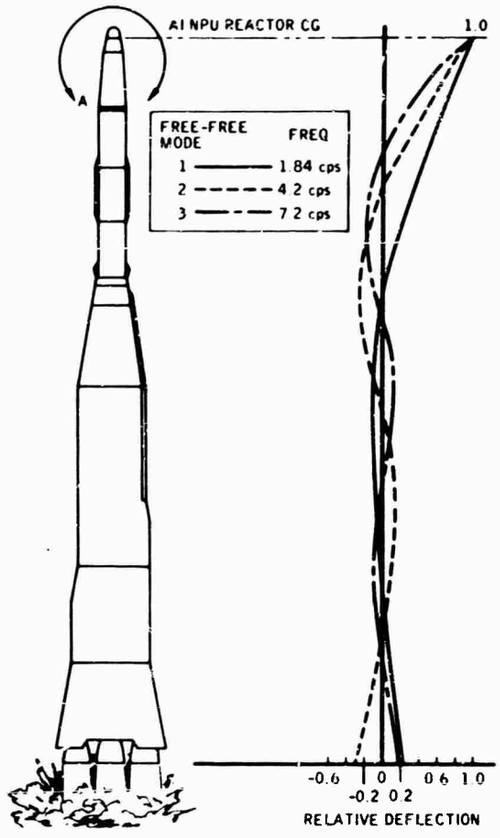

Fig. 2 - Launch configuration mode shapes normalized to maximum deflection

10A was indicated to be 3.8 g at the top of the reactor. The results of a subsequent analysis by the LMSC Agena structures people are also shown in the figure. Thus, in all SNAP 10A vibration tests at the qualification level, a fundamental maximum load limit of 3.8 g was observed at lateral frequencies below 100 cps. It can also be seen that the maximum acceleration level at the SNAP 10A system c.g. was about 1.5 g rather than 2.0 g. For acceptance test purposes, a load limit of approximately 25 percent less than qualification, or 3.0 g, was adopted.

FLIGHT TEST DATA

For the SNAPSHOT flight test, structural loading data were obtained from each of three principal axes at the SNAP 10A upper torque box, AI station 97, the SNAP 10A/Agena interface, AI station 0, and the Agena forward rack. The upper instruments were designated as AI-86 X-axis, AI-87 Y-axis, and AI-88 Z-axis.

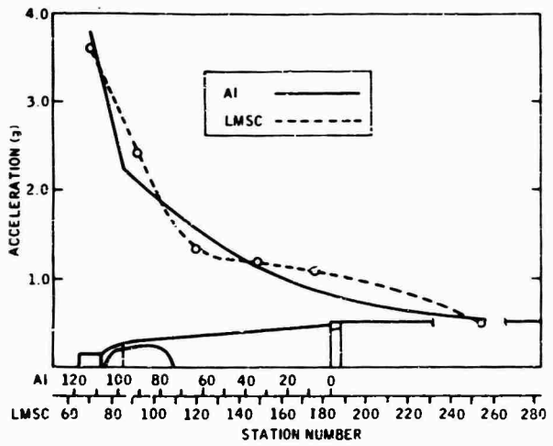

Fig. 3 - SNAP 10A maximum lateral acceleration levels

The interface instruments were designated as A-10 X-axis, A-11 Y-axis, and A-12 Z-axis. Oscillograph records of flight vibration data are shown in Figs. 4, 5 and 6 for the lift-off and Agena firing sequences. The most critical part of the flight occurred within 1 sec after lift-off when the maximum vibration-induced lateral bending moment and shear occurred at the SNAP 10A/Agena interface. Lateral loads were maximum for SNAP 10A at 9 cps in both Y-Y and Z-Z axes. The oscillograph records indicate these peak accelerations were in phase for approximately 2 sec at lift-off. Their vector sum was 2.2 g as measured at the AI-87 and AI-88 pickups. If the calculated mode shape was normalized to these data, an acceleration level of 3.3 g would be indicated at the top of the reactor. This flight test result at 9 cps was, for all practical purposes, the same structural mode for SNAP 10A that developed at 11 cps during acceptance vibration tests of the flight unit. The frequencies were different primarily due to impedance differences between a shaker slip plate, and a continuous elastic structure.

A more meaningful comparison of loads can be made in terms of lateral shear and interface bending moments, rather than indirect quantities such as frequency and acceleration

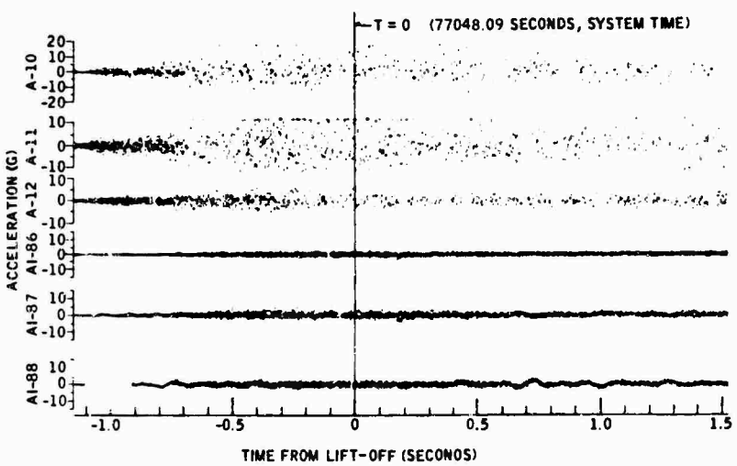

Fig. 4 - Flight vibration record -- lift-off

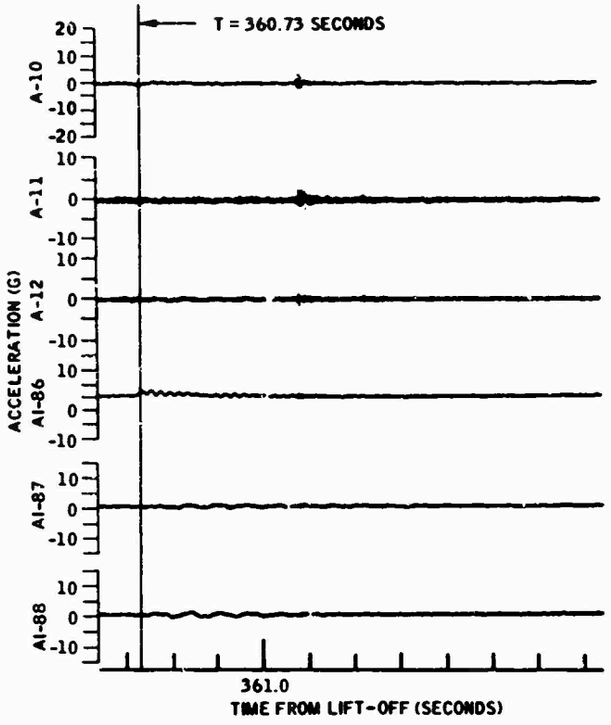

Fig. 5 - Flight vibration record — Agena first ignition

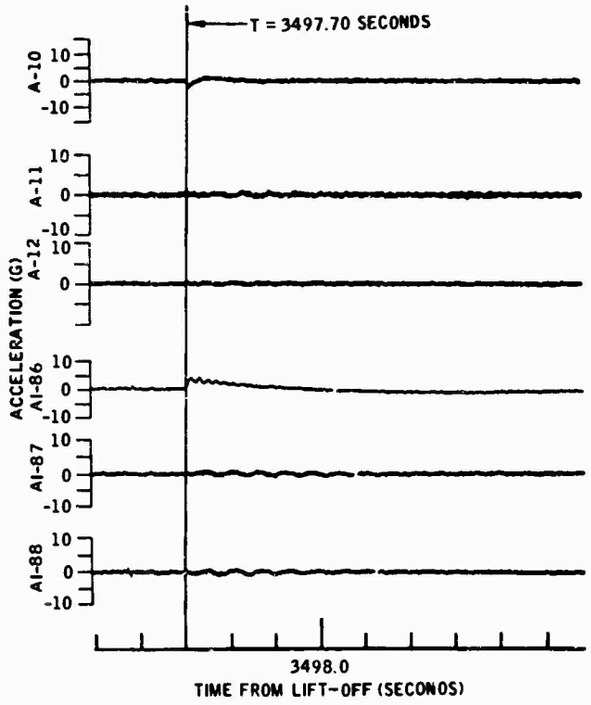

Fig. 6 - Flight vibration record — Agena second ignition

level measurements. Table 2 compares the basic flight loads with the SNAP 10A acceptance test structural loads.

CONCLUSIONS

The SNAP 10A flight test vibration data indicate that no critical design conditions were exceeded. The structural integrity of the entire SNAPSHOT vehicle was maintained during the critical ascent phase of flight. Detailed comparison of the flight test data with the design and test criteria of the SNAP 10A satellite has revealed that all loads encountered were near acceptance test levels and well within qualification levels for the system. The SNAP 10A structural design and test criteria were, therefore, near optimum for the launch environment. This flight test also verified the importance of instrumenting for responses of a total system rather than just the spacecraft interface levels. Thus, it has been possible to make realistic comparisons between flight test loads and their simulations in the laboratory.

TABLE 2
SNAP 10A/Agena Structural Interface
Lateral Shears and Bending Moments

Condition	Bending Moment (in./lb)	Shear (lb)	Remarks
Flight	171,000	1,940	9 cps elastic mode
Acceptance	165,000	1,950	11 cps vibration test

DISCUSSION

Mr. Kaplan (General Electric Co.): To what extent was your flight vehicle instrumented? How many transducers did you have? Were they over the effective length of the SNAP 10A, or were they confined to one or two locations?

Mr. Robb: There was a large vibration pickup package on the total launch configuration. We only had three at the top of the SNAP 10A, the three in the three principal axes, which were mounted in such a way that we could tell what the principal masses, that is, the reactor and the shield, would do. We had three at the interface station 0 between the Agena and the SNAP 10A, and then there was the standard Agena instrumentation at the Agena c.g. In addition, there was a large array of instrumentation which, as I understood it, was to be reduced only if the structure did not make it. We did make it, so data were not reduced, and the data I show in the report are the best and most explicit we have.

Voice: You showed a bending moment from flight. Was that estimated from the accelerometer readings using the mode shapes, or did you have strain gages on the vehicle?

Mr. Robb: No, we worked entirely with accelerometers.

* * *

GROUND-WIND-INDUCED OSCILLATIONS OF GEMINI-TITAN AIR VEHICLE AND ITS ERECTOR

John E. Tomassoni and William H. Lambert
The Martin Company
Baltimore, Maryland

Although the Gemini-Titan air vehicle appears to be a typical uncomplicated rocket structure, it does have peculiarities which cause the effect of ground winds to be rather important to its operations. Not only is this true from the standpoint of loads on the air vehicle, but also because of the limited clearance separating it from the erector used to service and protect the booster and spacecraft, as the erector is raised or lowered. To avoid interference and damage, a knowledge of the total deflections is necessary, particularly for operations in periods of high winds.

The program to evaluate the effects of ground winds on the Gemini-Titan system encompassed three phases:

1. Full-scale vibration tests in which dynamic characteristics of the air vehicle and erector were measured. The data were obtained specifically for, and used directly in, scale model design.

2. Model wind tunnel tests from which static and dynamic data were obtained for both the air vehicle and erector, covering all wind azimuths and various erector positions.

3. Measurement of full-scale wind-induced responses of the air vehicle and erector.

In the model tests, maximum base bending moments on the air vehicle were induced when it was in the turbulent wake of the erector. Dynamic responses of the model erector were small compared with static loads.

The full-scale air vehicle data correlated well with the wind tunnel results, although the full-scale data are limited with respect to range of wind velocity and direction. With respect to load magnitude, the full-scale data appear somewhat higher than model responses, possibly because of the added effects of atmospheric turbulence.

Dynamic wind responses of the full-scale erector were very small, as the model results indicated. However, the transient responses induced by mechanical operations of raising and lowering the erector unexpectedly proved so significant that a wind restriction was imposed on the erector operations when the launch vehicle was erected.

J. E. Tomassoni

INTRODUCTION

Dynamic wind-induced oscillations of erect slender structures historically have been best described by experimental methods. Except for limited regions of flow, associated with low Reynolds numbers, analytical tools for predicting the dynamic response of a specific structure to lateral fluid flow have been inadequate. Respect for the large loads which may be developed by the oscillatory response has forced designers to accept one of two possible alternatives: the inclusion of large margins of safety

or, where this is not feasible, an experimental determination of the magnitude of response with a model. In the last decade, studies of wind-induced oscillations have been expanded and accelerated by the advent of large rocket boosters. While the Gemini-Titan air vehicle appears to be a typical uncomplicated example of this type, and some progress has been made in the analytical "expectation" of problem areas, it has peculiarities which made the effects of ground winds significant to its operations. This was true not only from the typical standpoint of loads on the vehicle, but also in relation to the limited clearance between the vehicle and folded platforms on the erector during its raising or lowering operations. Additional unknowns were the effects of turbulence and vortices on the air vehicle generated by the erector and umbilical tower.

A program to assess wind-induced oscillations was, therefore, instituted early in the Gemini program encompassing three phases: (a) full-scale vibration tests, (b) wind tunnel model test, and (c) measurement of full-scale wind-induced oscillations. A descriptive outline of each of these phases follows.

FULL-SCALE VIBRATION TEST

The full-scale vibration test was conducted in two parts: one on the fully loaded air vehicle (GT-1) while it was erected on its stand at Cape Kennedy, and the other on the erector. Excitation of both structures was accomplished manually. The purpose of the full-scale vibration tests was to determine the fundamental frequencies and damping characteristics which were to be used in the design of the wind tunnel dynamically scaled models. Damping is particularly important to wind-induced oscillation test models.

Data for the air vehicle were obtained for both east-west (pitch) and north-south (yaw) planes of excitation. The first cantilevered bending frequency was the same in both planes, 0.4 cps, which correlated well with analysis. The structural damping coefficient $g = 2c/c_c$ in the N-S plane had an average value of 0.012, and in the E-W plane averaged 0.008.

Cables were used to excite vibrations of the erector manually while it was positioned in six attitudes: up-locked, up-unlocked, 11, 30, 50 and 88 deg from the vertical. The resulting frequencies, naturally different between the unsymmetrical axes of the structure, were scaled in the corresponding planes of the model erector.

WIND TUNNEL TEST

The dynamic and static loads resulting from steady winds were obtained from tests conducted in the NASA Langley 16-ft transonic dynamics tunnel. The model was in essence a 7.5 percent scale replica of the complete system complex as shown in Fig. 1. This includes a dynamically scaled air vehicle and a frequency scaled erector. The umbilical towers (primary and Stage II) and the spacecraft crane were geometrically scaled only. The air vehicle structural damping obtained from the full-scale vibration measurements was duplicated in the model with the aid of a viscous damping device developed and provided by NASA Langley.

Test configurations included the launch vehicle without the erector (simulating the prelaunch condition), the vertical and fully curtained erector, and the launch vehicle in the presence of the erector positioned at angles of 6, 33, and 50 deg from the vertical.

Instrumentation was provided for the measurement of base bending moments and tip accelerations of the launch vehicle and erector models over a range of wind velocities and directions. The wind azimuth producing the largest total (dynamic plus static) response for each configuration was investigated at velocities up to a test Mach number of 0.4, equivalent to the full-scale specification velocity limit of 47.5 mph.

The maximum base bending moment on the air vehicle occurred when it was in the wake of the erector (which was 33 deg off vertical). This condition caused the air vehicle to experience very little static load. The large dynamic load was apparently induced by a field of unsteady forces in which the body was immersed, i.e., vortices and turbulence generated by the erector rather than vortices shed from the body alone. A somewhat lower but similar response occurred when the air vehicle was in the wake of the primary umbilical tower. This wake influence was found to be sensitive to wind azimuths.

As in the case of the air vehicle, maximum dynamic responses of the erector were found to exist when it was in the wake of the air vehicle, although all dynamic responses were relatively low. Maximum total loads of the erector model were invariably static in nature, generally by large margins (65 to 95 percent of total).

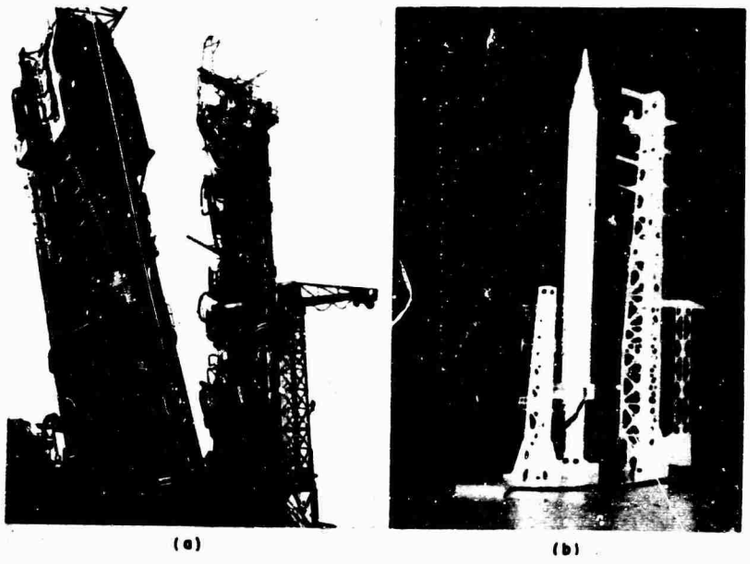

(a) (b)

Fig. 1 - (a) Gemini launch complex, and (b) 7-1/2 percent wind-induced oscillation model

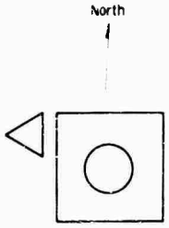

Fig. 2 - Schematic illustrating relative proximity of launch vehicle erector and umbilical tower

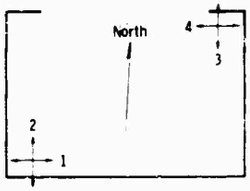

Fig. 3 - Location and orientation of CVE accelerometers, 109-ft elevation

FULL-SCALE WIND-INDUCED OSCILLATION TEST

Test Setup

A measurement system was set up at Pad 19 from which wind-induced oscillatory responses were obtained on the first five Gemini launch vehicles and the complete vehicle erector (CVE). Figure 2 illustrates the relative proximity of the structures. The launch vehicle responses were measured during the "wet mock" simulated launch and prelaunch periods when the vehicle was completely assembled, fueled, and the erector retracted. Loads data in the form of bending moments and side forces in both the pitch and yaw planes were obtained from load cells located at the base of the vehicle support frame. The data were recorded, without interference to the launch operations, on magnetic tape regardless of ground wind conditions and were presented for analysis in strip chart form. The output of 2-g accelerometers located in the vicinity of the spacecraft/launch vehicle interface was also recorded, but their signal strength was not sufficient for accurate analysis.

Responses of the erector to ground winds were recorded on a slow-speed strip chart using four accelerometers located at the 109-ft elevation. These were oriented as illustrated in Fig. 3. Although this system could operate unattended for a 24-hr period, its primary function was to obtain data when the wind velocities were in excess of 20 mph.

Continuous measurements of wind velocity and direction were also recorded on the slow-speed recorder using a wind vane anemometer and two NASA-developed drag spheres. These

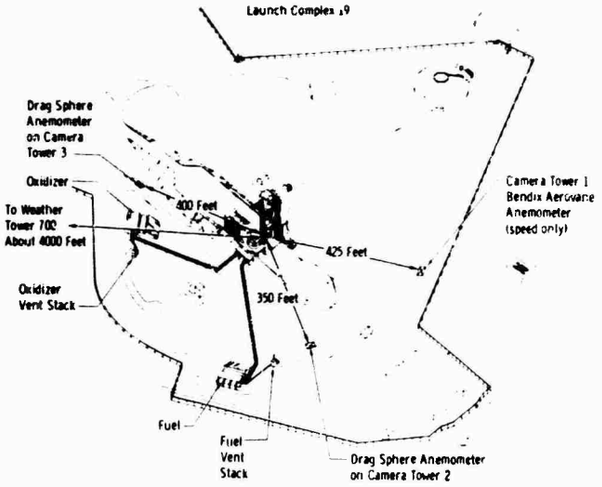

Fig. 4 - Anemometer locations

Fig. 5 - Aerovane anemometer installation, Tower No. 1

were mounted 57 ft above the ground on towers located on the complex as shown in Fig. 4. A typical tower installation is shown in Fig. 5. All measurements were time correlated. Supplementary data from meteorological towers were also used.

Results for Launch Vehicle

The launch vehicle bending moment data obtained from the load cell system (corrected to vehicle base bending moments through vibration modal analysis) are shown in Fig. 6. These

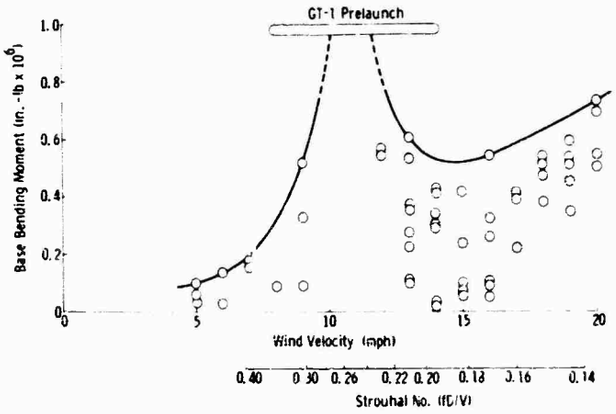

Fig. 6 - Full-scale wind-induced oscillatory loads

data represent the total amount obtained and are not defined with respect to wind direction. Note that the maximum recorded wind velocity was 20 mph. Although the data are somewhat scattered, the existence of a response trend associated with the discrete vortex shedding phenomenon is evident in that the peak response occurs close to the critical Strouhal number of 0.22 for circular cylinders. The wind vectors which produced these bending moments are illustrated in Fig. 7. The symbols indicate the direction in which the wind was blowing.

A correlation of the full-scale data with the model test results is presented as a function of wind azimuth in Fig. 8. In this figure, the upper curve represents an envelope of maximum base bending moments obtained from the model tests for the design wind velocity of 47.5 mph. The symbols represent the same full-scale data contained in Fig. 6. Since the maximum full-scale wind velocity occurring during data measurement was 20 mph, it appears that the model data may be unconservative, particularly for the wind azimuth of 135 deg and the GT-1 data point at 176 deg. Full-scale responses may have been increased because of an unknown level of low-frequency turbulence. Note that the maximum model loads occurred in the azimuth range of 300 to 340 deg, where the primary umbilical tower is generally upstream of the launch vehicle. The relative proximity of the tower to the vehicle is illustrated in Fig. 2. For this wind azimuth region, a correlation of full-scale data with model test results as a function of wind velocity is presented in Fig. 9. The model data were obtained for a constant wind azimuth of 325 deg, and the full-scale data cover an azimuth range of 285 to 360 deg. For the limited amount of full-scale

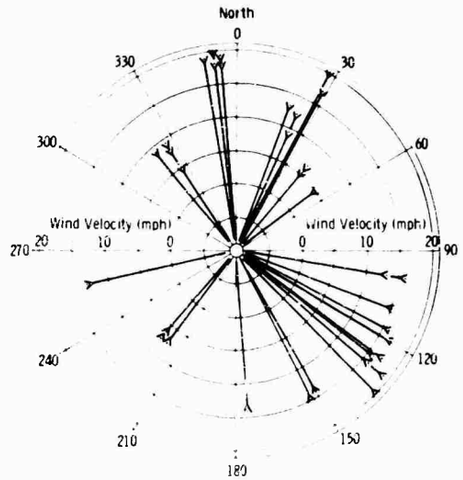

Fig. 7 - Gemini wind exposures

data obtained in this range, the correlation appears to be reasonably good.

The maximum measured full-scale base bending moment was 980,000-in.-lb, which is well within that allowed for wind-induced oscillations. However, projecting the full-scale data to the design wind velocity of 47.5 mph (neglecting effects of turbulence), the bending moment would exceed the model data by approximately 150 percent, thus bringing the wind-induced oscillatory loads to within 3 percent of that allowable.

The maximum full-scale deflection at the spacecraft/launch vehicle interface based on

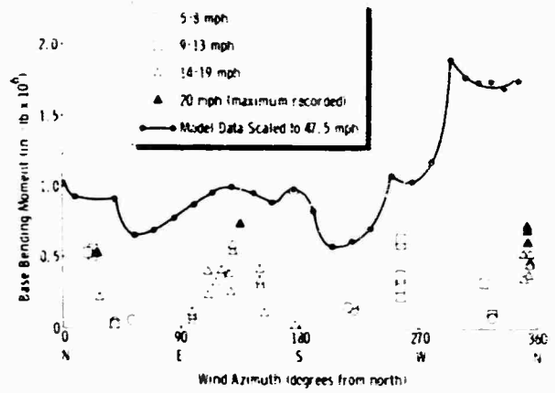

Fig. 8 - Correlation of full-scale wind-induced oscillatory loads with model test results

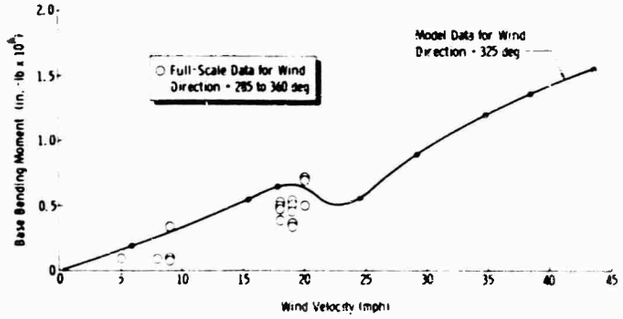

Fig. 9 - Correlation of full-scale Gemini wind-induced oscillatory loads with model test results

vibration modal data under the observed conditions was only ± 0.36 in.

To supplement the Gemini launch vehicle full-scale data, dynamic wind-induced base bending moments were obtained from a series of Titan II military rocket vehicles. The significant differences which existed between the Gemini and Titan II were the shape of their respective payloads (nose shape) and the fact that certain packages were externally mounted on some of the Titans just forward of the staging plane. The corresponding wind data were obtained from meteorological tower measurements.

It was determined that the base bending moment response trend with wind velocity for the Titan II is quite similar to the envelope of Gemini data. A comparison is shown in Fig. 10. The solid symbols represent the "clean" Titan (no external packages), which mose closely resembles the Gemini. The open symbols for the Titans with external packages contain illustrations of their approximate location. The arrows on these symbols indicate the wind azimuth for each data point. This effect has not been isolated from the results.

Results for Complete Vehicle Erector

The erector responses to various wind conditions in the upright and locked position were obtained between 27 August 1964 and 15 July 1965. A 350-deg wind at 45 mph which included low-frequency gusts was the maximum recorded during this period. The wind vectors are displayed in Fig. 11, with the symbols indicating the direction in which the wind was blowing.

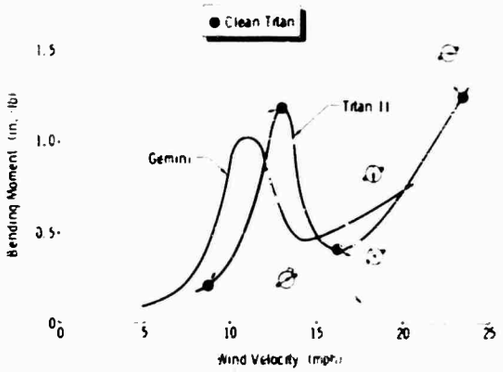

Fig. 10 - Comparison of Titan II with Gemini wind-induced oscillatory bending moments

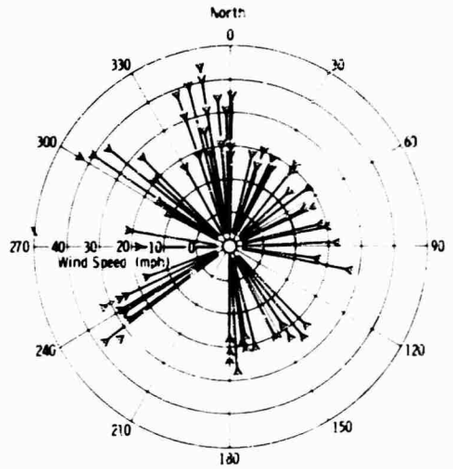

Fig. 11 - CVE recorded wind vectors

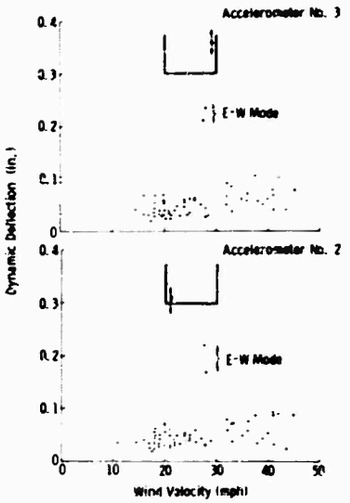

Fig. 12 - Full-scale erector wind-induced oscillatory responses, north-south mode

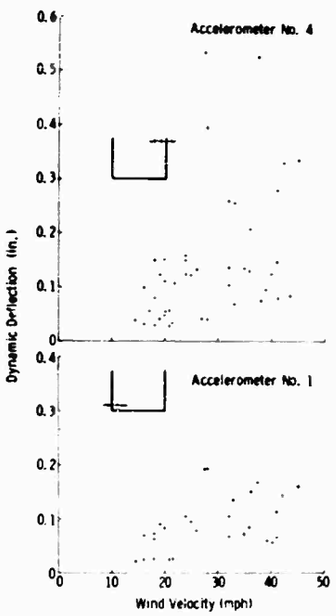

Fig. 13 - Full-scale erector wind-induced oscillatory responses, east-west mode

The resulting erector responses were small as indicated by the data in Figs. 12 and 13. These data were obtained from the four accelerometers mounted at the 109-ft elevation. Although the data are quite scattered, their envelope suggests a general increase of response with increasing wind velocity as would be expected. These data have also been examined to determine an effect due to wind direction because of the rectangular erector shape and differences between the modes of the east-west (E-W) and north-south (N-S) planes. No conclusive trends were evidenced except that the E-W modal amplitudes were, in general, greater than those of the N-S mode regardless of wind direction. The E-W mode, which is a coupled bending-torsion mode, is different from the N-S mode because the erector is nonaxisymmetric in both weight and stiffness. The corresponding frequencies are 0.75 and 1.25 cps, respectively.

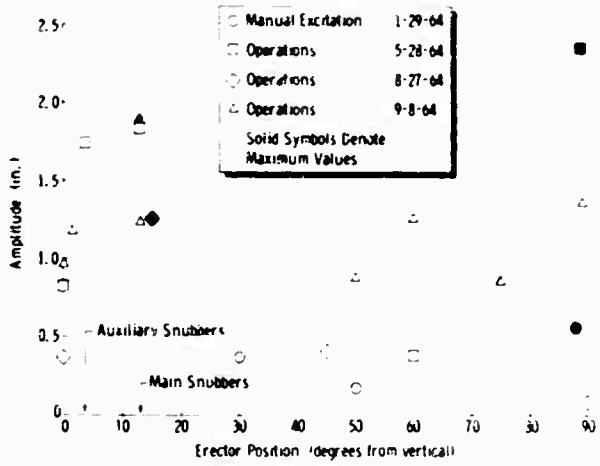

Fig. 14 - Erector dynamic amplitudes, 109-ft elevation

The maximum measured displacement was ±0.53 in. which occurred on accelerometer No. 4 in the E-W mode. It is of interest to note that the maximum response on all accelerometers occurred at 27.5 mph with the wind from 234 deg. Since this response was evident on all accelerometers, the torsional aspect of the mode is indicated.

The response amplitudes of the erector under the recorded wind exposures were, in reality, very small, and the data scatter did not allow for an adequate trend correlation with the wind tunnel model test results. However, the full-scale measurements were in the same order of magnitude as those obtained from the model tests, both indicating low-wind-induced dynamic loads.

Results - Clearance

A knowledge of the total relative deflection between the air vehicle and the erector work platforms, resulting from both static and dynamic behavior, was required so that maximum allowable winds could be determined for safe erector operations, particularly if the erector was to be raised to protect the vehicle from high winds.

Records taken during the full-scale wind-induced oscillation program disclosed that the erector dynamic response to transients induced by raising and lowering operations were significant. This necessitated the examination of their effect on the clearance between the erector and vehicle.

The minimum clearance occurred when the erector was approximately 3.5 deg from the vertical which was also the position at which transients were induced by engagement of the auxiliary snubbers. The critical structure on the erector was the easternmost corner of a kickplate protruding from the double folded work platform on the northwest corner of the 91-ft elevation. The critical vehicle structure was a spacecraft/launch vehicle mating lug. The maximum nominal clearance at this point was 4-1/8 in. with no wind loads.

The erector frequencies and accelerations were obtained from the same four accelerometers described previously, and corresponding deflections were calculated. The results from a series of erector operations revealed that an amplitude of ±1.75 in. occurred at the erector critical clearance position (3.5 deg) in the E-W mode which was, of course, the direction critical to the clearance problem. The maximum operational transient data are summarized in Fig. 14 for the various erector positions at which transients occurred. The amplitudes generated during the manual excitation test are also indicated on the figure.

The operational transient amplitudes, when combined with deformations due to winds (steady plus gust) and wind-induced oscillations and corrected to the critical clearance elevation by vibration modal analysis, resulted in a maximum allowable wind of only 22 mph from the west. This was the wind under which the erector could be operated without making contact with the erected air vehicle. This, of course, was based on the total relative deflection

between the erector and the air vehicle under the same wind environment. Also included in this clearance analysis were misalignment tolerances.

Since the 22-mph wind velocity was considered to be much too restrictive, a simple modification to the kickplate was introduced, increasing the undeformed clearance to 7-1/2 in. This allowed the westerly wind restrictions to be increased to 41.5 mph which was sufficiently close to the air vehicle design wind speed of 47.5 mph. Clearance was nonrestrictive for all other wind directions.

CONCLUSIONS

Based on the results obtained from the wind-induced oscillation test program, both model and full scale, several conclusions were drawn.

Gemini Launch Vehicle

1. Under the design wind conditions, the maximum base bending moments were found to exist when the vehicle was in the turbulent flow field generated by the erector when it was 33 deg from the vertical. This indicates that the effect of nearby structures may be more significant than that of vortices shed from the body alone.

2. The trend of the measured full-scale dynamic data correlated well with the dynamically scaled model wind tunnel test results, although the full-scale data are somewhat limited with respect to wind velocity and direction. The model data appear to be unconservative in load magnitude, particularly for the southeasterly winds. However, the full-scale data projected to the design wind velocity, neglecting effects of turbulence, are still within the wind-induced oscillatory limit allowed.

3. A trend of increasing response exists with increasing wind velocity, and a peak response occurred close to the critical Strouhal number, $(fd)/V$, of 0.22 for circular cylinders.

4. The maximum dynamic bending moment experienced by the vehicle was 980,000 in.-lb which was 52 percent of the wind-induced oscillatory design limit. This occurred near the critical Strouhal number under a southerly wind of 8 to 14 mph.

Complete Vehicle Erector

1. Responses of the erector due to winds were observed in its first two structural modes (E-W and N-S). The largest responses, in general, occurred in the E-W mode (0.75 cps) regardless of the wind direction. The maximum amplitude was ±0.53 in. at the 109-ft elevation in the E-W mode.

2. Loads resulting from the wind-induced oscillations on the erector were very low.

3. Raising and lowering the erector induced responses greatly exceeding those caused by winds. These significantly contributed to an operational westerly wind restriction of 41.5 mph when the launch vehicle was erected.

DISCUSSION

Mr. Lyon (Bolt Beranek & Newman): Did your meteorological data show any significant wind profile near the ground, and if so, was there any attempt to simulate nonuniform wind as a function of height in the wind tunnel test?

Mr. Tomassoni: No, we took the wind tunnel test as it was for the winds as they were. Meteorological data were available to show profile data, but we did not consider this. Our reference point was the 57-ft level.

Mr. Lyon: Do you remember what variation there would have been over the height of the vehicle?

Mr. Tomassoni: Yes. The variation was not really very significant. It was slight from about 20 ft on up. The meteorological data were actually based on 5-min averages, so at a given instant there could have been significant changes.

Mr. Runyan (NASA Langley Res. Ctr.): In addition to this wind gradient, there is turbulence in the atmosphere. Of course, we spend millions to build wind tunnels having no turbulence, and now we would like to test with turbulence in the tunnel. So actually at Langley we are working on procedures not only to duplicate the wind profile which increases from zero on

the ground, but also to duplicate turbulence. We have not come up with a device yet that will fit into our 16-ft tunnel, but we are doing it with small scale models.

Mr. Tomassoni: Our data indicated that turbulence was pronounced in the extremely low frequency region and that it did not necessarily couple with the frequencies of the structure.

* * *

NOISE LEVEL MEASUREMENTS FOR IMPROVED DELTA, ATLAS/AGENA-D, AND TAT/AGENA-D LAUNCH VEHICLES

Lloyd A. Williams and William B. Tereniak
NASA Goddard Space Flight Center
Greenbelt, Maryland

This paper presents acoustic noise data obtained during the launch of three vehicles: the improved Delta, the TAT/Agena-D, and the Atlas/Agena-D. Acoustic noise data obtained within the shroud during major flight events, i.e., lift-off, transonic, and maximum dynamic pressure, are presented as well as levels measured external to the shroud during lift-off. Data comparisons of the various measurements, i.e., internal to external, vehicle to vehicle, and acoustic signature to spacecraft vibration signature, are made for the times of interest.

L. A. Williams

INTRODUCTION

Of the many mechanisms that cause random vibrations in spacecraft during launch, the sound field of the rocket engine during subsonic flight, especially during lift-off, is considered to be the primary generator of random vibrations measured in the spacecraft area. The other significant source is generated by aerodynamic buffeting and boundary layer turbulence at Mach 1 and the max Q periods of flight. In the past year, acoustic sound pressure level (SPL) and vibration measurements were made during the launch of three Goddard Space Flight Center spacecraft to establish design and environmental test criteria for later spacecraft. The vehicle/spacecraft configurations studied were the improved Delta (TAD)/OT-2 spacecraft, the thrust-augmented Thor (TAT) Agena-D/OGO-C spacecraft, and the Atlas/Agena-D/OAO spacecraft.

Acoustic noise data obtained within the shroud during the major flight events of lift-off, transonic, and max Q are presented, as well as levels measured external to the shroud during lift-off. Also given are vibration data measured at the spacecraft/adapter interface.

Data comparisons are made of the various measurements, i.e., internal to external acoustic noise, vehicle to vehicle acoustic noise, and acoustic signature to vibration signature. The comparisons are made to establish the noise reduction properties of the Nimbus shroud, to compare the noise spectra measured as a function of the vehicle and launch pad configurations, and to establish any similarities between the noise spectra and vibration spectra.

VEHICLE CONFIGURATIONS

Improved Delta (TAD)/OT-2 Spacecraft

The launch vehicle was a three-stage DSV-3E Delta vehicle designated Delta-37. The first stage (S/N 20204) was a modified liquid-propellant Thor booster powered by a Rocketdyne engine system rated at 172,000 lb of thrust at sea level. Three strapped-on Thiokol TX33-52 solid-propellant motors of 54,000 lb thrust each augmented the main engine to provide lift-off thrust in excess of 330,000 lb. The second stage (S/N 20203) was an Aerojet-General liquid-propellant engine system rated at 7800 lb of thrust in a vacuum. The third stage was

an Allegany Ballistics Laboratory X258-C4 solid-propellant motor (S/N RH-92) rated at 6000 lb of thrust in a vacuum.

The spacecraft shroud was of the Nimbus configuration made of epoxy-fiber glass material approximately 0.100 in. thick over its cylindrical portion and thicker at the forward end. The shroud diameter was 65 in.

Thrust-Augmented Thor (TAT) Agena-D/OGO-C Spacecraft

The thrust-augmented Thor booster used for OGO-C launch is considered identical to the one used during launch of OT-2. The Agena-D 6801 was used as the second stage. The shroud was of the Nimbus type and is considered identical to that used on the improved Delta, with the exception that a 3/4-in. microquartz felt thermal blanket was attached to the inside circumference of the OGO-C shroud from stations 110 to 210.

Atlas/Agena-D/OAO Spacecraft

The Atlas-D (LV-3A) booster/sustainer configuration produces 386,562 lb of thrust at lift-off. The Agena-D second stage was identical to that of the TAT/Agena-D used for launch of OGO-C. The shroud used for the OAO launch was considerably different from the Nimbus in that it was made of a high-temperature-phenolic/fiber glass honeycomb sandwich with a nominal thickness of 1.75 in. Shroud diameter was 120 in. as contrasted to the 65-in. diameter of the Nimbus shroud.

TRANSDUCER LOCATIONS

During launch of the OGO-C spacecraft, two microphones were mounted on the umbilical mast to obtain SPL's external to the shroud during lift-off; no internal SPL's were measured. Figure 1a shows an elevation view of the microphones located opposite to vehicle stations 172 and 247. The microphones were located 11 ft 5 in. from the yaw axis and 4 in. down range of the pitch axis. Also shown are accelerometer locations.

The Tiros OT-2 spacecraft contained a microphone mounted within the vehicle shroud at station 130 to measure internal SPL's. A second microphone was mounted on the umbilical mast to measure external SPL's during lift-off. Relative locations of the two microphones are given in Fig. 1b. No vibration

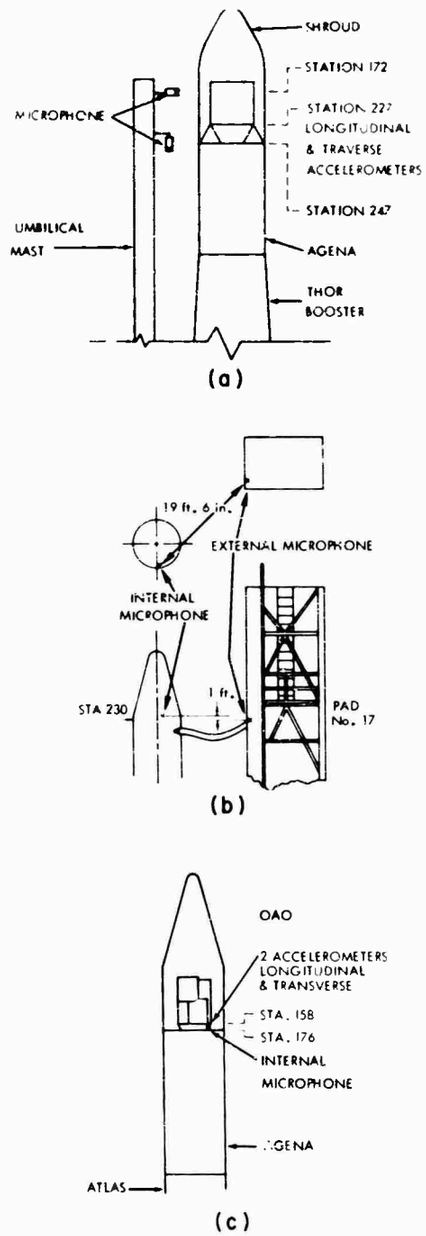

Fig. 1 - Microphone locations: (a) Thor Agena, OGO-C; (b) Delta, OT-2; and (c) Atlas Agena, OAO

measurements were made in the spacecraft area.

The OAO was instrumented with one internal microphone mounted on the spacecraft

adapter at spacecraft station 174. Figure 1c illustrates its relative location, as well as the accelerometer locations.

DISCUSSION AND RESULTS

The rocket engine exhaust and aerodynamic disturbances are the principal sources of the high-intensity noise environment for launch vehicles. During the lift-off phase, the rocket engine exhaust is the major source. Maximum internal acoustic noise levels were registered during this time period (T + 0 to T + 2 sec). The internal acoustic spectrum during lift-off is affected by the type of rocket booster (i.e., thrust output, nozzle diameter, number of engines, etc.), launch pad structural configuration, the topography of the local terrain, noise reduction properties of the shroud, and acoustic properties of the interior volume.

After lift-off, the maximum in-flight internal acoustic noise levels occurred during transonic and maximum dynamic pressure flight times and were lower than those measured at lift-off. The in-flight noise levels are generated by shock wave and separated flow effects over the vehicle body. These in turn are dependent on the shroud configuration, vehicle angle of attack, atmospheric conditions, noise reduction properties of the shroud, and acoustic properties of the interior volume.

TAT/Agena-D

During launch of the OGO-C, maximum overall (OA) external SPL's measured about 148 db over a bandwidth of 10 Hz to 10 kHz, between T + 0 and T + 1.25 sec. A graph displaying the spectral levels (octave bands) for the two microphone locations is given in Fig. 2.

Maximum levels were determined to be in the 400-Hz octave band for both microphones, and the octave band SPL's were 144.5 and 142.5 db for stations 247 and 172, respectively. Station 172 is approximately 85 ft above main engine nozzle exit plane. Station 247 is 76-3/4 ft above the nozzle exit plane. The octave band levels fall off on both sides of the 400-Hz octave band; however, it is noted that there is a significant increase in the 12.5-Hz band. The wave shape of the low-frequency data (<20 Hz, termed infrasonic region) is given in Fig. 3 for both microphones during OGO-C lift-off. The cause of this low-frequency noise is attributed to the ignition transient of the three solid-propellant motors rather than the main engine ignition.

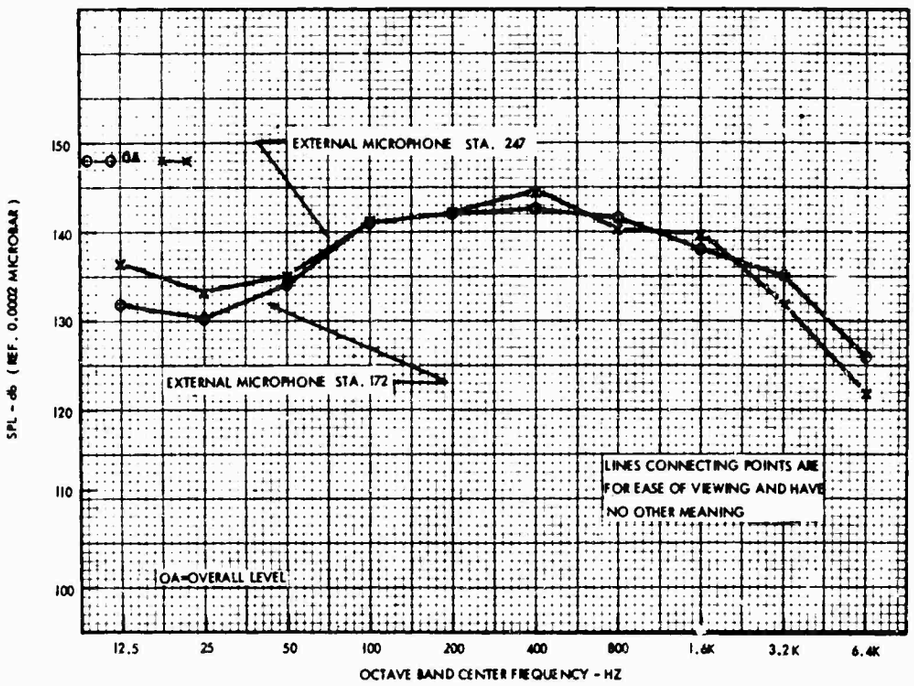

Fig. 2 - OGO-C Thor-Agena octave band acoustic noise level

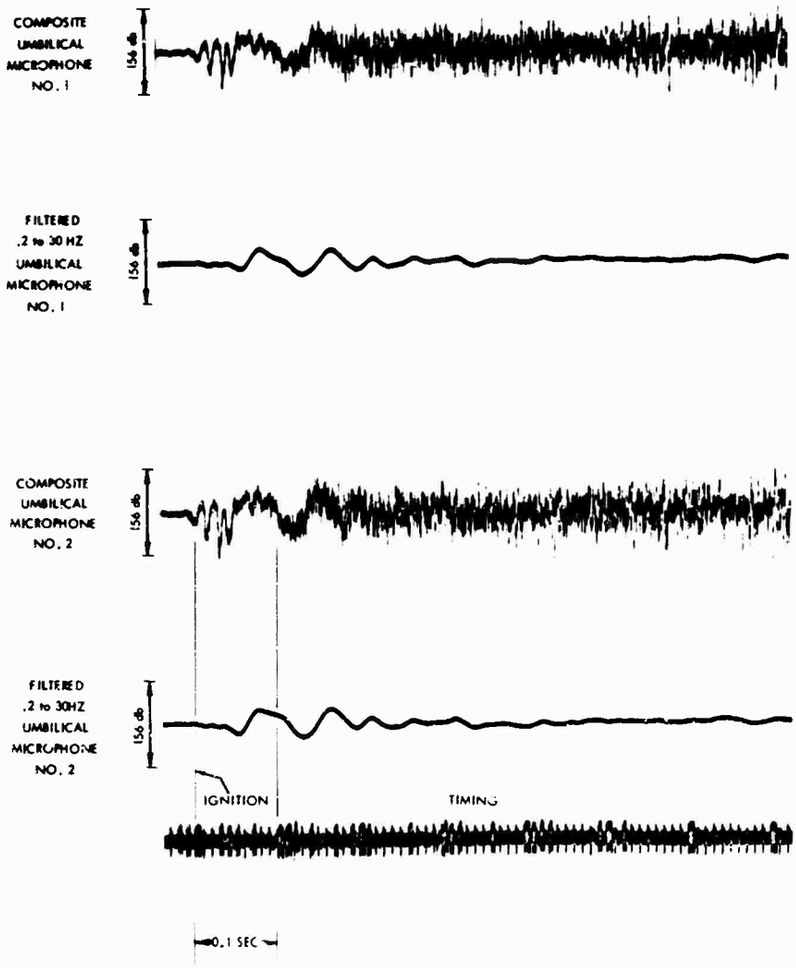

Fig. 3 - OGO-C Thor-Agena peak sound pressure

Chamber pressure traces of the solids show a buildup in pressure in less than 0.1 sec, whereas the main engine pressure buildup takes 0.4 sec. Therefore, since the maximum noise level in the 12.5-Hz octave band occurs within 0.1 sec after solid ignition, this low frequency can only be attributed to the solid-propellant motors. Similar low-frequency responses of internal and external SPL measurements have been measured during the TAD launch and are cited below.

TAD

A graph of acoustic noise level (db) vs octave band center frequency of the microphone data obtained during OT-2 launch is displayed in Fig. 4. The plotted values consist of internal and external microphone data at lift-off and also internal microphone data from the transonic and max Q portions of flight. Maximum overall noise level measured during lift-off was 138 db (10-Hz to 10-kHz bandwidth) for the internal microphone. The maximum internal OA SPL during transonic was 133 db (10 Hz to 10 kHz). The highest octave band levels obtained from the internal microphone were 132.5 db at 800 Hz and 130.5 db at 400 Hz during lift-off and transonic, respectively. Also shown on this graph are octave band levels during the max Q portion of flight. A pronounced shift in the acoustic energy from lower to higher frequencies can be seen as the vehicle passed from transonic to the max Q portion of flight.

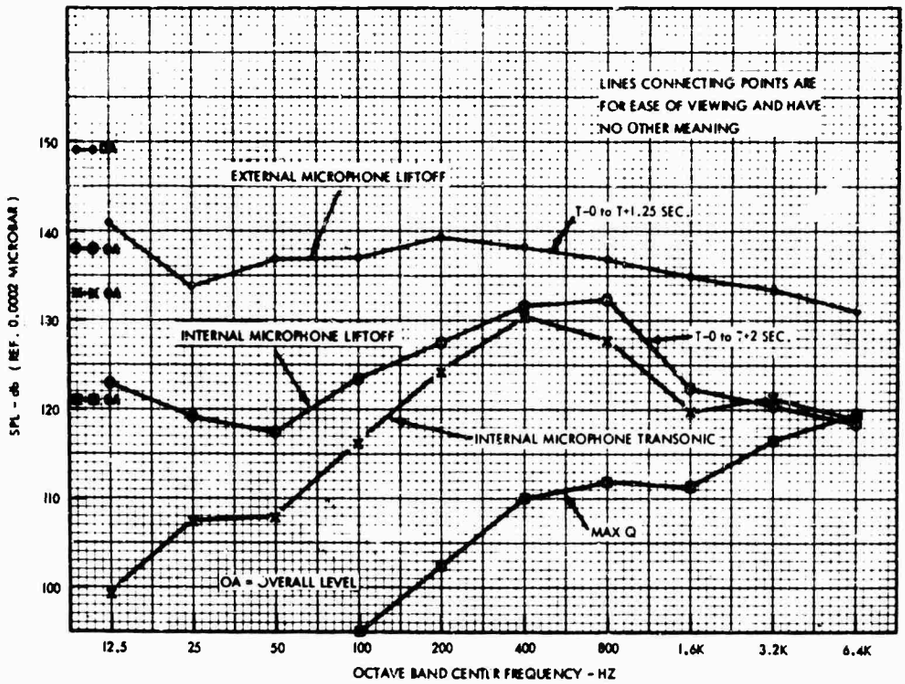

Fig. 4 - OT-2 improved Delta octave band noise level

The maximum overall noise level measured during lift-off was 149 db (10-Hz to 10-kHz bandwidth) for the external microphone. The highest octave band level obtained from the external microphone was 141 db at 12.5 Hz. The waveshapes (filtered traces) of these low-frequency data are shown in Fig. 5 for the internal and external microphones at lift-off; also shown are composite (unfiltered) traces of the two microphones. The shroud microphone signal is clipped between T + 0.3 and T + 0.5 sec. The similarity of the infrasonic data of both microphones is quite apparent. Also significant is the comparability of Fig. 3 with Fig. 5. This comparison is not too unexpected since the OGO-C and OT-2 launch vehicles utilized identical boosters (thrust-augmented Thor), but different launch pad configurations. Noise levels of launch pads of different configurations are compared later in this paper.

Atlas/Agena-D

Figure 6 is a display of internal acoustic noise level vs octave band center frequency for the Atlas/Agena-D/OAO. The graph displays results obtained during lift-off, transonic, and max Q portions of flight. The maximum overall levels were 136.5, 128.5, and 122.6 db for lift-off, transonic, and max Q, respectively, for a 10- to 1600-Hz bandwidth. Maximum octave band levels were 134 db at 400 Hz during lift-off and 122 db at 1600 Hz during transonic. The maximum octave band level during max Q was 119 db at 1600 Hz.

Pad Configuration Effects

Presented in Figs. 7 and 8 are comparisons of the near field acoustic noise levels generated by the thrust-augmented Thors (TAD and TAT/Agena-D) on two launch pads of different configurations. The TAD vehicle was launched from an ETR (Cape Kennedy) pad. The exhaust from the main engine and the three strap-on solid-propellant motors pass through the launch deck level to a water-cooled 90-deg deflector plate. The bottom of the plate is at ground level. The TAT/Agena-D was launched from a WTR (Vandenberg) pad. At this pad the main engine jet gases are exhausted into a water-cooled 90-deg bucket deflector which exhausts the jet gases into a trench. The jet gases from the three strap-on solid-propellant motors exhaust directly onto the three sliding plate deflectors located at the launch level. These

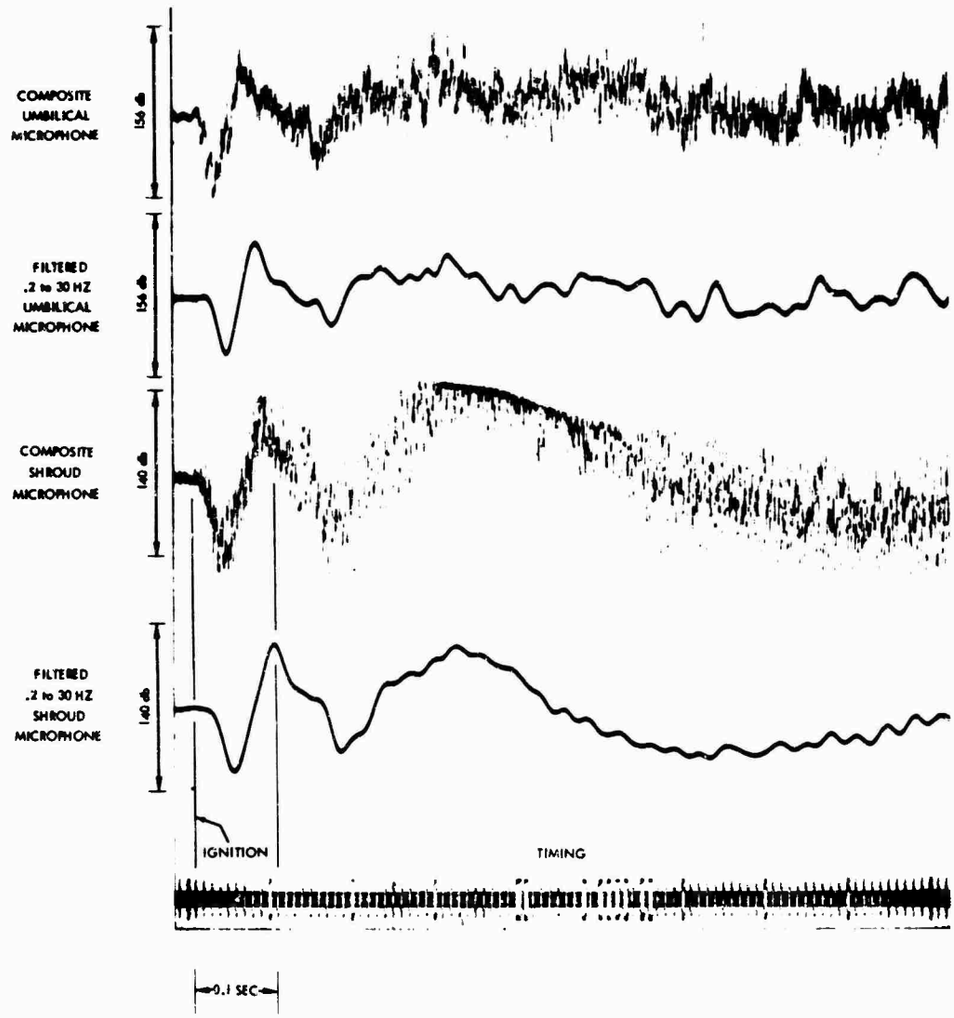

Fig. 5 - OT-2 improved Delta peak sound pressure

sliding plates are not water-cooled and deflect the jet gases back up at an angle slightly above the horizontal. The OA and octave band levels are influenced by these differences in pad design. Figure 7 is a plot showing the comparison of the acoustic noise measured by the umbilical microphones during T + 0.2 to T + 0.3 sec (altitude 0.7 to 1.6 ft). The acoustic noise levels above the 80-Hz center frequency band are generally greater for the TAT/Agena launch than the TAD launch. This phenomenon may be explained by the reduction in source-to-receiver distances brought about by jet gases of the solid-propellant motors deflecting upwards on the launch level rather than those exhausting on the lower level plate deflector. Also, with a lower level plate deflector for the solid exhaust stream, some of the noise source lies under the platform with respect to the umbilical microphones. These are usually high-frequency sources, and platform (launch level) shielding would result in lower SPL in this frequency band [1]. Figure 8 shows the same microphone data comparison at T + 0.8 to T + 1.2 sec (altitude 11.5 to 26 ft).

Comparison of Internal Noise

Figure 9 is a graph showing the internal SPL at lift-off and transonic for the Atlas/Agena-D and TAD vehicles. At lift-off the

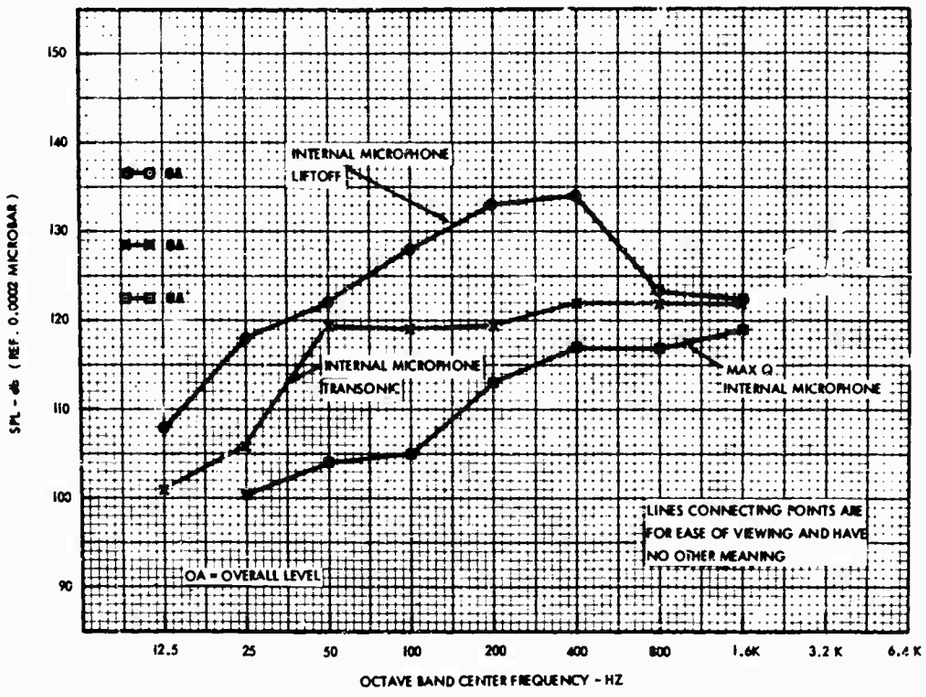

Fig. 6 - OAO Atlas/Agena octave band acoustic noise level

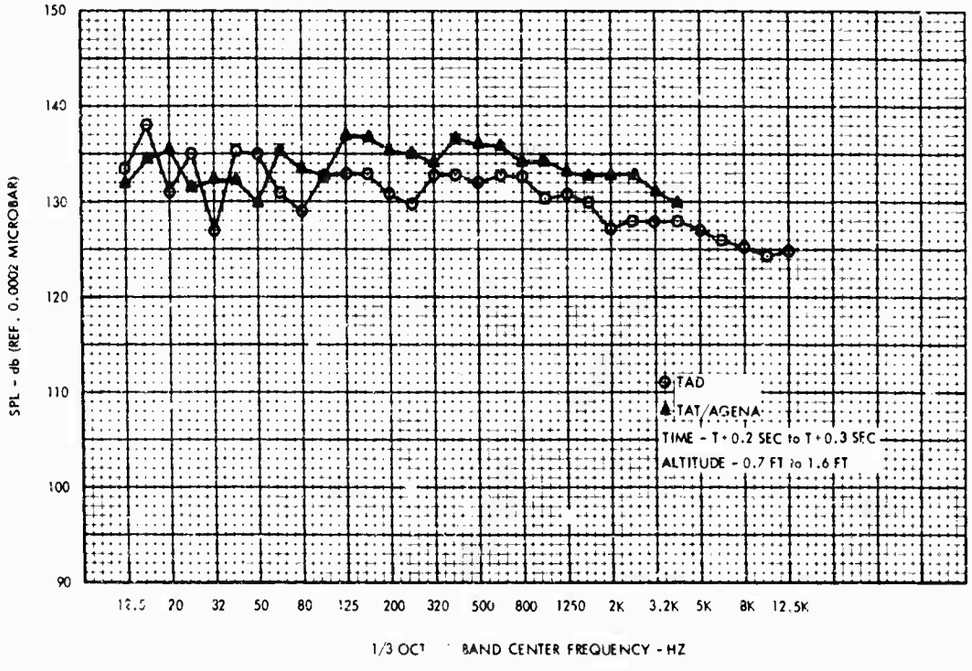

Fig. 7 - Comparison of noise levels between TAD and TAT/Agena launch pads (T + 0.2 to T + 0.3 sec)

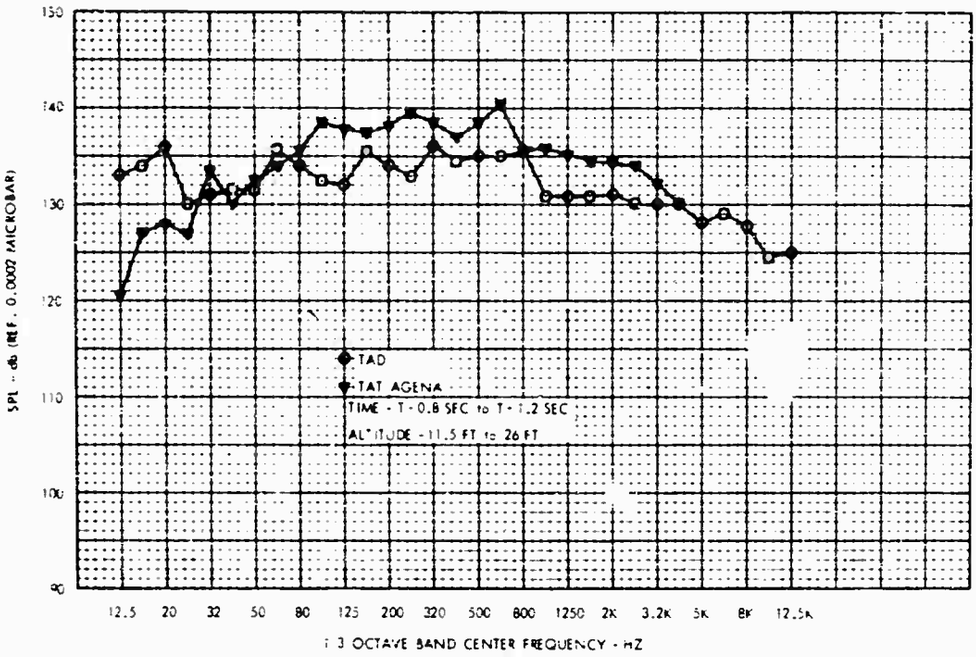

Fig. 8 - Comparison of noise levels between TAD and TAT/Agena launch pads (T - 0.8 to T - 1.2 sec)

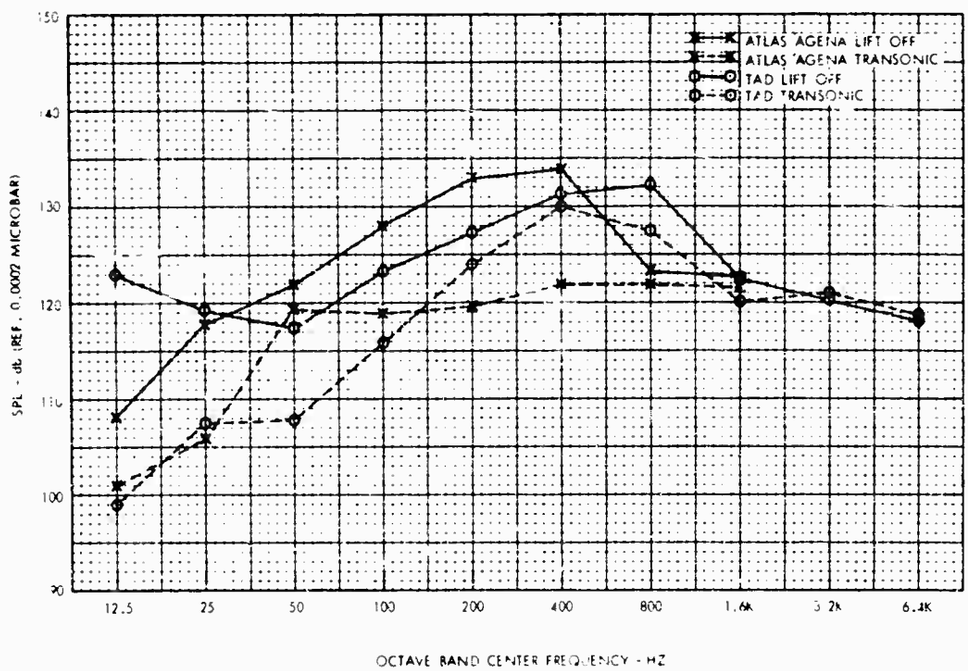

Fig. 9 - Comparison of noise levels inside vehicle shrouds (TAD and Atlas/Agena)

graph shows the maximum noise levels in the 400- and 800-Hz octave band for the Atlas/Agena-D and TAD, respectively. These bands contain the ring frequencies of the two types of shrouds. The ring frequency for cylindrical shells is defined as the frequency where the longitudinal wavelength is equal to the circumference of the cylinder [2]. The ring frequency is equal to the shell material's longitudinal wave speed divided by the circumference of the cylinder. The TAD lift-off curve would approach the slope of the other curves in the 12.5- and 25-Hz bands if the first 0.3 sec of data (ignition noise transient) are ignored. This can be seen in Fig. 5. Figure 9 also shows a greater SPL for the TAD vehicle than for the Atlas/Agena at transonic.

Nimbus Shroud Attenuation

Nimbus shroud acoustic attenuation vs octave bands, based on measurements of the shroud and umbilical microphones, is presented in Fig. 10 at T + 0.2 and T + 1.0 sec. This graph shows an attenuation of 5.5 to 6 db in the 800-Hz center frequency octave band. The ring frequency for this shroud is located in this octave band.

Comparison of Noise and Vibration Spectra

Figure 11 presents plots of external mean squared sound pressure density and the mean squared acceleration density in the longitudinal and transverse directions at the spacecraft/adapter interface during lift-off of the TAT/Agena-D. The frequencies less than 100 Hz shown in the acceleration traces are attributed primarily to the vehicle longitudinal and bending modes excited by impulses of main engine and solid motor ignitions. The higher frequencies are primarily attributed to the response of the spacecraft/adapter interface to acoustic excitation with maximum levels observed in the 500- to 1000-Hz band. This is in the region of the ring frequency of the Nimbus shroud which was calculated to be approximately 660 Hz. Figure 11 shows that the comparison of acceleration spectra with the external SPL spectra is quite poor. This is not very surprising, since the shroud is transparent to only certain frequencies.

Some of the vibratory energy is also transmitted to the measuring points by way of the forward Agena/adapter structure which is excited by the sound pressure and by direct

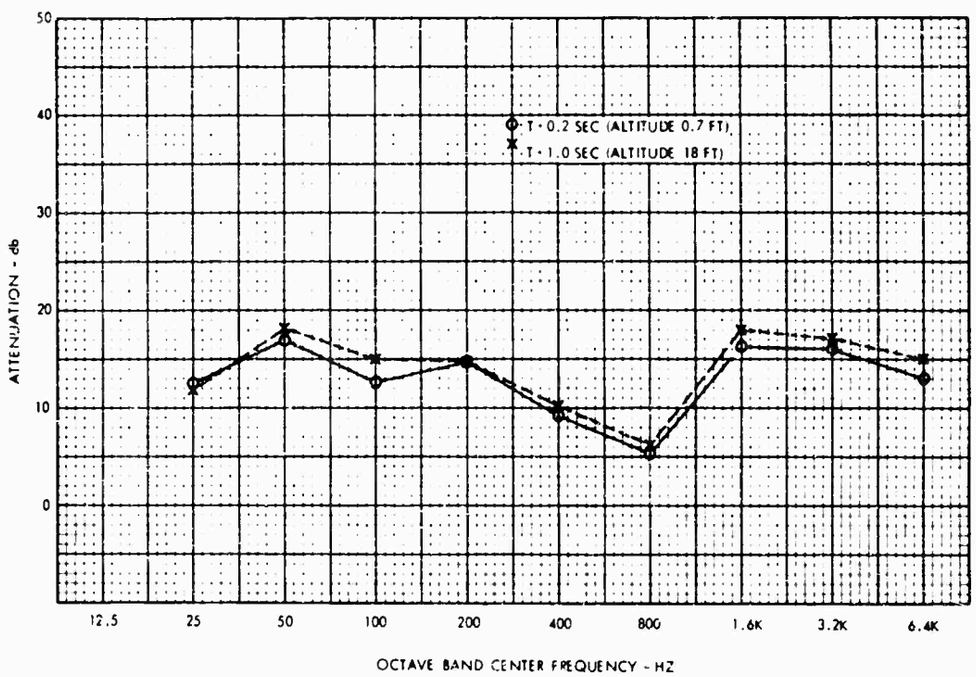

Fig. 10 - OT-2 shroud (Nimbus type) acoustic transmission loss

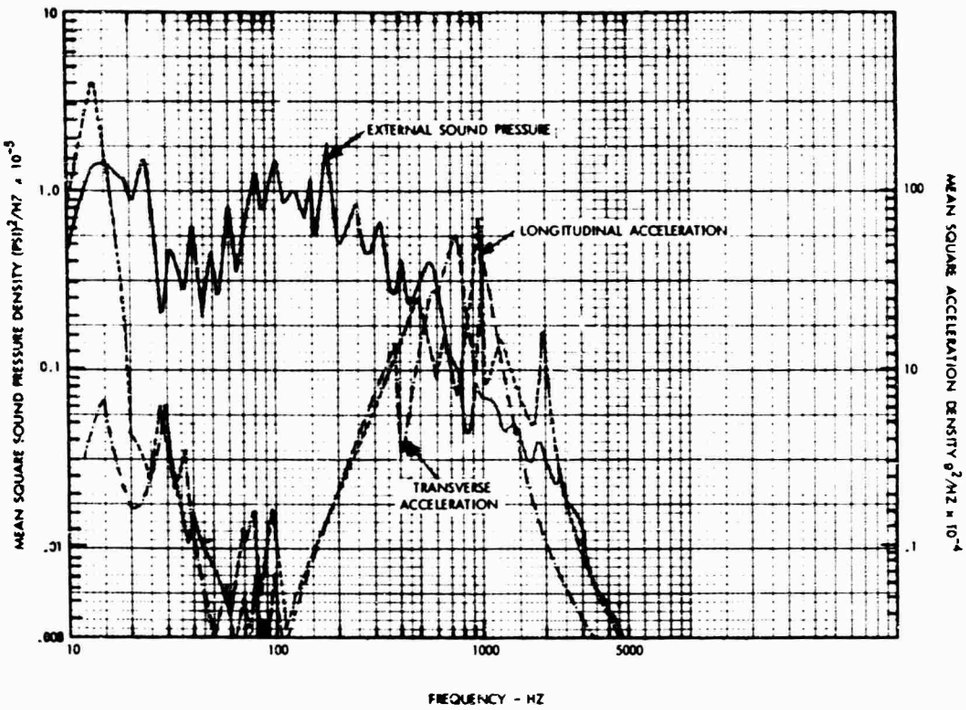

Fig. 11 - Comparison of noise and vibration spectra of TAT/Agena during lift-off

structural transmission from the rocket engine. The latter effect is not considered significant because of the attenuating effects of the transmission path.

The external overall SPL was 66×10^{-3} psi over a 10-Hz to 10-kHz bandwidth. The acceleration overall levels were 1.57 g rms (10- to 1980-Hz bandwidth) and 2.0 g rms (10- to 2615-Hz bandwidth) for the transverse and longitudinal directions, respectively.

Figure 12 presents plots of the internal SPL and acceleration spectra obtained during Atlas/Agena lift-off. The maximum vibration responses occurred in the 200- to 500-Hz band for both the longitudinal and transverse axes. The highest levels were observed to occur in the transverse direction at 500 Hz, while the maximum longitudinal acceleration response was measured at about 260 Hz. The most predominant peaks in the internal SPL spectrum occurred at 220 and 360 Hz. The ring frequency for this shroud was calculated to be about 380 Hz.

The overall levels measured during lift-off were 19.5×10^{-3} psi (10- to 2615-Hz bandwidth), 1.3 g rms (10- to 1125-Hz bandwidth), and 1.98 g rms (10- to 1125-Hz bandwidth) for the internal SPL, the longitudinal acceleration and transverse acceleration, respectively.

Figure 13 presents SPL and acceleration spectra measured during the transonic region of flight. The SPL spectrum shows that the highest levels occur at 80 and 200 Hz; a downward shift from those measured at lift-off. The highest transverse acceleration frequency also shifted downwards from 500 Hz at lift-off to 400 Hz at transonic. The longitudinal acceleration spectrum shows the same 260-Hz frequency as was measured at lift-off, but its level was reduced from 20×10^{-3} to 3.0×10^{-3} g^2/Hz. Also a corresponding reduction in SPL from 140×10^{-8} psi^2/Hz at lift-off to 5×10^{-8} psi^2/Hz at transonic was observed to occur at this frequency.

The overall SPL during this time period was 11.5×10^{-3} psi^2/Hz (10- to 2615-Hz bandwidth) were 0.79 and 0.63 g rms for the longitudinal and transverse directions, respectively.

Figure 14 shows the acceleration and SPL responses measured during max Q. The SPL spectrum shows that the higher frequencies

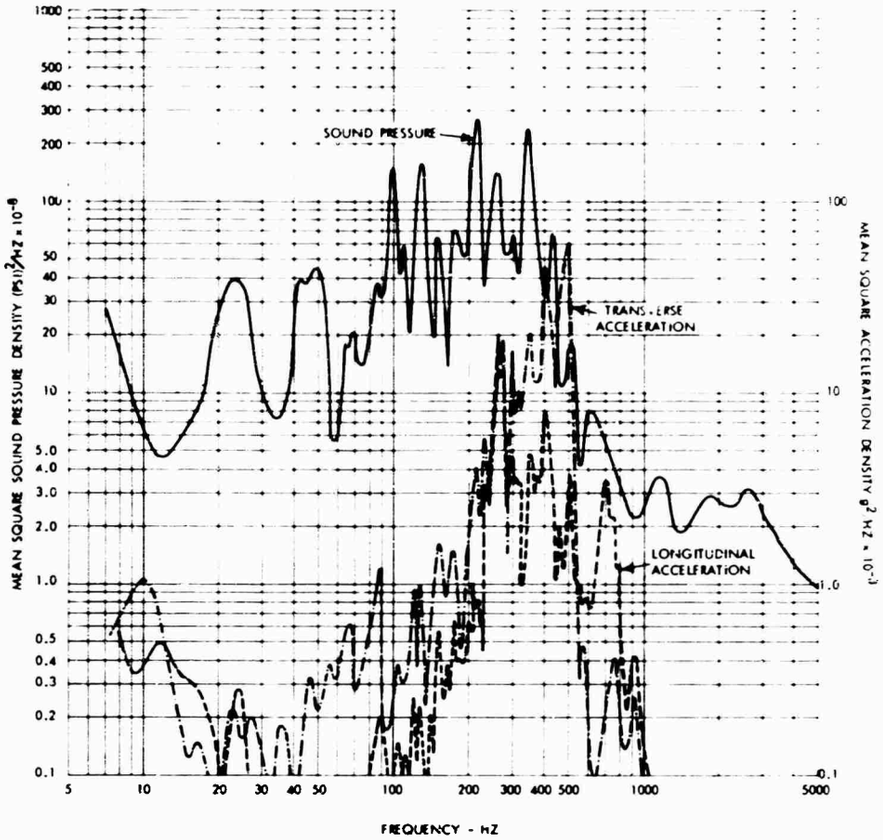

Fig. 12 - Comparison of noise and vibration spectra of Atlas/Agena-D during lift-off

become more predominant during max Q than at transonic; however, the highest peak was measured at 100 Hz. The transverse acceleration became more prominent in the 280- to 500-Hz band with maximum peaks occurring at 430 and 500 Hz. The longitudinal acceleration spectrum shows similarity to that spectrum measured during lift-off with the most predominant peak occurring at 260 Hz.

The overall acceleration levels (10- to 1125-Hz bandwidth) during max Q were 0.79 and 0.88 g rms for the longitudinal and transverse directions, respectively. The overall SPL (10 to 2615 Hz) was 11.0×10^{-3} psi.

From the data given in Figs. 12 through 14, it can be seen that there is little or no comparison between the narrow-band SPL spectra obtained within the shroud and the narrow-band vibration spectra obtained at the spacecraft/adapter interface, and that the vibration spectra predominate in the same octave band (400 Hz) as the ring frequency of the shroud.

CONCLUDING REMARKS

The data presented in this paper indicate:

1. The maximum acoustic noise levels generated during launch and flight of the three vehicle designs occurred at lift-off.

2. Noise energy in the infrasonic range (below 20 Hz) occurred during lift-off and was attributed to the ignition transient noise of the three strap-on solid-propellant motors.

3. After lift-off, the next maximum noise level event occurred during transonic flight and not during max Q for the TAD and Atlas/Agena vehicles.

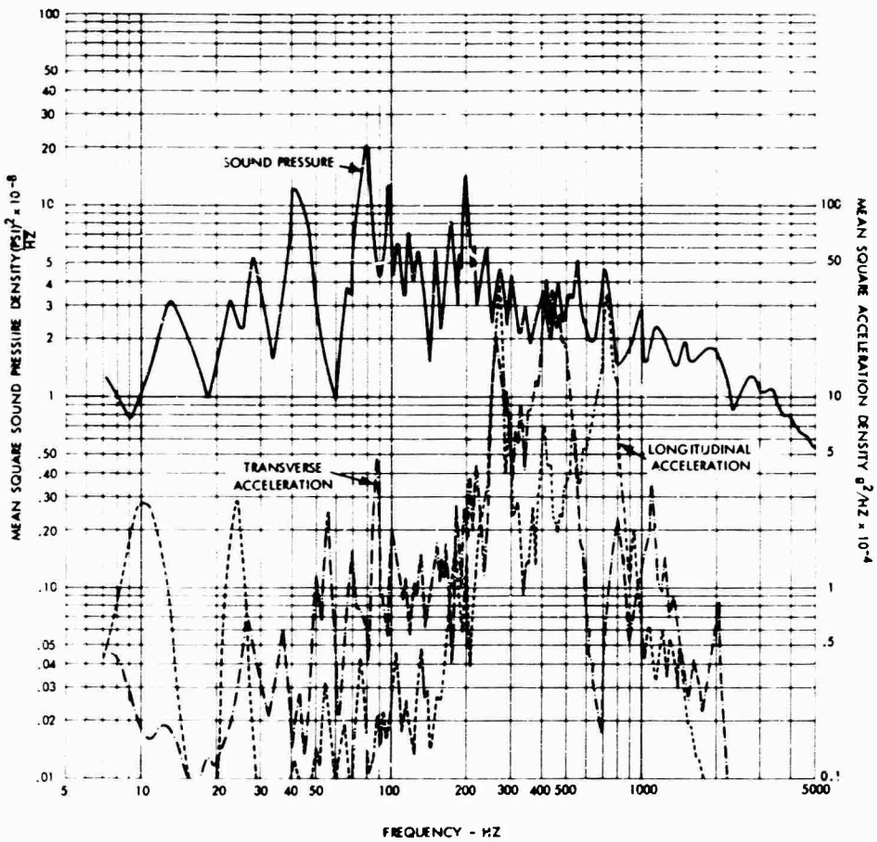

Fig. 13 - Comparison of noise and vibration spectra of Atlas/Agena-D during transonic

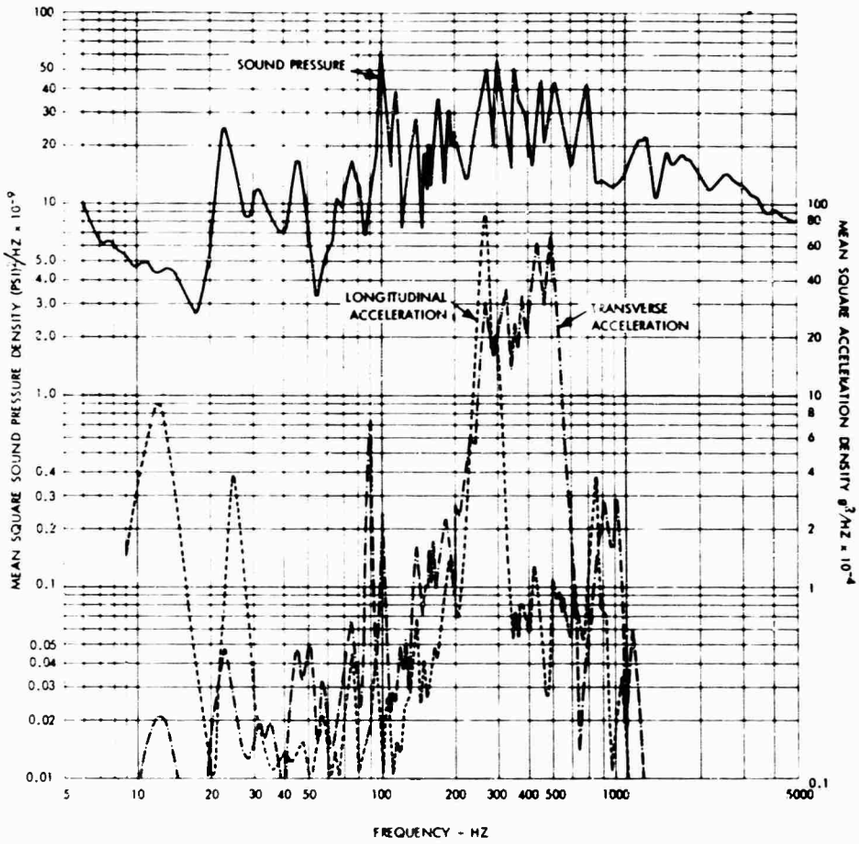

Fig. 14 - Comparison of noise and vibration spectra of Atlas/Agena-D during max Q

4. Acoustic noise levels generated by thrust-augmented Thors launched from launch pads of different configuration (ETR vs WTR design) result in higher noise levels in the 1/3-octave bands above 80-Hz band at WTR.

5. The maximum octave band internal noise levels were located in the 400- and 800-Hz bands for the Atlas/Agena and TAD vehicles, respectively. These bands contain the ring frequency for the different shrouds.

6. There is little or no comparison between the sound pressure and acceleration narrow-band spectra.

7. The narrow-band acceleration spectra measured at the spacecraft/adapter interface peak in the same octave band as the ring frequency of the shroud.

REFERENCES

1. R. W. Peverley and E. B. Smith, "A Practical Method of Predicting the Acoustical Dynamic Environment for Large Booster Launch Facilities," Shock and Vibration Bull. No. 33, Part 2, pp. 89-101, Feb. 1964

2. J. E. Manning and G. Maidanik, "Radiation Properties of Cylindrical Shells," J. Acoust. Soc. Am., Vol. 36, No. 9, Sept. 1964

DISCUSSION

Mr. Kaplan (General Electric Co.): Has instrumentation been planned or developed to define the relative transmission of the energy through the shroud, to determine what portion of it is acoustical and caused by sound pressure generated inside the shroud by the shroud response, and what portion of the excitation of the shroud is transmitted as vibration to the spacecraft in through the adapter?

Mr. Williams: There is such a program on the OGO satellite. We do not have the full report yet, but the data which I have seen shows that most of the noise at transonic really is generated by the acoustic field and not the structural transmission path of the shroud.

Mr. Jackman (General Dynamics/Pomona): Apparently these levels are not nearly as severe as had been anticipated. We have been thinking in terms of 140 to 160 db. Was it a surprise to you to obtain 130 and 140 db as a maximum at any point as compared with some of the Saturn/Apollo predictions of about 170 and 175 db?

Mr. Williams: I do not know very much about the Saturn, but since the noise field level in the spectrum is a function of the thrust of the vehicle, as thrust is increased, the noise level will increase.

Mr. Jackman: You didn't anticipate higher levels than this and were not surprised by the lower levels?

Mr. Williams: No, we measured 149 db overall. We set the systems up for 156 db.

Mr. Rice (Goodyear Aerospace Corp.): Was that dip in your attention curve due to the ring mode?

Mr. Williams: Right, the actual frequency of the ring mode was 630 Hz which was in the 800-Hz band. That dip is due to the transmission of acoustic radiation at the ring frequency.

Mr. Rice: Was the mode shape of the ring a four-lobe shape with two cross-nodal lines?

Mr. Lynn (Bolt Beranek and Newman): For a structure of this size, there are a series of modes that resonate near that frequency, and all are well coupled to the acoustic field. There is a purely breathing mode that is resonant at this frequency, but there are a series of modes that will contribute to the high transmission in this frequency band.

* * *

THE "VACUUM SPRING" *

K. D. Robertson
U. S. Army Materials Research Agency
Watertown, Massachusetts

In many instances a suspension system is required to protect equipment from the combined effects of both shock and vibration. Good isolation against one effect, however, may result in poor isolation against the other. This occurs because the parameters (spring rate and weight) which influence shock isolation also influence vibration isolation. Consequently, it is difficult to satisfy both shock and vibration requirements simultaneously since only one of these parameters (spring rate) is arbitrary.

A new nonlinear spring, the "Vacuum Spring," has been developed which may resolve this difficulty and satisfy both shock and vibration requirements simultaneously. This spring combines high energy absorption and vibration attenuation over a wide range of forcing frequencies. This unusual behavior is produced by a stepwise nonlinearity in its loading curve which is composed of two straight-line segments of differing slopes representing two independent spring rates. The slopes of these line segments and the point of intersection can be adjusted to suit any particular design requirements. A spring-mass system involving this concept has been simulated on an analog computer. Results indicate that it is possible to construct a suspension system which will not resonate at any frequency (under certain loading conditions) but will absorb large amounts of energy while remaining elastic.

K. D. Robertson

INTRODUCTION

Suspension systems are frequently required to isolate equipment from the combined effects of shock and vibration, but good isolation against one effect may result in poor isolation against the opposite effect; i.e., a good shock isolator may be a poor vibration isolator. This occurs because the parameters, spring rate and weight, which govern the vibration behavior of the system, also govern the shock response of the system. Generally, only one of these parameters, the spring rate, is arbitrary. Consequently, it is difficult to satisfy both shock and vibration requirements simultaneously.

A new nonlinear suspension system, the "Vacuum Spring," has been developed which may help to solve this dilemma. This suspension system involves three arbitrary parameters which can be adjusted to accommodate any particular combination of shock and vibration. The unique properties of this system stem from its nonlinear load deflection behavior. The curve representing this behavior consists of two straight-line segments which, because of the difference in slopes (one high and one low), resemble a step function. The slopes of these lines, i.e., the spring rates, are arbitrary and

*U. S. Patent Pending, Reference AMC 3370.

constitute two independent parameters. The point of intersection of these lines is also arbitrary and represents a third independent parameter. These parameters can be chosen to satisfy any particular design requirement.

The quality of a suspension system is determined by its shock and vibration isolation characteristics. An indication of the shock absorption characteristics of a system can be obtained by measuring the area under the loading curve. In the present case this area approaches the theoretical maximum for a given fragility level, since the loading curve approximates a step function. The behavior of this system under vibratory loads was not as easily evaluated. That behavior was the subject of this investigation.

"VACUUM SPRING" SYSTEM

The "Vacuum Spring" is exceedingly simple in design. It is a self-contained unit and requires no auxiliary equipment such as reservoirs or pumps. In principle, this spring uses the atmosphere as its reservoir. Details of two systems employing the "Vacuum Spring" principle are illustrated in Fig. 1. The essential features of both systems are identical, consisting of a flexible bellows, diaphragms, stops, and a loading mechanism. The major difference between the two systems shown is in the loading mechanism. In one instance loading is accomplished through flexible cables; in the second instance it is accomplished through rods. The choice of loading mechanism depends on the application.

During assembly, the bellows is partially collapsed and completely evacuated. A void is maintained between the diaphragms by stops. Atmospheric pressure acts on one face of the diaphragm, while a vacuum acts on the opposite face. This creates an unbalanced force across the diaphragms and causes precompression in the stopping mechanism. When a load is applied through the loading mechanism (rods or cables), the preload is gradually transferred from the stopping mechanism to the loading mechanism. Thus, the initial spring rate k (Fig. 2) of the system is determined by the combined spring rate of the loading and stopping mechanisms. This initial spring rate is generally very high. When the applied load exceeds the preload in the stopping mechanism, the bellows expand axially and radially. The radial expansion of the bellows exposes more surface area of the diaphragm to the differential pressure across it and results in a net gain in the total force. This factor, plus the increased tension in the bellows, is responsible for the subsequent low spring constant k_1 (Fig. 2).

A "Vacuum Spring" similar to the one illustrated in Fig. 1b was tested statically. The

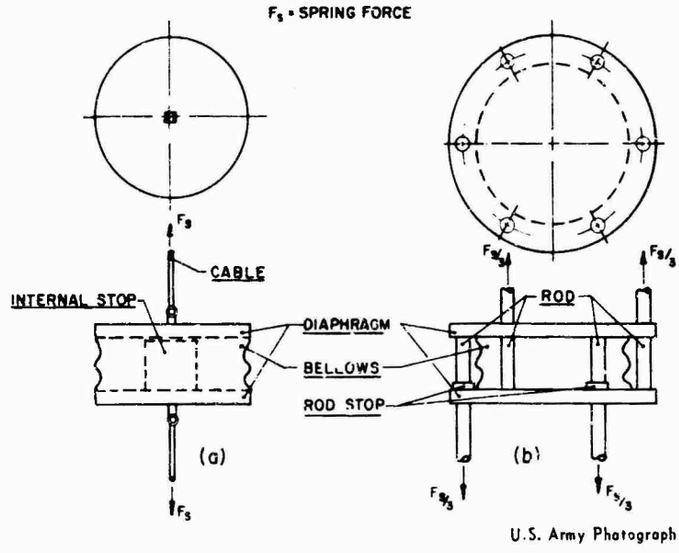

Fig. 1 - "Vacuum Spring": (a) loaded through flexible cables, and (b) loaded through rods

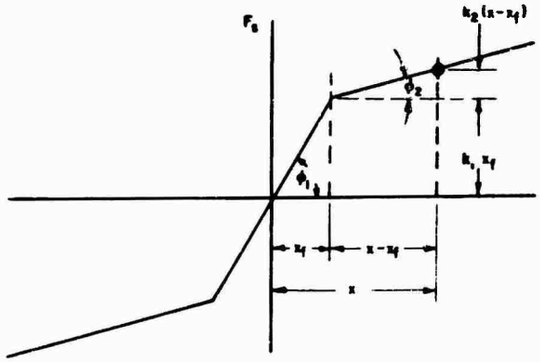

$\phi_1 = \tan^{-1} k_1$ $\quad F = k_1 g(x)$, $|x| < |x_f|$ $\quad g(x) = x$

$\phi_2 = \tan^{-1} k_2$ $\quad F_s = k_1 g(x) + k_2 \left[x - g(x) \right]$, $|x| > |x_f|$

$g(x) = +x_f$, x POSITIVE

$g(x) = -x_f$, x NEGATIVE

U.S. Army Photograph

Fig. 2 - Idealized load deformation diagram

actual test setup is shown in Fig. 3. The spring tested had a diameter of 10-1/2 in. and an initial height, excluding attachments, of 3-1/2 in. The maximum deflection was 3 in. and was limited by the test setup rather than by the bellows. The maximum load attained by the spring (Fig. 4) was 1180 lb at approximately 2.9 in. deflection. The initial spring rate k_1 was 92,000 lb/in. and the secondary spring rate k_2 was 96 lb/in.

U.S. Army Photograph

Fig. 3 - Static test fixture

NOMENCLATURE

- W weight (lb),
- M mass (lb/sec^2/in.),
- F_o amplitude of forcing function (lb),
- F_s spring force (lb),
- x displacement (in.),
- x_f maximum displacement of stiff spring (in.),
- g function of x (in.),
- k_1 initial spring rate (lb/in.),
- k_2 secondary spring rate (lb/in.),
- ω_f forcing frequency (rad/sec),
- ω_1 higher natural frequency of vacuum spring (rad/sec),
- ω_2 lower natural frequency of vacuum spring (rad/sec),
- A_n amplification factors of vacuum spring (n = 1 or 2),

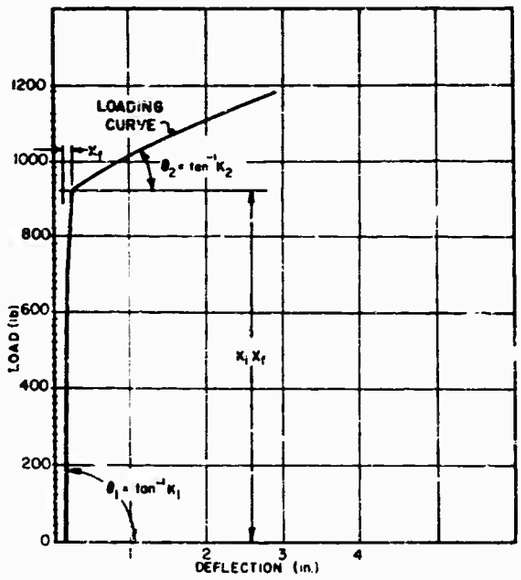

U.S. Army Photograph

Fig 4 - Actual load deflection diagram

K_n potentiometer setting ($n = 1, 2, 3$, etc.), and

t time (sec).

ANALYSIS

The system analyzed is illustrated diagrammatically in Fig. 5. It consists of a mass M supported by a vacuum spring. The mass is disturbed by a time varying forcing function $F(t)$. The loading curve and the force displacement relations for the vacuum spring are shown in Fig. 2. The governing equation for the system is

$$M \frac{d^2x}{dt^2} = \Sigma F = F(t) - F_s , \qquad (1)$$

where F_s is the spring resisting force. From Fig. 2,

$$F_s = k_1 g(x) + k_2 \{x - g(x)\} , \qquad (2)$$

where

$$\begin{aligned} g(x) &= x , \text{ when } |x| \leq |x_f| , \\ &= + x_f , \text{ when } |x| > |x_f| \text{ and } x \text{ positive.} \\ &= - x_f , \text{ when } |x| > |x_f| \text{ and } x \text{ negative.} \end{aligned} \qquad (3)$$

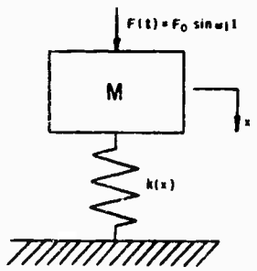

U.S. Army Photograph

Fig. 5 - Spring-mass system

With the proper substitution, Eq. (1) can be written as follows:

$$\frac{d^2x}{dt^2} + \omega_2^2 \{x - g(x)\} + \omega_1^2 g(x) = \frac{F(t)}{M} , \qquad (4)$$

where

$$\omega_1^2 = \frac{K_1}{M}$$

and

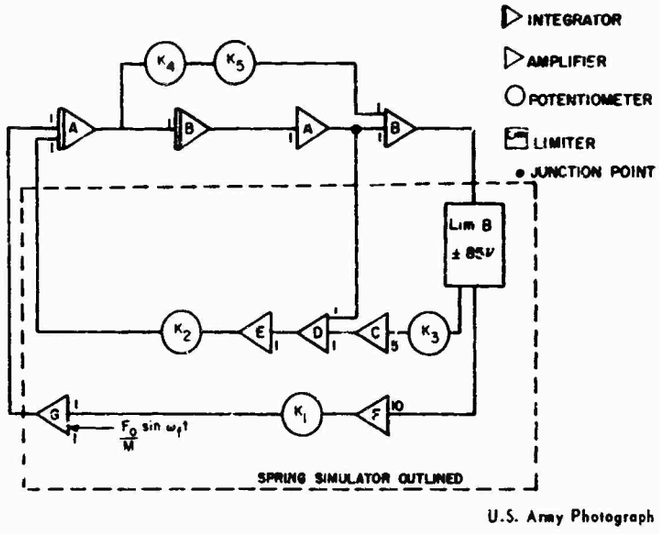

U.S. Army Photograph

Fig. 6 - Computer program

$$\omega_2^2 = \frac{K_2}{M} .$$

Solutions to Eq. (4) were obtained with an analog computer for the condition that

$$F(t) = F_o \sin \omega_f t .$$

SIMULATION

The spring-mass system described by Eq. (4) was simulated on an analog computer. The complete computer program is diagrammed in Fig. 6. It is an ordinary second-order system with a stepwise nonlinearity introduced to represent the spring. The spring simulator, separately illustrated in Fig. 7, consists of two separate feedback paths. One or both of these paths may be in the circuit at any particular time. The path ABC is always open and its output is a nonlinear function of x. When $|x| < |x_f|$, the output is $-\omega_1^2 x$, but when $|x| > |x_f|$, the output is a constant equal to $-\omega_1^2 g(x)$. When the sign of x is positive, $g(x) = +x_f$, and when x is negative, $g(x) = -x_f$. The output of the path ADE is also a nonlinear function of x. When $|x| < |x_f|$, the output of path ADE is zero, but when $|x| > |x_f|$, the output is $-\omega_1^2 \{x - g(x)\}$, where again the sign of

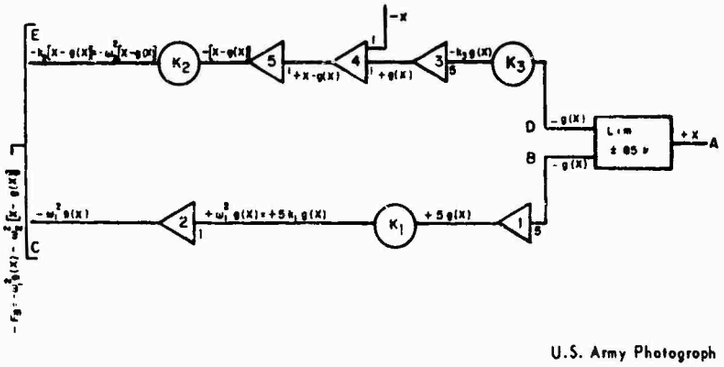

U.S. Army Photograph

Fig. 7 - Spring simulator

$g(x)$ is determined by the sign of x. The sum of these two paths, ABC and ADE, represents the spring force.

The analog simulation of the system shown in Fig. 4 was unstable at all frequencies when potentiometers K_4 and K_5 were set at zero. This instability was caused by positive feedback through the integrators. To counteract this condition, a certain amount of negative feedback was required. This amount of negative feedback does not represent damping, however, since it merely corrects for certain imperfections in the integrators.

The following procedure was used to determine the correct amount of feedback required. The nonlinearities in the system were eliminated, which reduced the governing equation to the standard second-order harmonic equation:

$$\frac{d^2x}{dt^2} + \omega_1^2 x = \frac{F_o}{M} \sin \omega_f t \qquad (5)$$

Equation (5) represents the motion of the system when $x < x_f$ or when only the stiff spring constant k_1 was active. Since the exact solution of this equation is known, the computer solution could be forced to match the known solution by introducing sufficient negative feedback through potentiometers K_4 and K_5. This amount of negative feedback corresponds to the no-damped condition. The potentiometer settings determined as stated above were then used in the solution of Eq. (4).

LINEAR SPRING-MASS SYSTEM

The "Vacuum Spring" is a combination of two linear spring systems. This is shown by the idealized load deformation diagram for this spring (Fig. 2) which is simply a combination of two linear spring rates. Consequently, the dynamic behavior of the "Vacuum Spring" and its associated mass can be described by two sequential linear differential equations in place of the single piecewise linear equation as was done in the previous analysis. The behavior of the complex system can then be examined in terms of the known behavior of its separate parts. For this purpose, Eq. (4) will be rewritten as two sequential linear equations as follows:

$$\frac{d^2x_m}{dt^2} + \omega_1^2 x_m = \frac{F(t)}{M} \qquad (6)$$

where $x = x_m$ when $x_m < x_f$, $m = 1, 2, 3$, etc., and

$$\frac{d^2x_n}{dt^2} + \omega_2^2 x_n = H(t), \qquad (7)$$

where $x = x_n$ when $x_n > x_f$, $n = 1, 2, 3$, etc., and

$$H(t) = \frac{F(t)}{M} + \left\{\omega_2^2 - \omega_1^2\right\} g(x) \qquad (8)$$

with $g(x)$ as defined in Eq. (3).

Methods of solution of these equations are given in any standard text on advanced mathematics [1]. The solutions of these equations for the case where $F(t) = F_o \sin \omega_f t$ are as follows:

$$x_m = \frac{F_o M \omega_1^2}{\omega_1^2 - \omega_f^2}\left\{\sin \omega_f t - \frac{\omega_f}{\omega_1} \sin \omega_1 (t - t_{n-1})\right\} + x_{n-1} \cos \omega_1 (t - t_{n-1}) + \frac{\dot{x}_{n-1}}{\omega_1} \sin \omega_1 (t - t_{n-1}) \qquad (9)$$

and

$$x_n = \frac{F_o M \omega_2^2}{\omega_2^2 - \omega_f^2}\left\{\sin \omega_f t - \frac{\omega_f}{\omega_2} \sin \omega_2 (t - t_{n-1})\right\} + x_{n-1} \cos \omega_2 (t - t_{n-1}) + \frac{\dot{x}_{m-1}}{\omega_2} \sin \omega_2 (t - t_{m-1}). \qquad (10)$$

These equations must be solved sequentially, using the final values of x and $\dot{x}$ of Eq. (9) as the initial values for Eq. (10). In these equations the times, t_{m-1} and t_{n-1}, are measured from zero to the time at which x_{m-1} or x_{n-1} is equal to x_f. Numerical evaluation of Eqs. (9) and (10) is very cumbersome and, in the present case, unnecessary. The behavior of the system can be determined from an examination of the equations. These equations indicate that amplification affects only the first term, i.e., terms involving the forcing function. The remaining terms involving x and $\dot{x}$ are affected by previous amplifications; i.e., these terms store the effects of all previous amplifications, but are not directly affected by amplification. The maximum amplifications in these equations occur when one of the following conditions prevail:

$$\sin \omega_f t = \sin \omega_1 (t - t_{n-1}) = 1 \qquad (11)$$

or

$$\sin \omega_f t = -\sin \omega_2 (t - t_{m-1}) = 1. \quad (12)$$

The maximum amplifications for the conditions cited above are

$$A_m = \frac{1}{1 - \frac{\omega_f}{\omega_1}} \quad (13)$$

and

$$A_n = \frac{1}{1 - \frac{\omega_f}{\omega_2}}. \quad (14)$$

When the system is started from rest, i.e., $x_o = \dot{x}_o = t_o = 0$, only the stiff spring portion will be active if the amplitude of the applied load does not exceed the value given by

$$F_o < \left(1 - \frac{\omega_f}{\omega_1}\right) x_f (M \omega_1^2) = \left(1 - \frac{\omega_f}{\omega_1}\right) k_1 x_f. \quad (15)$$

When F_o exceeds these limits, the soft spring portion will become active.

The period of the displacements described by Eqs. (9) and (10) does not coincide with the period of the forcing function. Only the period of the first terms in Eqs. (9) and (10) agrees with the period of the forcing function. All other terms represent free vibrations at the period of the natural frequencies. Hence, the period of vibration of the displacement x is always different from the period of the forcing function for the condition when the applied load exceeds the value given by Eq. (15). This allows the resultant vibrations to get out of phase with the forcing function and a result similar to damping occurs. This effect was probably responsible for some of the attenuation observed in this investigation.

DISCUSSION OF RESULTS

Results of this investigation are plotted in nondimensional form in Fig. 8. In this figure the transmissibility (F_s / F_o) is plotted as a function of the frequency ratios (ω_f / ω_1) and (ω_f / ω_2). These results were obtained at three different levels of input force. Each curve on Fig. 8 represents a specific value of the ratio $F_o / k_1 x_f$. The ratios investigated were $F_o / k_1 x_f$ = 0.9, 1.53, and 3.74. The lowest value of this ratio represents value at which resonance will not occur at the lower natural frequency ω_2.

The results obtained are a consequence of the nonlinearities in the load-displacement behavior of this spring. As shown in Fig. 2, the spring rate of the "Vacuum Spring" is amplitude dependent. When the displacement is less than a certain value, $x < x_f$, the spring rate is k_1 and the natural frequency associated with this spring rate is $\omega_1 = \sqrt{k_1 / M}$. If the displacement exceeds this value, $x > x_f$, the spring rate becomes k_2 and the natural frequency becomes $\omega_2 = \sqrt{k_2 / M}$. Under these circumstances it is natural to expect that the vibration behavior of the associated vacuum spring-mass system will also be displacement amplitude dependent.

This dependence of behavior on displacement amplitude was noted throughout the frequency range investigated, $1 < \omega_f / \omega_2 < 14.4$, and was particularly evident at the natural frequencies $\omega_f / \omega_1 = \omega_f / \omega_2 = 1$ as shown by the

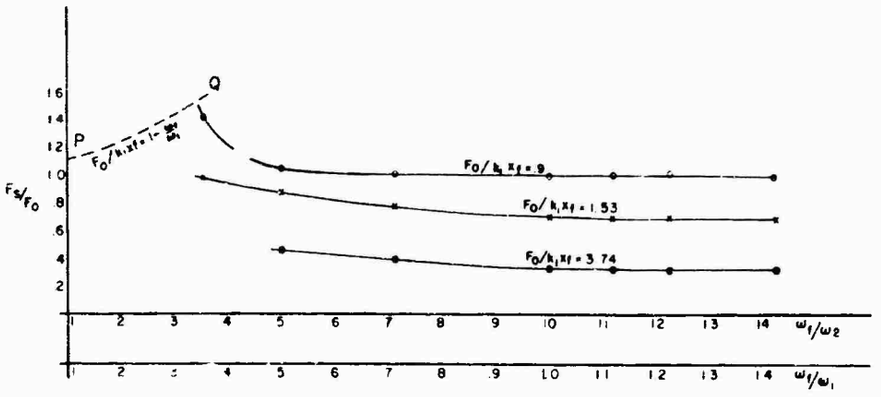

U.S. Army Photograph

Fig. 8 - Transmissibility curves

absence of resonance at these frequencies under certain loading conditions.

At the lower natural frequency, $\omega_f/\omega_2 = 1$, the spring-mass system did not resonate for input loads less than a certain value, $F_o < 0.9k_1x_f$. Under these loading conditions only the stiff spring constant was involved and the natural frequency of the spring-mass system was ω_1; hence, resonance should not and did not occur. This effect is represented in Fig. 8 by the isolated point (P_1) at $F_s/F_o = 1.11$, $\omega_f/\omega_2 = 1$.

When the amplitude of the input force was increased at the lower natural frequency, i.e., $F_o > 0.9k_1x_f$ and $\omega_f/\omega_2 = 1$, the soft spring constant k_2 became operative. Then, at least for a portion of the cycle, the natural frequency of the system became ω_2 and a resonant condition developed.

In the frequency region $1 < \omega_f/\omega_2 < 2$, amplification occurs as a result of both the soft and stiff spring constants (Eqs. (13) and (14)). In this region the computer overloaded and the results were considered unreliable. Rescaling was attempted but this introduced other inaccuracies. Consequently, the behavior of the system in this region was not determined. From a practical point of view, that behavior is of no great significance since in this region the system should be operated with $F_o < 1/[1 - (\omega_f/\omega_1)^2]$, i.e., with only the stiff spring portion active as shown by the dashed curve in Fig. 8. In this case, the amplification would be given by Eq. (13).

The behavior of the system for the load ratios investigated is shown in Fig. 8 for frequency ratios greater than $\omega_f/\omega_2 > 3.5$. As shown in that figure, the transmissibility decreases with increasing load ratios and increasing frequency ratios. For those load ratios investigated, the maximum transmissibility was 1.46 and occurred at $\omega_f/\omega_2 = 3.5$, $F_o/k_1x_f = 0.9$. At the higher natural frequency $\omega_f/\omega_1 = 1$, the greatest transmissibility, $F_s/F_o = 1$, occurs at a load ratio of $F_o/k_1x_f = 0.9$, and the lowest transmissibility, $F_s/F_o = 0.34$, occurs at a load ratio of $F_o/k_1x_f = 3.74$.

The behavior of the system at the higher natural frequency was a curious combination of amplification, limiting and attenuation. If the applied load was small, $F_o < k_1x_f$, such that the displacement did not exceed x_f, i.e., $x < x_f$, a resonant condition initially developed, since all displacements occurred in the stiff spring region and the spring was operating at its natural frequency. As the resonant condition built up, the displacement increased and finally exceeded the value $x > x_f$. When this condition occurred, the soft spring portion became active and the natural frequency switched to the lower value ω_2. Since the forcing frequency was still ω_1, the system was operating well above its natural frequency and attenuation resulted. This combination of effects limited the output to approximately k_1x_f for the conditions cited above. At higher load ratios attenuation increased.

The frequency of vibration of the "Vacuum Spring"-mass system did not coincide with the forcing frequency when $x < x_f$, i.e., when the soft spring constant became active. This effect appeared to be a phase shift at low frequencies, but at high frequencies, where the effect was most noticeable, this spring acted as a frequency divider. The cause of this effect is discussed in the section of this report on the linear spring-mass system. A pronounced shift in frequency occurred at a frequency ratio of $\omega_f/\omega_1 = 1$. At this frequency ratio, the output frequency was only half the input frequency.

CONCLUSIONS

The following conclusions are derived from static test results and computed dynamic results of a "Vacuum Spring" system. Time and expense did not permit dynamic evaluation of a mechanical model. It should be borne in mind that the computed results did not consider any mechanical damping. Since damping is always present in a mechanical system, the computed values of transmissibility would be reduced in an actual mechanical system.

1. A practical nonlinear suspension system can be constructed, incorporating three arbitrary parameters, which can be used to satisfy both shock and vibration mitigation requirements simultaneously.

2. The "Vacuum Spring" system incorporating a stepwise nonlinear load deformation diagram, will maximize energy absorption at any specified fragility level.

3. A resonance-free suspension system can be constructed using the "Vacuum Spring" principle.

4. The "Vacuum Spring" can be used as a mechanical frequency divider.

REFERENCE

1. F. B. Hildebrand, Advanced Calculus for Applications, pp. 8-13. Prentice-Hall, Englewood Cliffs, N. J., 1962

DISCUSSION

Voice: In your analog simulation, did you simulate the actual nonlinear system, or the reduced linear equation?

Mr. Robertson: I simulated the nonlinear system. It can be broken down into two sequential linear equations, so it is really a linear system.

Voice: But your response is amplitude dependent?

Mr. Robertson: Yes.

Mr. Ungar (Bolt Beranek & Newman): Some time ago we worked on a system that involved a buckled column with force deflection characteristics very much like the one you are considering. Are you aware of this work and have you considered using something much simpler than your vacuum spring?

Mr. Robertson: No, I am not aware of this work.

Mr. Ungar: Have you compared the results of your analysis with some more classical work that Stoker has in his book on nonlinear vibrations?

Mr. Robertson: No, I have not.

Mr. Ungar: Do you have any idea what the damping is in your spring?

Mr. Robertson: No, but I did simulate a certain type of damping in another portion not shown and the results were practically identical. I knew the response of the stiff spring or what it should be on the analog computer either with the ordinary solution or with the solution without damping. In other words, if the free vibration term is included, two terms are obtained in the solution. Otherwise, only one is obtained. I computed the output with only one of these terms because I knew the response of the system. In this way, I introduced damping at least into the stiff spring.

Mr. Ungar: The spring appears to me to have very little damping. If you hit it, wouldn't it keep bouncing back and forth for a long time?

Mr. Robertson: It may have only small amounts of damping, so that it may not absorb energy or damp it out.

Mr. Langland (Naval Ordnance Test Station, China Lake): Have you tried to take into account an increased stiffness at the far end that would simulate an effect such as bottoming?

Mr. Robertson: No, I have considered it, but I have not tried it. This would actually eliminate the critical area near the lower natural frequency, so you would actually get no resonance anywhere in the frequency region. At the lower natural frequency if the critical value which would activate the soft spring is exceeded, a resonant condition would build up, but if, when the displacement approached this other spring, the effect of bottoming out, this would again change the natural frequency and this effect would actually more or less limit the resonant condition.

Mr. Runyan (NASA Langley Research Center): At Ames Research Center they are working on a vacuum spring, but not with this double spring constant. They are looking for a spring that a launch vehicle could be placed on and vibrated with negligible interference with the support, that is, with large separation of the first structural mode with the spring constant. If anybody is interested in this, they can contact Al Erickson at Ames.

* * *

SELF-ADAPTIVE VIBRATION BALANCING DEVICE FOR HELICOPTERS

W. Euan Hooper
The Boeing Company
Morton, Pennsylvania

Rotor-induced vibration in helicopters is a major problem. At the present time, vibration levels are being minimized by costly structural modifications occurring late in the development life of the aircraft, or by the introduction of necessarily heavy vibration absorbers of the classic spring-mass type.

This paper describes a vibration-balancing device which is under development for incorporation at the initial design phase of a helicopter. The device balances out the exciting forces at the point at which it is situated and keeps that point nodal in the presence of vibration emanating from any other point. It is self-adaptive to changes in excitation from zero to maximum and has a very rapid response time. Similarly, it adapts rapidly to changes in the rotor speed and in the phase of the excitation relative to the rotating system. The device takes its drive from the rotating system and is as light as an inertial balancing system can be. It requires no external power supplies in the form of hydraulics or electrics, and once installed would be sealed for life.

The operating principles have been intensely investigated through theoretical and model means. Certain dynamic requirements of the mounting point, which correspond approximately to those of a supercritical shaft, have to be satisfied. The behavior of the device when accelerating through critical frequencies has been analyzed and tested, and the results of this work are summarized.

Aspects of an installation in a helicopter are discussed and it is concluded that, for a modest expenditure in weight and mechanical complexity, the device can virtually eliminate helicopter n/rev vibration as an operational problem.

W. E. Hooper

INTRODUCTION

The vibration of a helicopter during the course of a routine mission illustrates the unique nature of the problem. In common with many other vehicles, the vibration frequencies are keyed to multiples (n, $2n$, $3n$, etc.) of rotor speed (where n is the number of blades per rotor). Less common, however, is the fact that the levels of excitation may change from near zero to a maximum in some conditions of operation on the ground and in the air, and that the relative phase between forcing at different points and directions in the aircraft can change over a wide range of steady flight conditions (e.g., hover, transition, and high speed in forward flight; vertical and forward autorotation; low-speed sideways and backward flight). In addition, the helicopter normally encounters a large number of transient situations (e.g., gusts and rapid pilot-induced maneuvers), all of which cause a temporary or semipermanent change in the excitation environment. This can result in short-term (1 to 10 sec) doubling or even tripling of the excitation levels, with consequent

discomfort and possible alarm to the occupants of the helicopter. An illustration of the vibration levels that might be encountered in a typical rescue operation in a hot and mountainous hostile area is given in Fig. 1.

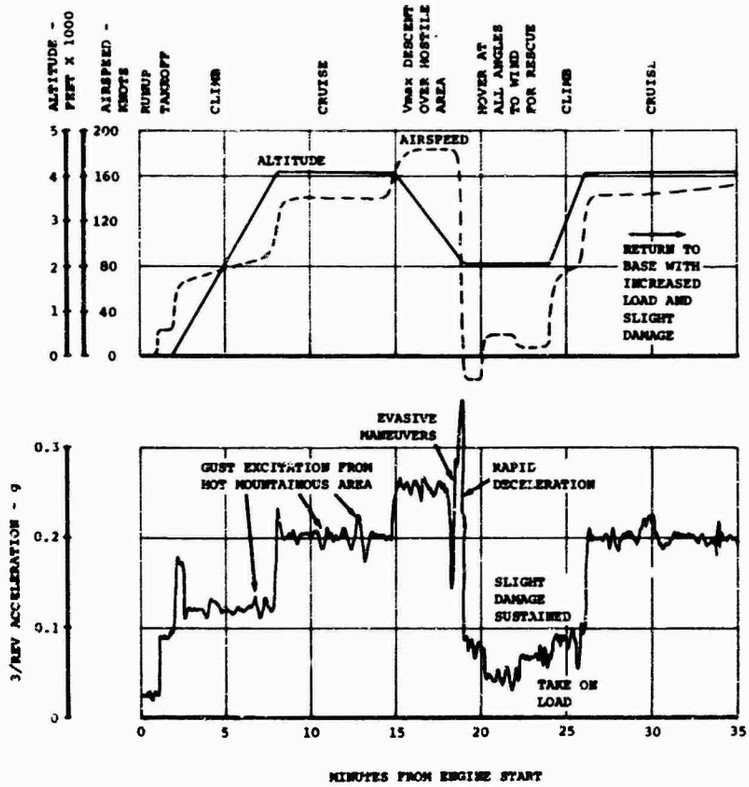

Fig. 1 - Typical 3/rev vibration levels during rescue mission

The approach of the dynamics engineer to this problem has been to concentrate on the steady-state aspect and to design rotor components and fuselage structures away from resonance with principal excitation frequencies. Particularly in the case of the fuselage, practice has frequently fallen short of prediction, and fuselages have too often been modified even after the prototypes have flown. The classic spring-mass vibration absorber appears in many current helicopters (CH-46A, SH-3A, UH-2A, OH-6A) as tacit admission that the best efforts to minimize response by structural modification either cost too much, weigh too much, or are insufficiently effective.

The cheap but heavy vibration absorber does an excellent job of reducing local vibration to acceptable levels, but it has significant disadvantages:

1. Its high weight stems from the fact that the vibrating mass will only move through about 20 times the motion of its mount, which will typically give it accelerations of only 5 to 6 g; i.e., weights of 200 lb are required to give reaction forces of up to 1200 lb.

2. It is sensitive to changes in rotor speed and thus has a narrow band of operation. This is reasonable in powered flight — when the rotor speed is automatically governed by the engines — but the absorber can actually aggravate the basic situation in autorotation, when the rotor speed may increase by 10 percent.

3. The beneficial effect of the vibration absorber is limited to the area in which it is placed (normally under the seats of those most likely to complain).

4. The operational life of a unit may well be limited by the arduous requirements for the springs.

These disadvantages provided the spur for the development of the subject device. While confirmation by flight test is awaited for final demonstration of its effectiveness, it should achieve not only lower vibration levels than the type of vibration absorber discussed, but the disadvantages of the latter either no longer apply or are significantly reduced. The device is named UREKA, for Universal Rotor Excitation Kinematic Absorber, and a description of its operation follows.

OPERATION AND PHYSICAL PRINCIPLES

The operation of UREKA depends on balance weights swinging freely about a shaft which is rotating at the excitation frequency. The simplest illustration of the device is shown in Fig. 2, in which subcritical and supercritical vibrations of a shaft with an unbalanced rotor are shown. The basic behavior is treated in many textbooks [1]. Subcritically, the rotor center of gravity will fall outside the shaft eccentric motion. Supercritically, the reverse occurs. If two balance weights which are free to assume any position about the shaft are now added to the subcritical case, they will gravitate to the largest radius under the influence of centrifugal forces and cause an additional imbalance, thereby magnifying the eccentric shaft motion. If the weights are added to the supercritical case, however, they still gravitate to the largest radius as before, but now this puts them opposite the imbalance and the eccentric motion will be reduced. If heavier weights are added progressively, the motion will be reduced gradually until the weight is sufficient to balance perfectly the initial imbalance.

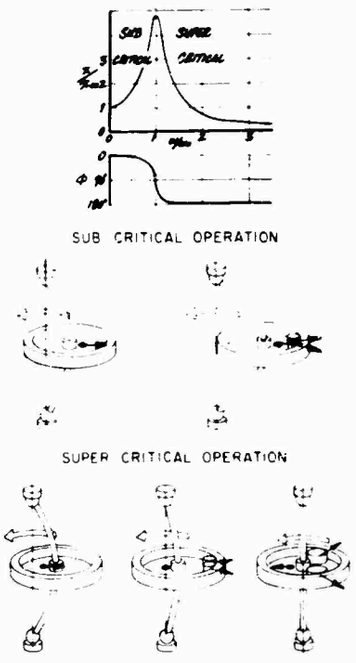

Fig. 2 - Effect of free balance weights on an unbalanced shaft

Up to this point, one weight could have been used to nullify the initial imbalance. However, if the number of weights is now increased so that the total is in excess of that required to counter the initial imbalance, the self-adaptive feature becomes evident. Too much balance weight causes the initial situation to be reversed, and the weights now find that the point of maximum radius is at the opposite side of the rotor. They start to move toward this point, but then the initial situation prevails again with the result that the weights separate and execute an oscillatory (in general) motion, converging on the positions required for complete balance. They will not stop moving until the geometric center of the track is nodal.

The offset center of gravity is representative of an applied external force vector having a circular locus. This type of excitation is, of course, most commonly caused by mass imbalance, whereas helicopter excitation – for example, in the vertical/longitudinal plane at the forward rotor of a tandem rotor helicopter – will vary from a near zero locus when running up on the ground to elliptical loci of various major/minor dimensions, inclinations, and directions of rotation when flying in various conditions (Fig. 3). An elliptical locus can be constructed from two counterrotating circular loci whose magnitudes and phases can be independently defined. The circular loci that produce the elliptical loci of Fig. 3 are shown in Fig. 4. Clearly, two independent counterrotating devices as described will provide the required circular force loci, and such a combination constitutes the UREKA system. Each element of the counterrotating pair sees only the eccentric motion which is the circular portion of the total elliptical motion rotating in the same direction as the shaft. The suspicious dynamicist will require more evidence that such a counterrotating system will work as described.

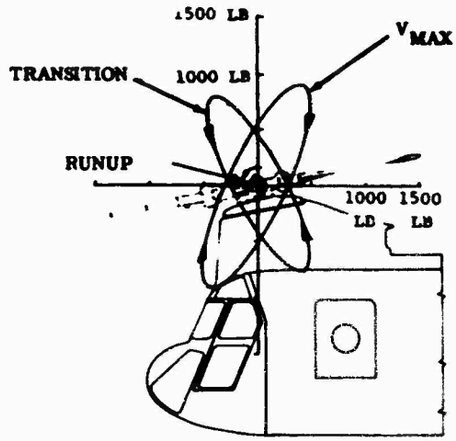

Fig. 3 - Typical rotor hub force loci

DEMONSTRATION AND PROOF OF OPERATION

The most direct proof of the basic principles is given with a simple model made from a toy mechanical construction set (Fig. 5). This model provides dynamic proof of Fig. 2 and can be operated using steel balls for balance weights (Fig. 5b), or any number of not necessarily equal pendulums (Fig. 5c). Not only is the imbalance convincingly negated, but vibration due to a slightly bent and much used shaft is also nullified.

The 4-degree-of-freedom equations of motion for a single rotating system have been derived and solved by both analog and digital means [2]. The equations are nonlinear and involve third-order products of the variables and, of course, no small angle assumptions can be made for the motion of the balance weights. The extension of the 4-degree-of-freedom single rotating equations to 6-degree-of-freedom counterrotating equations is straightforward [3], but the magnitude of the equations proved to be on the limit for acceptable analog solution and a very successful incremental digital solution has been written. Runge-Kutta extrapolations were used [4] and the resulting time histories of an initially disturbed motion are automatically plotted from a magnetic tape.

This program is now used to illustrate the behavior of UREKA in a variety of situations. Examples of behavior on a simple isotropic support have already been published [2]. Now consider a counterrotating unit mounted on a nonisotropic support having spring/mass/damper characteristics in the X and Y directions. Let the natural frequency in the X direction N_x be one-half the shaft speed ($N_x = 0.5$),

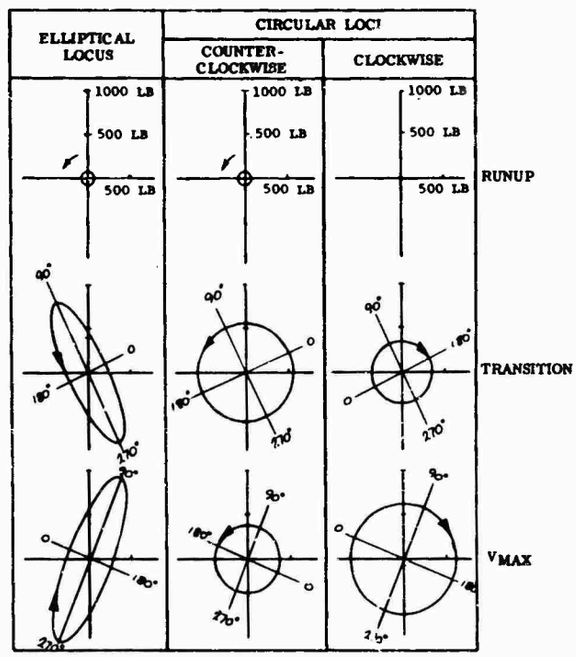

Fig. 4 - Synthesis of elliptical force loci

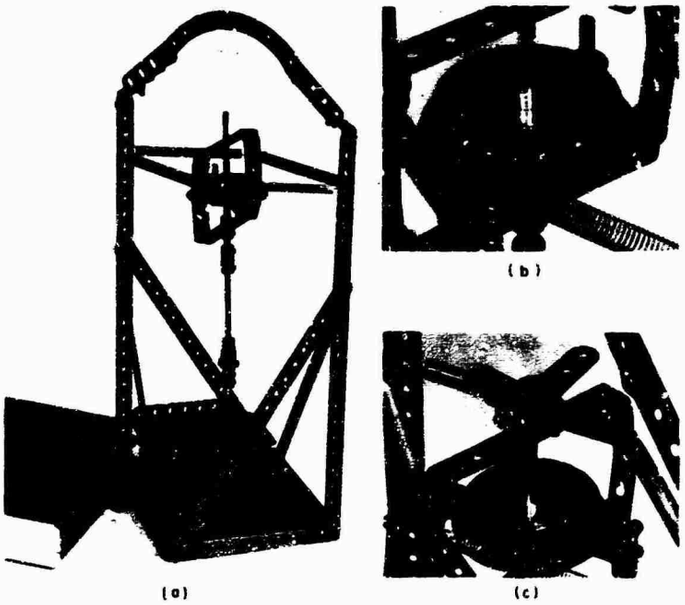

Fig. 5 - UREKA demonstration model: (a) model and controller, (b) using steel balls, and (c) using pendulums

the natural frequency in the Y direction N_y be two-thirds the shaft speed ($N_y = 0.667$), the mass ratio in the X direction $\mu_x = 0.001$, the mass ratio in the Y direction $\mu_y = 0.005$, and the structural damping ratio in the X and Y directions be given by $\delta_x = \delta_y = 0.05$. Let elliptical forcing be imposed suddenly on the system which was initially in balance; i.e., the balance weights were at ±90-deg locations from rotating references as shown in the small sketch, and the X and Y motions were zero. In Fig. 6a, counterclockwise circular forcing (an extreme case of elliptical) is applied and the Y response, after an initial transient disturbance, converges rapidly to zero. The X response is very small, partly because it is further removed from its natural frequency and partly because of the symmetrical starting position of the weights. To illustrate the effectiveness of UREKA, the hatched lines indicate the level of vibration that would have occurred without UREKA. Note that the counterclockwise weights reach new balance positions after about 10 rev, but that the clockwise weights, after a slight disturbance, return to their initial positions since there is no excitation for them to balance in this sense. A clockwise circular force would, of course, produce a mirror image of this behavior.

In Fig. 6b, linear forcing, which is another extreme case of elliptical forcing, is applied. The X direction now shows all the motion which again quickly dies out. The balance weights of both systems converge to new positions and do so symmetrically, with the result that no motion is seen in the Y direction.

Diagonal linear forcing of the same magnitude is applied in Fig. 6c. Most of the motion is in the Y direction and the weights settle down to the same separation angle, but about different mean positions. This motion took a little longer to converge, underlining the nonlinearity of the system wherein the time to stabilize depends on the initial displacements. In Fig. 6d, the same forcing is applied, but the weights are in different starting positions. Note that there is still only small response in the X direction, but that the weights converged to their final positions in 5 rev.

Now using the forcing and initial conditions of Fig. 6d, let the dynamic properties in one direction be varied as in Fig. 7. The X direction frequency remains at 0.5 times shaft speed, and the Y direction frequency changes from 0.667 to 0.8 to 1.0 times shaft speed. Figure 7a is a repetition of Fig. 6d. Figure 7b shows greater transient Y motion due to the increased proximity to resonance. Note that the balance weights reach their final positions in about the same time, but that a little more damping would reduce their oscillatory motion. Figure 7c is an extreme case to demonstrate the alternate

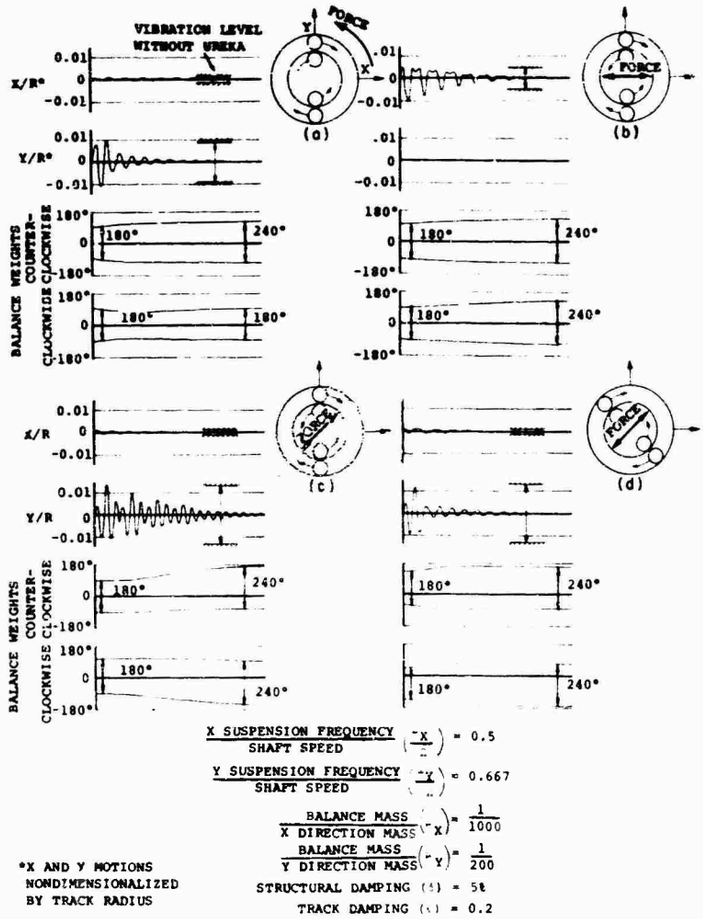

Fig. 6 - UREKA behavior with circular and linear forcing when mounted on a nonisotropic support: (a) counterclockwise circular forcing, (b) linear forcing, (c) and (d) diagonal linear forcing

mode of UREKA behavior discussed in the next section. Note that the balance weights rapidly come together and then move steadily backward relative to the shaft, completing 1 rev approximately every 10 rev of the shaft, i.e., an absolute speed equal to 90 percent of shaft speed. The Y motion shows a beat between the two frequencies. No amount of damping will rectify this situation, as the dynamic response of the suspension in this case is basically unsuitable for UREKA.

Figure 8 illustrates the importance of balance weight damping, even when the suspension dynamics are correct. The nonisotropic system and diagonal forcing of Fig. 7b are used, and the motion is illustrated for nondimensional balance weight damping coefficients (λ defined in the appendix) of 0.1, 0.2, and 0.3. Figure 8a with λ equal to 0.1 shows a very interesting case, with marginal stability between the balanced and acceleration modes. The damping is clearly too low, so that the weights oscillate excessively, but they do not come together as in Fig. 7c. If the record had been allowed to continue, the oscillation might have eventually died down. The nonlinear equations dictate that a smaller initial disturbance would have just balanced, while a larger disturbance would have pushed the system rapidly into the acceleration mode. Figure 8b is a repetition of Fig. 7b (note the change in scales) and shows complete stability, but the balance weight motion is too oscillatory. Figure 8c shows near-optimum

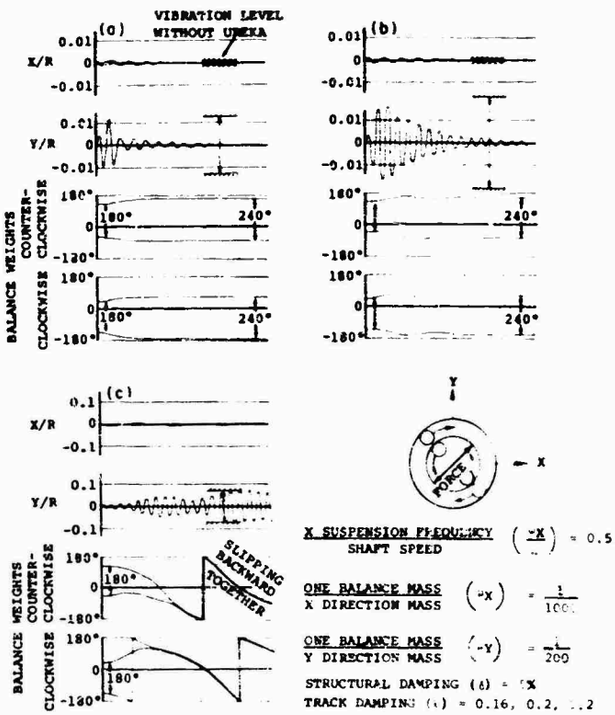

Fig. 7 - UREKA behavior with stiffness variation in Y direction: (a) ω_y/Ω = 0.667, (b) ω_y/Ω = 0.8, and (c) ω_y/Ω = 1.0

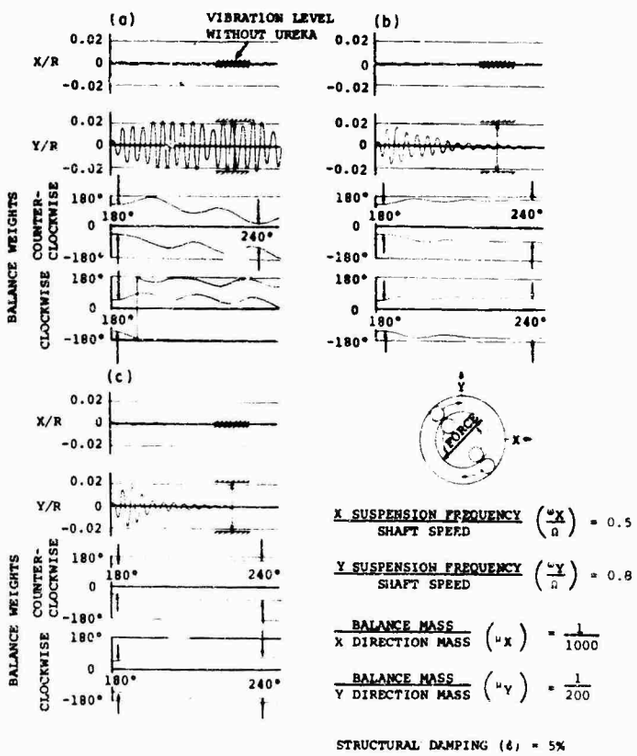

Fig. 8 - UREKA behavior with variation in balance weight damping: (a) λ = 0.1, (b) λ = 0.2, and (c) λ = 0.3

behavior, with the weights converging again within 4 to 5 rev. A further increase in damping would extend the time for the balance weights to converge and degrade the ability of URELA to adapt to a sudden change in forcing, although the balance weight motion would be quite stable.

An instrumented model was built [5] to provide more precisely controlled conditions than the mechanical model could give, and to demonstrate the counterrotating feature (Fig. 9). Counterrotating coplanar tracks were driven by a speed-controlled motor. The gearbox and tracks were mounted through springs and dampers to a rigid frame, giving a critical speed at about 500 rpm. The tracks contained liquid for damping the motion of the 1-1/2-in. diameter steel balls that were used for balance weights; each track was provided with a Plexiglas cover to allow stroboscopic illumination of the balls.

Electromagnetic shakers that could be turned on or off suddenly were used to evaluate transient behavior. It was important that shaking be provided at precisely shaft speed, so sine waves were generated by potentiometers on the rotating shaft to provide the inputs for the shakers. By this means, any elliptical form of forcing could be generated by controlling the shakers independently. The positions of the balance weights were effectively recorded by the use of a light beam which was reflected onto a photocell by a ball in passing; the photocell then superimposed a blip onto a 1-per-rev sawtooth. By joining the blips on the oscillograph record, the angular position of the weights was given. X-Y motions and shaker forces were also recorded. A wide range of test conditions was covered, using damping fluids of 20 to 2000 s viscosity at various depths in the tracks.

With this model it was possible to confirm all the phenomena mentioned so far. Stroboscopic illumination showed clearly the balance weight motions and corroborated all the preceding explanations. One major parameter evaluated with the instrumented model was the balance weight damping. Figure 10 shows the

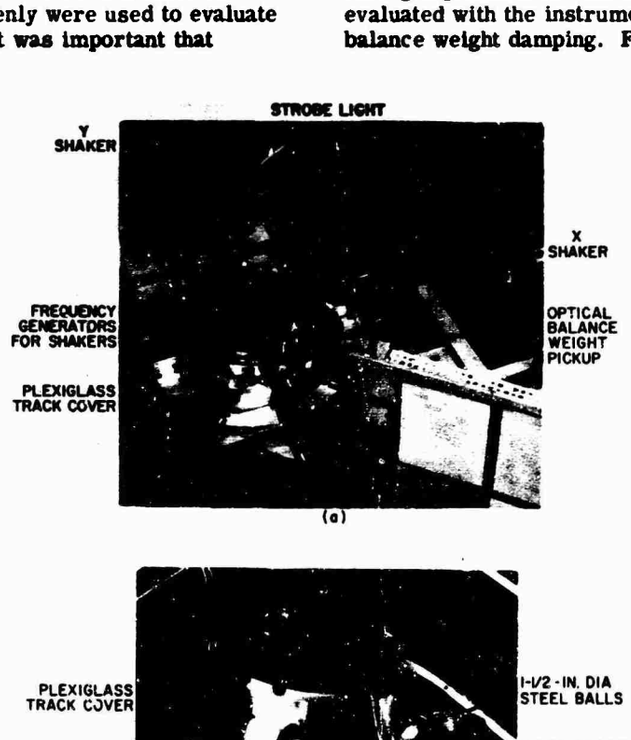

Fig. 9 - Instrumented counterrotating model: (a) test arrangement, and (b) balance weights in inner track

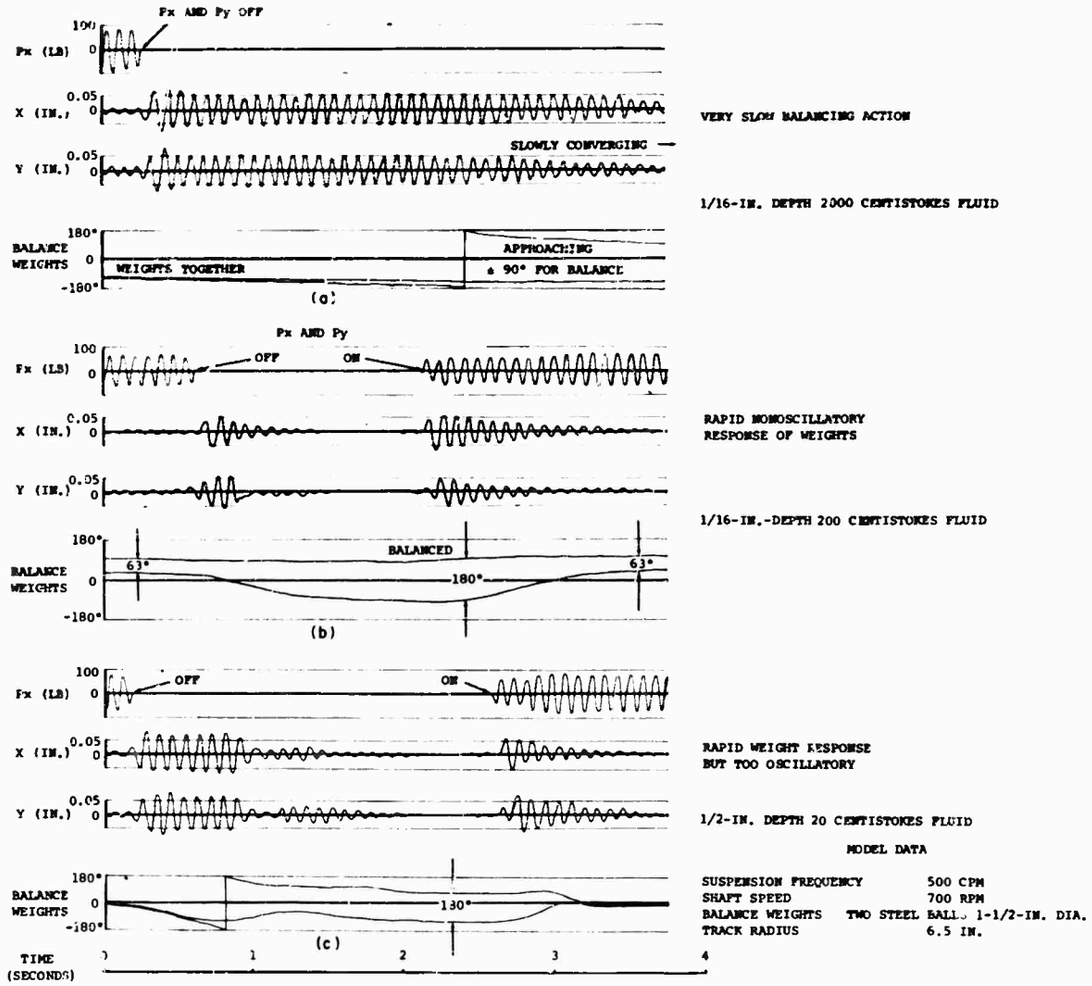

Fig. 10 - Model test data -- effect of track damping on single rotating system with circular excitation: (a) overdamped, (b) optimum damping, and (c) underdamped

influence of balance weight damping on the transient behavior following a sudden change in the forcing. These data are for a single rotating system on an isotropic mount. The X and Y motions show a slight initial vibration due to nonmatching of the shakers. In Fig. 10a an excessive amount of damping was obtained with a syrup-like fluid. When the forcing in the X and Y directions was switched off, the balls relocated very slowly, taking about 15 sec to reach their final positions and meanwhile causing unwanted vibration. Using a damping fluid with 1/10 of the viscosity, the model showed optimum behavior as seen in Fig. 10b. The weights took up their new positions with no oscillation in as little as 7 to 8 rev of the shaft with a correspondingly short period of disturbance to the X and Y motions. With an additional reduction in viscosity, the weights became too oscillatory, as seen in Fig. 8, and the stabilization time for the system increased again. Too great a disturbance can cause a reversion to a completely different motion in which UREKA will not balance correctly. This will be discussed next.

ACCELERATION BEHAVIOR

When UREKA is run up from rest it will be initially in the subcritical situation (Fig. 2), if the structure is grounded. With no external excitation, the balance weights begin to cause an eccentric motion which lags the weights

themselves by an angle approaching 90 deg as the speed approaches the structural resonance. The weights gravitate toward the peak radius of the eccentric motion, but in so doing cause the peak radius to move away from the weights. The result is that, as resonance is approached, the weights move steadily backward with respect to the shaft at a speed determined by the damping between the shaft and the weights. This backward slipping was analyzed [2], and the results are summarized in Fig. 11. It is apparent that once the weights themselves can be coaxed above the resonant speed, they immediately separate and converge onto shaft speed. A very clear demonstration of this was obtained with the instrumented model, as shown in Fig. 12. Note the rapidity of the change which is completed in about 10 rev. After converging onto shaft speed, the balance weights are very stable and the shaft speed can be reduced below the critical speed before reversion to the acceleration mode takes place. During an unexcited rundown to zero speed, the weights normally stay in place, i.e., balanced. Experience has shown that a balance weight damping that gives about 10 percent overshoot during acceleration has optimum behavior in the balancing mode. The implication is that operation of UREKA should be planned at least 10 percent above the critical frequency if normal operation requires acceleration through this frequency.

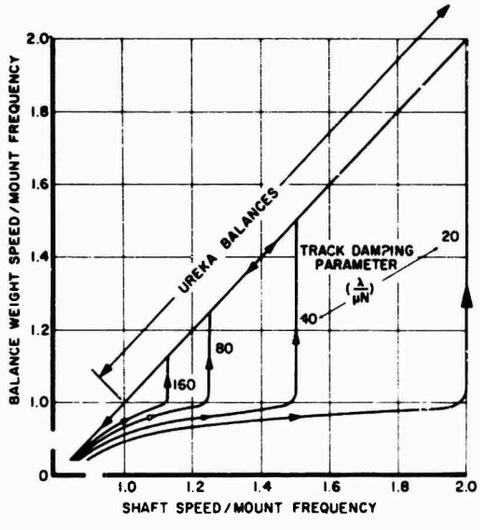

Fig. 11 - Balance weight slippage during acceleration

As an alternate design, a centrifugally operated bi-stable clamp can be used to hold the weights until the critical speed is exceeded. This has the advantage of retaining the weights in a balanced position on shutdown. On the next runup, the weights will not excite the structure.

DYNAMIC REQUIREMENTS FOR MOUNTING UREKA

The simple system of Fig. 2 shows that UREKA works in a supercritical shaft environment. A practical situation is rarely as simple as this, and a helicopter hub is no exception. A more complex system will behave as shown in Fig. 13, in which the acceleration (g's) of a mounting point per unit applied force is plotted against frequency, together with the phase lag of the displacement relative to the force. For an isotropic system UREKA requires that the phase lag lie between 90 and 180 deg for successful balance. The regions where UREKA will not balance are shaded in Fig. 13. Typically, UREKA will not function immediately below the frequency of a mode that has significant motion at the point of attachment. It will function immediately above such a mode, and it will function right through a mode that has only

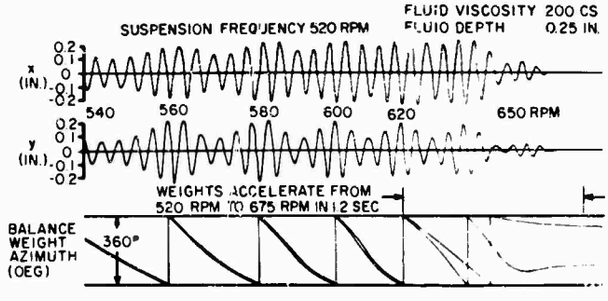

Fig. 12 - Final stage of acceleration of single rotating balance weights

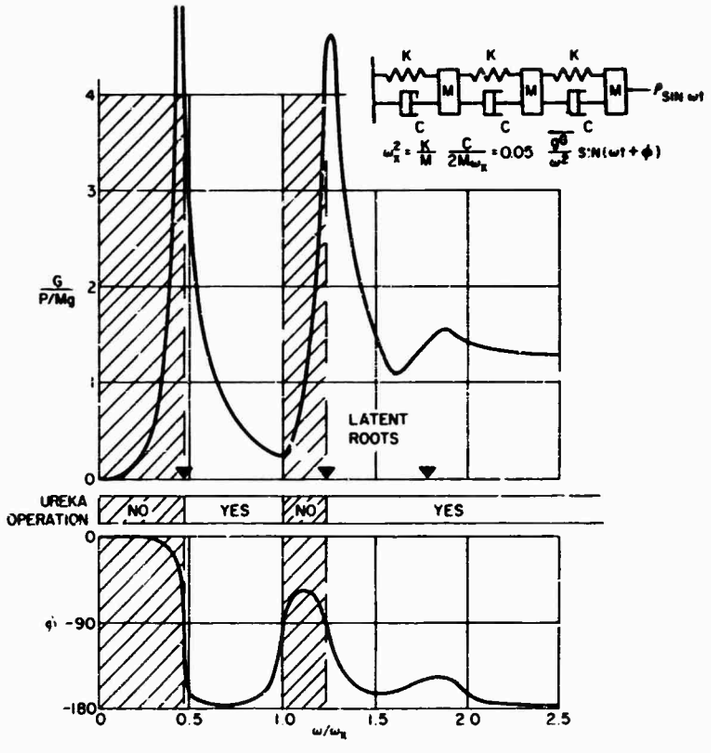

Fig. 13 - Typical multiple freedom structure showing regions for UREKA operation

small motion at the point of attachment, e.g., the third mode in Fig. 13.

The requirements for the nonisotropic case are more complicated. These were discussed [2] and can be summarized by saying that UREKA (a) balances if the phase lags of both directions lie between 90 and 180 deg, (b) does not balance if the phase lags of both directions lie between 0 and 90 deg, and (c) balances if the phase lag of one direction lies further in the 90- to 180-deg range than the phase lag of the other direction lies in the 90-to 0-deg region. (When the responses are different, only a calculation will determine the result).

Mounting conditions that are satisfactory for UREKA are often provided as a matter of course. For example, of the various helicopters considered for running a flight evaluation, about 50 percent already have satisfactory dynamics of the mounting point. A structure that is essentially rigid and freely suspended is ideal. A structure which has many modes of vibration will typically be satisfactory for UREKA operation above the 3rd or 4th mode. For operation in and around the first few modes, a shake test will be required to determine the suitability, and structural modification may be required to move a principal natural frequency by 20 percent or so. For an aircraft at the preliminary design stage, the requirement will be satisfied by incorporating semi-isolation in the hub mounting; that is, a degree of flexibility which will make the hub a major antinode and give a natural frequency that is 50 to 60 percent of the operating frequency.

APPLICATION TO A HELICOPTER

The plane of maximum n/rev forcing for a helicopter is typically the vertical/longitudinal plane. Application of the unit to an existing helicopter is shown diagrammatically in Fig. 14. This is a vertical/longitudinal counterrotating unit located at the rotor hub to prevent the n/rev motions from entering the fuselage. In this way the vibration of the fuselage will be reduced at all points.

The efficiency of such a unit is very high compared to the type of spring-mass absorber already described. This is because the balance

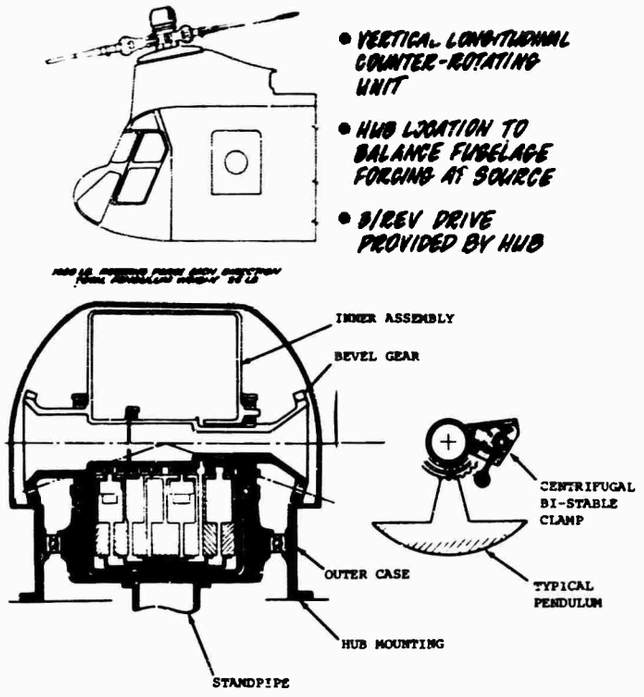

Fig. 14 - UREKA installation in a forward hub location

weights are typically operating at about 90 g, compared to 5 to 6 g for the absorber; i.e., 10-lb weights can produce up to 900 lb of useful force and cause zero motion of the mounting point, in contrast to the spring-mass absorber which leaves a small residual motion.

The unit operates in the following manner. The outer case is fixed to the rotor hub and carries a large bevel ring gear. The inner assembly contains the counterrotating pendulums, all of which rotate about an airframe lateral axis. The lateral axis is provided by bearings mounted in nonrotating structure carried on a standpipe which passes through the rotor shaft to the airframe. The bevel ring gear drives mating bevel gears at n/rev on opposite sides of the inner assembly and in opposite directions of rotation. Each gear drives a shaft which carries two freely swinging pendulums. Each pendulum is split into two equal parts which are placed on either side of the vertical/longitudinal plane of symmetry and are rigidly coupled together. In this manner, torsional excitation of the rotor hub is avoided. Each shaft carries one centrifugally operated clamp which clamps both weights of that shaft until the rotor speed is above the critical frequency.

Ideally, the unit would be designed to be buried inside the hub to provide minimum profile; this can be achieved when UREKA is incorporated at the preliminary design stage.

LIMITING EFFECT OF BALANCE WEIGHT FRICTION

It has already been shown that the balance weights make use of high g's to get large forces from small weights. In the interests of a light system, it would be beneficial to have the weights operating at as large a radius as possible and have proportionately lighter weights giving the same force.

Friction emerges as a factor limiting this trend. Whether the balance weights are pendulums on a small diameter bearing or balls rolling in an outer track, the friction between a weight and the shaft will exert a restraining torque. As the eccentric motion of the shaft tends to zero in the balancing process, there comes a point where the tangential component of centrifugal force directing the weights to their balance positions equals the friction force. The weights can stop moving at this point and thereby leave residual vibration.

This phenomenon is analyzed in the Appendix, and it is deduced that if no more than 5 percent of maximum obtainable residual force is allowed from UREKA, the operating limitations are given by

$$\frac{\mu r}{\mu_F b} \geq 10 .$$

where

μ = mass ratio,

μ_F = bearing friction coefficient,

r = balance weight radius, and

b = bearing radius.

This is plotted in Fig. 15, which shows the importance of keeping friction low and r/b high. Practically attainable values of μ_F vary from 0.0005 to 0.002, and this would give a lowest usable μ of 0.001, that is, a total single rotating balance weight of 1/500 of the effective weight of the mounting point (1/250 for counter-rotating). This still gives a very light system compared to ratios of 1/20 to 1/50 which are typical for a spring-mass absorber.

Note that the criterion given is pessimistic in neglecting the presence of vibration at other frequencies, which will tend to keep the balance weights on the move.

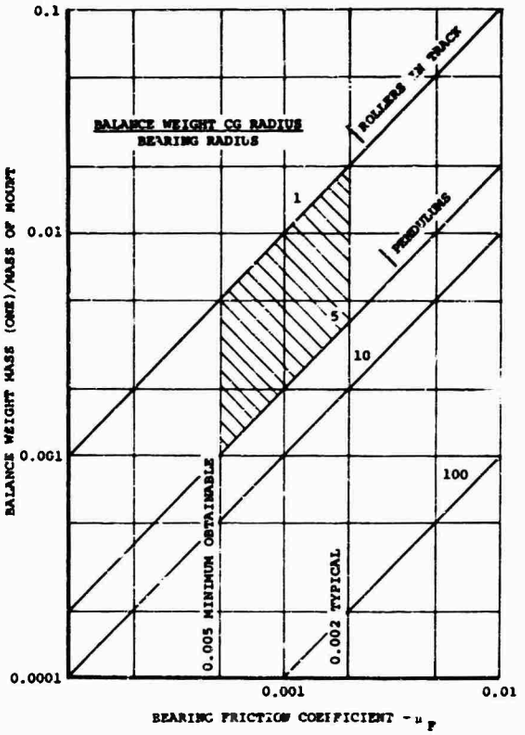

Fig. 15 - Limiting effect of friction on UREKA mass ratio

CONCLUSIONS

1. A vibration balancing device has been described which should be capable of reducing helicopter n/rev vibration to negligible levels.

2. The device is self-adaptive to changes in rotor speed, forcing levels, and phase.

3. It has a rapid response to transient loading, such as those produced by gusts and maneuvers.

4. Dynamic properties of the mounting point must approximate those of a supercritical shaft. Many installations have the required properties as an inherent part of their design.

5. Satisfactory acceleration through critical frequencies dictates either a minimum balance weight damping requirement or a speed-controlled clamp.

6. Friction between balance weights and the shaft must be minimized to avoid an undesirable level of residual exciting force.

7. The device is conveniently and effectively mounted on or integrated with a helicopter rotor hub. It requires no external power supplies (other than rotational drive) and can be sealed for life. It combines the virtues of simplicity, high efficacy, and reliability with moderate cost, complexity, and weight.

REFERENCES

1. J. P. Den Hartog, Mechanical Vibration (4th ed.), p. 237 McGraw-Hill, New York, 1956

2. W. E. Hooper, "UREKA – A Vibration Balancing Device for Helicopters," J. Am. Helicopter Soc., Vol. 11, No. 1, pp. 28-43, Jan. 1966

3. D. Reed and L. Mirandy, "UREKA – Analog Study of Counter-Rotating System," Boeing Doc. D8-0164, May 1965

4. J. Brass, "UREKA 6 – Digital Computing Program for Counter-Rotating System," Boeing Doc. D8-0165, May 1965

5. A. Mayer and J. Czarnecki, "UREKA – Model Test Report," Boeing Doc. D8-6166, May 1965

Appendix

BALANCE WEIGHT FRICTION AND RESIDUAL FORCING

NOMENCLATURE

- b Bearing radius, in.
- C Linear damping rate of suspension in X and Y directions, lb sec/in.
- C_β Balance weight rotational damping rate, lb in. sec.
- K Linear spring rate of suspension in X and Y directions, lb/in.
- M Suspension mass in X and Y directions, lb sec^2/in.
- m Mass of one balance weight, lb sec^2/in.
- N Natural frequency (X and Y directions) ratio = ω/Ω, nondimensional
- P External force in X and Y directions, lb
- r Radius of balance weight c.g., in.
- S Amplitude of eccentric suspension motion, in.
- t Time, sec
- x, y Linear displacements of suspension, in.
- ζ Damping ratio in X and Y directions = $C/(2M\omega)$, nondimensional
- ζ_{res} Residual force ratio = $\cos\psi$, nondimensional
- ζ Force ratio in X and Y directions = $P/(2mr\Omega^2)$, nondimensional
- ζ Balance weight damping ratio = $C_\beta/(mr^2\omega)$, nondimensional
- μ_F Bearing friction coefficient, nondimensional
- μ Mass ratio = $m/(M+4m)$, nondimensional
- ϕ Phase lag angle of suspension displacement behind external force, deg
- ψ Semi-angle between balance weights, deg
- ω Suspension frequency in X and Y directions = $[K/(M+4m)]^{1/2}$, nondimensional
- Ω Shaft angular velocity, rad/sec

ANALYSIS

As the weights approach their final positions for balance, the force compelling them to move approaches zero. When it drops below the friction force, the weights may stop short of their balance positions and cause residual forcing. This is most easily evaluated by considering an isotropically mounted single rotating UREKA (Fig. A-1).

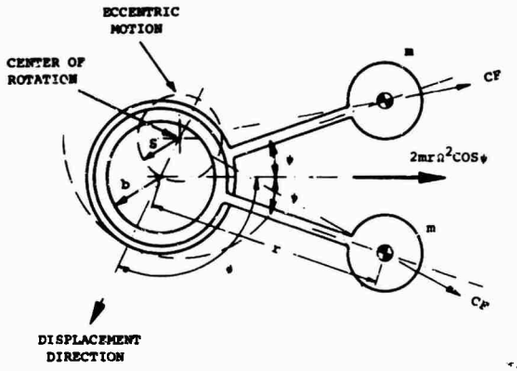

Fig. A-1 - Balance weights and eccentric shaft motion

Let the unit be rotating with balance weights separated by an angle 2ψ, thus causing a residual forcing of $2mr\Omega^2\cos\psi$.

The component of centrifugal force (CF) tending to rotate each balance weight on its bearing causes a moment,

$$mS\Omega^2 r \sin(\phi+\psi),$$

as shown in Fig. 5 of Ref. 2.

When the friction restraining torque equals this moment, we have

$$mr\Omega^2 b\mu_f = mS\Omega^2 r \sin(\phi \pm \psi),$$

or

$$\mu_f = \frac{S}{r}\frac{r}{b}\sin(\phi \pm \psi). \qquad \text{(A-1)}$$

The eccentric ratio S/r resulting from the applied circular force is obtained from the equation of motion,

$$M_x\ddot{x} + C_x\dot{x} + K_x x = 2mr\Omega^2 \cos\psi \cos\Omega t,$$

from which, dropping the subscripts for clarity,

$$\frac{x}{r} = \frac{2\mu\cos\psi}{(N^2-1) + 2i\delta N}\cos\Omega t,$$

$$\frac{S}{r} = \frac{2\mu\cos\psi}{\left[(N^2-1)^2 + (2\delta N)^2\right]^{1/2}}, \qquad \text{(A-2)}$$

and

$$\tan\phi = \frac{2\delta N}{N^2-1}. \qquad \text{(A-3)}$$

Therefore,

$$\frac{\mu_f}{\mu}\frac{b}{r} = \frac{2\cos\psi\sin(\phi \pm \psi)}{(N^2-1)^2 + (2\delta N)^2}. \qquad \text{(A-4)}$$

putting $\cos\psi = \zeta_{res}$ as a measure of the residual force (maximum residual force occurs when $\zeta_{res} = 1$). By substituting Eqs. (A-1), (A-2) and (A-3) in Eq. (A-4), we get

$$\frac{\mu_f b}{\mu r} = 2\zeta_{res}\left[\frac{2\delta N\zeta_{res} \pm (N^2-1)\sqrt{1-\zeta_{res}^2}}{(N^2-1)^2 + (2\delta N)^2}\right].$$

This relationship is plotted in Fig. A-2, for $\delta = 0.05$, to illustrate how the residual force depends on the natural frequency ratio N and the parameter $\mu r/\mu_f b$. This parameter should be as large as possible, thus emphasizing the importance of low friction and low bearing radius. It is also evident that, as N approaches unity, the requirement for low friction is less severe because a small residual force causes larger eccentric motions, thus causing greater balancing moments on the weights. A pendulum with a small bearing clearly has an advantage over a roller on a track in this respect because of the larger value of the ratio r/b.

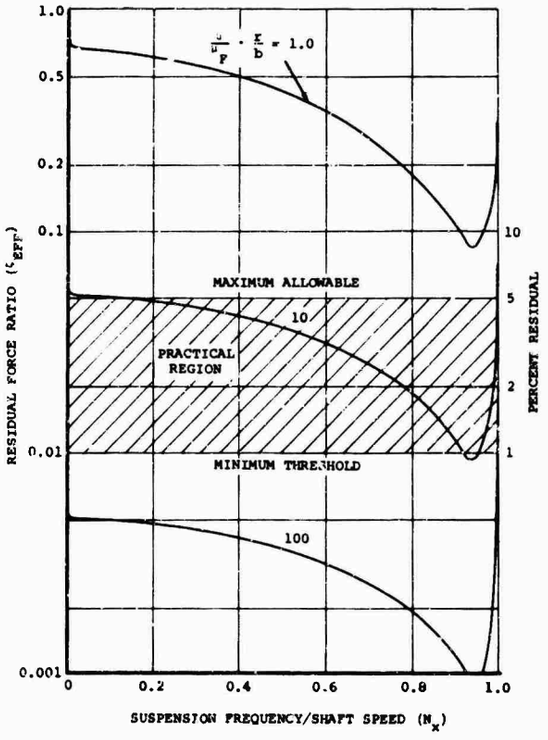

Fig. A-2 - Maximum residual force as a result of bearing friction

SHOCK RESPONSE OF ELECTRONIC EQUIPMENT CABINETS BY NORMAL MODE METHOD

T. K. Hasselman and C. M. Hwang
TRW Systems
Redondo Beach, California

The usefulness of the normal mode method for computing the dynamic shock response of base-excited cabinet-type structures is illustrated. The detailed dynamic loads which are obtained eliminate many of the uncertainties encountered in a load factor approach to the design problem. A structure can be "analytically tested" long before the hardware is available, which results in a more efficient development process. New configurations are particularly suited to the treatment.

Several sonar system cabinets were analyzed which averaged 65 in. in height and weighed approximately 300 to 1200 lb. Excitation consisted of an acceleration pulse recorded during prior testing of similar equipment on the Navy medium weight shock machine using the 25- to 30-cps simulated deck.

Insight into the excitation-system-response relationship can be provided by examination of plotted mode shapes and a comparison of their corresponding frequencies with the frequency content of the excitation. Isometric representation and orthographic projection of overall maximum displacements help to focus attention on critical areas and indicate how certain load conditions arise. They supplement corresponding sets of member loads in tabular form. The results of this analysis depend on the validity of the various assumptions which are made and therefore should be qualified by actual testing of the equipment.

INTRODUCTION

Shock testing of shipboard equipment has illustrated the need to consider dynamic loading in its design. Dynamic load factors are commonly used as a design guide but are generally inadequate for design evaluation since details regarding load distribution, stiffness and mass properties, and interconnection of structural members are omitted.

With the present availability of high-speed computing machines, the normal mode method can be a useful tool for handling more of these details in their proper relationship. Once a suitable dynamic model is established, its equations of motion can be written in matrix form. A modal analysis yields a transformation matrix which uncouples the equations of motion so that they may be solved individually for a known excitation. Solutions to the uncoupled equations of motion together with the transformation matrix constitute sufficient information for computing structural response. Member loads are obtainable from a knowledge of relative displacements and subsequent stress analyses can be made.

DYNAMIC MODEL

Modeling techniques must yield a model which is compatible with available computer programs. In this case, the task was to represent a basic cabinet structure, like the one shown in Fig. 1a, by a three-dimensional lattice-type structure, as shown in Fig. 1b. Since this cabinet was symmetric, only half of it was modeled. Each member of the lattice, being one dimensional, was given axial, torsional, and bending stiffness. Members were connected to each other by either pinned or rigid joints. The original mass distribution of the cabinet and its equipment was modeled by lumping it at the joints of the model. Thus, a system with distributed parameters was modeled as a lumped parameter system.

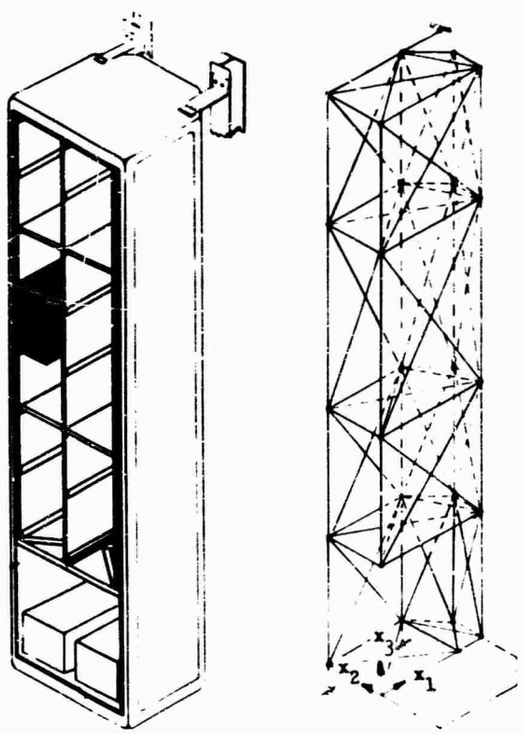

Fig. 1 - Idealization from (a) actual cabinet structure to (b) analytic model

Certain idealizations were made. The structure was assumed to have linear elastic properties. Beams of nonsymmetric cross section in the structure were replaced by doubly symmetric beams of equivalent bending stiffness in the model. Shear panels were replaced by planar lattices of axially stiff members with no torsional or bending stiffness using the methods of Hrennikoff [1] and Pestel [2]. Plates were replaced in a like manner by planar lattices of beam-type members which had out-of-plane bending stiffness but no axial, torsional, or in-plane bending stiffness. Structural component which did not fit the beam, panel, or plate categories were accounted for by directly including their force-deflection properties in the overall stiffness matrix. System damping was represented by light proportional viscous damping. The structure to which the cabinet was mounted was assumed to be much more rigid than the cabinet itself.

ANALYSIS

The analytical solution to the problem of determining the dynamic response of a complex structure to a deterministic transient input by the normal mode method is straightforward and well-known [3]. It is outlined here for clarity and completeness.

The equations of motion for a base-excited structure can be written in the following matrix form:

$$[m]\{\ddot{y}(t)\} + [c]\left(\{\dot{y}(t)\} - \{\dot{x}(t)\}\right) + [k]\left(\{y(t)\} - \{x(t)\}\right) = \{0\} . \quad (1)$$

where

$[m]$ = diagonal mass matrix,

$[c]$ = damping matrix,

$[k]$ = stiffness matrix,

$\{y(t)\}$ = time-dependent vector of cabinet displacement relative to ground, and

$\{x(t)\}$ = time-dependent vector of base displacement relative to ground.

If we let $y_i(t) - x(t) = z_i(t)$, where the subscript i denotes a coordinate number, Eq. (1) becomes

$$[m]\{\ddot{z}(t)\} + [c]\{\dot{z}(t)\} + [k]\{z(t)\} = -[m]\ddot{x}(t) \quad (2)$$

$\{z(t)\}$ is the time-dependent relative displacement vector of the cabinet with respect to its base. The equations of motion in the z coordinate system are coupled. With a knowledge of $[m]$ and $[k]$, a modal analysis is made to determine a set of eigenvalues ω_r^2 and eigenvectors $\{\phi^{(r)}\}$ which yield the natural frequencies and corresponding mode shapes for the system. r denotes the mode number. The eigenvectors, when arranged in matrix form, constitute a transformation matrix $[\Phi]$ which can transform the equations of motion in the coordinate system to a new coordinate system, q, where the equations become uncoupled:

$$\{z(t)\} = [\Phi]\{q(t)\} , \quad (3)$$

where $q_r(t)$ are the normal coordinates. Upon substitution of Eq. (3) into Eq. (1) and premultiplication by $[\Phi]^T$,

$$[\Phi]^T[m][\Phi]\{\ddot{q}(t)\} + [\Phi]^T[c][\Phi]\{\dot{q}(t)\} + [\Phi]^T[k][\Phi]\{q(t)\} = -[\Phi]^T[m]\{\ddot{x}(t)\} .$$

or

$$[M_r]\{\ddot{q}(t)\} + 2[\zeta_r \omega_r][M_r]\{\dot{q}(t)\} + [\omega_r^2][M_r]\{q(t)\} = -[\Phi]^T[m]\{\ddot{x}(t)\} \quad (4)$$

where

$$[\Phi]^T[m][\Phi] = [M_r] ,$$

the generalized mass matrix, and

$$[\Phi]^T[c][\Phi] = 2[\zeta_r \omega_r][M_r]$$

for proportional damping. ζ_r denotes the percent of critical damping for the rth mode. Let

$$\{\ddot{x}(t)\} = \{\alpha\}\ddot{x}_o(t) .$$

where $\ddot{x}_o(t)$ is the time-dependent magnitude of the input acceleration vector as shown in Fig. 2a which was recorded during prior testing of similar equipment on the Navy medium weight shock machine using the 25- to 30-cps simulated deck [4] and for n joints

$$\{\alpha\} = \begin{Bmatrix} \{\alpha\}_1 \\ \{\alpha\}_2 \\ \vdots \\ \{\alpha\}_n \end{Bmatrix} .$$

In addition,

$$\{\alpha\}_j = \begin{Bmatrix} \alpha_{j1} \\ \alpha_{j2} \\ \alpha_{j3} \\ 0 \\ 0 \\ 0 \end{Bmatrix} ,$$

$\alpha_{j1} = \cos \alpha_1$,

$\alpha_{j2} = \cos \alpha_2$,

$\alpha_{j3} = \cos \alpha_3$,

α_1 = angle between input vector and X_1 axis,

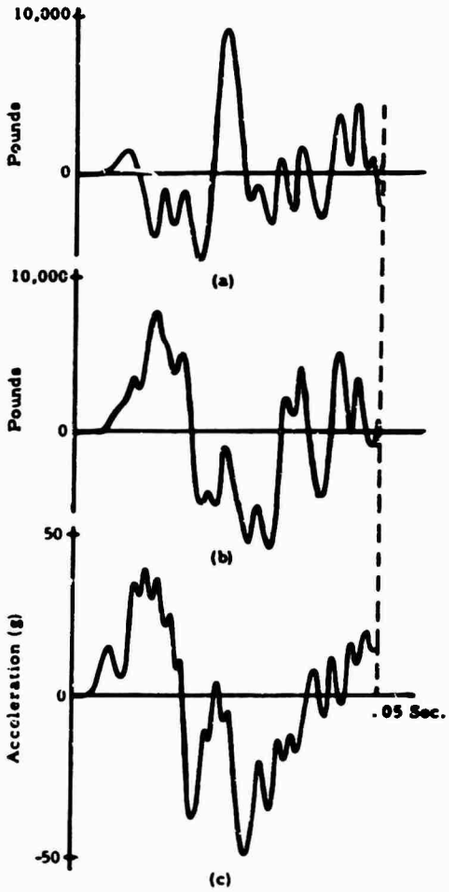

Fig. 2 - Cabinet response to base excitation: (a) right top support axial load, (b) left top support axial load, and (c) base acceleration

α_2 = angle between input vector and X_2 axis, and

α_3 = angle between input vector and X_3 axis.

The X_1, X_2, X_3 axes are shown in Fig. 1b. $\{\alpha\}$ may be called the direction cosine vector of the input. We define

$$[M_r]^{-1}[\Phi][m]\{\alpha\} = \{\Gamma_r\} .$$

where Γ_r is a modal participation factor which is a measure of the extent to which the rth mode participates in synthesizing the total dynamic load on the structure. The equations of motion in normal coordinates may be written in the matrix form,

$$\{\ddot{q}(t)\} + 2[\zeta_r \omega_r]\{\dot{q}(t)\} + [\omega_r^2]\{q(t)\} = -\{\Gamma_r\}\ddot{x}_o(t) \quad (5)$$

They may be solved individually as

$$\ddot{q}_r(t) + 2\zeta_r \omega_r \dot{q}_r(t) + \omega_r^2 q_r(t) = -\Gamma_r \ddot{x}_o(t) \quad (6)$$

A big advantage in using the normal mode method is the simplification that results from neglecting higher modes. This brings up the question of modal convergence. Specifically, how many modes must be included in a summation for relative displacement $\{z(t)\}$ or for absolute acceleration $\{\ddot{y}(t)\}$ to achieve satisfactory convergence?

Consider Eq. (3) and

$$\{\ddot{y}(t)\} = \{\ddot{z}(t)\} + \{\ddot{x}(t)\} = [\Phi]\{\ddot{q}(t)\} + \{\alpha\}\ddot{x}_o(t) \quad (7)$$

In fact, $\{z(t)\}$ converges faster than $\{\ddot{y}(t)\}$ because $\{z(t)\}$ depends on $\{q(t)\}$ and $\{\ddot{y}(t)\}$ on $\{\ddot{q}(t)\}$, and since $\{q(t)\}$ is of the order

$$[\omega_r^2]^{-1}\{\ddot{q}(t)\},$$

its rate of convergence is increased by the rate at which $1/\omega_r^2$ becomes smaller. If only stresses are required, satisfactory convergence of $\{z(t)\}$ is all that is necessary, since stress depends on strain, and strain on relative displacement. Of course, if we choose to evaluate $\{z(t)\}$ from Eq. (2),

$$\{z(t)\} \approx -[k]^{-1}[m]\{\ddot{y}(t)\} = -[k]^{-1}[m]\left([\Phi]\{\ddot{q}(t)\} + \{\alpha\}\ddot{x}_o(t)\right) \quad (8)$$

where second order damping forces are neglected. $\{z(t)\}$ still converges at the same rate as it did in Eq. (3). However, if an acceleration distribution is required (e.g., for evaluation of brackets and fasteners which attach electronic components to the cabinet), then convergence of $\{\ddot{y}(t)\}$ must be achieved. Another way to compute absolute acceleration is

$$\{\ddot{y}(t)\} \approx -[\Phi][\omega_r^2]\{q(t)\}. \quad (9)$$

which also ignores damping forces.

If all terms of Eq. (9) are included, the accuracy of the approximation depends only on damping being small. However, when higher modes are neglected, convergence of Eq. (9) becomes poor in regions near the support points. Equations (7) and (9) are commonly known as the modal acceleration and modal displacement methods, respectively. The latter was not used because of its convergence problems [3,5]. Satisfactory convergence of the former was usually achieved in 12 modes.

RESULTS

The quantity $\{z(t)\}$ represents a complete time history of response for the entire structure. Quantitatively, our concern was only for those points in time at which critical stresses occurred. It was generally difficult to identify these times, not only because of the large quantities of response information to be examined, but also because stresses in the model sometimes differed significantly from those in the actual structure, depending on how the structure was modeled. However, support forces were found to be a good indicator since peaks in support force time histories tended to coincide with large relative displacements of the overall structure. Since these structures are usually supported at only a few points, it was convenient to obtain machine plots of the support force time histories. Other displacement or acceleration vs time plots were sometimes helpful, particularly for unusual configurations. In any case, engineering judgment was required. Several times, t_i, were selected for which complete sets of member loads were computed. Corresponding to each set was a relative displacement vector $\{z(t_i)\}$ which could be plotted to give a visual picture of structural deformation (Fig. 3).

A typical dynamic side load is shown in Fig. 4 for the cabinet shown in Fig. 1. Each plotted point represents the magnitude of a concentrated dynamic side load occurring on the left front corner post. The points are connected by straight lines for visual continuity. In contrast is the straight vertical line which represents an empirical load factor. A load factor can be no better than a straight line representing a spacewise average load, and for some cabinets it may be hard to predict this average.

The results of this type of analysis depend on the validity of the assumptions which are made and, therefore, should be qualified by actual testing of the equipment.

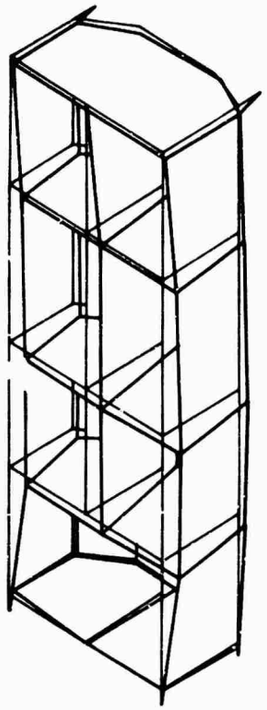

Fig. 3 - Isometric representation of relative displacements

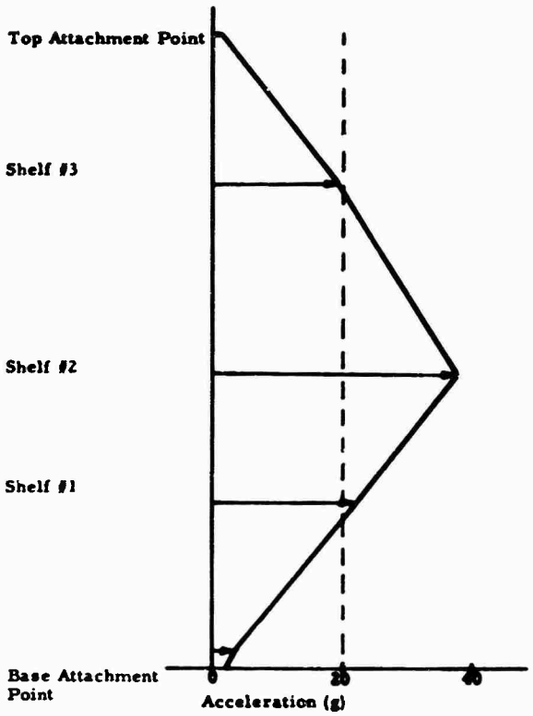

Fig. 4 - Side load on front of cabinet

ACKNOWLEDGMENTS

This work was performed under Navy Contract NOw 66-0393d. The authors wish to acknowledge the cooperation of the ASW Program Office, Ships Systems Command, and the U.S. Navy Underwater Sound Laboratories.

REFERENCES

1. A. Hrennikoff, "Soiution of Problems of Eiasticity by the Framework Method," J. Appi. Mech., Vol. 8, pp. A-169—A-175, 1941
2. E. C. Pestel, "Investigation of Plate and Shell Modeis by Matrices," Technische Hochschuie, Hannover, Germany, 1963
3. W. C. Hurty and M. F. Rubinstein, Dynamics of Structures. Prentice Hail, Englewood Cliffs, N. J., 1964
4. C. J. Floyd, "A Simulated 25-30 CPS Deck for Shock Testing," Shock and Vibration Buil., No. 35, Part 1, March 1966
5. R. L. Bisplinghoff, H. Ashley, R. L. Halfman, Aeroelasticity. Addison-Wesley, Cambridge, Mass., 1955

BIBLIOGRAPHY

Barton, M. V., V. Chabotov, and Y. C. Fung, "A Collection of Information on Shock Spectrum of a Linear System," TRW Systems Rept. EM 11-9, July 1961

Pestel, E. C., and F. A. Leckie, Matrix Methods in Elastomechanics. McGraw-Hill, New York, 1963

Wada, B., "Stiffness Matrix Structural Analysis," JPL Tech. Rept. 32-774, 1965

"Military Specification Shock Tests, H.I. (High Impact): Shipboard Machinery, Equipment and Systems, Requirements For," Mil. Spec. MIL-S-901C (Navy)

DISCUSSION

Mr. Tomassoni (Martin Co.): Did you attempt to investigate various degrees of end fixity on the cabinets, that is, the different flexibilities that the structures may have had where they were tied in.

Mr. Hasselman: These cabinets were mounted at both the cabinet base and generally to two points on the top. The boundary conditions were applied to the portions of the brackets that attached to the rigid test fixture, and these were assumed perfectly fixed. The cabinet did feel the intermediate fixity, so to speak, because of flexibility of the mounting brackets.

Mr. Tomassoni: Was this analysis made with components in the cabinet?

Mr. Hasselman: The mass of the components to be included in the cabinet was lumped along with the cabinet mass at the joints of the lattice. As far as structural contributions from the components were concerned, this was ignored.

Mr. Tomassoni: Was there any correlation with test results?

Mr. Hasselman: We do not have any test results yet with which we can compare our analysis. However, we were able to compare order of magnitude results with the tests that were performed on similar cabinets on this machine. This is the best comparison we have been able to make.

Mr. Lou (General Dynamics/San Diego): You show a cabinet that is supported down the center. Is this open-front cabinet what you have actually assumed, or did you assume literally two small cabinets bolted together structurally?

Mr. Hasselman: Our structural model was a cabinet shell, open in the front. Since the structure was symmetric, both elastically and inertially, we only modeled half of the cabinet but the restraints on the plane of symmetry were such that the modes that we got were either antisymmetric or symmetric, and then these were combined later in the modal synthesis.

* * *

DAMPED VIBRATIONS OF ELASTICALLY SUPPORTED RIGID BODY WITH COUPLING BETWEEN TRANSLATION AND ROTATION

Francis H. Collopy
Itek Corporation
Lexington, Massachusetts

F. H. Collopy

INTRODUCTION

In certain engineering applications, elastically supported systems having two degrees of freedom, rotation and translation, have system requirements which necessitate negligible rotational motion response to vibrational inputs. One such application is elastically supported optical equipment which requires a minimum rotational movement of the optimal axis so as to ensure high-quality resolution. The vibrational inputs may consist of translational and/or rotational ground motion or may be induced by a force excitation at any arbitrary point on the rigid body.

For systems which require a minimum of coupling motion between translation and rotation, it would seem adequate to locate the resultant of the spring system at the body center of gravity. This would apparently be accomplished by a center of gravity mounting system. However, the presence of a small eccentricity between the center of gravity of the isolated body and the spring resultant could cause a crosscoupling effect which would result in undesirable motions.

Although the simplicity of the subject matter suggests the possibility of previous exposure in the technical literature, apparently no discussion exists which includes damping effects. The Shock and Vibration Handbook contains a chapter [1] which abounds with various isolation systems analyses and includes damping effects. However, none of the results apply to the system under consideration in this paper. The text by Jacobsen and Ayre [2] does contain the undamped solution for "an elastically supported rigid body having two degrees of freedom, one in translation, X, and the other in rotation, Θ." Lord Manufacturing Company also released a report [3] which presents the solution to the undamped case. Since present specifications include motions which are defined over a broad frequency range (which usually includes resonant conditions), it is desirable to have a knowledge of the nature of the damped solutions.

It is the purpose of this paper to provide the solution to the damped system for a certain range of dimensionless parameters and to describe the means for future analytical extensions.

APPROACH

Assumptions

For the purposes of this paper it is assumed that the distance e as shown in Figs. 1 and 2 is relatively small (on the order of 1 in.). This is a realistic assumption for systems for which it is desirable to minimize crosscoupling effects. However, to illustrate the effects of large values of e, some curves of nondimensional response ratios are presented in this paper (Fig. 3).

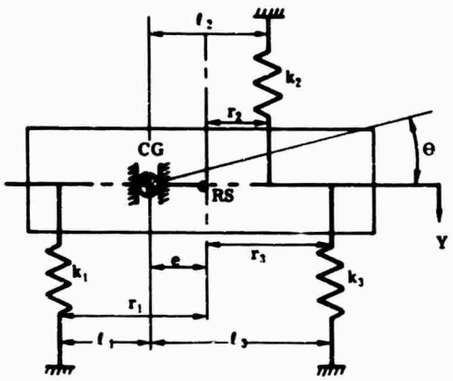

CG — Center of gravity
RS — Location of resultant spring

Fig. 1 - Single mass system having two degrees of freedom

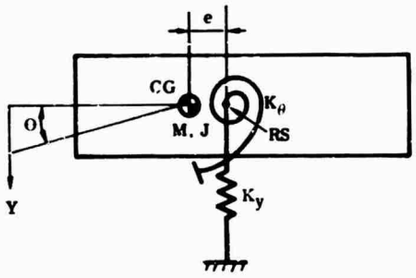

CG—Center of gravity
RS—Location of resultant spring
M—Mass of rigid body
J—Moment of inertia of rigid body

Fig. 2 - Equivalent system of Fig. 1

Equations of Motion

To acquaint the reader better with the system under consideration and the differential equations of motion which govern this system, attention is called to Fig. 1. A similar figure appears in the text of Jacobsen and Ayre [2]. The equations of motion for free vibration of this system are

$$M\ddot{Y} + (k_1 + k_2 + k_3)Y + (k_1\ell_1 - k_2\ell_2 - k_3\ell_3)\theta = 0$$

and

$$J\ddot{\theta} + (k_1\ell_1^2 + k_2\ell_2^2 + k_3\ell_3^2)\theta + (k_1\ell_1 - k_2\ell_2 - k_3\ell_3)Y = 0 . \quad (1)$$

Jacobsen and Ayre [2] show that by substituting a set of resultant springs for the spring system, a simpler form of Eqs. (1) can be obtained. If we choose the relationship that the resultant translatory spring constant K_y is simply the sum of the individual spring constant, then $K_y = k_1 + k_2 + k_3$, or, in general,

$$K_y = \sum_1^n k_i .$$

If r_1, r_2 and r_3 denote the distances from the individual springs to the line of action of the resultant, the following equation holds true:

$$-k_1r_1 + k_2r_2 + k_3r_3 = 0 . \quad (2)$$

The following relationships also hold true (Fig. 1):

$$r_1 = \ell_1 + e ,$$

$$r_2 = \ell_2 - e ,$$

$$r_3 = \ell_3 - e .$$

Making these substitutions in Eq. (2) and solving for e, we find

$$e = \frac{-k_1\ell_1 + k_2\ell_2 + k_3\ell_3}{k_1 + k_2 + k_3} ,$$

or

$$e = \frac{\sum_1^n k_i\ell_i}{K_y} . \quad (3)$$

Furthermore, the resultant rotational spring constant is given by

$$K_\theta = k_1r_1^2 + k_2r_2^2 + k_3r_3^2 ,$$

or

$$K_\theta = \sum_1^n k_i r_i^2 . \quad (4)$$

By use of Eqs. (2), (3), and (4), Eqs. (1) can be written

$$M\ddot{Y} + K_yY - eK_y\theta = 0$$

and

$$J\ddot{\theta} + (K_\theta + e^2K_y)\theta - eK_yY = 0 . \quad (5)$$

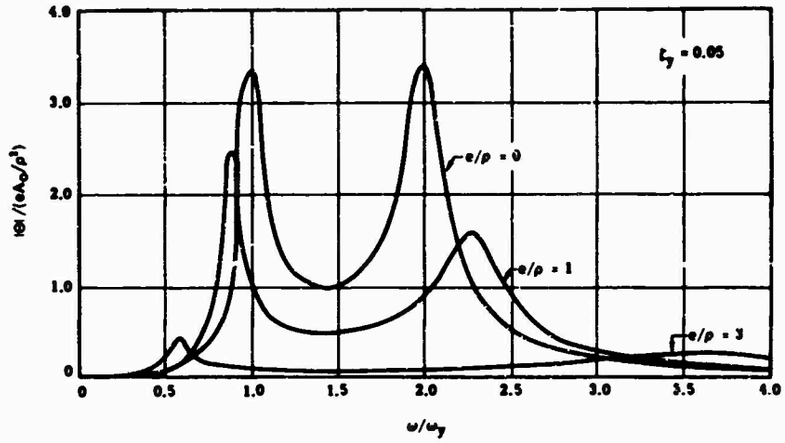

Fig. 3 - Dependence of rotational amplitude ratios on variation of e/ρ values

Jacobsen and Ayre [2] describe this derivation in finer detail; it is reproduced in this work merely to complete the discussion.

Equations (5) are the governing equations for the resulting system as shown in Fig. 2. If the springs shown in Fig. 2 have corresponding dampers C_y and C_θ, then the differential equations of motion are

$$M\ddot{Y} + C_y\dot{Y} - eC_y\dot{\theta} + K_yY - eK_y\theta = 0$$

and (6)

$$J\ddot{\theta} + (C_\theta + e^2C_y)\dot{\theta} - eC_y\dot{Y} + (K_\theta + e^2K_y)\theta - eK_yY = 0.$$

Definition of Terms

To present the results in a nondimensional form, it is necessary to use various parameters:

$$\omega_y = \sqrt{K_y/M},$$

$$\rho = \sqrt{J/M},$$

$$\frac{C_y}{M} = 2\zeta_y\omega_y,$$

$$r = \zeta_\theta/\zeta_y,$$

$$\omega_\theta = \sqrt{K_\theta/J},$$

$$a = \sqrt{K_\theta/K_y},$$

and

$$\frac{C_\theta}{J} = 2\zeta_\theta\omega_\theta.$$

It is evident from these definitions that $\omega_\theta/\omega_y = a/\rho$.

FORCED VIBRATION

Ground Displacement

If the system of Fig. 2 is subjected to a steady-state vibrational ground motion Y_0 then the equations of motion become

$$M\ddot{Y} + C_y\dot{Y} - eC_y\dot{\theta} + K_yY - eK_y\theta = K_yY_0 + C_y\dot{Y}_0$$

and (7)

$$J\ddot{\theta} + (C_\theta + e^2C_y)\dot{\theta} - eC_y\dot{Y} + (K_\theta + e^2K_y)\theta - eK_yY = -eK_yY_0 - eC_y\dot{Y}_0.$$

At this point it is best to introduce the concept of complex amplitude to describe the driving motion and subsequent response. This concept simplifies tremendously the treatment of forced vibrations of systems of more than one degree of freedom [4]. The function

$$Y = \underline{Y}\cos(\omega t - \alpha)$$

using complex notation can be written as

$$Y = \underline{Y}e^{i(\omega t - \alpha)} = \underline{Y}e^{-i\alpha}e^{i\omega t} = \bar{Y}e^{i\omega t},$$

where $\bar{Y} = \underline{Y}e^{-i\alpha}$ is called the complex amplitude.

Letting the ground motion be expressed as $Y_0 = A_0e^{i\omega t}$, the steady-state vibration may be

expressed by $Y = \bar{Y} e^{i\omega t}$ and $\theta = \bar{\theta} e^{i\omega t}$. By substitution of these expressions into Eq. (7) and performance of the mathematical steps involved, it can be shown that the solutions are equal to

$$Y = \frac{\left\{\frac{\omega^2}{\omega_y^2}\left[-1 - 4r\zeta_y^2\frac{a}{\rho}\right] + \frac{a^2}{\rho^2}\right\} + i\left\{2\zeta_y\frac{\omega}{\omega_y}\left[\frac{a}{\rho}\left(r + \frac{a}{\rho}\right) - \frac{\omega^2}{\omega_y^2}\right]\right\} A_0 e^{i\omega t}}{D} \quad (8)$$

and

$$\theta = \frac{\left(\frac{eA_0}{\rho^2}\right)\left(\frac{\omega^2}{\omega_y^2}\right)\left(1 + 2\zeta_y\frac{\omega}{\omega_y}i\right)e^{i\omega t}}{D}. \quad (9)$$

where

$$D = \left[\frac{\omega^4}{\omega_y^4} - \frac{\omega^2}{\omega_y^2}\left(1 + \frac{e^2}{\rho^2} + \frac{a^2}{\rho^2} + 4r\frac{a}{\rho}\zeta_y^2\right) + \frac{a^2}{\rho^2}\right] + i\left[-\frac{\omega^3}{\omega_y^3}(2\zeta_y)\left(1 + \frac{a}{\rho}r + \frac{e^2}{\rho^2}\right) + \frac{\omega}{\omega_y}\left(2\zeta_y\frac{a}{\rho}\right)\left(\frac{a}{\rho} + r\right)\right]. \quad (10)$$

When D in Eq. (10) is set equal to zero, the resulting equation is the dimensionless frequency equation. The graph of this equation is shown in Fig. 4, and it depicts the dependence of the frequencies on the value of e/ρ and a/ρ. For the purposes of this discussion, it is assumed that the eccentricity e is small and e/ρ is much less than 1.0 (i.e., $e/\rho = 0.01 \rightarrow 0.1$). Thus in Eq. (10), the term e^2/ρ^2 can be eliminated for ease of presentation. From Fig. 4, when $e/\rho = 0$, the two natural frequencies ω/ω_y are 1.0 and a/ρ.

Complex Algebra Simplification

The equations for Y and θ are in the complex form of

$$\frac{a + bi}{c + di}. \quad (11)$$

When this equation is expanded, using the algebraic laws pertaining to complex numbers, the following relationship appears:

$$\frac{ac + bd}{c^2 + d^2} - i\frac{ad - bc}{c^2 + d^2}, \quad (12)$$

which is in the form of $e - if$. This expression for the complex amplitude yields the real amplitude, $\sqrt{e^2 + f^2}$, with the phase angle described as

$$\alpha = \tan^{-1}\frac{f}{e}. \quad (13)$$

By referring to Eq. (12) and letting $e = (ac + bd)/(c^2 + d^2)$ and $f = (ad - bc)/(c^2 + d^2)$, we can express the real amplitude, $\sqrt{e^2 + f^2}$, as

$$\sqrt{e^2 + f^2} = \sqrt{\frac{a^2 + b^2}{c^2 + d^2}}. \quad (14)$$

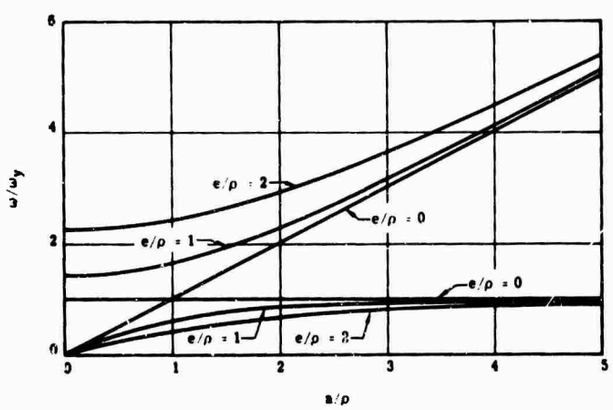

Fig. 4 - Dimensionless frequency curves as functions of length ratios e/ρ and a/ρ

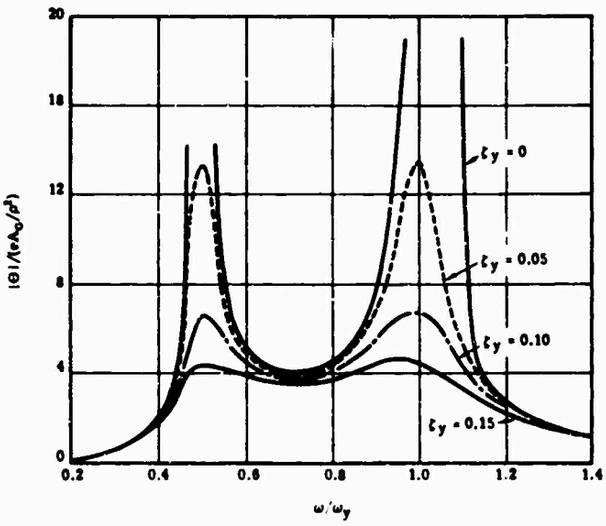

Fig. 5 - Dimensionless rotational amplitude ratios ($a/\rho = 1/2$, $r = 1$)

and the phase angle as

$$\alpha = \tan^{-1}\left(\frac{ad - bc}{ac + bd}\right).$$

Nondimensional Amplitude Ratios

Since Eqs. (8) and (9) are in the complex form of $(a+bi)/(c+di)$, as mentioned before, the results of Eq. (14) can be used to obtain the dimensionless amplitude ratios $|Y|/A_0$ and $|\Theta|/(eA_0/\rho^2)$. It is unnecessary to expand the equations here. These dimensionless ratios and their dependence on the many parameters can be calculated very nicely with a high-speed computer. The plots of the resulting rotational amplitude ratios are presented in Figs. 5 through 8. No plots are necessary for $|Y|/A_0$, since the mathematical operations on Eq. (8) suggested by Eq. (14) simply yield the transmissibility curve for a one-degree-of-freedom system.

Referring to the curves for $|\Theta|/(eA_0/\rho^2)$, we observed that the peaks occur at $\omega/\omega_y = 1$ and a/ρ. These frequencies are the translational and rotational uncoupled frequencies ω_y and ω_θ. When these frequencies are equal to each other ($a/\rho = 1$), only one peak occurs, as illustrated in Fig. 6. The curves presented herein represent only a small sample of the many possibilities available by varying the parameters.

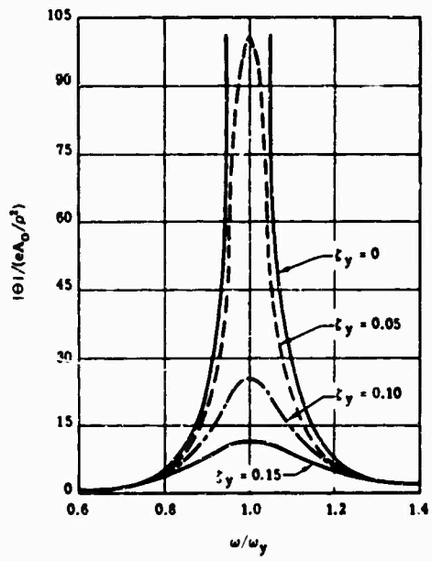

Fig. 6 - Dimensionless rotational amplitude ratios ($a/\rho = 1$, $r = 1$)

Another set of curves that might prove useful would be a plot of the peak values of $|\Theta|/(eA_0/\rho^2)$ vs a/ρ. This is simply a cross plot of the peaks of the family of curves similar to those in Figs. 5 through 8. This is illustrated in Fig. 9. The peak values marked m can be plotted vs a/ρ. These represent the maximum rotational amplitudes occurring when the

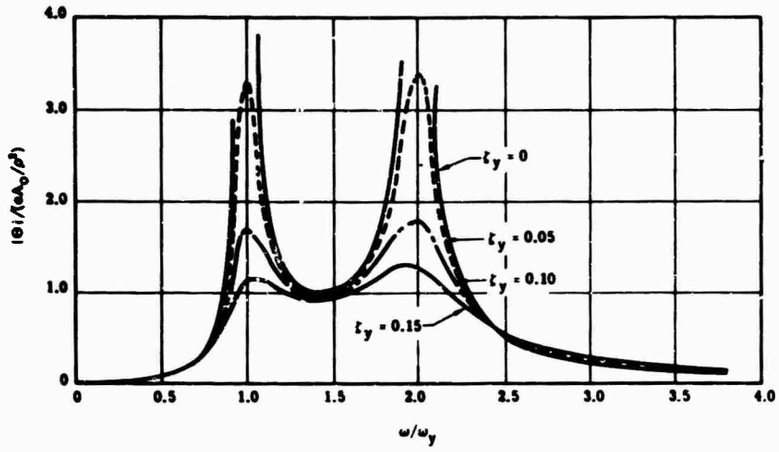

Fig. 7 - Dimensionless rctational amplitude ratios ($a/\rho = 2$, $r = 1$)

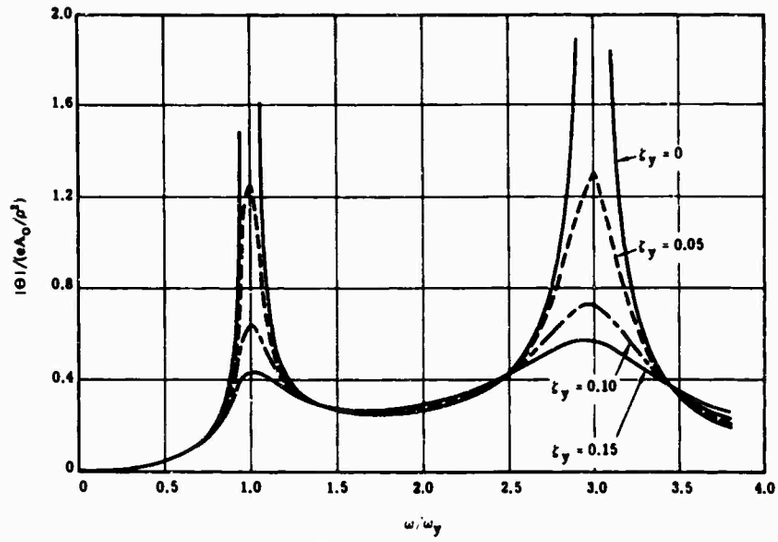

Fig. 8 - Dimensionless rotational amplitude ratios ($a/\rho = 3$, $r = 1$)

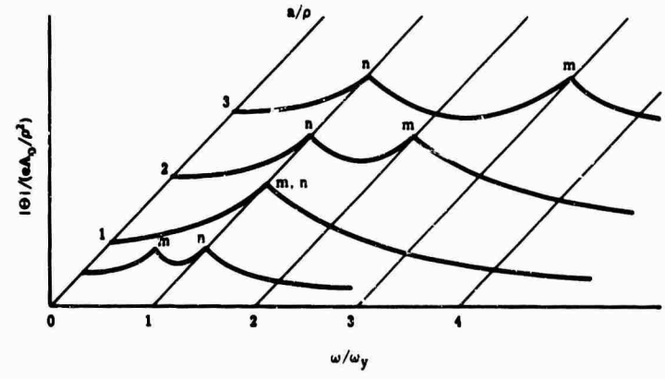

Fig. 9 - Family of curves, $|\theta|/(eA_0/\rho^2)$

forcing frequency ω equals the uncoupled rotational frequency ω_θ. The peaks marked n are the maximum rotational amplitudes when ω equals the uncoupled translational frequency ω_y. Mathematical expressions of these plots can be derived from Eqs. (9) and (14). The mathematics involved will not be given here.

For $\omega/\omega_y = 1$, we obtain

$$\frac{|\Theta|}{eA_0/\rho_2} = \frac{1}{2r_y}\sqrt{\frac{1+4\zeta_y^2}{4r^2\left(\frac{a}{\rho}\right)^2\zeta_y^2+\left[\left(\frac{a}{\rho}\right)^2-1\right]^2}}. \quad (15)$$

For $\omega/\omega_y = a/\rho$, we obtain

$$\frac{|\Theta|}{eA_0/\rho_2} = \frac{1}{2r\zeta_y}\sqrt{\frac{1+4\zeta_y^2\left(\frac{a}{\rho}\right)^2}{4\left(\frac{a}{\rho}\right)^2\zeta_y^2+\left[\left(\frac{a}{\rho}\right)^2-1\right]^2}}. \quad (16)$$

The graphs of Eq. (15) are shown in Figs. 10, 11, and 12. The graphs of Eq. (16) are shown in Figs. 13, 14, and 15.

Ground Rotation

If the system of Fig. 2 is subjected to a steady-state vibrational ground rotation Θ_0 instead of a ground displacement A_0, the following relationships hold:

$$\frac{|Y|}{e\Theta_0} = \frac{|\Theta|}{eA_0/\rho^2};$$

that is, the ordinate of Figs. 5 through 15 can be either $|\Theta|/(eA_0/\rho^2)$ or $Y/e\Theta_0$, and

$$\frac{|\Theta|}{\Theta_0} = \frac{|Y|}{A_0}$$

(same as for one degree of freedom).

Force Excitation at Arbitrary Point ($e/\rho \ll 1$)

If a force P_0 is applied at any arbitrary point on the body at a distance ℓ from the center of gravity, then the following nondimensional equation results:

$$\frac{\frac{\Theta}{\ell P_0}}{K_y\rho^2} = \frac{\left(\frac{\omega^2}{\omega_y^2}-1\right)+i\left(-2\zeta_y\frac{\omega}{\omega_y}\right)}{D}.$$

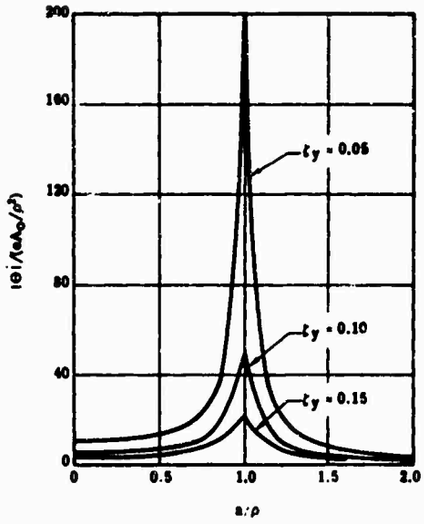

Fig. 10 - Plot of rotational amplitude ratios at uncoupled translational frequency ω_y (r = 1/2)

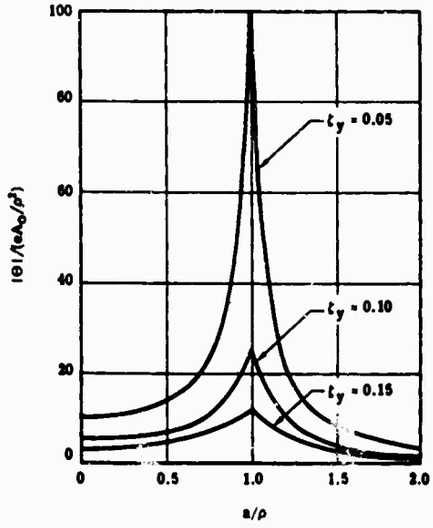

Fig. 11 - Plot of rotational amplitude ratios at uncoupled translational frequency ω_y (r = 1)

This equation is now in the complex form of Eq. (11) and can be evaluated as demonstrated previously.

DISCUSSION

The results as shown in Figs. 5 through 15 reveal some interesting, but not necessarily startling, facts:

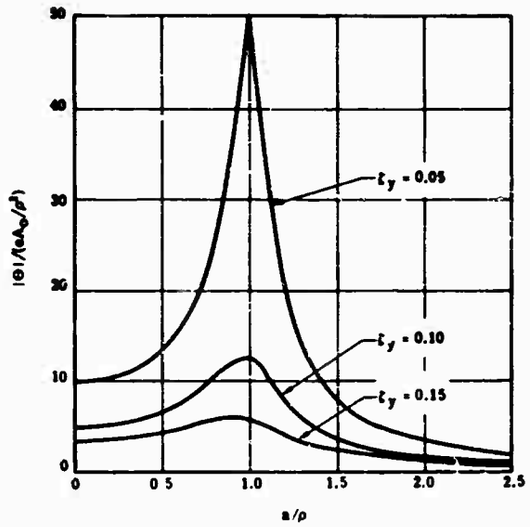

Fig. 12 - Plot of rotational amplitude ratios at uncoupled translational frequency ω_y (r = 2)

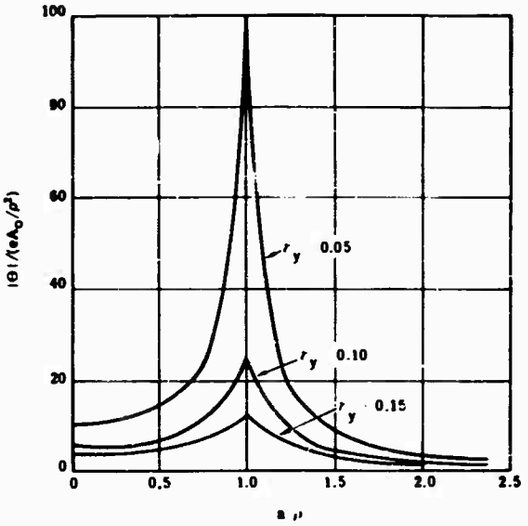

Fig. 14 - Plot of rotational amplitude ratios at uncoupled rotational frequency ω_θ (r = 1)

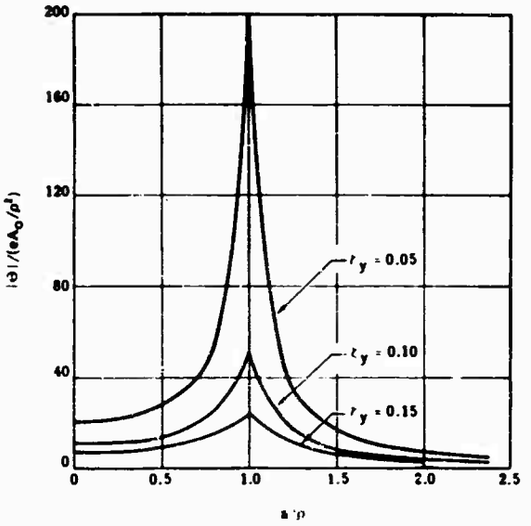

Fig. 13 - Plot of rotational amplitude ratios at uncoupled rotational frequency ω_θ (r = 1/2)

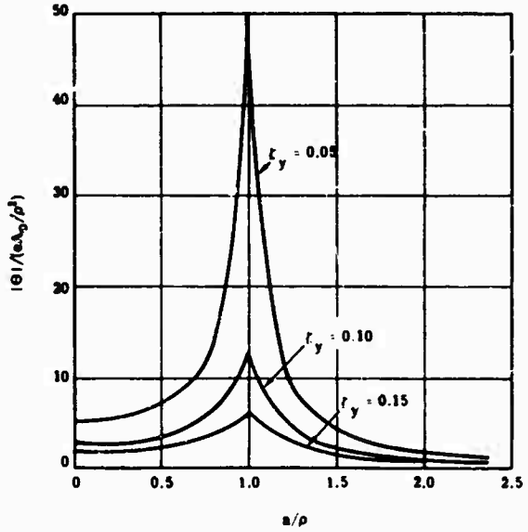

Fig. 15 - Plot of rotational amplitude ratios at uncoupled rotational frequency ω_θ (r = 2)

1. The amount of damping present in the system directly affects the response ratio.

2. The two uncoupled natural frequencies should be separated as far as practicable.

3. Figure 11 indicates that at the uncoupled translational natural frequency, the maximum rotational response ratio $|\theta/(eA_0/\rho^2)|$ is equal to $(1/2\zeta_y)^2$, and this occurs when $a/\rho = 1$; that is, when ω_y and ω_θ are equal.

4. Figure 11 ($r = 1$) also indicates that the value of $\theta/(eA_0/\rho^2)$ at $a/\rho = 0$ is $1/2\zeta_y$. In fact, at all points on the curve, the response ratio is equal to $1/2\zeta_y$ multiplied by the relative motion magnification curve of a one-degree-of-freedom system [4, p. 91].

Items 3 and 4 are not too unexpected and can be shown to be mathematically correct: (a) when $\omega/\omega_y = 1$, the relative deflection of the spring K_y is equal to $(1/2\zeta_y)A_0$ (for small damping); (b) the force from the spring acting on the mass at a distance e from the center of gravity is $K_y(1/2\zeta_y)A_0$; (c) this force results in a moment, $M = eK_y A_0/2\zeta_y$, acting on the very weakly coupled rotational system ($e/\rho \ll 1$); (d) the nondimensional ordinate for the magnification factor of a single-degree-of-freedom [4] rotational system is

$$\frac{\theta}{\theta_{static}} = \frac{\theta}{M/K_\theta} = \frac{1}{\sqrt{\left(1 - \frac{\omega^2}{\omega_n^2}\right)^2 + 4\zeta^2 \frac{\omega^2}{\omega_n^2}}};$$

(e) the forcing frequency is ω_y and the natural frequency of the rotational system is ω_θ; therefore, (ω/ω_n) which appears in the preceding relationship is ω_y/ω_θ or ρ/a; (f) expanding $\theta/(M/K_\theta)$, we obtain

$$\frac{\theta}{M/K_\theta} = \frac{1}{\sqrt{\left(1 - \frac{\omega^2}{\omega_n^2}\right)^2 + 4\zeta_y^2 \frac{\omega^2}{\omega_n^2}}}$$

$$= \frac{1}{\sqrt{\left(1 - \frac{\rho^2}{a^2}\right)^2 + 4\zeta_y^2 \frac{\rho^2}{a^2}}}.$$

Therefore,

$$\theta = \frac{\frac{eK_yA_0}{2\zeta_yK_\theta}}{\sqrt{1 - \left(\frac{\rho^2}{a^2}\right)^2 + 4\zeta_y^2 \frac{\rho^2}{a^2}}}.$$

It can be shown that this becomes

$$\frac{\theta}{eA_0/\rho^2} = \frac{\frac{\rho^2}{a^2} \cdot \frac{1}{2\zeta_y}}{\sqrt{\left(1 - \frac{\rho^2}{a^2}\right)^2 + 4\zeta_y^2 \frac{\rho^2}{a^2}}}. \quad (17)$$

which is $1/2\zeta_y$ times the relative magnification curve for a single degree of freedom. For small damping, it can be seen that Eq. (17) is equal to Eq. (15).

Referring to Eq. (17) and item 3 above, when $a/\rho = 1$,

$$\frac{\theta}{eA_0/\rho^2} = \left(\frac{1}{2\zeta_y}\right)^2.$$

Referring to item 4, when $a/\rho = 0$, the limit of $\theta/(eA_0/\rho^2)$, as a/ρ approaches 0, is $1/2\zeta_y$.

Fig. 9 is most useful in understanding the interdependence of the various parameters in three-dimensional space.

CONCLUSIONS

The curves presented illustrate the interdependence of the following parametric quantities: mass, mass moment of inertia, translational and rotational spring rates and damping constants, and the distance between the center of gravity of the system and the excitation. The curves are not drawn for all possible combinations of the parameters, but are readily obtainable from the equations presented.

Although most of this presentation is applicable to a system with e/ρ much less than one, some curves are presented for higher values of e/ρ. Fig. 3 illustrates the rotational amplitude ratios for e/ρ equal to 1 and 3.

As mentioned previously, these values of e/ρ are not realistic for most representative systems. However, there surely exists among the theorists the desire to learn of the dependence among the parameters for all ranges of e/ρ. This can be accomplished by using the approach of this paper to establish the governing equations, and a high-speed computer to evaluate these equations.

REFERENCES

1. H. Himelblau and S. Rubin, "Vibration of a Resiliently Supported Rigid Body," Shock and Vibration Handbook, Chap. 3, pp. 3-1 to 3-52. McGraw-Hill, New York, 1961

2. L. S. Jacobsen and R. S. Ayre, Engineering Vibrations, pp. 335-344. McGraw-Hill, New York, 1956

3. James T. Gwinn, Jr., Lord Manufacturing Co. Eng. Rept. 03001-11, March 1961

4. N. O. Myklestad, Fundamentals of Vibration Analysis, pp. 220-221. McGraw-Hill, New York, 1956

* * *

MISSILE HANDLING ANALYSIS

C. R. Brown and Alex J. Avis
Westinghouse Electric Corporation
Sunnyvale, California

The handling of POLARIS missiles from submarine tenders to submarines has been studied by analyses and full-scale tests. Results are given of a rigid body shock analysis and of loading tests at a selected harbor and at the San Francisco Bay Naval Shipyard. The test results indicate that the existing POLARIS loading fixture without shock absorbers will protect the missile up to a vertical impact velocity of 0.7 to 1.0 fps. With shock absorbers, the system operates safely up to about 4.0 fps. The calculated values were more conservative, showing a lower safe operating range.

An alternate system, which automatically controls the position of the loading fixture relative to the submarine deck, is also discussed. This alternate system, called Yo-Yo, provides negligible impact or lift-off velocities. Larger tender crane motors and new gears, brakes, and controls would be required to install the Yo-Yo system on existing tenders. A model Yo-Yo unit was tested, and good operating characteristics were noted. It is concluded that the shock loading problem can be eliminated by using either shock absorbers or a constant relationship crane system. The Navy has selected a shock absorber system for POSEIDON handling system.

INTRODUCTION

The handling of POLARIS missiles from submarine tenders to submarines has recently been reexamined by Westinghouse under Navy Special Projects Office contract NOw 60-0642. The purpose of the study was to verify the adequacy of present POLARIS handling shock absorber equipment and to lay the groundwork for the design and development of POSEIDON missile handling equipment. Since a small percentage of POLARIS missiles must occasionally be examined for proper performance as part of a missile surveillance program, it is necessary to load and unload POLARIS submarines at several harbors throughout the world. Most of these harbors are well protected, so relative motions between the tender and the submarine will be very small most of the time. However, one of these harbors is relatively unprotected from ocean winds and waves, which occasionally effect large relative motions. Therefore, this harbor was chosen as the site for recently completed handling tests [1]. It was a problem, however, to plan the trip schedule of the test personnel to coincide with a storm. Data from this selected harbor were supplemented by data from a simulated test at the San Francisco Bay Naval Shipyard (SFBNSY).

Figure 1 shows a profile view of the missile, loading fixture, submarine, and tender. The missile is supported inside a liner from a small hoist as shown. A funnel guide is temporarily installed on top of the launcher tube to guide and mate the loading fixture to the launcher tube. Part of the funnel guide may be seen at the submarine deck. In rough weather, an outrigger type shock absorber is added to the loading fixture (Fig. 2). In this case, four small funnel guides are attached to the submarine deck to receive the legs of the shock absorber assembly. This same rough weather gear also provides potential capability for at-sea transfer of missiles under mild sea states. The outrigger design has been satisfactory, but during rough weather additional precautions must be taken to keep it from striking the exposed submarine hatch. However, no damage has ever been reported.

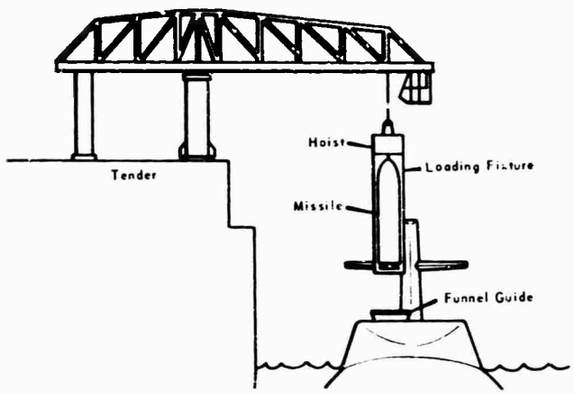

Fig. 1 - On-loading POLARIS missiles

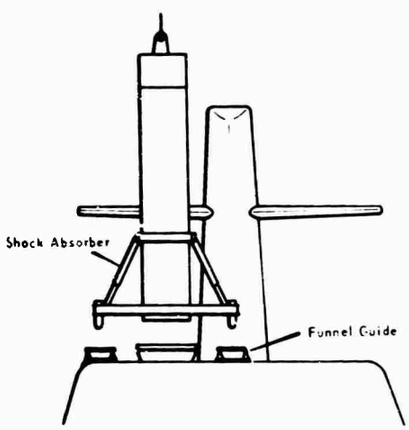

Fig. 2 - POLARIS outrigger shock absorber system

ANALYSIS

Prior to conducting the handling tests at the selected harbor and the SFBNSY, an analysis was made to predict missile response and system performance. A mathematical model, as shown in Fig. 3, represented the missile, liner, hoist, hoist cable, crane cable, and foundation stiffness. The foundation stiffness represented the resiliency of the funnel guide. Shock absorbers were represented by simply using a softer foundation stiffness and adding viscous damping. Coulomb damping was used to simulate friction as the missile slides vertically in the liner. A viscous damping term was included with the shock absorber spring and with the hoist cable spring. All masses but one were assumed to be rigid bodies; the liner was represented as a two-mass unit with a connecting spring. The upper half of the liner mass was lumped with the hoist mass, and the lower half was represented as shown.

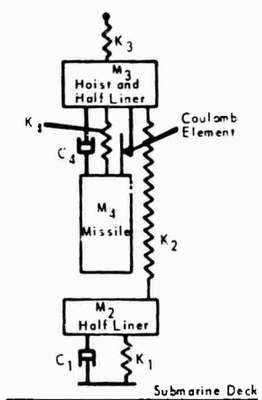

Fig. 3 - Mathematical model of handling system

Several parametric runs were made with various values of damping, spring constants, and landing velocities. Shock absorbers were simulated in several locations, including in the hoist block and in the funnel guide [2]. The mathematical representation would be approximately the same for a shock absorber located in the funnel guide, in the liner base, or for an outrigger-type shock absorber.

TEST CONDITIONS

Variables recorded during the handling test at the selected harbor included wave heights,

missile or handling fixture impact velocity, missile and hoist decelerations, and relative heave, sway, and surge between the submarine and the tender. Cable jerk impact tests were also made at the selected harbor and at the SFBNSY. Figure 4 shows how some of the more important measurements were obtained. The missile in a handling fixture is shown approaching the submarine deck. Accelerometers were located on the missile nose fairing and base flange. A third accelerometer was located on the hoist base flange, as shown. The impact velocity was measured by means of a wire and a linear motion transducer.

RESULTS OF TEST AND ANALYSIS

Figure 5 shows missile deceleration over a range of impact velocities without a shock absorber. The solid line represents the calculated values and the small circles represent the test data obtained at the selected harbor. The data from SFBNSY are also shown on the curve. Both the flat pad and the submarine were estimated to have high stiffness as compared to that of the loading fixture. The test results and calculated values show general agreement. The reduced slope of the test points up to 1.1 fps is attributed to the taking up of joint looseness

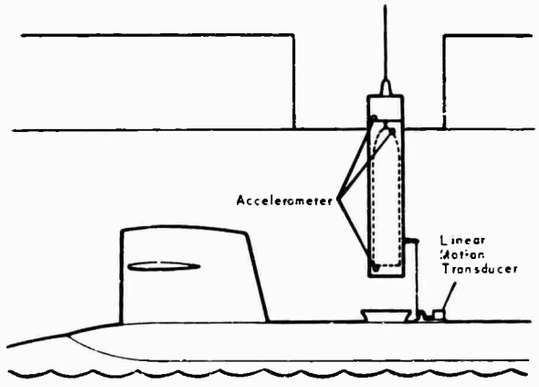

Fig. 4 - Instrumented missile loading operation

During the test, only mild to medium harbor conditions were available. It was also impossible to take full advantage of the maximum relative ship motions that were available, since the crane operators consistently landed the load at the crest of the heave cycle. The impact between the submarine deck and the loading fixture usually occurred at the point of almost zero relative motion. This reaction of the operators was natural since they were well aware of the nature and fragility of the load. However, the reluctance of the crane operators to land hard was disappointing to the test crew, who had anticipated obtaining a range of impact values. It was also difficult to keep the recorder from jamming and the instruments operating properly in the cold, wind, and rain encountered in the test area in January.

The test setup at the SFBNSY consisted of similar equipment, except that the funnel guide or launch tube extension was bolted to a concrete pad, and a yard crane replaced the tender crane. Also, an A-3 structural test vehicle known as an STV-3M was used instead of live missiles.

over this range of compression. When this looseness is eliminated, the components become effectively stiffer. Off-center landings may also have contributed to the scatter of the test points. If the loading fixture initially strikes the funnel guide on one side, a reduced shock level will be produced, since the foundation spring constant would be effectively lowered. In any event, the test points were fairly repeatable and included the readings of two separately mounted accelerometers (one on the missile base and one on the nose cone), and a load cell attached to the missile nose cone. The load cell readings were converted to deceleration values by dividing the readings by the missile weight. It may also be noted that the load cell readings differ from the accelerometer readings. This difference is probably due partly to the vertical friction between the missile and the liner. Measurement of this friction on previous tests at low velocities has shown a value of from 7000 to 12,000 lb. At a limiting missile nose cone loading of 1.9 g, it appears that impact velocities of from 0.7 to 1.0 fps would be safe. The calculated results are more conservative, showing a lower limit.

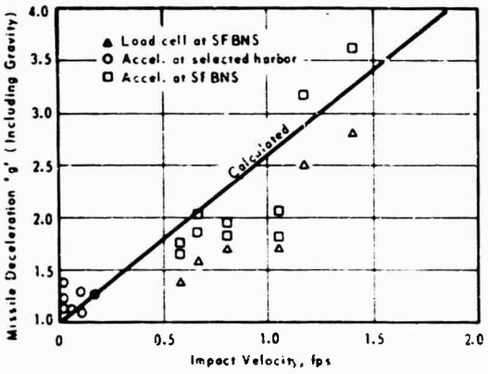

Fig. 5 - Landing shock without shock absorbers

Shock absorbers were not evaluated at the selected harbor because of lack of rough weather conditions. However, they were evaluated during the SFBNSY test. Figure 6 shows missile deceleration vs impact velocity with shock absorbers using a structural test vehicle. Test points from a load cell and an accelerometer mounted in the missile nose and an accelerometer mounted on the missile base are shown. All of the test points follow the same trend, showing a gradual reduction in missile deceleration as the velocity increases, until the springs bottom at about 4.5 fps impact velocity. The exact shape of the curve between zero and 1.0 fps is not known, but all curves must go through the 1.0-g point at zero velocity. From the test results it is evident that loadings up to a velocity of about 4.0 fps can be made safely. Again, the calculated values are more conservative.

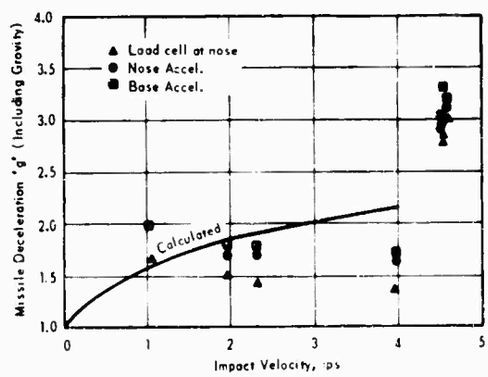

Fig. 6 - Landing shock with shock absorbers

The phenomenon of decreasing response with increasing velocity was not expected prior to the test. Such an occurrence is not normal even with a preloaded spring system; however, with the large number of springs and masses in the tested assembly, random phasing with the shock pulse may occur. A check of the test data traces has shown that such may be the case. When the loading fixture was released from the yard crane through a constant velocity hydraulic valve, an oscillation occurred in the missile accelerometer and load cell traces. For high-velocity drops, the oscillation did not have time to develop before impact occurred. For low-velocity drops, several cycles of oscillation were noted. The phasing of these oscillations and the shock pulse may have resulted in some higher loads on the missile at the lower input velocities. Off-center impact, as previously mentioned, or tilted impacts, may have contributed to the unusual test results. This would be especially likely when shock absorbers were used, since landing on one leg of the shock absorber assembly would provide a much softer spring effect.

The calculated values do not show the same negative slope characteristics as the tested values, even though an effort was made to simulate the complete system. However, the results are close enough to assure that performance of new designs can be adequately predicted. Further analysis is planned including flexible representations of the missile and liner.

Once a missile and loading fixture have been landed on the funnel guide, a jerking of the crane cable may occur if the crane operator does not provide sufficient slack, and the relative heave motions of the ships suddenly lift the fixture from the deck. This cable jerk phenomenon can also produce shock loads on the missile. During the test at the selected harbor, only mild cable jerks were produced, which resulted in an acceleration on the missile of only 1.05 g, including gravity. From the 2.75-cps oscillations of the accelerometer readings, it was possible to determine that the combined crane cable and boom had a stiffness of about 49,400 lb/in., which will be helpful information for future calculations. Figure 7 shows the results of a cable jerk test at SFBNSY. For this test, the loading fixture and missile were suspended from the yard crane and suddenly released, using a constant velocity valve. The assembly underwent a severe jerk as the end of the valve was reached. The calculated and test values of deceleration show good correlation up to a velocity of about 3.0 fps for the few available test points. Above this level, the

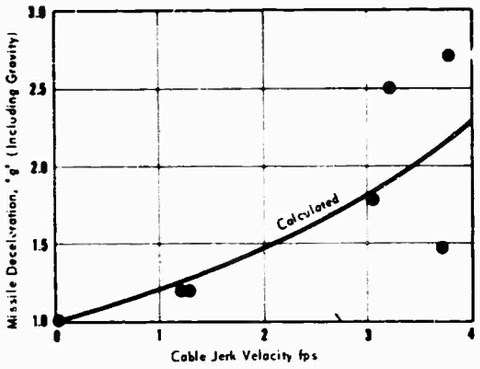

Fig. 7 - Cable jerk shock test

scatter in the test points becomes fairly large. The scatter appears to be due to the reaction of the yard crane, which is approximately 1/4 as rigid as the tender crane, and to the sudden change in load as the constant velocity valve was activated. The crane boom oscillated when the load was suddenly reduced, causing an oscillation in the missile accelerometer trace. As in the case of the previously discussed drop tests, with or without a shock absorber, the system had time to oscillate through about two cycles before impact occurred for the low-velocity tests. At the higher velocities, only a fraction of a cycle was possible. It appears that phasing of the shock pulse and the system oscillation has a large influence on the resulting system response. Both the calculated and test results show th missile limit of 1.9 g is reached at slightly over 3.0 fps when using the SFBNSY yard crane. A value of 1.75 fps has been calculated as the cable jerk velocity limit using the tender crane. It was assumed in these calculations that all components were initially at rest for the tender cable jerk situation and for the SFBNSY test simulation. Then the cable was suddenly given an upwa d velocity impulse. Additional analysis using a flexible representation of the missile and liner and more accurate simulation of test conditions may further clarify these results.

During the test period at the selected harbor, only medium size waves and ship motions were available. The waves were measured by a wave gage, located on the bottom of the harbor, just off the starboard bow of the tender. The relative motions between ships were measured by using linear-motion potentiometers attached to one ship and a light wire stretched to the adjacent ship. Temporary booms were used where necessary to position the wires properly. Figure 8 shows a typical trace of wave amplitude and ship relative motion as a function of time. The displacement scale is on a relative basis. To understand the ship motion characteristics better, a spectrum analysis has been made of the wave, heave, and surge motions. Figure 9 shows a typical Fourier spectrum of the wave motions. The predominant waves on this particular day had a period of approximately 7 sec. Figure 10 shows a spectrum plot of relative heave motion at the same time. The heave motion is characterized by a dominant period of 8 to 9 sec. Significant motions are also evident at a period of about 12 sec. Most of the relative heave motion is due to the submarine motion, with the tender remaining relatively quiet. Since the frequency content of the waves is close to the fundamental heave frequency of the submarine, the submarine responds with large heaving motions. Figure 11 shows that the relative surge motion between the submarine and the tender has a characteristic period of about 60 sec on the same day. Submarine roll was found to be about 2.5 times the roll amplitude of the tender during most of the testing period.

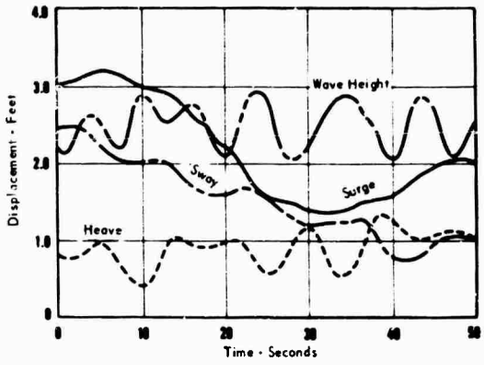

Fig. 8 - Typical ship motion trace

ALTERNATE SYSTEM

The shock absorber system previously described, or any equivalent shock system, would undoubtedly provide adequate protection to the missile under limited rough weather harbor conditions or even in limited open sea environments. An alternate method, called a Yo-Yo system, provides a constant differential distance between the load and the submarine, with the operator controlling only the rate of approach. This differential control system automatically regulates the speed and direction of the crane motor, so as to provide low impact or lift-off velocities of the load with the deck [3]. This is accomplished as shown schematically in

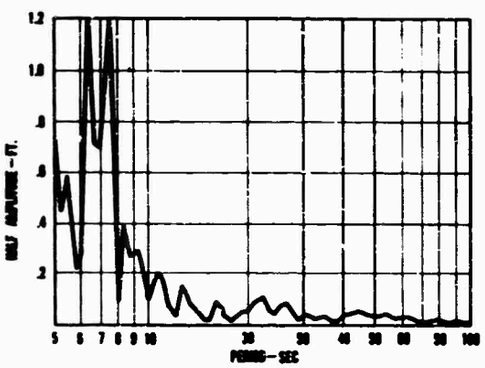

Fig. 9 - Frequency spectrum plot of wave motion

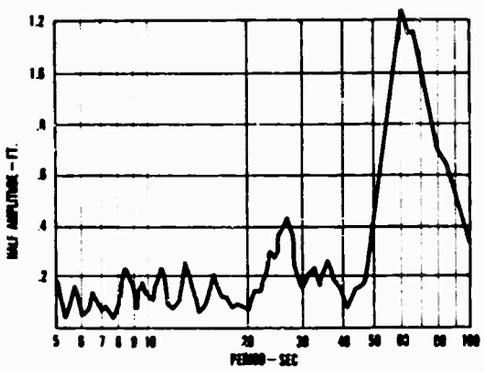

Fig. 11 - Frequency spectrum plot of relative surge

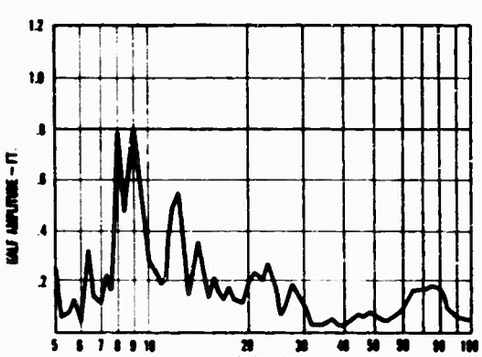

Fig. 10 - Frequency spectrum plot of relative heave

Fig. 12. With the loading fixture suspended from the tender crane over the submarine deck, a tag line is attached to the deck from a reel, which drives a synchro on the crane boom. The hoist motor and gears are controlled by composite inputs from the reel synchro and from the operator. If the operator does not choose to raise or lower the load, the synchro control system will maintain the load at a fixed distance above the submarine deck, even though the two ships are heaving and pitching. Relative downward or upward motion can then be introduced by movement of a control lever by the operator.

Figure 13 shows the horsepower required to eliminate relative motion between the load and the deck for POSEIDON missile and loading fixtures over a range of relative heave

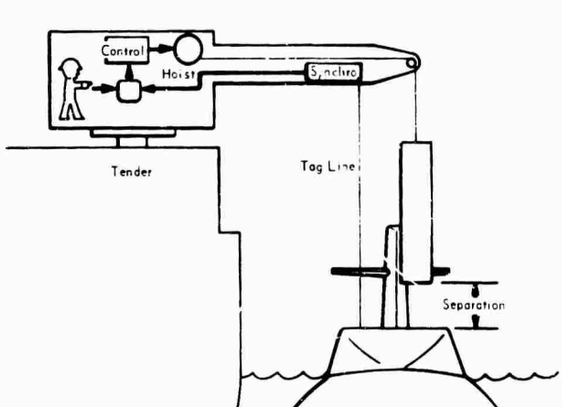

Fig. 12 - Schematic of Yo-Yo system

velocities. It may be seen that the horsepower requirements are reasonable. For example, to accommodate a 2.5-fps relative heave, a 250-hp motor would be necessary. New motor controllers, gears, and larger brakes would be required. A space check has shown that all components can probably be fitted into the existing machinery space in the tender cranes.

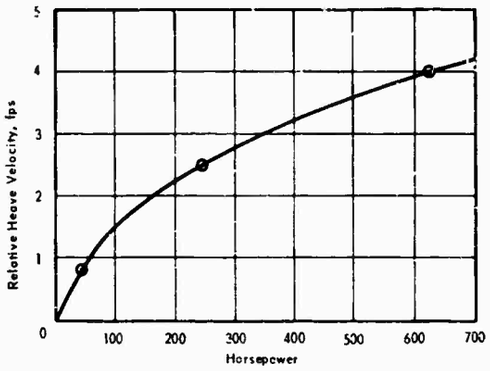

Fig. 13 - Yo-Yo horsepower requirements

A working model of the Yo-Yo was built several years ago for demonstration purposes using a 4000-lb test weight. Rough weather conditions were simulated in a test tank. In spite of the violent barge motions from the man-made waves, the crane and Yo-Yo controls were able to maintain an almost constant position of the load relative to the barge. By moving the control lever in the downward direction, the load could be set down at almost zero impact velocity. Lift-offs were also performed with almost zero relative velocity by reversing the control lever.

With the Yo-Yo system, shock absorbers and skilled crane operators are not required, and loading fixture designs can be lightened. The effect of lateral ship motions are reduced, since the operator does not have to worry about vertical impact. The Yo-Yo system can adequately handle not only missiles but other delicate items, such as warheads, torpedoes, and ammunition, even in rough weather.

CONCLUSIONS

Protection of POLARIS or POSEIDON missiles during loading operations can be accomplished either by adding a shock absorbing system to the loading fixture or by effectively eliminating the relative motion between the load and the submarine deck. The feasibility of both methods has been established; in fact, the POLARIS outrigger shock absorbers have been in service for several years. Indications are that the POLARIS program will retain the outrigger shock absorbing system for possible use in rough weather conditions, and that a shock absorber between the missile and liner will be developed for the POSEIDON program.

ACKNOWLEDGMENTS

The writers appreciate the assistance given by Otis R. Walton, V. Stroud, Charles Kelley, E. D. Pabst, and R. S. Elberty in planning and performing the test and analysis.

REFERENCES

1. A. J. Avis, E. D. Pabst, and C. R. Brown, "Missile Handling Test Report," Westinghouse TN-543, July 6, 1966
2. O. R. Walton, "C-3 Vertical Shock During Loading Operations," Westinghouse TN-529, Nov. 17, 1965
3. C. R. Brown, E. J. Barakauskas, and R. C. Raffaeli, "Landing System Analysis," Westinghouse TN-544, May 20, 1966

DISCUSSION

Mr. Forkois (Naval Research Laboratory): Was there any roll motion in any of your tests?

Mr. Brown: Yes, we measured roll, heave, sway, and surge of the two ships. Actually, heave was influenced by roll so there was an error, but we feel it was relatively small. With the time we had, this was about the best we could do.

Mr. Forkois: I thought maybe some of the apparent discrepancies might have been due to neglecting the roll of the submarine.

Mr. Brown: No, most of the test data were collected during tests at the San Francisco Bay Shipyard where we used a concrete pad. There was no roll there at all.